Technische Universität München

Fakultät für Medizin

Klinische Forschergruppe der Frauenklinik des Klinikums rechts der Isar

Effects of the GTPase Rab31 on breast cancer cell proliferation, adhesion, and expression of other tumor-associated genes

Mag. Susanne Sölch

Vollständiger Abdruck der von der Fakultät für Medizin der Technischen Universität München zur Erlangung des akademischen Grades eines

Doctor of Philosophy (Ph.D.)

genehmigten Dissertation.

Betreuer: apl. Prof. Dr. V. Magdolen

Vorsitzender: Univ.-Prof. Dr. C. Zimmer

Prüfer der Dissertation:

1. apl. Prof. Dr. A. Krüger

2. Priv.-Doz. Dr. G. H. S. Richter

Die Dissertation wurde am 22.01.2014 bei der Fakultät für Medizin der Technischen Universität München eingereicht und durch die Fakultät für Medizin am 17.02.2014 angenommen.

There is a theory, which states that if ever anyone discovers exactly what the Universe is for and why it is here, it will instantly disappear and be replaced by something even more bizarre and inexplicable. There is another theory which states that this has already happened.

Douglas Adams

So eine Arbeit wird eigentlich nie fertig, man muss sie für fertig erklären, wenn man nach Zeit und Umständen das Mögliche getan hat.

Johann Wolfgang von Goethe

1 - ABSTRACT 6

2 - ACRONYMS AND ABBREVIATIONS 8

3 – INTRODUCTION 11

3.1 - CANCER IS A MULTISTEP PROCESS 11
3.2 - CANCER METASTASIS FORMATION 13
3.3 - BREAST CANCER 16
3.4 - THE UROKINASE SYSTEM 18
3.4.1 - THE UROKINASE PLASMINOGEN ACTIVATOR (UPA) 19
3.4.2 - THE PLASMINOGEN ACTIVATOR INHIBITOR 1 AND 2 (PAI-1 AND PAI-2) 20
3.4.3 - THE UROKINASE RECEPTOR (UPAR / CD87) 21
3.4.4 - UPA-UPAR CELL SIGNALING 22
3.4.5 - UPAR IN CANCER 23
3.4.6 - UPAR MRNA VARIANTS 23
3.4.7 - UPAR-Δ4/5 AS A PROGNOSTIC MARKER 25
3.5 - RABGTPASES 28
3.5.1 - STRUCTURE OF RAB PROTEINS 30
3.5.2 - RAB GTPASES IN MEMBRANE TRAFFICKING 31
3.6 - RAB31 34
3.6.1 - RAB31 FUNTIONS AND INTERACTION PARTNERS 35

5 - METHODS AND MATERIALS 39

5.1 - MOLECULAR CLONING 39
5.1.1 - DESIGN OF OLIGONUCLEOTIDES FOR SITE DIRECTED MUTAGENESIS 39
5.1.2 - SITE-DIRECTED MUTAGENESIS 41
5.1.3 - DESIGN OF SHRNAI 43
5.1.4 - CLONING OF SHRNAI INTO THE RNAI-READY PSIREN-RETROQ VECTOR 44
5.1.5 - TRANSFORMATION OF PLASMID DNA INTO COMPETENT BACTERIA BY HEAT PULSE 44
5.1.6 - SMALL-SCALE PLASMID PREPARATION (MINI-PREP) 45
5.1.7 - RESTRICTION ENZYME ANALYSIS 46
5.1.8 - MEDIUM SCALE PLASMID PREPARATION (MIDI-PREP) 47
5.1.9 - GLYCEROL STOCKS OF BACTERIA 48
5.2 - CELL CULTURE 48
5.2.1 - CULTIVATION OF ADHERENT MAMMALIAN CELLS 48
5.2.2 - THAWING OF ADHERENT CELLS 48
5.2.3 - FREEZING OF ADHERENT CELLS 48
5.2.4 - LIPOSOME BASED STABLE TRANSFECTION OF ADHERENT MAMMALIAN CELLS 49
5.2.5 - TRANSIENT TRANSFECTION OF MDA-MB-231 CELLS WITH RAB31-SIRNA 51
5.2.6 - STABLE RAB31 KNOCK-DOWN IN MDA-MB-231 CELLS BY SHORT HAIRPIN RNA INTERFERENCE 53
5.2.7 - SUBCLONING OF CELL LINES *VIA* SINGLE SELECTION OF CELLS 56
5.2.8 - DETECTION OF MYCOPLASMA CONTAMINATION IN CULTURED CELLS 56
5.2.9 -TREATMENT OF MYCOPLASMA INFECTIONS 57
5.2.10 - 3D CELL CULTURE 57
5.3 - CELLULAR ASSAYS 58
5.3.1 - PREPARATION OF CELLULAR ASSAYS *IN VITRO* 58
5.3.2 - COUNTING PROLIFERATION ASSAY 58
5.3.3 - PROLIFERATION MEASUREMENT WITH ALAMARBLUE 58
5.3.4 - PROLIFERATION MEASUREMENT WITH CYQUANT 59
5.3.5 - PROLIFERATION MEASUREMENT BY MEASURING THE CELLULAR IMPEDANCE 61
5.3.6 - ADHESION ASSAYS 61
5.3.7 - INVASION ASSAY 62
5.3.8 - TGF-β ACTIVITY ASSAY 63
5.4 - FLOW CYTOMETRY 64

5.4.1 - Annexin V staining 64
5.4.2 – Determination of the percentage of cells in S-phase 66
5.5 - Immunocytochemistry 66
5.5.1 - Immunocytochemistry staining of cells on chamberslides 66
5.6 - Western blot analysis 67
5.6.1 - Cell lysis for SDS-PAGE 67
5.6.2 - Western blot analysis (semidry and wet blot) 67
5.7 - ELISA 68
5.7.1 - Rab31 ELISA 68
5.7.2 - TGF-β1 ELISA 69
5.8 - qPCR 70
5.8.1 - Isolation of RNA 70
5.8.2 - Reverse transcription for qPCR 70
5.8.3 - qPCR with linear fluorescent probes 71
5.8.4 - SABiosciences array qPCR 73
5.9 - Statistics 75

6 - RESULTS 76

6.1 - Generation of breast cancer cells co-overexpressing Rab31 and uPAR-Δ4/5 76
6.1.1 - Stable transfection of breast cancer cells 77
6.1.2 Characterization of the overexpression of Rab31 and uPAR-Δ4/5 overexpression in MDA-MB-231 cells 78
6.1.3 - Proliferation of MDA-MB-231 cells overexpressing Rab31 and uPAR-Δ4/5 80
6.1.4 - Adhesive characteristics of MDA-MB-231 cells overexpressing Rab31 and uPAR-Δ4/5 81
6.2 - Knock-down of Rab31 mRNA levels in MDA-MB-231 cells 82
6.2.1 - Transient transfection of siRNAs in MDA-MB-231 cells 82
6.2.2 - Expression of two different shRNAs directed to Rab31 mRNA in MDA-MB-231 cells 84
6.2.3 - Analysis of MDA-MB-231 cells expressing Rab31-shRNAi 87
6.2.4 - Proliferative charactersistics of MDA-MB-231 cells with reduced Rab31 mRNA levels 88
6.3 - Rab31 mutants 89
6.3.1 - Design of Rab31 mutants affecting the GTP/GDP cycle or membrane association 89
6.3.2 - Generation of stably transfected breast cancer cells overexpressing Rab31-mutants 95
6.3.3 - Proliferative charactersistics of breast cancer cells overexpressing Rab31-WT/-mutants 99
6.3.4 - Adhesive properties of breast cancer cells overexpressing Rab31-WT/-mutants 101
6.3.5 - Invasive capacity of breast cancer cells overexpressing Rab31-WT/-mutants 103
6.4 - Molecular effects of Rab31 overexpression 104
6.4.1 - Breast cancer cells overexpressing Rab31 104
6.4.2 - Proliferative properties of Rab31-overexpressing cells 107
6.4.3 - Identification of differentially expressed candidate genes in Rab31-overexpressing *versus* control cells by mRNA analysis (SAB EMT array) 115
6.4.4 - Validation of differential VCAN expression in Rab31-overexpressing *versus* vector control breast cancer cells 122
6.4.5 - Validation of differential TGF-β1 mRNA expression in Rab31-overexpressing *versus* vector control breast cancer cells 124
6.4.6 - Validation of differential TGF-β1 expression in Rab31 low *versus* high expressing cells on the protein level 126
6.4.7 - Validation of differential TGF-β activity levels in Rab31-overexpressing *versus* vector control cells 132
6.4.8 - Identification of further differentially expressed candidate genes using another mRNA array (SAB TGF-β array) 134
6.4.9 - Validation of differential mRNA expression of selected candidate genes in Rab31-overexpressing *versus* vector control cells by qPCR 136

7 - DISCUSSION **139**

8 - REFERENCES **155**

9 - PUBLICATIONS **169**

10 - ACKNOWLEDGEMENTS **170**

1 - ABSTRACT

The urokinase receptor (uPAR) is a member of the proteolytic plasminogen activator system, which plays an important role in tumor growth, invasion and metastasis. High mRNA levels of the uPAR splice variant uPAR-Δ4/5 are associated with poor prognosis of lymph node-negative (LNN) breast cancer patients. Its overexpression in breast cancer cells leads to reduced cell adhesion and invasion and to modulation of mRNA levels of tumor-associated genes, including up-regulation of the matrix metalloproteinase MMP-9. Thus, uPAR-Δ4/5 may influence the metastatic potential of breast cancer cells.

RAB31 was identified as a differentially expressed gene associated with uPAR-Δ4/5 expression in breast cancer. Vesicle transport, signal transduction, receptor internalization as well as receptor recycling is regulated by Rab proteins the large family of Rabs constitutes of monomeric, small GTP-binding proteins. Elevated Rab31 mRNA expression is associated with poor prognosis of LNN breast cancer patients, similar to the overexpression of uPAR-Δ4/5. In breast cancer cells, overexpression of Rab31 leads to enhanced cell proliferation associated with reduced adhesion towards several extracellular matrix (ECM) proteins and decreased invasive capacity.

The aim of the thesis was to further explore the tumor biological role of Rab31 in breast cancer cells compared with the effect of various mutants of Rab31 or Rab31 knock-down and to assess the biological effects of co-overexpression of Rab31 with the splice variant uPAR-Δ4/5 in these cells.

MDA-MB-231 breast cancer cells, simultaneously overexpressing Rab31 and uPAR-Δ4/5, were generated in order to investigate any additive or synergistic effects of these biomarkers on cell proliferation or adhesion, compared to vector control cells. No additive or synergistic effects were detected when both Rab31 and uPAR-Δ4/5 were co-overexpressed in comparison to overexpression of either Rab31 or uPAR-Δ4/5 alone, regarding cell proliferation or adhesion towards different ECM proteins.

To prove that Rab31 acts as a molecular switch on cell proliferation, depending on its expression level, Rab31 mRNA levels were stably knocked down by short hairpin RNA interference (shRNAi) in MDA-MB-231 wild-type cells, which express moderate endogenous Rab31 levels. Reduction of Rab31 mRNA/protein expression led to significantly lower cell proliferation rates, which matches the effects observed upon Rab31 overexpression.

To analyze whether Rab31 GTPase activity and/or distribution within the breast cancer cell is necessary for its effects on cell proliferation, adhesion and invasion, expression plasmids for (i) a constitutively active form of Rab31, Rab31-Q64L, (ii) a constitutively inactive form, Rab31-S19N, and (iii) a mutant unable to insert into the Golgi membrane, Rab31-ΔCC, were generated. MDA-MB-231 and CAMA-1 cell lines were stably transfected with the mentioned plasmids. Whereas Rab31-Q64L-overexpressing cells

exhibit the same phenotype as Rab31-WT-overexpressing cells concerning proliferation, adhesion and invasion, Rab31-ΔCC-overexpressing cells are characterized by a phenotype comparable to that of vector control cells. These results show that on one hand a constitutively active Rab31 does not intensify the effects of wild-type Rab31 regarding these processes. On the other hand, membrane localization is a pre-requisite for Rab31-mediated effects on cell proliferation, adhesion and invasion. Unfortunately, the constitutively inactive Rab31-S19N variant was not expressed, neither in the MDA-MB-231 nor in the CAMA-1 cells. This may be due to non-tolerated, dominant-negative scavenger effects (*i.e.* competition with the wild-type vesicle transport machinery for Rab-associated proteins), which have been previously described for constitutively inactive mutants of other Rab family members.

Since biological processes such as cell proliferation and adhesion depend on the expression and activity of a plethora of genes, we investigated whether overexpression of Rab31 in breast cancer cells would modulate the expression of other tumor biologically relevant genes. For this, a low-density microarray carrying gene probes known to be involved in epithelial to mesenchymal transition (EMT) was screened for differentially expressed genes in Rab31-overexpressing *versus* vector control cells. Initially, two candidate genes, VCAN1 and TGFB1, were identified. VCAN1, which encodes the extracellular matrix proteoglycan versican, upon Rab31-overexpression, is up-regulated in both the MDA-MB-231 and the CAMA-1 cells, whereas TGFB1, encoding transforming growth factor-beta 1 (TGF-β1), was found down-regulated. Further studies showed that TGF-β1 is strongly reduced in Rab31-overexpressing MDA-MB-231 and CAMA-1 cells as well, both at the protein expression and the activity level. In normal epithelial cells and at early stages of oncogenesis, TGF-β1 acts as an anti-proliferative factor.

To further elucidate the effects of Rab31 overexpression on the TGF-β signaling pathway, the search for differentially regulated genes in Rab31-overexpressing *versus* vector control CAMA-1 cells was extended using another low-density microarray, this time focusing on genes of the TGF-β superfamily and related factors. By this, several genes affected by Rab31 overexpression were identified, including TGFB2, BMP7 and SMAD6 (all down-regulated) as well as B2M, FAS and TNFSF10 (all up-regulated), and their differential expression pattern was confirmed by independent qPCR assays in Rab31-overexpressing *versus* vector control cells.

In conclusion, the data presented provide novel insights into some of the molecular changes triggered by overexpression or repression of the GTPase Rab31 in breast cancer cells, eliciting their switch from an invasive to a proliferative phenotype, or *vice versa*.

2 - Acronyms and Abbreviations

%	percentage
*	statistically significant p-value ≤0.05
**	statistically significant p-value ≤0.01
***	statistically significant p-value ≤0.001
≤	greater, equal then
≤	smaller, equal then
°C	degree Celsius
µl	micro liter
2D	two dimensional
3D	three dimensional
A	adenine
AGO	Arbeitsgemeinschaft Gynäkologische Onkologie e.V.
Ago2	argonaute RISC catalytic component 2
AKT	murine thymoma viral oncogene homolog 1
ALS2	amyotrophic lateral sclerosis 2
ALS2CL	amyotrophic lateral sclerosis 2 C-terminal like
Amp	ampicillin
APT	aminophospholipid translocase
ASCO	American Society for Clinical Oncology
Asn	asparagine
ATP	adenosine triphosphate
Bak	BCL2-antagonist/killer
Bax	BCL2-associated X protein
BMP	bone morphogenic protein
bp	base pairs
BSA	bovine serum albumin
C	cysteine (protein context)
C	cytosine (DNA context)
Ca^{2+}	calcium ion
Cdc42	cell division control protein 42
cDNA	complimentary DNA
CHO	chinese hamster ovary
c-jun	jun proto-oncogene
CLSM	confocal laser-scanning microscope
cm	centi meter
c-suPAR	soluble D2-D3-uPAR
Ct	cycle temperature
Cys	cysteine
D1	domain 1 of uPAR
D2	domain 2 of uPAR
D3	domain 3 of uPAR
DF	disease-free
DFS	disease-free survival
DMEM	Dulbecco's modified eagle medium
DMFS	distant metastases free survival
DNA	deoxyribonucleic acid
DOC	double overexpressing cells
ds RNA	double stranded RNA
ds	double stranded
ECM	extracellular matrix
EDTA	ethylendiamintetraacetic acid
EEA1	early endosome antigen 1
EGFR	epidermal growth factor receptor
EHS	Engelbreth-Holm-Swarm mouse sarcoma
ELISA	enzyme-linked immunosorbent assay
EMT	epithelial to mesenchymal transition
ERK	elk-related tyrosine kinase
ERα	estrogen receptor α
FACS	fluorescence-activated cell sorting
FAK	focal adhesion kinase
FAM	fluorescein
FCS	fetal calf serum
FPRL1	formyl peptide receptor 1
FRET	fluorescence resonance energy transfer
FSTL3	follistatin-like 3
g	gram
G	guanine
GAP	GTPase activating protein
GAPDH	Glyceraldehyde 3-phosphate dehydrogenase
Gapex-5	GTPase activating protein 5
GDF	GDI displacement factor
GDI	GDP-dissociation inhibitor
GDP	guanosine diphosphate
GEF	guanine exchange factor
GGT	geranylgeranyl transferase
Gln	glutamine
GLUT4	glucose transporter type 4
Gly	glycine
GPI	glycosylphosphatidylinositol
GST	glutathione S-transferase
GTP	guanosine triphosphate
GTT	geranylgeranyl transferase
h	hour
HEK	human embryonic kidney
HEPES	(4-(2-hydroxyethyl)-1-piperazineethanesulfonic acid
Her2	human epidermal growth factor receptor 2
HPRT	hypoxanthine-guanine-phosphoribosyltransferase
HRP	horseradish peroxidase
ICC	immunocytochemistry
ICD	International Classification of Diseases
IGF-II	insulin-like growth factor II

IgG	immunoglobulin G
INHα	inhibin, alpha
INHβ	inhibin, beta
JAK	janus kinase
JNK	mitogen-activated protein kinase 8
kb	kilo bases
KD	knock-down
kDa	kilo Dalton
L	leucine
LAP-1	latent associated protein 1
LB	lysogeny broth
LDL	low-density lipoprotein
Leu	leucine
LNN	lymph node-negative
LRP-1	LDL receptor-related protein-1
Lys	lysine
M-6-PR	mannose 6-phosphate receptor
MAP	mitogen activated kinase
MAPK	mitogen-activated protein kinase
MET	mesenchymal to epithelial transition
mg	milli gram
Mg^{2+}	magnesium ion
min	minute
miRNA	micro ribonucleic acid
MIS	anti-Mullerian hormone
ml	milli liter
mm	milli meter
MMP	matrix metalloprotease
mRNA	messenger ribonucleic acid
MUC-1	mucin 1-C
MW	molecular weight
Myc	avian myelocytomatosis viral oncogene homolog
N	asparagine
NF-kB	nuclear factor of kappa light polypeptide gene enhancer
ng	nano gram
nM	nano Molar
nm	nanometer
nt	nucleotides
NTC	non target control
OCRL-1	oculocerebrorenal syndrome of Lowe 1
ORF	open reading frame
OS	overall survival
p38	mitogen-activated protein kinase 14
PAGE	polyacrylamide gel electrophoresis
PAI	plasminogen activator inhibitor
PBS	phosphate buffered saline
PCR	polymerase chain reaction
PDG	platelet-derived growth factor
PEG	polyethylene glycol
PFA	paraformaldehyde
PI	propidium iodide
PI3K	phosphatidylinositol 3-kinase
PLS	phospholipid scramblase
PR	progesterone receptor
PS	phosphatidylserine
PVDF	polyvinylidene difluoride
Q	glutamine
Q64L	pointmutation at position 64 from glutamine to asparagine
qPCR	quantitative polymerase chain reaction
Rabex5	RAB guanine exchange factor 1
Ras	rat sarcoma
REP	Rab escort protein
RhoA	ras homolog family member A
RhoB	ras homolog family member B
RI	TGF-β-receptors type I
RII	TGF-β-receptors type II
RIII	TGF-β-receptors type III
RIN3	Ras and Rab interactor 3
RISC	RNA-induced silencing complex
RNA	ribonucleic acid
RNAi	ribonucleic acid interference
rpm	rounds per minute
RT	room temperature
S	serine
S29N	pointmutation at position 29 from serin to leucine
SBE	smad binding element
SCR	scrambled
SDS	sodium dodecyl sulfate
SEAB	secreted alkaline phosphatase
sec	second
Ser	serine
shRNA	short hairpin ribonucleic acid
shRNAi	short hairpin ribonucleic acid interference
siRNA	short interfering ribonucleic acid
Smad	Smad family member
SMB	somatomedin B
ss	single stranded
STAT	signal transducer and activator of transcription
suPAR	soluble uPAR
SV40	simian virus 40
T	tyrosine
TAK1	nuclear receptor subfamily 2, group C, member 2
TBS	Tris buffered saline
TGF-β1	transforming growth factor beta 1
TGF-β2	transforming growth factor beta 2
TGF-β3	transforming growth factor beta 3
TGN	trans-Golgi network
TIMP-1	tissue inhibitor of metalloproteases 1
TJP1	tight junction protein 1
TMB	3,3',5,5'-tetramethylbenzidine
TNF	tumor necrosis factor

tPA	tissue-type plasminogen activator
TRAIL	tumor necrosis factor (ligand) superfamily, member 10; TNFSF 10
Tris	tris-(hydroxymethyl)-aminomethan
uPA	urokinase-type plasminogen activator
uPAR	urokinase plasminogen activator receptor
uPAR-Δ4/5	urokinase receptor splice variant with deletion of exon 4 and 5
uPAR-Δ5	urokinase receptor splice variant with deletion of exon 4
v/v	volume per volume
VCAN	versican
VEGF	vascular endothelial growth factor
VN	vitronectin
w/v	weight per volume
Wnt	wingless-type MMTV integration site family
WT-1	Wilms tumor 1
XF	XerumFree
ΔC4	deletion of the four C-terminal cysteines
ΔCC	deletion of the two C-terminal cysteines
Ψ^+	packaging signal for virus particles
λ-DNA	lambda DNA

3 – INTRODUCTION

3.1 - CANCER IS A MULTISTEP PROCESS

Cancer is a complex disease, which is only partially understood. Principally, cancer is based on unregulated cell growth caused by dynamic changes in the genome, which involve stepwise accumulation of genetic modifications and progressive alterations in gene expression. Extensive cancer research has shown the importance of dominant gain of function mutations, such as in proto-oncogenes, as well as in tumor suppressor genes with recessive loss of function mutations. Both classes of cancer genes have been identified through their altered expression pattern in human and in animal cancer models. Diverse lines of evidence suggest that tumorigenesis is a multistep process and that these steps reflect successive genetic alterations that drive transformation of normal cells into highly cancerous ones. It has been proposed (Hanahan and Weinberg 2000) that most probably all types of tumors share six altered capabilities (Figure 1). These are listed as:

1. Self-sufficiency in growth signals. Tumor cells show a greatly reduced dependence on exogenous growth factors by generating autocrine growth signaling cascades and constitutively active receptors, thereby becoming independent of their microenvironment.

2. Insensitivity to growth-inhibitory signals. Antigrowth signals can hinder proliferation by two distinct mechanisms: cells are either driven out of active proliferation into a temporary quiescence (G0) or proliferation is permanently stopped by induction of a post-mitotic state. Incipient cancer cells must evade these signals in order to proliferate continuously.

3. Evasion of apoptosis. The ability of tumor cells to expand is not only determined by cell proliferation but also by evading programmed cell death. Apoptosis is a program present in all types of cells, therefore, most cancer cells, must become resistant to apoptotic signals.

4. Unlimited replicative potential. Uncoupling of a cell's growth program from its environment alone is not sufficient for unrestricted growth. It has been hypothesized that all cell types have an intrinsic, cell-autonomous program to limit multiplication. This program relies on telomere shortening during consecutive mitotic divisions and is disrupted in cancer cells, for example, by constitutive expression of telomerase, which reestablishes the shortened telomeres in each cycle.

5. Constitutive angiogenesis. In order to proliferate continuously, cancer cells must ensure their supply of energy and oxygen. Since proliferating cancer cells have no intrinsic ability to induce the formation of blood vessels or stimulate their growth, malignant cells have to develop angiogenic abilities, for example, by expressing angiogenesis-initiating signals such as the vascular endothelial growth factor (VEGF).

6. Tissue invasion and metastasis. One critical step in the progression of cancer is the formation of metastases. Primary tumors can spawn pioneer cells that travel to distant, secondary sites where they can found new colonies. These distant settlements finally cause most cases of deaths in humans. Successful invasion and metastasis depends on the five other acquired hallmarks described above. Invasion and metastasis formation utilize similar operational strategies, which involve changes in the physical coupling of cells to their microenvironment, activation of extracellular proteases as well as changes in integrin expression and loss of epithelial polarity. Each of these cellular changes is a novel capability acquired during tumor development and represents the successful breaching of multiple anticancer defense mechanisms (Figure 1) (Hanahan and Weinberg 2000).

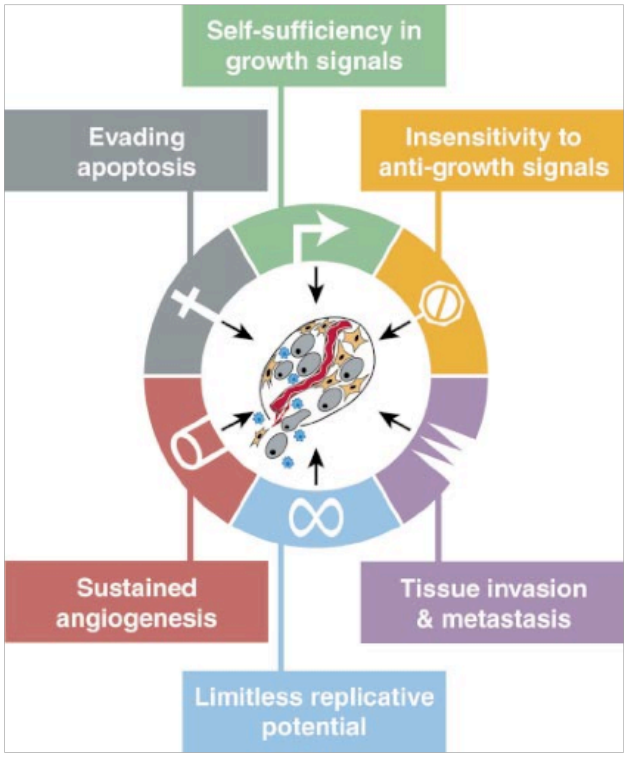

Figure 1 | Acquired hallmarks of cancer
It is suggested that most, if not all, cancers have acquired the same set of functional capabilities during their development, albeit through various mechanistic strategies (Hanahan and Weinberg 2000).

At least two additional hallmarks were added in the last decade, one involves the capability to modify the cellular metabolism in order to most effectively support proliferation and the other allows cancer cells to evade the immune system. The energy metabolism in cancer cells is distinct to normal cells: The ATP production of tumor cells is less efficient because they exclusively use anaerobic glycolysis even in the presence of oxygen (Warburg effect). This is compensated by the up-regulation of glucose

transporters. The proteins responsible for the metabolic switch are also involved in many other processes of the core hallmarks of cancer, so it may be described as another phenotype of proliferation-induced oncogenes. As immune surveillance recognizes and eliminates the majority of cancer cells, the second new hallmark implies that the surviving cancers and metastases must have a way of evading this immunological response. This theory remains to be confirmed and thus is considered only an emerging hallmark so far. In addition to these emerging and old hallmarks two consequential characteristics are important to facilitate development of cancer: Firstly, genomic instability enables cancer cells to alter the genome in a way to constantly adapt to challenges during tumor progression. It was found that evolving premalignant cells are able to accumulate favorable malignant genotypes by destabilization of gene copy numbers and gene sequences in human tumors and that these defects in genomic maintenance selectively accelerate the rate at which tumors progress (Hanahan and Weinberg 2011). Secondly, the inflammation generated by innate immune cells can result in the support of the aforementioned hallmarks. For example, inflammation in the microenvironment can foster the development of benign lesions into full-blown cancers (Figure 2) (de Visser et al. 2006; Qian and Pollard, 2010). The release of inflammatory compounds can increase the selective pressure and thereby cause nearby cancer cells to evolve towards a higher grade of malignancy thus compensating for the harsher environment (Hahn and Weinberg 2002; Grivennikov et al. 2010; Hanahan and Weinberg 2011).

Together, the gain of these hallmarks enables tumor cells to leave their site of origin and to spread to a secondary site, leading to metastasis formation. Metastasis of carcinomas is responsible for more than 80% of cancer-associated cases of deaths. Nevertheless, the mechanisms underlying the formation of metastases are poorly understood so far (Gupta and Massague 2006).

3.2 - CANCER METASTASIS FORMATION

The so-called epithelial to mesenchymal transition (EMT) and the reciprocal process mesenchymal to epithelial transition (MET) play key roles in tumor metastasis formation. As a characteristic, epithelial cells adhere to each other by specialized membrane structures to form a tight monolayer and are strongly connected to the extracellular matrix (ECM). The core elements of the cell-cell interactions are (i) tight junctions which are built up by claudin and occludin, (ii) adherent junctions which are formed by cadherins, and (iii) gap junctions which are made from connexins. Binding of cells to the ECM is predominantly accomplished by integrins. Integrins are a large family of cell adhesion receptors, which are involved in cell-extracellular matrix and cell-cell interactions. They are composed of long extracellular domains, which adhere to their ligands, and short cytoplasmic domains that link the receptors to the cytoskeleton of

the cell. The polarity of the epithelium is defined by the organization of the junctions as a lateral belt with localized distribution of adhesion molecules and the polarized organization of the actin cytoskeleton apical of the ECM. Therefore, epithelial cells can only move within the epithelial layer (Berx et al. 2007; Hugo et al. 2007).

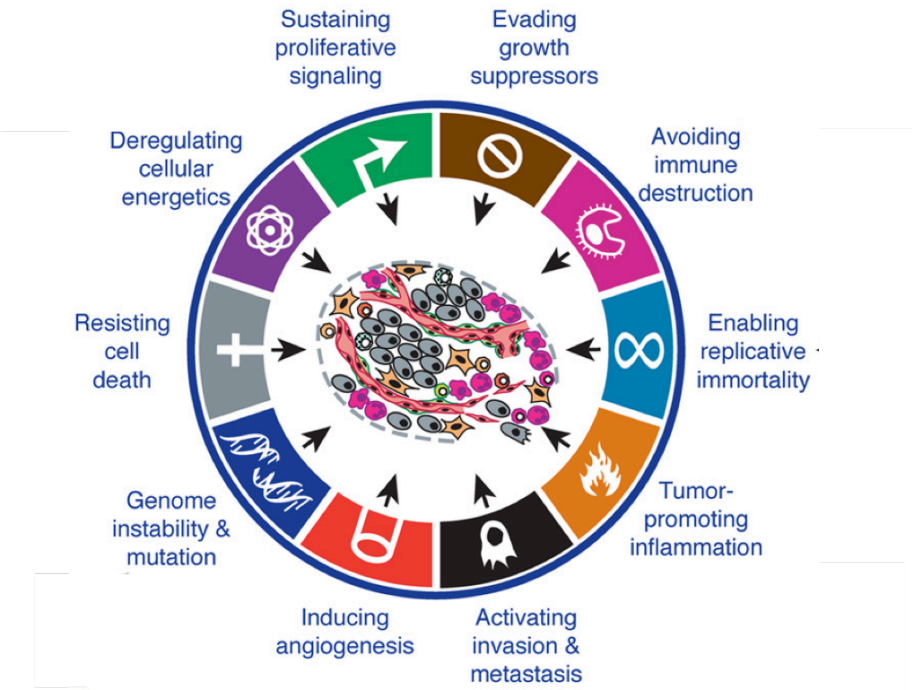

Figure 2 | Emerging hallmarks and enabling hallmarks
Increasing evidence suggests that additional hallmarks of cancer are involved in the pathogenesis of cancer. Emerging hallmarks affect the capability to modify or reprogram cellular metabolism in order to most effectively support neoplasia. Enabling hallmarks allow cancer cells to evade immunological destruction, in particular by T-, B- and natural killer cells as well as by macrophages. Genomic instability and thus mutability equip cancer cells with genetic alterations that drive tumor progression. Inflammation by innate immune cells layed out to fight infections and heal wounds can instead ensure the support of multiple hallmarks, thereby illustrating tumor-promoting consequences of inflammatory responses (Hanahan and Weinberg 2011).

Mesenchymal cells, in contrast, form irregular structures with focal adhesions that are less strong than tight junctions. The mesenchyme has no apical-basolateral polarization, but instead some polar organization of their leading and tailing and also during motility, which is generated by a dynamic polarization of the actin cytoskeleton along the axis of migration. Thus, mesenchymal cells can move in all three dimensions by reorganizing the actin cytoskeleton according to the changes in the direction of migration. Thus, EMT describes the process in which epithelial cells lose their sessile phenotype and gain migrant features which is an important step in tumor progression (Figure 3).

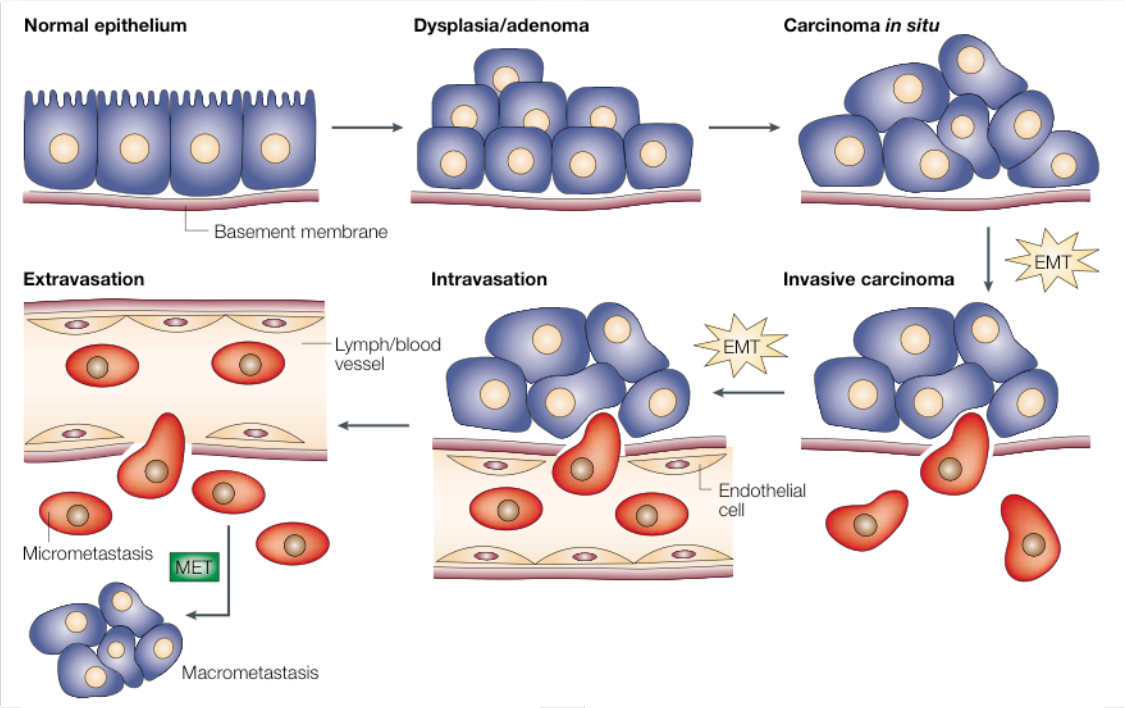

Figure 3 | Metastasis formation
Epithelial carcinoma cells undergo epithelial to mesenchymal transition (EMT) to escape the primary cancer and invade lymph or blood vessels. After intravasation, the cancer cells must survive the shear forces of the circulation allowing their passive transport to distant organs. To form micro-metastases the cells undergo mesenchymal to epithelial transition (MET) after extravasation from a vessel (Thiery 2002).

In healthy individuals, EMT takes place in early embryogenesis when mesoderm and endoderm are formed (Thiery and Sleeman 2006). Later in the development, EMT is responsible for organ and tissue formation. It also plays an important role in the regeneration process during wound healing. In the pathological context of cancer and other diseases, EMT is involved in fibrosis and metastasis formation. Besides prominent structural morphological differences, epithelial *versus* mesenchymal cells show big differences in their gene expression profiles. Some of the differentially expressed genes can be used as biomarkers to distinguish between these two cell types. One example for an epithelial cell marker is E-cadherin. It is a transmembrane protein that is localized to adherent junctions at the basal membrane and mediates cell-cell contact in a Ca^{2+} dependent manner. E-cadherin is not (or only weakly) expressed in mesenchymal cells. Another established marker for epithelial cells is tight junction protein 1 (TJP1). This protein is only present on the cytoplasmic side of tight junctions, where it interacts with claudin, occludin and with the actin cytoskeleton. Thus, TJP1 provides a linkage between the actin cytoskeleton and the tight junctions.

Vimentin, on the other side is a typical marker for mesenchymal cells. It forms intermediate filaments, which provide flexibility to the cell with their dynamic nature, and plays a significant role in positioning and anchoring of organelles in the cytosol.

Therefore, vimentin is the cytoskeletal component, which is responsible for maintaining cell integrity under mechanical stress *in vivo*.

During EMT, the loss of E-cadherin is a very crucial step. E-cadherin is a strong tumor suppressor and indeed, E-cadherin reintroduction is sufficient to partially or even completely reverse EMT in certain cell types (Christofori and Semb 1999; Arias 2001). EMT is a complex process, which requires alterations in morphology, cellular architecture, adhesion and migration capacity. This diversity of changes might explain why EMT is controlled by at least six pathways (Wnt, TGF-β, Hedgehog, Notch, RTK and NF-κB) (Huber et al. 2004). During tumor progression, these pathways and their cross talk are often deregulated and drive cells into EMT (Grünert et al. 2003; Gotzmann et al. 2004; Huber et al. 2004; Berx et al. 2007).

3.3 - Breast cancer

Cancer is a leading cause of death worldwide, accounting for 7.6 million cases of deaths, which are around 13% of all cases of deaths, in 2008. Death rates from cancer are predicted to increase worldwide, with an estimated 13.1 million deaths in 2030 (www.who.int). The most frequent cancer in women in the US is breast cancer (Figure 4).

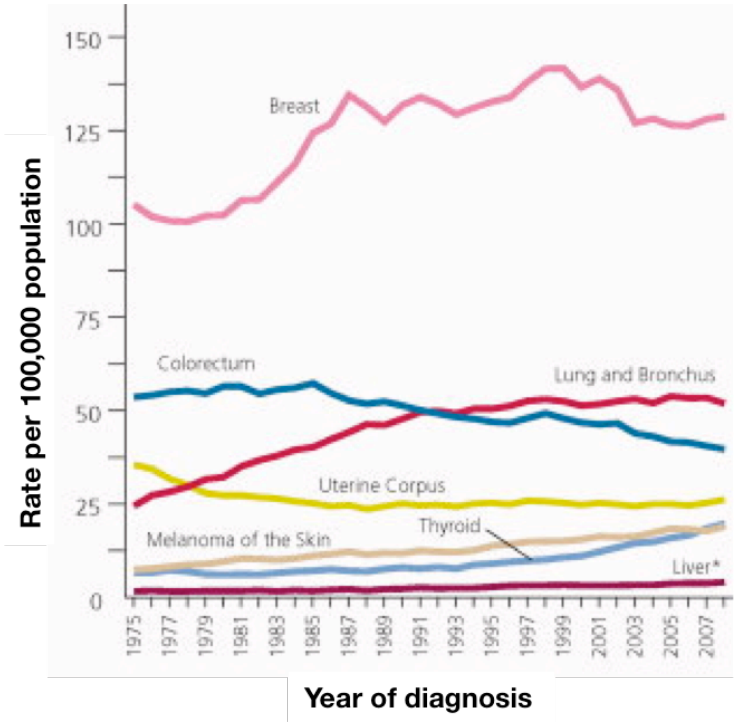

Figure 4 | Frequency of diagnosis of different cancer types in women in the US
Breast cancer was diagnosed most frequently within the observed period (1975-2008). Incidence rates of women from 1975 to 2008 are depicted. Rates are age-adjusted to the 2000 US standard population and adjusted for delays in reporting. Picture modified from Siegel et al. 2012.

Approximately 232,340 new cases of invasive breast cancer and 39,620 breast cancer deaths are expected to occur in the US in 2013. One in eight women is estimated to develop breast cancer in the US (and the western world) in her lifetime (Siegel et al. 2012). Nevertheless, due to improvement in therapy of breast cancer patients, nowadays lung cancer causes the highest number of cancer death in women in the US (Figure 5).

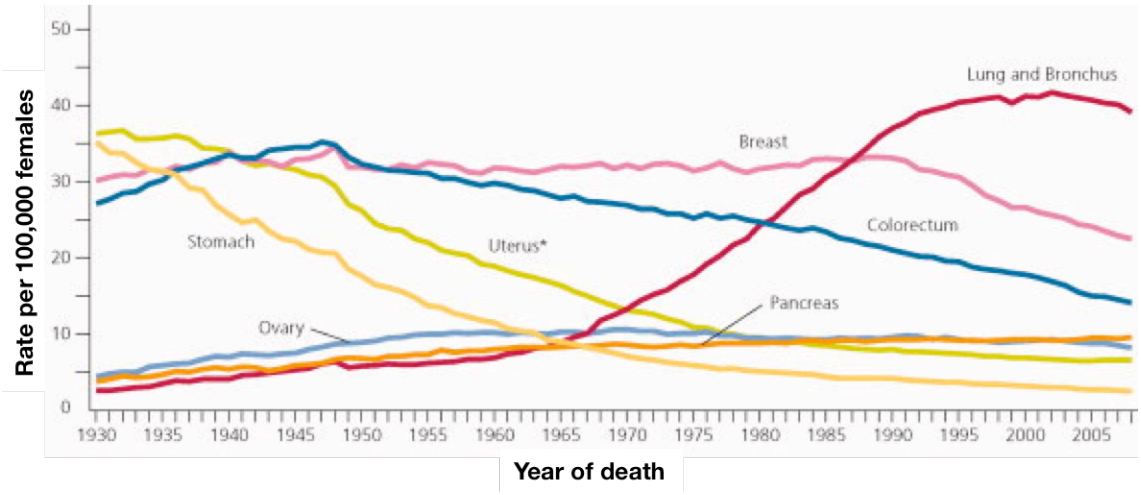

Figure 5 | Frequency of deaths caused by different cancer types in women in the US
From 1953-1985 breast cancer and from 1986-2008 lung cancer caused the highest number of cancer death among US women. Rates are age adjusted to the 2000 US standard population. Due to changes in International Classification of Diseases (ICD) coding, numerator information has changed over time. Rates for cancers of the uterus, ovary, lung and bronchus, and colorectum are affected by these changes. Picture modified from Siegel et al. 2012.

Well-known prognostic factors for breast cancer are expression of the estrogen receptor α (ER α), the progesterone receptor (PR), overexpression of the oncoprotein Her2 (human epidermal growth factor receptor 2), as well as the metastasis status of the lymph nodes (de Bock and Wang 2004). In 2007, in addition to the above-mentioned conventional markers, the American Society for Clinical Oncology (ASCO) and the German Arbeitsgemeinschaft Gynäkologische Onkologie (AGO) recommended urokinase plasminogen activator (uPA) and plasminogen activator inhibitor 1 (PAI-1) levels in tumor tissue as valuable prognostic factors (Harbeck et al. 2004).

In an analysis comprised of 18 different data sets with over 8,300 patients with primary breast cancer PAI-1 and uPA were the strongest prognostic factor for overall survival (OS) and disease-free (DF) (Look et al. 2002). This also holds true for the clinically relevant subgroup of the lymph node-negative (LNN) patients without adjuvant therapy. This is why today, in addition to the above-mentioned conventional markers, uPA and PAI-1 are highly recommended for assessment of the breast cancer status. uPA and PAI-1 allow optimization of breast cancer therapy by identifying patients with high (levels of uPA and/or PAI-1) or low (levels of uPA and PAI-1) risk of disease recurrence (Mengele et al. 2010; Schmitt et al. 2010). LNN patients with low uPA and PAI-1 levels

have a low recurrence risk and do not need to be over-treated by adjuvant chemotherapy. In contrast, in LNN patients with high uPA and PAI-1 levels the risk of relapse is high and systemic adjuvant chemotherapy is indicated (Harbeck et al. 2004).

3.4 - THE UROKINASE SYSTEM

The uPA-system, on one hand, is a key regulator in embryogenesis, inflammation and wound healing. On the other hand, it is involved in the development of cancer and metastasis formation, shown by the elevated expression of members of the uPA-system in a wide range of solid tumors. The uPA-system is involved in processes of cell migration and invasion of tissues. In order to promote migration and invasion, cells have to detach from their surrounding matrix. Detachment is initiated by focused degradation of the ECM by plasmin, a serine protease. Plasmin is the active form of plasminogen and triggers a proteolytic cascade. The uPA-system includes the ligand uPA, its cell membrane receptor (uPAR), the ECM protein vitronectin and the two main inhibitors PAI-1 and PAI-2. After binding of uPA to its cell surface receptor uPAR, plasminogen is efficiently activated at the cell surface resulting in high plasmin activity in the pericellular space (Figure 6) (Montuori et al. 2005; Ulisse et al. 2009; O'Halloran et al. 2013).

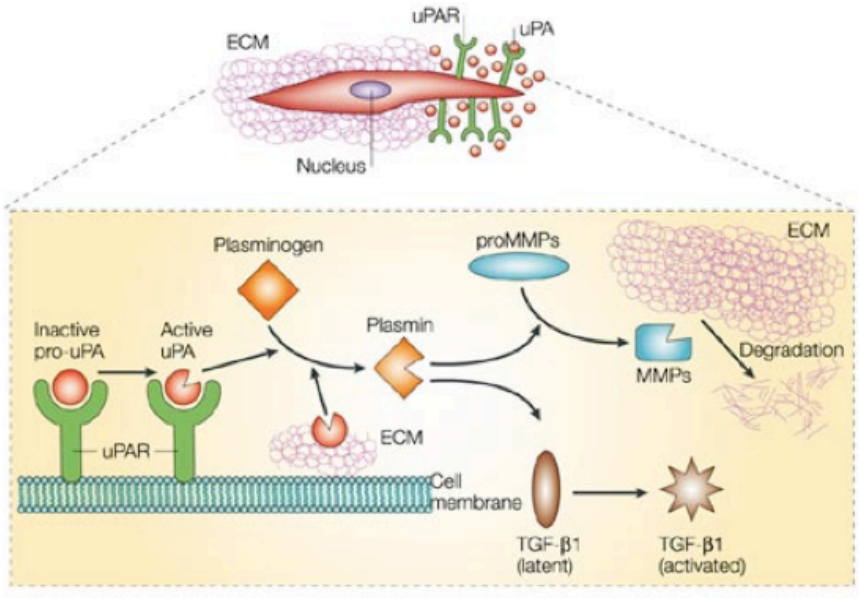

Figure 6 | Schematic representation of the uPA/uPAR system
At the leading edge of migrating cells, uPAR binds the inactive urokinase (pro-uPA), which then is converted to active uPA. Active uPA proteolytically activates plasminogen to active plasmin, which then breaks down ECM components and/or activates latent growth factors such as TGF-β1. Plasmin can also degrade the ECM indirectly through activation of pro-matrix metalloproteinases (MMPs) (Blasi et al. 2002).

Plasmin is a broad-spectrum serine protease, which can digest nearly all proteins in the ECM. Additionally, plasmin has several other functions: firstly, plasmin and uPA create a feedback loop where plasmin proteolytically activates pro-uPA to uPA and *vice versa*. Secondly, plasmin can activate distinct matrix metalloproteases (MMPs) such as MMP-3, MMP-9, MMP-12, and MMP-13, resulting in further degradation of the ECM. Thirdly, plasmin can also activate or release several cytokines and growth factors, for example TGF-β1 (Duffy and Duggan 2004). Hence, the uPA system regulates extracellular proteolysis as well as intracellular signaling by interacting with numerous receptors such as integrins and receptor tyrosine kinases (Figure 7).

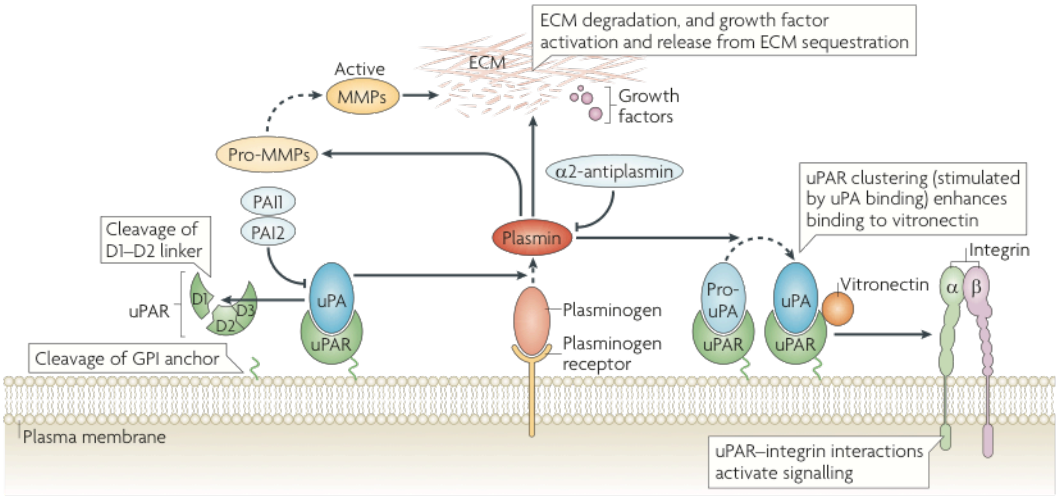

Figure 7 | Function and regulation of uPAR in the plasminogen activation system
uPAR can bind uPA in its active and inactive (zymogen) form. uPA cleaves plasminogen thereby generating the active protease plasmin. Plasmin in turn can activate pro-uPA. Plasmin cleaves and activates also MMPs. Both plasmin and MMPs degrade ECM components, activate growth factors or liberate them from the ECM.
The proteolytic activities of uPA and plasmin are antagonized by PAI-1 and PAI-2 as well as α_2-antiplasmin. uPA–uPAR binding promotes clustering of uPAR in the plasma membrane, in sphingolipid- and cholesterol-enriched domains (lipid rafts), and raise its ability to bind the ECM protein vitronectin. Complexes of uPAR and ligands interact with integrin co-receptors for intracellular signaling.
uPA also cleaves uPAR in the linker region between its first and second domain (D1 and D2), thereby generating a soluble fragment (D1) and a membrane-associated fragment (D2-D3). uPAR cleavage inactivates uPA binding to uPAR during proteolysis, and also inactivates or modifies the signaling functions of uPAR. Both full-length uPAR and D2–D3-uPAR can be shed through removal of the GPI anchor by proteases or phospholipases (Smith and Marshall 2010).

3.4.1 - The urokinase plasminogen activator (uPA)

uPA is a 53 kDa serine protease. Like almost all mammalian serine proteases, uPA is initially synthesized as a catalytically inactive single-chain polypeptide. Structurally, uPA can be divided into three main domains: an N-terminal growth factor domain, which contains the binding site for uPAR, a kringle domain, and a C-terminal sequence, which

catalyzes activation/cleavage of target proteins. Mature uPA is a two-chain protein linked by a disulfide bond between cysteine 148 and cysteine 279 (Duffy and Duggan 2004).

There are two physiologically active plasminogen activators, uPA and the tissue-type plasminogen activator (tPA). Migrating leading-edge keratinocytes express uPA and uPAR, whereas tPA has been detected only in a some keratinocytes late in the re-epithelialization of wounds in humans (Jögi et al. 2010). tPA is involved in the dissolution of fibrin rich blood clots (Blasi and Carmeliet, 2002). Of note, mainly tPA is not able to bind to uPAR.

The feedback loop in which uPA activates plasminogen to plasmin and then plasmin activating pro-uPA to uPA is regulated in two different ways: PAI-1 inhibits uPA while plasmin is inhibited by α_2-antiplasmin and α_2-macroglobulin (Figure 7) (Andreasen et al. 1997; Mengele et al. 2010; Smith and Marshall 2010).

3.4.2 - The plasminogen activator inhibitor 1 and 2 (PAI-1 and PAI-2)

Both PAI-1 and PAI-2 belong to the serpin (serine protease inhibitor) family of protease inhibitors, a super-family of proteins that fold into a conserved structure and employ a unique suicide substrate-like inhibition mechanism (Duffy and Duggan 2004). PAI-1 is a single-chain glycoprotein of 43 kDa and is thought to be the primary physiological inhibitor of the uPA protease activity. It reacts rapidly with uPA by forming a stable covalently bound complex with a 1:1 stoichiometry. Another important property of PAI-1 is its ability to induce the clathrin-mediated internalization of the ternary uPAR-uPA-PAI-1 complex. This complex associates with members of the low-density lipoprotein (LDL) family (mostly LDL receptor-related protein-1; LRP-1), which is secluded into clathrin-coated endosomes. The internalization of the trimetric complex can activate adhesion, migration, invasion, proliferation and survival (Mengele et al. 2010). After fusion of these endosomes with lysosomes, the covalently bound uPA/PAI-1 complex is degraded and uPAR itself is, at least partly, transported back to the cell surface (Czekay et al. 2001). PAI-1 can also attach to the ECM protein vitronectin and thus might modulate cellular adhesion and migration (Duffy and Duggan 2004). This behavior indicates that increased overall proteolytic activity can not be responsible for all pro-oncogenic effects, since also high expression levels of a proteolytic inhibitor like PAI-1 can have oncogenic effects (Binder and Mihlay 2008).

PAI-2 exists in two forms, a 47 kDa intracellular, non-glycosylated form and a 60-kDa secreted, glycosylated form. Both forms result from translation of the same mRNA and possess comparable anti-protease activity. PAI-2 acts in the same way as PAI-1 and also forms a 1:1 suicide complex with uPA. Although PAI-2 is an efficient inhibitor of uPA, it binds more slowly than PAI-1 (Duffy and Duggan 2004).

3.4.3 - THE UROKINASE RECEPTOR (UPAR / CD87)

uPAR, also known as CD87, is anchored to the extracellular surface of the cell membrane with a glycosylphosphatidylinositol (GPI) tail. The amino acid based molecular weight of the unmodified uPAR protein is 35 kDa, but as it is highly glycosylated, its actual molecular weight lies between 50-60 kDa (Ploug and Ellis 1994). uPAR is synthesized as a single chain polypeptide of 335 amino acids with 21 amino acids acting as signal peptide. This signal peptide is cleaved off in the lumen of the endoplasmatic reticulum, and the GPI anchor is attached. (Behrendt et al. 1991; Ploug et al. 1991; Montuori et al. 2005). The three structurally homologous domains each comprise about 90 amino acids and are numbered from the N-terminus of the protein. Part of exon 1 encodes most of the hydrophobic leader sequence, while the sequence necessary for GPI-anchor attachment is encoded by exon 7 (Figure 8) (de Bock and Wang 2004).

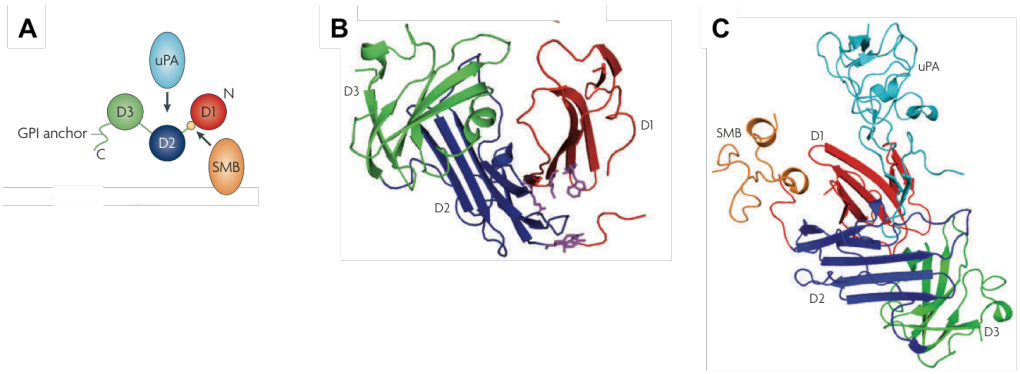

Figure 8 | Structure of uPAR
A: Systematic representation of uPAR including its GPI anchor. The three domains of uPAR are designated D1, D2 and D3. Arrows indicate the binding sites of uPA and the somatomedin B (SMB) domain of vitronectin, respectively. The SMB domain is a cysteine-rich N-terminal domain of vitronectin that interacts with uPAR and PAI-1. Interaction of SMB with both uPAR and PAI-1 is managed mainly *via* the same amino acid residues.
B: 3D structure of uPAR, with domains colored as in **A**. Residues of the vitronectin-binding site are shown in purple. The uPA-binding site is located in the central cavity formed by the concave arrangement of the three domains.
C: 3D structure of soluble uPAR bound to uPA and the SMB domain of vitronectin in a triple complex. uPAR domains are colored as in **A**. Images in **B** and **C** were created using the data of (Huai et al. 2008; Smith and Marshall 2010)

uPA and other proteases (trypsin, elastase, MMPs and plasmin) have the ability to cleave uPAR between D1 and D2. The resulting fragments of uPAR can no longer bind uPA and therefore cleavage disables all cell signaling functions as well as all proteolytic functions of the uPA-uPAR complex (Montuori et al. 2005). It has been hypothesized that proteases cleave uPAR and the truncated D2-D3-uPAR forms on the extracellular side of the membrane, soluble uPAR (suPAR) and soluble D2-D3-uPAR (c-suPAR) occur in the extracellular space (Smith and Marshall 2010). Phospholipases (C and D) can shed uPAR or cleaved c-suPAR from the plasma membrane by removing the GPI

anchor. suPAR can bind the same extracellular ligands uPA and vitronectin as the GPI-bound receptor. Therefore, suPAR can compete with membrane-bound uPAR for the binding of extracellular ligands, resulting in reduced cell surface-associated uPA activity and cell adhesion to vitronectin. suPAR has been detected in breast cancer patients and high levels of suPAR correlate with a poor prognosis (Smith and Marshall 2010). The crystal structure of suPAR is shown in Figure 8 B (Llinas et al. 2005). The domains generate a deep internal cavity and a large external surface (Tang and Wei 2008). uPAR binds uPA at its N-terminal domain in the central cavity (Figure 8 C). Binding involves residues from all three domains. The vitronectin binding site of uPAR is found in D1 and in the D1-D2 linker (Figure 8 A) (Madsen and Sidenius 2008; Smith and Marshall 2010).

3.4.4 - uPA-uPAR CELL SIGNALING

uPAR is unable to directly transduce signals on its own due to the lack of transmembrane and cytosolic domains (Tang and Wei 2008). It is generally believed that uPAR associates and activates transmembrane receptors on the cell surface. uPAR has been reported to associate with various proteins like integrins, receptor tyrosine kinases (*e.g.* EGFR) and G-protein coupled receptors (*e.g.* FPRL1), thus affecting cell proliferation, adhesion and migration . The direct interaction of uPAR with vitronectin has been mentioned to be involved in the induction of at least a part of the uPAR-induced cell signaling. This results in drastic changes in the morphology oft cells and so in increased cell motility (Cortese et al. 2008). As a GPI-anchored protein, uPAR is found in a specialized form of lipid rafts called lipid micro-domains. Lipid rafts partitioning of uPAR is associated with uPAR dimerization and binding to vitronectin. The activation of plasminogen by uPAR-bound uPA is independent of the lipid environment (Cortese et al. 2008). Lipid raft partitioning of uPAR is promoted by uPA binding, revealing another mechanism by which uPA can enhance uPAR binding to vitronectin. Accumulation in lipid rafts might increase protein–protein interactions between uPAR, its co-receptors and intracellular effectors, thereby enhancing downstream signaling. Signaling through uPAR and its interacting proteins has been demonstrated to activate the Ras-mitogen-activated protein kinase (MAPK) pathway, the tyrosine kinase focal adhesion kinase (FAK), Src and Rac proteins. The latter proteins are members of a subfamily of the Rho-family of GTPases (Blasi and Sidenius 2009).

Other pathways such as the janus kinase (JAK)-signal transducer and activator of transcription (STAT) as well as PI3K-Akt, have also been implicated in uPAR signaling (Smith and Marshall 2010).

In addition to its proteolytic properties, uPA also exerts several other important biological effects in a non-proteolytic manner. These functions are largely related to the regulation of the interactions between the cell and the surrounding matrix. Moreover,

uPAR signaling can be induced by uPA binding to uPAR, which is independent of the proteolytic activity of uPA (Smith and Marshall 2010).

3.4.5 - uPAR IN CANCER

In the healthy organism, uPAR is moderately expressed in various tissues (lungs, kidneys, uterus, spleen, vessels, bladder, thymus, liver, heart and testis). High uPAR expression is observed in organs undergoing major tissue remodeling, such as trophoblast cells and migrating keratinocytes at the edge of wounds (Blasi and Sidenius 2010). uPAR is expressed during ECM remodeling, *e.g.* in tissues during embryo implantation and placental development (Smith and Marshall 2010). The expression of uPAR is increased in many pathological conditions, like inflammation, infections and especially in cancer (Blasi et al. 2002). For instance, uPAR is overexpressed in kidneys during chronic proteinuric disease as well as in the central nervous system following trauma. uPAR expression is strongly induced during leukocyte activation and differentiation, suggesting a role in inflammatory and immune responses (Smith and Marshall 2010). uPAR is overexpressed in cancerous diseases of the breast, the lung, the bladder, the colon, the liver, the pleura, the pancreas, and the brain as well as in leukemia (Sidenius and Blasi 2003). High expression of uPAR is found particularly at the advancing fronts of invasive breast carcinoma and in those epithelial cells protruding into the stroma. The presence of uPAR on the invasive front of breast cancer cells suggests that uPAR is the decisive feature for the role of the uPA-system in cancer cell invasion (de Bock and Wang, 2004). Higher expression of uPAR has also been observed in tumor-associated macrophages and fibroblast at the invasive front (Smith and Marshall 2010). Moreover, suPAR, lacking the GPI-anchor, has been detected in conditioned medium of breast cancer cell lines and in the ascites fluid of ovarian cancer patients (Andreasen et al. 1997). Elevated expression of uPAR is linked with tumor progression and shortened disease-free and/or reduced overall survival of patients with malignant solid tumors (Schmitt et al. 1997). In normal breast tissue the expression of uPAR has been found to be either completely absent or at extremely low levels (Biermann et al. 2008). High levels of uPAR in breast cancer are also associated with unfavorable outcome. The prognostic impact of uPAR antigen determined in tumor tissue extracts, however, is less powerful than that of either uPA or PAI-1 (Kotzsch et al. 2008).

3.4.6 - uPAR mRNA VARIANTS

The human uPAR gene is located on the long arm of chromosome 19 (19q13). The wild-type uPAR gene is composed of seven exons and six introns comprising 21.67 kb. Exons 2/3, 4/5 and 6/7 encode domains D1, D2, and D3, respectively (Figure 9) (Ploug

et al. 1991). Transcription of different mRNA variants, from the same gene is a common observation for a growing number of proteins (Luther et al. 2003). These mRNA variants can result either from alternative splicing, sustained intronic sequences and utilization of alternative transcription initiation or polyadenylation sites. During tumor progression, alterations of the splicing process occur and therefore, alternative splicing may play an important role in tumorigenesis. For cancer-associated genes encoding proteins, such as CD44, WT-1, survivin, mdm2, MUC-1, and VEGF a broad spectrum of alternatively and/or aberrantly spliced mRNA variants with different and often oncogenic functions have been identified. In 1993, an uPA receptor was described where the exon 7 was exchanged for another final exon (Pyke et al. 1993). Alternatively spliced forms of human uPAR mRNA lacking exon 5 (uPAR-Δ5) were described by Casey et al. (1994). Luther et al. (2003) analyzed non-malignant and malignant human cells, as well as breast cancer tissue with respect to the expression of alternatively spliced uPAR mRNA variants. Two splice variants were detected with high frequency, an exon 5 deletion variant (uPAR-Δ5) and a variant lacking both exons 4 and 5 (uPAR-Δ4/5) (Figure 9). In Chinese hamster ovary (CHO) cells, lacking intrinsic uPAR-Δ4/5, the presence of both soluble and GPI-anchored uPAR-Δ4/5 protein was shown to be transcribed and secreted after stable transfection with a uPAR-Δ4/5 vector. The proteins were detected by Western blot analysis (Luther et al. 2003).

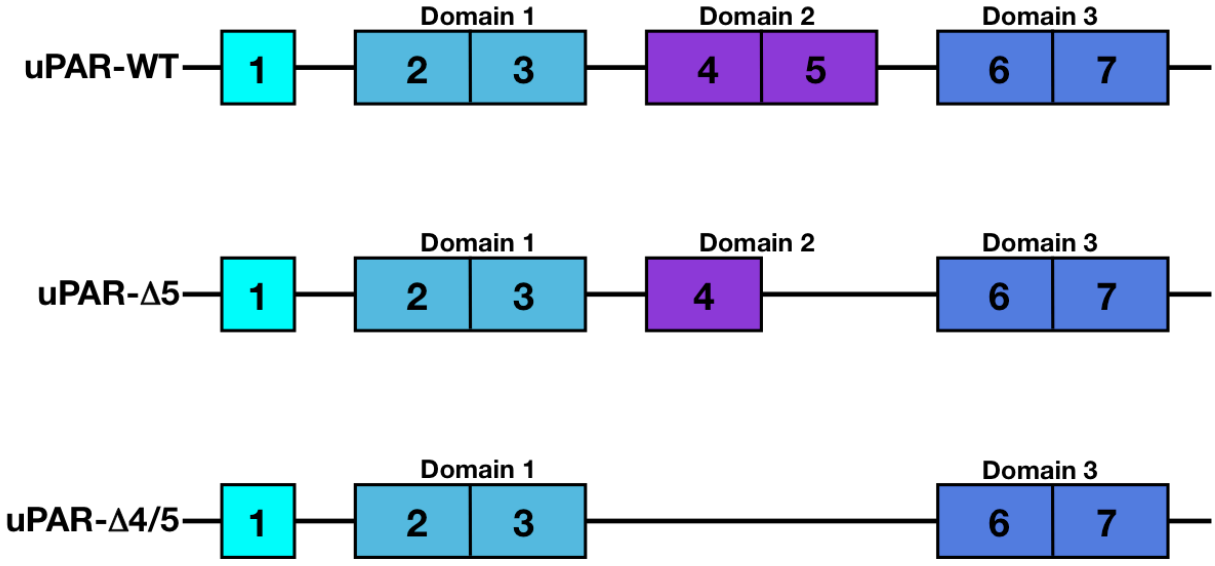

Figure 9 | Schematic representation of the mRNA of wild-type (WT) uPAR and two different splice variants
The uPA wild-type receptor is composed of three homologous domains (D1, D2 and D3), each encoded by 2 exons. The signal peptide is encoded by exon 1. The uPAR-Δ5 variant lacks exon 5. In the uPAR-Δ4/5 splice variant exon 4 and 5, encoding the complete domain 2 are absent (Luther et al. 2003).

Moreover, the uPAR-Δ4/5 mRNA is frequently present in cultured malignant human cells (breast, prostate, bladder) as well as in breast cancer tissue. In 2003, Luther et al. showed that high uPAR-Δ4/5 mRNA expression is correlated with a shorter disease-free survival (DFS) of breast cancer patients (Figure 10). This initial study included 43 node-negative and node-positive patients, treated with adjuvant systemic therapy.

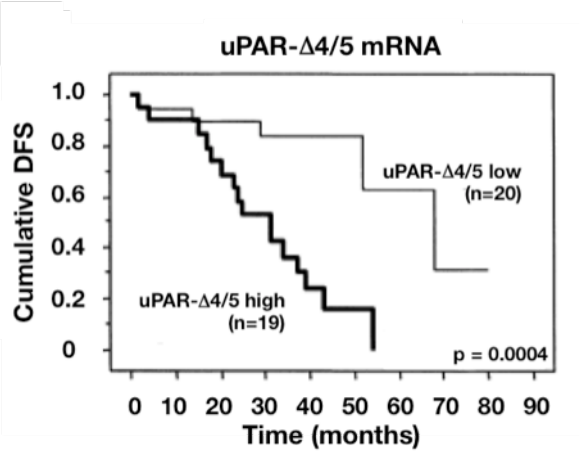

Figure 10 | Correlation of disease-free survival (DFS) and expression of uPAR-Δ4/5 mRNA in breast cancer patients
Kaplan Meier plot shows cumulative DFS of patients with low and high uPAR-Δ4/5 mRNA expression in tumor tissue. The graph shows that high uPAR-Δ4/5 mRNA levels are a significant marker for shorter DFS (Luther et al. 2003).

3.4.7 - uPAR-Δ4/5 AS A PROGNOSTIC MARKER

Correlation between expression of uPAR-Δ4/5 mRNA and survival was further analyzed in a study comprising 280 patients with lymph node-negative (LNN) breast cancer that did not receive systemic adjuvant therapy (Kotzsch et al. 2008) (Figure 11).

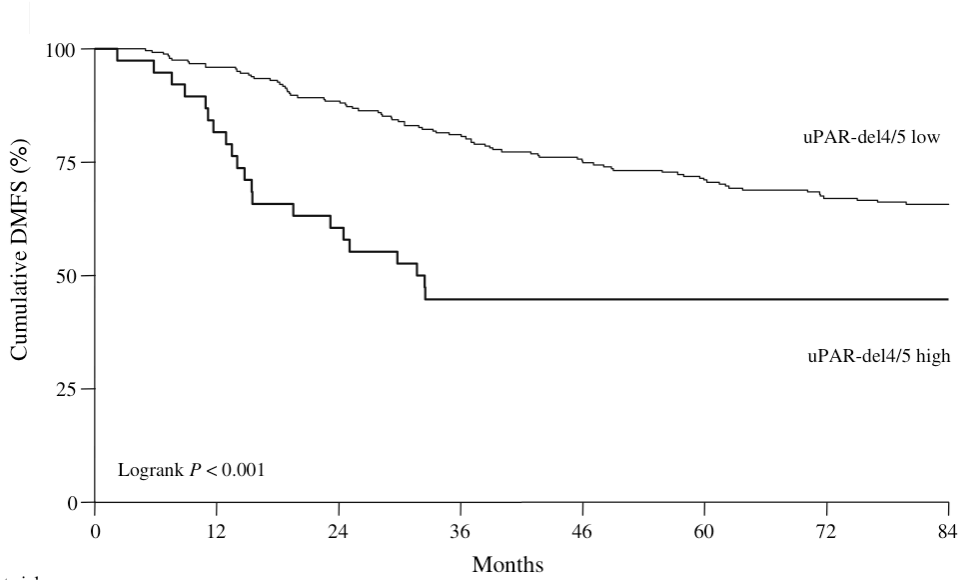

Figure 11 | Distant metastasis-free survival (DMFS) as a function of the of uPAR-Δ4/5 mRNA expression levels in lymph node-negative (LNN) breast cancer patients
The level of uPAR-Δ4/5 mRNA was measured by qPCR. In patients with low uPAR-Δ4/5 mRNA expression the DMFS was significantly longer than in patients with a high uPAR-Δ4/5 expression (Kotzsch et al. 2008).

The uPAR-Δ4/5 mRNA expression analysis revealed a significant shorter DMFS and overall survival (OS) (data not shown) of patients expressing uPAR-Δ4/5 at high levels (Figure 11). Furthermore, when the uPAR-Δ4/5 mRNA values were added to a base model encompassing age, menopausal status, tumor size, tumor grade, estrogen and progesteron receptor in a multivariate regression analysis, uPAR-Δ4/5 still contributed significantly to the base model, demonstrating that uPAR-Δ4/5 mRNA is an independent, pure prognostic factor in breast cancer.

In advanced ovarian cancer, however, it was recently shown that uPAR-Δ4/5 displays no prognostic relevance (Kotzsch et al. 2011).

To analyze potential tumor biological functions of uPAR-Δ4/5, Kotzsch et al. (2008) conducted microarray analyses of two different breast cancer cohorts. The aim was to identify other differentially expressed genes in breast cancer tissue with high *versus* low uPAR-Δ4/5 mRNA expression levels. The genes encoding proteins like dermatopontin, cadherin-11, homeobox B6, TIMP-3, tropomyosin-1, olfactomedin-like protein, and Rab31 turned up as promising candidates. For further analysis, Rab31 was selected since Rab proteins have been previously described to be involved in the progression of breast cancer in other respects (Kotzsch et al. 2008) (see also chapter 3.5.3).

Indeed, the analysis of the above-mentioned cohort of 280 LNN breast cancer patients for Rab31 mRNA expression levels revealed a significant relation between high Rab31 mRNA and an unfavorable outcome (Figure 12), similar to the relation of uPAR-Δ4/5 levels with prognosis.

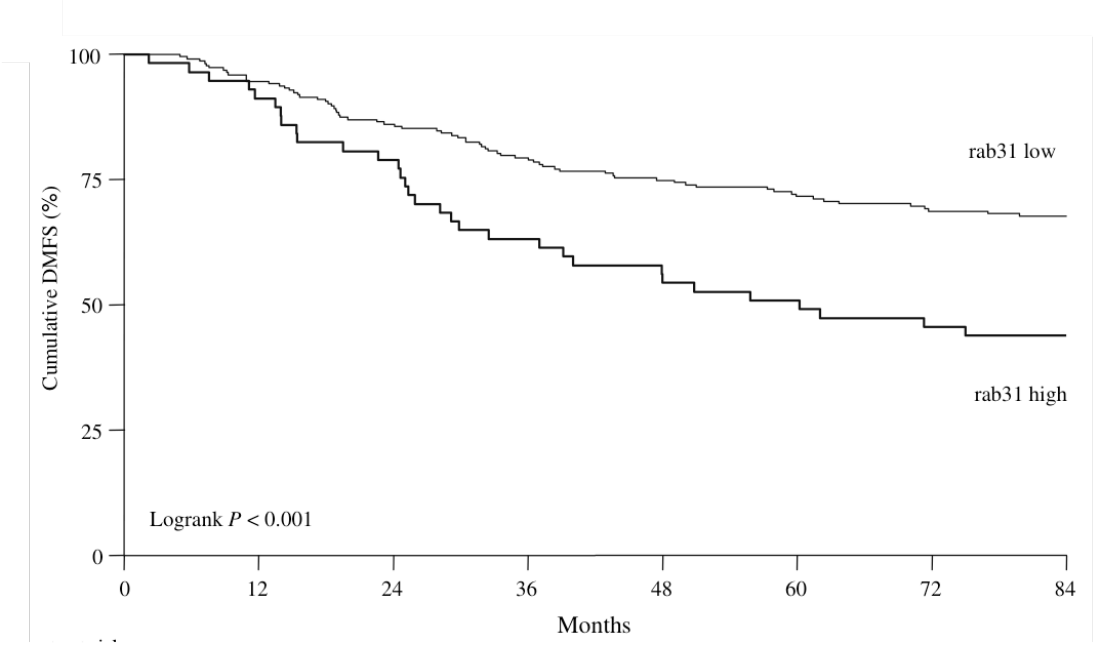

Figure 12 | Distant metastasis-free survival (DMFS) as a function of the Rab31 mRNA expression levels in lymph node-negative (LNN) breast cancer patients
The level of Rab31 mRNA was measured by qPCR. In patients with low Rab31 mRNA expression levels the DMFS was significantly longer than in patients with a high Rab31 expression (Kotzsch et al. 2008).

Importantly, Rab31 mRNA levels were shown to contribute significantly to a multivariate model, which included clinical and histomorphological parameters as well as uPAR-Δ4/5. Therefore, Rab31 can be considered as an independent prognostic marker for breast cancer (Kotzsch et al. 2008). Another study identified Rab31 and ten other genes that are overexpressed in ER-positive breast cancer patients (Abba et al. 2005). In advanced ovarian cancer however, it was demonstrated that Rab31 mRNA has no prognostic significance, similar to uPAR-Δ4/5 mRNA (Kotzsch et al. 2011).

Interestingly, DMFS and OS of breast cancer patients expressing both uPAR-Δ4/5 and Rab31 mRNA at high levels is shorter than all other sub-groups analyzed (Figure 13). Taken together, Rab31 and uPAR-Δ4/5 mRNA values have independent but additive pure prognostic relevance in LNN breast cancer patients (Kotzsch et al. 2008).

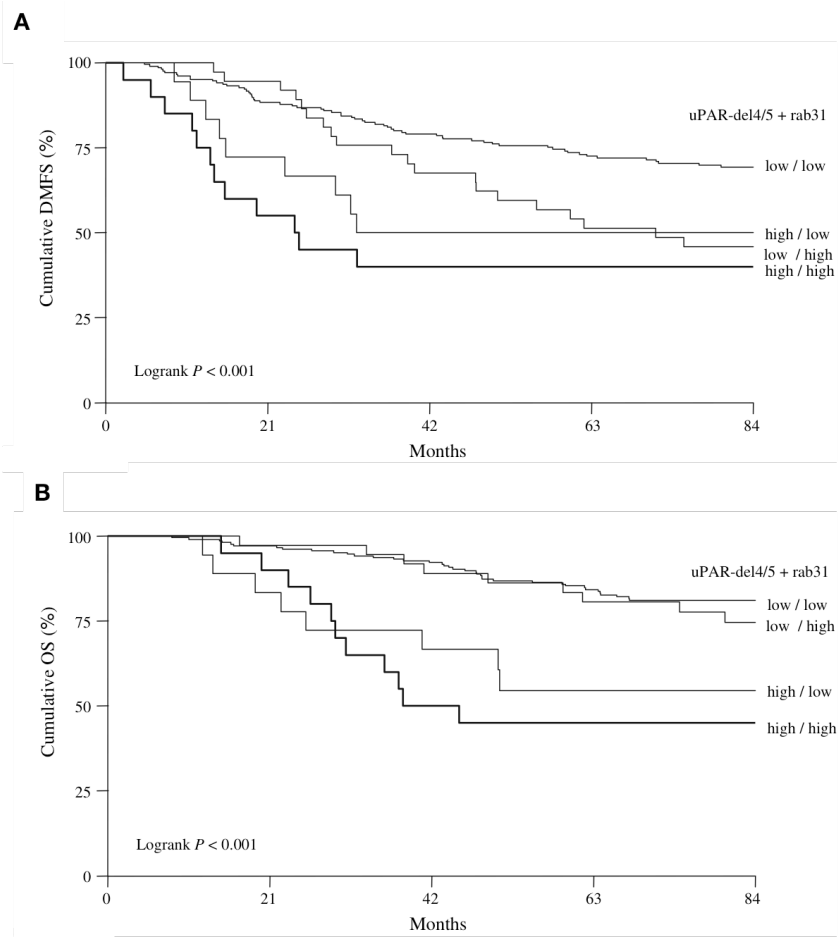

Figure 13 | Distant metastasis-free survival (DMFS) as a function of the of Rab31 and uPAR-Δ4/5 mRNA expression levels in lymph node-negative (LNN) breast cancer patients

A: Distant metastasis-free survival as a function of the combined mRNA expression of uPAR-Δ4/5 and Rab31. The subgroup of patients expressing uPAR-Δ4/5 and Rab31 at high levels show a significant shorter overall survival compared to patients expressing both mRNAs at low levels.

B: Overall survival as a function of the combined mRNA expression of uPAR-Δ4/5 and Rab31. The subgroup of patients expressing uPAR-Δ4/5 and Rab31 at high levels show a significant shorter overall survival compared to patients expressing both mRNAs at low levels (Kotzsch et al. 2008).

3.5 - RabGTPases

The Ras superfamily of small GTPases (20-25 kDa) includes the five different sub-family members Ras, Rab, Rho, Arf and Ran. Originally, Rabs were described as Ras-like proteins in the brain. The Rab family itself so far contains 70 putative human family members. Rab genes are located on different human chromosomes. Interestingly, Rab GTPases have been found in all eukaryotes investigated, e.g., *C. elegans* (29 members), *D. melanogaster* (26 members), and *S. cerevisiae* (11 members) (Stenmark and Olkkonen 2001).

Their large number and the wide distribution of Rab GTPases suggest a key role in cell metabolism. Rab GTPases have been shown to complement the yeast homologs demonstrating conservation of functions of these enzymes within eukaryotes (Stenmark and Olkkonen 2001). Rab GTPases are characterized by conserved GTP binding sites and variable C-termini, thus specifically controlling downstream effector interactions. Overall, the Rab GTPases regulate various steps of dynamic assembly and disassembly of multi-protein scaffolds, which are involved in vesicular traffic in both endocytic and secretory pathways. Moreover, Rab GTPases regulate endocytosis, recycling and degradation as well as exocytosis of cellular components, thus regulating overall tissue homeostasis (Mitra et al. 2011). Regulatory GTPases are inactive in the GDP-bound form and active in the GTP-bound form. Guanine exchange factors (GEFs) catalyze the exchange of GDP and GTP, since the spontaneous rate of GDP release is extremely slow. Another characteristic of Ras superfamily GTPases is their slow intrinsic rate of GTP hydrolysis. Therefore, hydrolysis of GTP is stimulated by a GTPase activating protein (GAP) (Itzen and Goody 2011) (Figure 14). Due to the high cytosolic concentration of GTP (~1 mM) a new molecule of GTP binds as soon as GDP is released (Stenmark 2009). At some point after hydrolysis, GDP-bound Rab re-forms the complex with Rab-GDI and dissociates from membranes to enter a recycling process (Kajiho et al. 2011). After *de novo* synthesis of Rab by cytosolic ribosomes the GDP-bound Rab is presented to a geranylgeranyl transferase (GGT) by the Rab escort protein (REP). GGT mediates prenylation of Rab-GDP by addition of the isoprenoid geranylgeranyl at C-terminal cysteine residues. Rab GTPases have a variety of different cysteine motifs (XCCXX, XXCCX, XXXCC, CCXXX, XXCXC and XCXXX; X represents any amino acid), all occurring with one or two highly hydrophobic geranylgeranyl groups (Stenmark and Olkkonen 2001, Itzen and Goody 2011). GDP dissociation inhibitor (GDI) binds to prenylated GDP-Rab by masking its isoprenyl anchor and, thereby, maintaining the Rab protein in the cytosol. Membrane attachment of Rab proteins requires the function of a GDI displacement factor (GDF). Moreover, REP is required to release the GDI from Rab molecules in a way that Rab31-GDP can be delivered to specific membranes (Figure 14). Once dissociated from GDI and associated with membranes the exchange of GDP for GTP is catalyzed by GEF (Mitra et al. 2011).

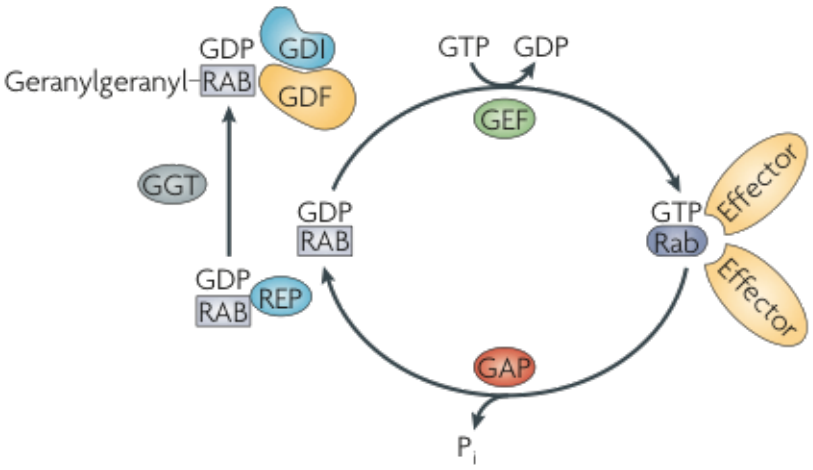

Figure 14 | The Rab switch and its circuitry
Conversion of Rab from the GDP-bound (inactive) into the GTP-bound (active) form is catalyzed by a guanine nucleotide exchange factor (GEF). Active Rab is recognized by numerous effector proteins. The hydrolysis of GTP is accelerated by GTPase-activating protein (GAP) and Rab is converted back to the inactive form. Newly synthesized Rab is in the inactive state and . is recognized by a Rab escort protein (REP) and presents the Rab to a geranylgeranyl transferase (GGT). GTT prenylates Rab at the carboxy-terminal cysteine residues once or twice. The geranylgeranylated, inactive Rab is recognized by Rab GDP dissociation inhibitor (GDI), which regulates the activation cycle of the Rab at the memabrane. The direction of the Rab–GDI complex to specific membranes is mediated by interaction with a membrane-bound GDI displacement factor (GDF) (Stenmark 2009).

3.5.1 - Structure of Rab proteins

The principle structure of the Rab31 protein is common to all small GTPases of the Ras superfamily. The fold consists of six β-sheets, comprising of five parallel strands and one antiparallel strand, surrounded by five α-helices. The binding sites for guanine nucleotides and Mg^{2+} as well as the active center are made up of the five loops (G1-G5) that connect the α-helices and β-strands (Figure 15). The G1 loop is conserved in many ATPases and some nucleoside/nucleotide kinases. The loops G2 and G3 are located in the so-called switch I and switch II regions respectively. The loops G4 and G5 specifically interact with the guanine base, thus, excluding other nucleotides such as ATP from hydrolysis (Itzen and Goody 2011). The amino acid residues that form this active site are closely associated with either the phosphate groups of the bound nucleotide and Mg^{2+} or the guanine base and are highly conserved within the entire Ras superfamily (Stenmark and Olkkonen 2001).

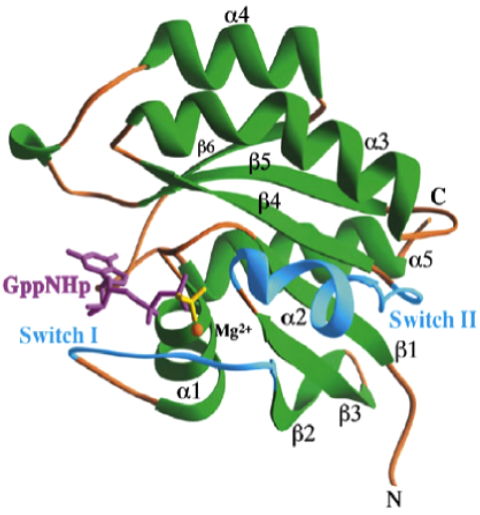

Figure 15 | Structural features of Rab GTPases
Ribbon drawing of Rab3A complexed with the GTP analog GppNHp. The bound nucleotide (purple) interacts with the Mg^{2+}-ion (orange sphere). Switch I and II regions are depicted in blue, the α-helices and β-sheets in green and loops in orange (Stenmark and Olkkonen 2001).

During GDP release the nucleotide-binding site is opened by conformational change of the switch I and switch II regions, resulting in interruption of important interactions between of the Rab GTPase. The GEF appears to get in contact with the switch II region, switch I is also involved in most cases (Itzen and Goody 2011). Sequence analysis studies have revealed the presence of five distinct amino acid stretches, called RabF regions, that are characteristic of the Rab GTPases. The RabF stretches assemble in the vicinity of switch I and II regions and are suggested to provide a means of clearly identifying Rab proteins. In addition, four regions (RabSF regions) have been identified that can be used to define different subfamilies of Rab GTPases (Stenmark and Olkkonen 2001). The C-terminus of Rab GTPases is a hypervariable region, which has been implicated, in subcellular targeting of these proteins (Hutagalung and Novik 2011).

3.5.2 - RAB GTPASES IN MEMBRANE TRAFFICKING

The compartmentalization of eukaryotic cells into distinct organelles enables them to perform diverse functions in parallel. With this complexity the need arises for a cellular machinery to actively transport materials between compartments. Membrane traffic events are highly dynamic, involving continuous recycling of regulatory proteins between the cytosol and membranes, and the fusion and transport of membrane-bound carriers between organelles. This complex membrane traffic requires different classes of molecules for regulation. One key set of proteins well established in membrane traffic regulation is the Rab family of small GTPases (Singan et al. 2012).

Vesicle formation is mediated by Rab GTPases, which leads to movement and membrane fusion along with actin and tubulin. Several Rabs are found in the endoplasmic reticulum (ER) and facilitate transport from ER to Golgi. Some Rabs are localized in endosomes, clathrin-coated vesicles, membrane ruffles, plasma membranes, as well as secretory granules. These Rabs have a broad variety of functions e.g. trafficking between Golgi and endosomes, the assembly of adherent junctions, phagocytosis, mitochondrial dynamics, trafficking of sonic hedgehog signaling components, and neuroendocrine secretion. The strictly regulated trafficking of all kinds of vesicles to the cell surface is fundamental for all cells. Rab GTPases, with the help of their effectors, ensure the regulation of vesicle trafficking in timely and specially manner throw-out the cell. This strict regulation of membrane trafficking is important for the respective identity of each membrane. The importance of Rabs is further underlined by the increasing number of diseases attributed to Rab protein dysfunction (Corbeel and Freson 2008; Stenmark 2009; Subramani and Alahari 2010; Mitra et al. 2011; Singan et al. 2012).

Rabs participate in receptor/cargo collection and sorting (Figure 16 A) and can trigger uncoating of transport vesicles (Figure 16 B). During transport Rabs facillitate motor proteins to cooperate with membranes to drive vesicle motility (Figure 16 C). Mediating the complex events of proper docking (Figure 16 D) and fusion of transport vesicles with their targets (Figure 16 E) is also accomplished by Rabs (Zerial and McBride 2001).

Membrane-bound GDI displacement factors have the vital function of recognizing the specific Rab-GDI-complexes and facilitating GDI release. This release helps in the association between Rab GTPases and appropriate membranes. GDI extracts GDP-bound Rab from the membrane back into the cytosol and, thereby, allows the process to re-initiate (Mitra et al. 2011).

Several Rabs have also been implicated in the progression of several types of cancer. Primarily, Rab proteins are involved in the loss of cell polarity and in the metastatic transformation of tumor cells. This includes various human cancers, e.g. up-regulation of Rab5 in malignant and metastatic lung cell adenocarcinoma, of Rab3 in cancers of the nervous system, and of Rab1 in tongue squamous cell carcinomas (Hutagalung and Novik 2011). Rab8 mediates exocytosis of a matrix metalloprotease that is knownt to be important for cell invasion. Another example is Rab23, which is in charge of sonic hedgehog signaling, has also been implicated in carcinogenesis. Loss of Rab21, which controls the endocytic trafficking of integrins, has been found to correlate with aneuploidy in cancer. This correlation is thought to reflect the need of Rab21-mediated integrin endocytosis for correct cytokinesis (Stenmark 2009). Rab20 is expressed in multiple organs and assumes a polarized localization in certain cells. It was found to be upregulated in pancreatic tumor cell lines, primary pancreatic carcinoma samples, as well as in pre-neoplastic pancreatic intraductal neoplasia lesions (Chia and Tang 2009).

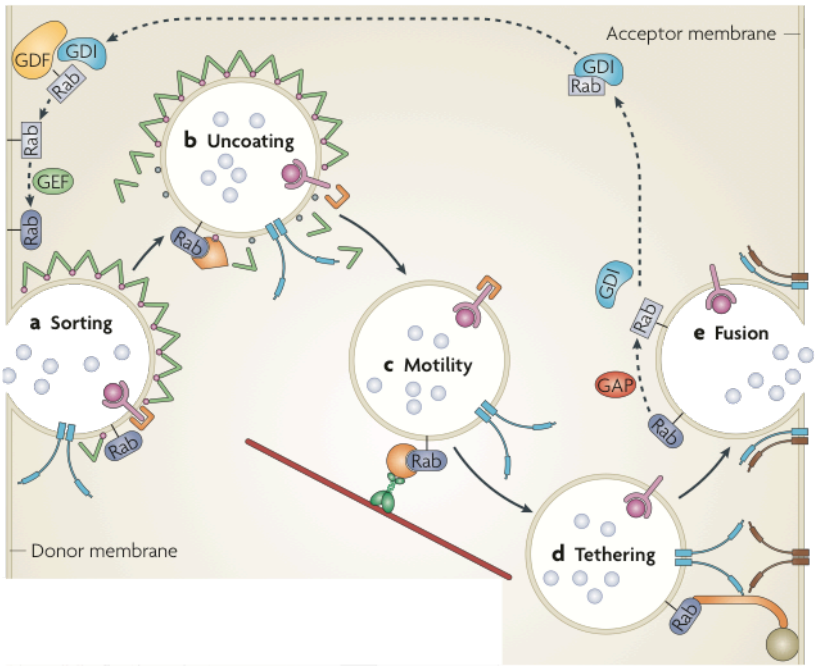

Figure 16 | Vesicle trafficking and the Rab GTPase functions in it
The steps in memabrane trafficking that can be controlled by Rab proteins and its effectors (orange).
a: Active Rab at a budding vesicle can manage that sorting proteins pack a certain receptor into it.
b: Through Rab different Rab effectors alter the the outer configuration of a transport vesicle and thereby uncoating through dissociation of coating proteins can occur.
c: Rab can mediate vesicle transport along a cytoskeletal tracks by recruiting motor adaptors or by binding directly to motor proteins.
d: Rab is able to facilitate vesicle tethering by recruiting tethering factors.
e: When the tethering factors interact with their counterparts the vesicle can fuse with the acceptor membrane.
Following membrane fusion and exocytosis of the carco, the Rab is hydorlysed to its inactive GDP-bound form due to the ,accelerated by a GAP. Inactive Rab is recycled back to the donor membrane by GDI. Rab is released from GDI by GDF and the cycle can start again (Stenmark 2009).

The best-characterized example of a Rab implicated in cancer is Rab25. Rab25 is closely related to Rab11, which regulates apical endocytosis and transcytosis in epithelial cells. The expression of Rab25 is increased in ovarian and breast cancers due to amplification of a chromosomal region in which the Rab25 gene resides. The resulting overexpression is associated with tumor metastasis and a lower patient survival rate (Hutagalung and Novik 2011). Rab25 expression increases the proliferation rate and severity of breast and ovarian cancer cells by rising Akt-phosphorylation, which in turn activates the phosphoinositide-3-kinase (PI3K) pathway. Rab25 expression is increased in prostate cancer as well as in transitional cell carcinoma of the bladder. Moreover, Rab25 has been shown to prevent cell death by down-regulation of the pro-apoptotic genes BAX and BAK (Cheng et al. 2005; Subramani and Alahari 2010). Accordingly, overexpression of Rab25 in cell culture, stimulates proliferation and inhibits apoptosis. The concrete mechanisms that determine the

effects of Rab25 with regards to proliferation and apoptosis are still unclear, it is speculated that they are caused by atypical recycling of signaling receptors, given the established role of Rab25 in trafficking by recycling endosomes. In addition, Rab25 is one of the few examples of a Rab directly found to interact with the transmembrane protein β1-integrin. The ability of Rab25 to control recycling of the fibronectin receptor α5β1 integrin, thereby, facilitating invasive cell migration, is also consistent with its pro-tumorigenic role in cancer (Stenmark 2009).

3.6 - RAB31

After the initial cloning of Rab31 from human melanocytes (Chen et al. 1996), a wild-type Rab31 BLAST search revealed 71 % identity with canine Rab22A. Another protein cloned from human melanocytes that was almost identical to Rab31 was named Rab22B (Bao et al. 2002). In 2001, Rodriguez-Gabin et al. identified a sequence expressed in rat oligodendrocytes with a high identity to human Rab31 (hRab31). It was designated rRab22B. A comparison of the rRab22B with the hRab31 DNA sequence showed 88 % identity and the predicted amino acid sequence had 94 % identity. These results show that rRab22B encodes the rat homolog of hRab31 (Figure 17).

Rab31, Rab21 and Rab22A are members of the Rab5-subfamily, which are all involved in the trafficking of early endosomes. Mechanisms controlling the activation of the Rab5 subfamily members remain unclear so far (Kajiho et al. 2011). Rab31 is a 194 amino acid protein (21.6 kDa) that was mapped to chromosome 18 (18p11.3) (Chen et al. 1996). It is expressed fairly ubiquitously in human tissue and is mainly localized at the trans-Golgi, the trans-Golgi network (TGN) and in endosomes. Rab31 is involved in vesicle transport from the Golgi apparatus to early and late endosomes, *e.g.* of mannose-phosphate receptors (Rodriguez-Gabin et al. 2009).

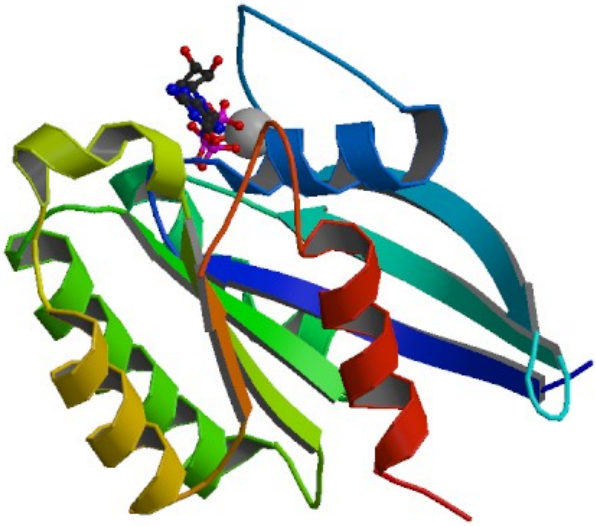

Figure 17 | Crystal structure of human Rab31 GTPase in complex with a GTP analogue
Ribbon drawing of Rab31 complexed with GTP analogue GppNHp (Park H. et al. unpublished). Picture taken from http://www.thesgc.org/structures/2fg5

3.6.1 - RAB31 FUNTIONS AND INTERACTION PARTNERS

In 2001, Rodriguez-Gabin et al. showed that Rab31 is present in small tubulo vesicular organelles trafficking from the trans Golgi/TGN to endosomes, and that the formation of these vesicles is regulated by Rab31. Moreover, the authors suggested that Rab31 controls the transport of the vesicles. In 2009, Rodriguez-Gabin et al. showed that Rab31 is part of the molecular mechanisms that regulate the transport of mannose 6-phosphate receptors (M-6-PR) from the TGN to endosomes. Furthermore, Rab31 is also involved in the formation of the vesicles at the TNG. Another function of Rab31 is the maintenance of the Golgi and the TGN. Interaction between rRab31 and OCRL-1 (oculocerebrorenal syndrome of Lowe 1) was demonstrated by Rodriguez-Gabin et al. (2010). Using oligodendrocyte lysates, a yeast two-hybrid system was applied with a GST-Rab31 bait. Pull-down experiments and co-immunoprecipitation found a direct Rab31 and OCRL-1 interaction. OCRL-1 is a phosphatidylinositol 4,5-diphosphate 5 (PI(4,5)$P_2$5)-phosphatase that regulates the levels of PI(4,5)P_2 and PI(4)P both signaling molecules are involved in Golgi/TGN organization and membrane trafficking. Furthermore, co-localization of ORCL-1 and Rab31 the TGN and endosomes was shown in HeLa cells as well as the correlation between ORCL-1 containing carriers containing M-6-PR (Rodriguez-Gabin et al. 2010).

Activation of Rabs is mediated by GEFs, which promote the exchange of bound GDP for GTP. Interaction of Rab5 subfamily members (Rab31, Rab21 and Rab22A) with GEF is mediated *via* a Vps9 domain. Lodhi et al. (2007) showed that Gapex-5 (also known as GAPVD1; GTPase activating protein and VPS9 domain 1), which contains a N-terminal Ras-GAP domain and a C-terminal Vps9 domain, could directly interact with Rab31 by

using pull-down assays with a GST-tagged Vps9 domain in Cos-1 cells overexpressing Rab31. The authors also showed that the GEF EEA1 (early endosome antigen 1) can interact with Rab31, with both its Vps9 domains (Lodhi et al. 2007).

In 2011, Kajiho et al. showed that RIN3 (Ras and Rab interactor 3) acts physiologically as a GEF to activate Rab31-dependent transport of M-6-PR between the TGN and early endosomes. This study also showed that all three RIN (Ras and Rab interactor) family members as well as ALS2 (amyotrophic lateral sclerosis 2) and ALS2CL (amyotrophic lateral sclerosis 2 C-terminal like) and Rabex5 (also known as RabGEF1; RAB guanine exchange factor 1) are capable of acting as GEFs for Rab31.

Another function of Rab31 was found by Ng et al. (2009). The authors showed that in addition to the M-6-PR transport, Rab31 plays a role in the regulation of epidermal growth factor receptor (EGFR) trafficking. This was demonstrated by affinity pull-down assays and co-immunoprecipitation analysis in A431 astroglia epidermiod carcinoma cells. Moreover, Rab31 was shown to associate with EGFR in a GTP-dependent manner and modulates internalization of EGFR.

Another protein interacting with Rab31 is the mRNA-binding protein HuR (also known as ELAVL 1; embryonic lethal abnormal vision like RNA binding protein 1). HuR is a ubiquitously expressed RNA-binding protein, which modulates gene expression at the transcriptional and posttranscriptional level. It is predominantly found in the nucleus, but can shuttle to the cytoplasm. Cytoplasmic HuR can stabilize target mRNA transcripts, which often encode proteins involved in carcinogenesis. In breast cancer, it is known that high HuR expression correlates with reduced survival of the patients (Heinonen et al. 2005; Heinonen et al. 2007). In MCF7 and 184B5Me cells HuR was found to directly bind to Rab31 mRNA, thus, stabilizing it (Heinonen et al. 2011).

MUC1-C (mucin 1-C) forms a complex with the estrogen receptor α (ERα) on the Rab31 promoter, which activates Rab31 transcription. Thus, Rab31 assists the up-regulation of MUC1-C in breast cancer cells by toning down the degradation of MUC1-C in lysosomes forming an auto-inductive loop. Analysis of databases from microarrays showed that Rab31 is expressed at higher levels in breast cancers as compared to normal, healthy breast tissues. Also, $MUC1^+$ and ER^+ breast cancers are characterized by increased levels of Rab31 expression. Moreover, the ten-year overall survival of patients with Rab31-positive breast tumors is significantly decreased compared to those with Rab31-negative tumors (Jin et al. 2012).

In initial experiments, we showed that overexpression of Rab31 is associated with enhanced proliferation of MDA-MB-231 and CAMA-1 breast cancer cells in a dose-dependent manner. In contrast, increased expression of Rab31 in these cells lines leads to reduced adhesion towards several ECM proteins and decreased invasive capacity through Matrigel also in a dose-dependent manner. Moreover, Rab31-overexpressing MDA-MB-231 breast cancer cells have been shown to be strongly

debilitated at metastatic dissemination to the lung in a xenograft invasion mouse model (Grismayer et al. 2012b).

4 - AIM OF THE THESIS

Aim of the thesis was to further explore (I) the tumor biological role of the small GTPase Rab31 in breast cancer cells compared with the effect of various mutants of Rab31 or Rab31 knock-down and (II) to assess the biological effects of co-overexpression of Rab31 with the urokinase receptor splice variant uPAR-Δ4/5 in these cells.

The following topics were investigated in detail:

1) High levels of uPAR-Δ4/5 or Rab31 mRNA in tumor tissue of breast cancer patients are significantly associated with shorter distant metastasis-free survival and overall survival. Such poor prognosis is reflected experimentally by overexpression of uPAR-Δ4/5 or Rab31 in breast cancer cell lines, which strongly affects tumor biologically important processes such as cell proliferation and/or adhesion. This raises the question whether simultaneous overexpression of uPAR-Δ4/5 and Rab31 in breast cancer cells would lead to an additive or synergistic effect on these tumor biologically relevant processes.

2) Previous data indicate that Rab31 may act as a molecular switch to allow breast cancer cells to convert from an invasive to a proliferative state, associated with increased cell proliferation in Rab31-overexpressing over vector control cells. Can this effect be reversed in breast cancer cells by knock-down of Rab31 mRNA expression employing the siRNA/shRNA technology?

3) Does overexpression of selected Rab31 variants (constitutively active, constitutively inactive, not membrane-associated) display similar effects as wild-type Rab31 overexpression on breast cancer cell proliferation, adhesion and invasion?

4) Does overexpression of wild-type Rab31 affect gene expression of other tumor-associated factors? Differential mRNA expression of candidate genes, initially identified by use of low-density microarrays, should subsequently be confirmed by independent quantitative PCR analyses and, if appropriate, also on the protein expression and activity levels, *e.g.* by Western blot analysis and cell-based activity assays.

5 - METHODS AND MATERIALS

5.1 - MOLECULAR CLONING

5.1.1 - DESIGN OF OLIGONUCLEOTIDES FOR SITE DIRECTED MUTAGENESIS

The mutagenic oligonucleotide primers used in this protocol were designed individually according to the desired mutation and based on the following considerations: (QuikChange site-directed mutagenesis kit manual; Agilent).

- Both of the mutagenic primers must contain the wanted mutation on both strands of the plasmid. Design the 3´-5´ primer, the 5´-3´ primer is then corresponding.
- Primers should be between 25 and 45 bases in length, with a melting temperature (T_m) of ≥78°C. Primers longer than 45 bases may be used, however the use of such primers increases the formation of secondary structures, which may affect the efficiency of mutagenesis

  The following formula was used for the estimation of primer T_m :

  $T_m = 81.5 + 0.41*(\%\ GC) - 675/N - \%$ mismatch

  N: primer length in bases; values for % GC and % mismatch are whole numbers.

  For T_m calculations of mutagenesis primers, a modified version of the above formula was used:

  $T_m = 81.5 + 0.41*(\%GC) - 675/N$

  N: primer length in bases except for inserted or deleted bases.
- The desired mutation (deletion or insertion) should be in the middle of the primer with ~10-15 bases of correct sequence on both sides.
- The primers should optimally have a minimum GC content of 40% and should terminate in one or more C or G bases (QuikChange site-directed mutagenesis kit manual; Agilent).

To identify the newly generated Rab31-Q64L mutant a new restriction site (*Stu* I) was introduced without changing the amino acid sequence in that particular part (Figure 18).

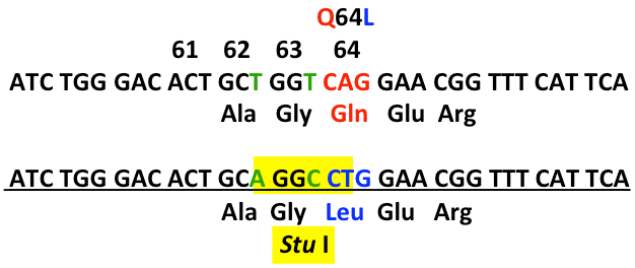

Figure 18 | Design of the primers used for the generation of the Rab31-Q64L mutant
The upper sequence shows part of the wild-type Rab31 cDNA nucleotide sequence with codon numbers and the amino acid sequence. The lower sequence depicts the newly designed mutated Rab31-Q64L site including the new *Stu* I restriction site (yellow). The amino acid sequence was mutated at codon number 64 from a glutamine to a leucine (red and blue). Nucleotides denoted in green letters were exchanged to generate a new *Stu* I restriction site without introducing further amino acid alterations. The underlined sequence represents the primer used in the PCR reaction.

In the case of the Rab31-S19N mutation a new *Pvu* I restriction site was created without changing the amino acid sequence. The Rab31-S19N mutant can be easily distinguished from the wild-type vector by restriction enzyme analysis (Figure 19).

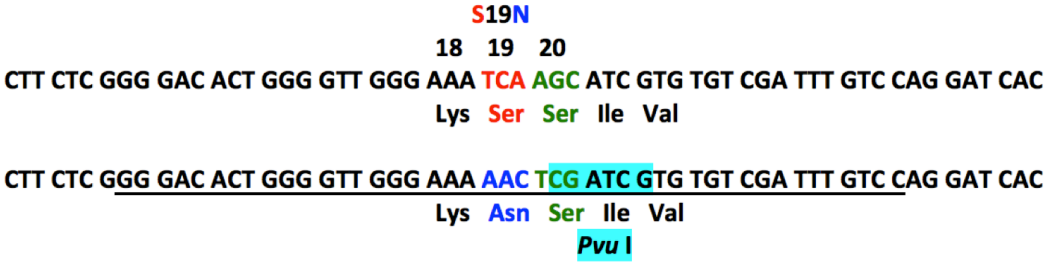

Figure 19 | Design of the primers used for the generation of the Rab31-S19N mutant
The upper sequence shows part of the Rab31 cDNA with codon numbers, and the amino acid sequence. The lower sequence depicts the newly designed mutated Rab31-S19N cDNA including the new *Pvu* I restriction site (light blue). The amino acid sequence was mutated at codon number 19 from serine to asparagine (red and blue). The green depicted nucleotides were changed to generate the new *Pvu* I restriction site without changing the amino acid sequence. The underlined sequence represents the primer used in the PCR reaction.

For the generation of the Rab31-ΔCC mutant a different approach was chosen. The *Xba* I restriction site from the Rab31 cDNA sequence was cloned, deleted and changed into a new stop codon. Thus the mutated sequence can be easily distinguished from the non-mutated sequence by restriction enzyme analysis (Figure 20).

Figure 20 | Design of the primers used for the generation of the Rab31-ΔCC mutant
The upper sequence shows part of the Rab31 cDNA nucleotide sequence including its corresponding amino acid sequence. The highlighted *Xba* I (green) restriction site was deleted as well as four codons. The lower sequence depicts the newly designed Rab31-ΔCC mutant with the generated stop codon (blue). The underlined sequence represents the primer used in the PCR reaction.

All mutant Rab31 constructs were generated by site-directed mutagenesis as described in chapter 5.1.2.

5.1.2 - Site-Directed Mutagenesis

The QuikChange *in vitro* site-directed mutagenesis kit (Agilent) allows for a site-specific mutation in a double-stranded plasmid DNA. The concept of site-directed mutagenesis is to replicate the plasmid DNA *via* PCR using primers carrying the desired mutation so that all replicated plasmids carry this mutation (Figure 21). The nicks in the plasmids will be repaired after transformation into competent bacteria. Since the freshly synthesized DNA is not methylated it can be easily distinguished from parental DNA *via Dnp* I digestion. *Dnp* I digests only methylated DNA; thus, the parental plasmid DNA carrying no mutation is eliminated from the sample.

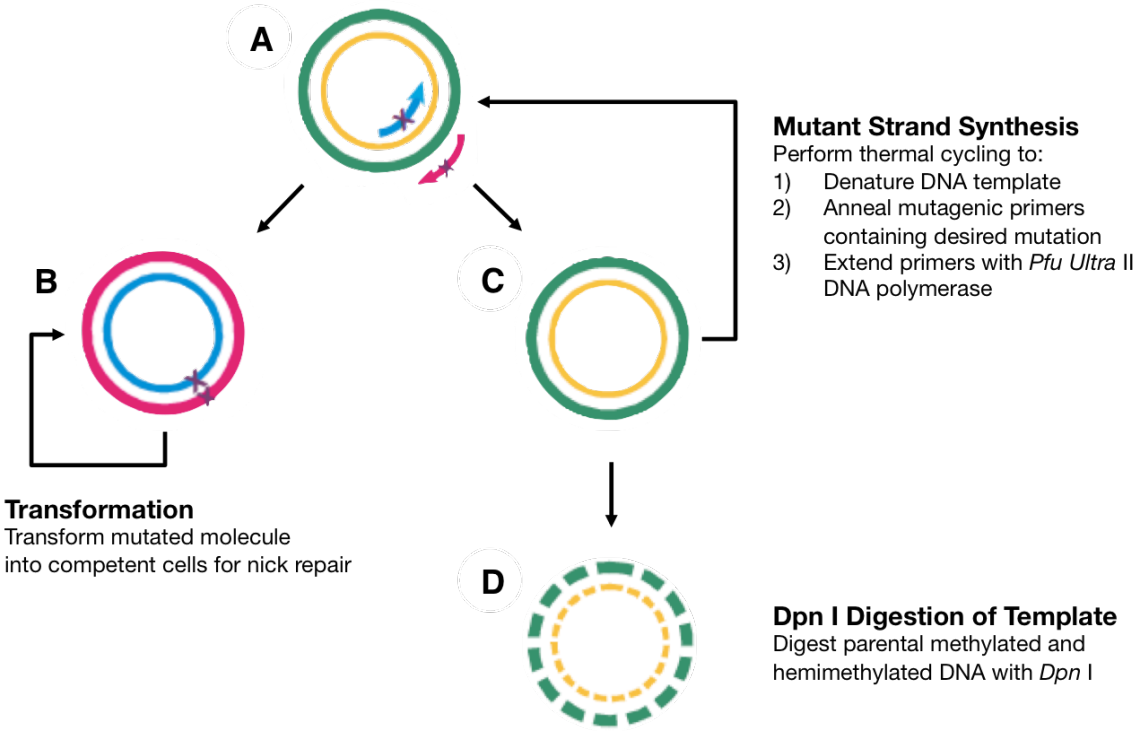

Figure 21 | Scheme of the QuikChange site-directed mutagenesis method
In the first step of the PCR the DNA is denatured followed by annealing of the mutagenic primers **(A)**. The *Pfu Ultra* II DNA polymerase is used for copying the vector plasmid. At the end of the first cycle the ratio of transformed mutated DNA to non-mutated DNA is 1:1 **(B/C)**. Methylated parental DNA is digested by *Dpn* I **(D)**. The undigested mutated plasmids are transformed into bacteria. The nick in the mutated plasmid is repaired in the competent bacteria. Picture modified from QuikChange II Site-Directed Mutagenesis Kit Instruction Manual www.agilent.com

Site directed mutagenesis PCR was carried out using the following sample composition **a)** and program **b)**:

a)

H_2O	33.0 µl
10x buffer (Agilent)	5.0 µl
Primer forward (10 µM)	1.25 µl
Primer reverse (10 µM)	1.25 µl
dNTPs (2.5 mM each)	6.0 µl
pRcRSV-Rab31 plasmid (4 ng/µl)	2.5 µl
Pfu Ultra II Fusion HotStart DNA polymerase (2.5 U/µl)	1.0 µl
	50.0 µl

b)

Step 1:	3 min	at	95°C
Step 2:	20 sec	at	95°C
Step 3:	20 sec	at	67°C
Step 4:	80 sec (15 sec per 1000 bp)	at	72°C
Step 5:	go to step 2		18x
Step 6:	3 min	at	72°C

After completing the PCR program, 1 µl of *Dpn* I (20,000 U/ml) (New England Biolabs) restriction enzyme and 5 µl NEB buffer 4 (New England Biolabs) were pipetted to the PCR products and mixed gently. During incubation for 1 h at 37°C the methylated, parental DNA is digested. The remaining mutated plasmid DNA is then transformed into competent bacteria (chapter 5.1.5).

5.1.3 - Design of shRNAi

To stably knockdown protein expression a specifically designed DNA sequence is integrated into the genome of cells. Following transcription of this sequence a hairpin-loop shaped RNA forms and interferes with target mRNA. This interference induces degradation of the double stranded RNA and thereby protein expression is knocked-down (Figure 29). To knock-down Rab31 expression, retroviral infection of target cells with the pSIREN-RetroQ vector (Clonetech) with two specially designed inserts (#3 and #5) was used (Figure 22).

Figure 22 | Rab31-shRNAi sequences for cloning into the pSIREN-RetroQ vector
The sequence was generated according to the specifications given in the Clontech manual (*Bam*H I restriction site; target sense sequence; hairpin loop; target antisense sequence; terminator and *Eco*R I restriction site) with an additional *Sal* I restriction site (blue) to identify correct inserts by restriction analysis. The hairpin loop is marked in green between the target sense and antisense sequences. The terminator sequence is highlighted in red. For cloning of this sequences into the pSIREN-RetroQ vector *Bam*H I and *Eco*R I restriction enzyme sites (gray) were necessary.

The oligonucleotides were synthesized by Metabion and cloned into the pSIREN-RetroQ vector as described in chapter 5.1.4.

5.1.4 - CLONING OF SHRNAI INTO THE RNAI-READY PSIREN-RETROQ VECTOR

The Rab31 shRNAi #3 and Rab31 shRNAi #5 (Figure 22) sequences were cloned in the linearized p-SIREN-RetroQ vector (Figure 23) using *Eco*R I and *Bam*H I.

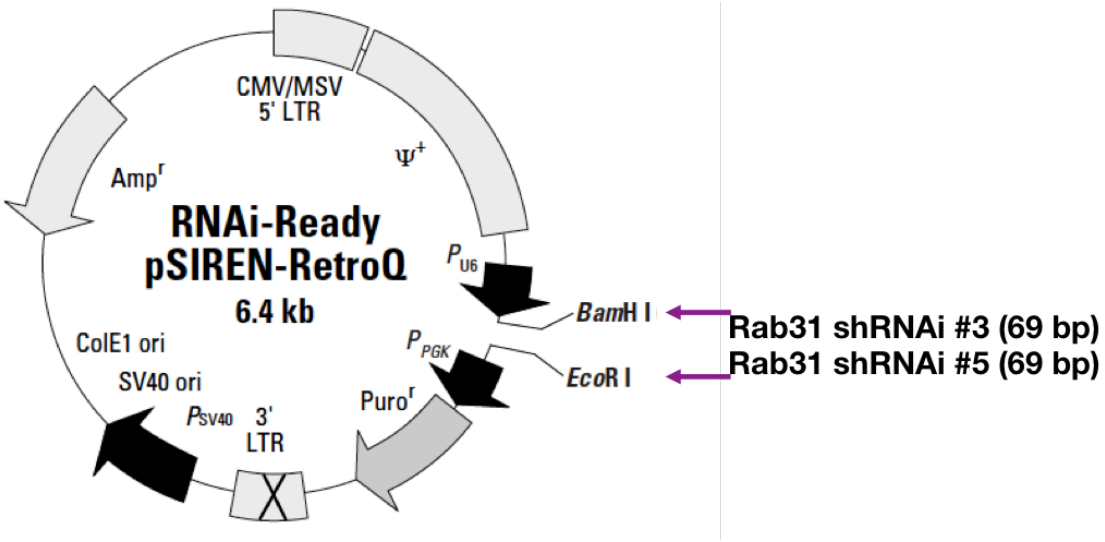

Figure 23 | Map of RNAi-Ready pSIREN-RetroQ retroviral vector
The map shows the features of the pSIREN-RetroQ vector: ampicillin / puromycin resistance; 3´ and 5´ long term repeat; Ψ^+ packaging signal; SV40 ori; unique restriction sites *Bam*HI and *Eco*RI where Rab31 shRNAi was inserted. Picture modified from RNAi-Ready pSIREN-RetroQ Vector information www.clontech.com

Ligation was carried out as follows:

pSIREN-RetroQ plasmid (25 ng/µl)	2.0 µl
T4-DNA ligase (400 U/µl)	0.5 µl
10x ligase buffer (New England Biolabs)	0.5 µl
H_2O	11.0 µl
	14.0 µl
Oligonucleotide Rab31 shRNAi #3/#5 (100 pmol/µl)	1.0 µl

The ligation mix was incubated at 25°C for 2-3 h. As a negative control the same ligation reaction without Rab31 shRNAi oligonucleotide was carried out.

5.1.5 - TRANSFORMATION OF PLASMID DNA INTO COMPETENT BACTERIA BY HEAT PULSE

Transformation of Rab31, Rab31 mutants and Rab31-shRNAi in *E. coli*

Supercompetent *E. coli* cells, XL1-Blue (Stratagene) were thawed on ice. For each reaction, 100 µl of the bacteria was aliquoted to a precooled 2 ml tube. Then 7µl of the ligation mix (chapter 5.1.4) and 44 µl TE [Tris 10 mM; EDTA 1 mM; pH 8] was added, gently mixed and incubated for 25 min on ice. After the addition of 800 µl LB medium [Bacto-Tryptone 1% (w/v); yeast extract 0,5% (w/v); 0.17 M NaCl; pH 7], the bacteria were incubated for 105 sec at 37°C with occasional gentle mixing. Subsequently, the sample was centrifuged at 500 g for 1 min. Then 800 µl supernatant was removed and

the cells were carefully resuspended in the remaining supernatant. The transformed bacteria were pipetted on an AMP-Agar-plate [100 µg/ml ampicillin; 10% (w/v) Agar] and spread with a sterile glass spatula. The plate was incubated at 37°C overnight. The next morning, two to three colonies were picked and placed into 5 ml LB-AMP medium [100 µg/ml ampicillin] and incubated at 37°C overnight while shaking at 200 rpm. The plasmid DNA of the bacteria was isolated *via* small-scale plasmid preparation (chapter 5.1.6). Analysis of correct insertions was done by restriction enzyme analysis (chapter 5.1.7).

5.1.6 - Small-scale plasmid preparation (Mini-Prep)

The following small-scale DNA preparation method was used to extract plasmid DNA from bacterial cultures. Subsequently, the plasmid DNA was characterized through restriction enzyme analysis and/or DNA sequencing. NucleoBond (Macherey-Nagel) uses an alkaline/SDS-based lysis protocol to prepare the bacterial cells for plasmid purification. Plasmid and chromosomal DNA are denatured under alkaline pH conditions. Potassium acetate is then added to the denatured lysate, which leads to the formation of a chromosomal DNA containing precipitate with some other cellular compounds. The potassium acetate buffer also neutralizes the lysate and allows the plasmid DNA to revert to its native supercoiled structure and to remain in solution. After equilibrating the NucleoBond Column with equilibration buffer the negatively charged plasmid DNA is bound to the anion-exchange resin. The DNA is eluted after extensive washing of the column with double distilled water. After precipitation of the eluted plasmid DNA it can easily be dissolved in water for further use (Figure 24) (Macherey-Nagel, Plasmid DNA Purification manual).

After inoculation of LB-AMP medium (5 ml) with a single colony picked from an Amp agar plate the sample was incubated overnight at 37°C while gently shaken. The culture was harvested by centrifugation (6,000 g for 15 min at 4°C) and the supernatant was discarded. The pellet of bacterial cells was resuspended in 400 µl buffer S1 + RNase A [50 mM Tris-HCl; 10 mM EDTA; 100 µg/ml RNase A; pH 8.0]. 400 µl of buffer S2 [200 mM NaOH; 1% SDS] were added to lyse the cells. The cell lysates were gently mixed by inverting the tube 6-8 times and incubated at RT for 2-3 min. To neutralize the solution, 400 µl cold (4°C) S3 buffer [2.8 M KAc; pH 5.1] was added. The mixture was gently inverted 6-8 times until a homogeneous suspension containing an off-white flocculate was formed. During incubation of the lysate on ice for 5 min the flocculate, containing chromosomal DNA and cellular compounds settled. The NucleoBond column was equilibrated with 1 ml buffer N2 [100 mM Tris; 15% ethanol; 900 mM KCl; 0.15% Triton X-100; pH 6.3]. To precipitate cell membranes the lysate was centrifuged at ≥12,000 g for 10 min at 4°C. The cleared lysate was pipetted onto the equilibrated NucleoBond column for binding of the plasmid DNA to the resin. The column was washed twice with 1.5 ml buffer N3 [100 mM Tris; 15% ethanol; 1.15 M KCl; pH 6.3].

The plasmid DNA was eluted with 1 ml buffer N5 [100 mM Tris; 15% ethanol; 1 M KCl; pH 8.5]. To precipitate the DNA, 750 µl isopropanol were added and carefully mixed. The DNA was pelleted by centrifugation at ≥15,000 g for 30 min at 4°C. The plasmid DNA was washed with 500 µl 70% ethanol and centrifuged at ≥15,000 g for 10 min at RT. After removal of the ethanol the DNA pellet was allowed to dry for 5-10 min at RT. The pellet was dissolved in an appropriate volume of sterile deionized H_2O under constant shaking for 10-60 min (Macherey-Nagel, Plasmid DNA Purification manual).

The Nanodrop device (Peqlab) was used to determine the plasmid concentration. To confirm the correct inserts/mutations within the plasmid DNA, restriction enzyme analysis was performed as described below (chapter 5.1.7).

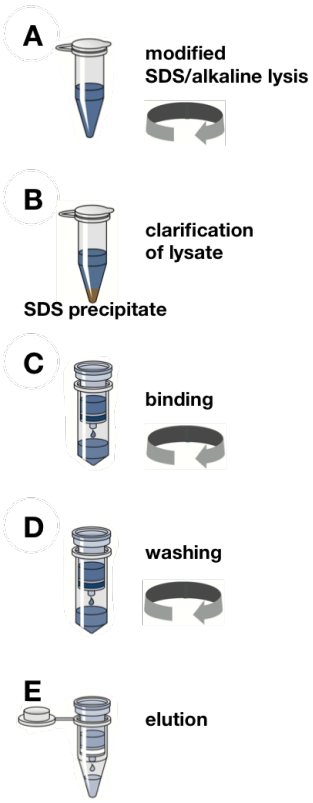

Figure 24 | Plasmid DNA purification (Mini-Prep)
Plasmid preparation is carried out in a five-step procedure. First, cells are lysed in an alkaline buffer **(A)**. Then the lysate is centrifuged to precipitate the solid cell fragments **(B)**. In the next step the plasmid DNA is bound onto the column (**C)**. After washing **(D)** the DNA is eluted from the column **(E)**. Picture modified form Qiagen http://www.qiagen.com

5.1.7 - RESTRICTION ENZYME ANALYSIS

Restriction enzyme analysis allows verification of the correct insertion of a DNA sequence and of successful performance of site directed mutagenesis. To control insertion of the two different Rab31 shRNAi oligonucleotides (#3, #5) into the pSIREN-RetroQ vector plasmid DNA was digested with *Sal* I. The pSIREN-RetroQ vector

without insert was linearized by *Sal* I restriction whereas after successful insertion of the Rab31 shRNAi (#3, #5) the digestion produced a second fragment. Restriction enzyme digestion was carried out using the following master mix:

Restriction enzyme (20 U/µl; NEB)	0.3 µl
10x buffer (according to enzyme; NEB)	1.0 µl
BSA (10 mg/ml)	0.1 µl
H_2O	5.1 µl
	6.5 µl
Plasmid DNA (~500 ng)	3.5 µl

The restriction enzyme digestion was incubated at 37°C for 1 h and the products were then separated on a 1% agarose gel with ethidium bromide. In all cases plasmid DNA was sequenced (Metabion) to confirm the correct sequence and to exclude undesired mutations.

5.1.8 - Medium scale plasmid preparation (Midi-Prep)

The medium-scale preparation was used to generate plasmid DNA for the transfection into cells. The preparation was similar to the mini-prep procedure, however larger volumes were used (Figure 24).

After inoculation of LB-AMP medium (50-100 ml) with a single colony picked from an Amp agar plate (chapter 5.1.5) the sample was incubated overnight at 37°C while gently shaken. The culture was harvested by centrifugation (6,000 g for 15 min at 4°C) and the supernatant was discarded. The pellet of bacterial cells was resuspended in 4 ml buffer S1 + RNase A [50 mM Tris-HCl, 10 mM EDTA, 100 µg/ml RNase A, pH 8.0]. 4 ml of buffer S2 [200 mM NaOH, 1% SDS] were added to lyse the cells. The cell lysates were gently mixed by inverting the tube 6–8 times and incubated at RT for 2-3 min. To neutralize the solution 4 ml cold (4°C) S3 buffer [2.8 M KAc; pH 5.1] was added. The mixture was inverted gently 6-8 times until a homogeneous suspension containing an off-white flocculate had formed. During incubation of the lysate on ice for 5 min the flocculate, containing chromosomal DNA and cellular compounds settled. The NucleoBond column was equilibrated with 2.5 ml buffer N2 [100 mM Tris; 15% ethanol; 900 mM KCl; 0.15% Triton X-100; pH 6.3]. To precipitate cell membranes, the lysate was centrifuged at ≥12,000 g for 10 min at 4°C. The cleared lysate was pipetted onto the equilibrated NucleoBond column for binding of the plasmid DNA to the resin. Washing the column twice was done with 10 ml buffer N3 [100 mM Tris; 15% ethanol; 1.15 M KCl; pH 6.3]. The plasmid DNA was eluted with 5 ml buffer N5 [100 mM Tris; 15% ethanol; 1 M KCl; pH 8.5]. To precipitate the DNA 3.5 ml isopropanol was added and carefully mixed. The DNA was pelleted by centrifugation at ≥15,000 g for 30 min at 4°C. The plasmid DNA was washed with 2 ml 70% ethanol and centrifuged at

≥15,000 g for 10 min at RT. After removal of the ethanol the DNA pellet was allowed to dry for 5-10 min at RT. The pellet was dissolved in an appropriate volume of sterile deionized H_2O under constant shaking for 10-60 min (Macherey-Nagel Plasmid DNA Purification manual). To determine the plasmid concentration the Nanodrop device (Peqlab) was used.

5.1.9 - Glycerol stocks of bacteria

Bacteria were added to 20 ml LB/Amp medium and cultured at 37°C overnight. The bacteria solution was centrifuged at 600 g for 5 min and resuspended in 2 ml of LB medium. The 2 ml of sterile glycerin was added to the bacteria suspension and mixed by pipetting. This glycerin/bacteria mixture was aliquoted and frozen at -80°C.

5.2 - Cell culture

5.2.1 - Cultivation of adherent mammalian cells

MDA-MB-231 and CAMA-1 cells were grown in plastic culture flasks in an incubator at 5% CO_2 (v/v), 95% humidity and 37°C. The cells were cultured in Dulbecco's Modified Eagle Medium (DMEM) with 10% fetal calf serum (FCS) and 10 mM Hepes (complete medium). The cells were passaged every 10 days. For this, the cells were detached with PBS / EDTA (1% w/v), washed with 5 ml PBS and transferred into a 15 ml Falcon tube. After centrifugation at 300 g for 3 min the supernatant was aspirated, the cells were resuspended in complete medium and transferred into a new culture flask.

5.2.2 - Thawing of adherent cells

Cells were thawed quickly and transferred to 10 ml complete medium. Thawed cells were centrifuged at 300 g for 5 min and the medium was discarded. Then the cells were resuspended in complete medium and seeded in an appropriate flask. After attachment of living cells, the medium containing dead cells was replaced by fresh medium.

5.2.3 - Freezing of adherent cells

Cells were detached and pelleted as described above (chapter 5.2.1), then quickly resuspended in 1 ml FCS containing 10% dimethylsulfoxid (DMSO). The cells were frozen at -80°C in cryogen micro tubes (Nalgene) for up to 24 h and transferred into liquid nitrogen at -196°C.

5.2.4 - LIPOSOME BASED STABLE TRANSFECTION OF ADHERENT MAMMALIAN CELLS

Lipofection is used to transport genetic material into a cell by means of liposomes. Liposomes are vesicles that can easily merge with the cell membrane since they are made of a phospholipid bilayer. Lipofection generally uses a positively charged lipid to form an aggregate with the negatively charged vector DNA. The lipoplex aggregate is positively charged at the surface, which increases the effectiveness of transfection through the negatively charged phospholipid bilayer (Figure 25).

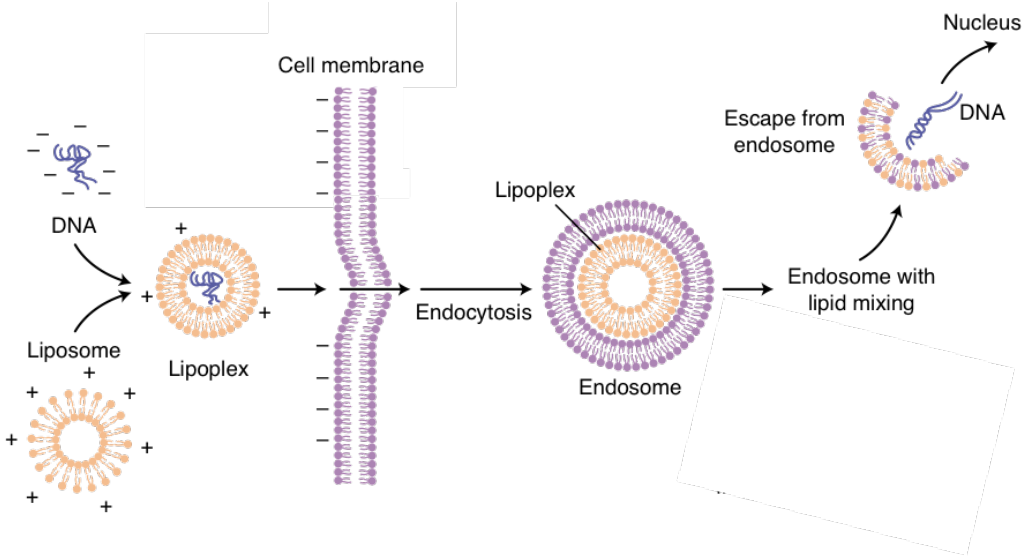

Figure 25 | Liposome based stable transfection of mammalian cells
The negatively charged DNA forms a so-called lipoplex with the positively charged liposome. The cationic lipoplex is endocytosed by the anionic cell membrane. In the resulting endosome the lipids mix and the DNA escapes to enter the nucleus. Picture modified form Parker et al. (2003)

The day before transfection, cells were seeded in a 6-well plate to 60-70% confluency. Prior to transfection, cells were washed once with 2 ml PBS and kept in 2 ml DMEM until addition of the transfection mixture. Next, the transfection mixture was prepared in tubes A and B. Tube A contained 2 µg of plasmid-DNA mixed with 300 µl DMEM, tube B contained 10 µl Lipofectin (Life Technologies) mixed with 300 µl DMEM. Both tubes were incubated for 5 min at RT. The content of tube A was pipetted into tube B, mixed thoroughly and incubated for 20 min at RT. Subsequently, 750 µl DMEM were added to the sample and the mixture was pipetted onto the cells and incubated for 6 h at 37°C. Afterwards, the transfection medium was carefully aspirated and replaced by complete medium. Having reached 80% confluency, cells were detached and transferred into small cell culture flasks (surface: 25 cm^2). Successful transfection of cells with the vector pRc/RSV (Life Technologies) (Figure 26) confers resistance to geneticin (G418; Life Technologies). Selection of stably transfected cells was performed by supplementation of 1 g/l (w/v) G418 into the complete medium. The pcDNA3.1 Hygro(+) vector (Life Technologies) (Figure 27) contained a hygromycin B resistance cassette

and cells were selected with 50 µg/µl hygromycin B (Life Technologies). Non-resistant cells were killed within ten days after addition of the antibiotics.

The cell lines MDA-MB-231 and CAMA-1 were stably transfected with the expression vector pRc/RSV (Figure 26), encoding the human full-length Rab31-WT and Rab31 mutant cDNAs. Control cells were transfected with the native pRc/RSV vector. MDA-MB-231 cells stably transfected with uPAR-D4/5, a splice variant of uPAR in the pcDNA3.1 Hygro(+) (Figure 27) vector were kindly provided by Bettina Grismayer. (Lutz et al. 2001; Luther et al. 2003; Grismayer et al. 2012b).

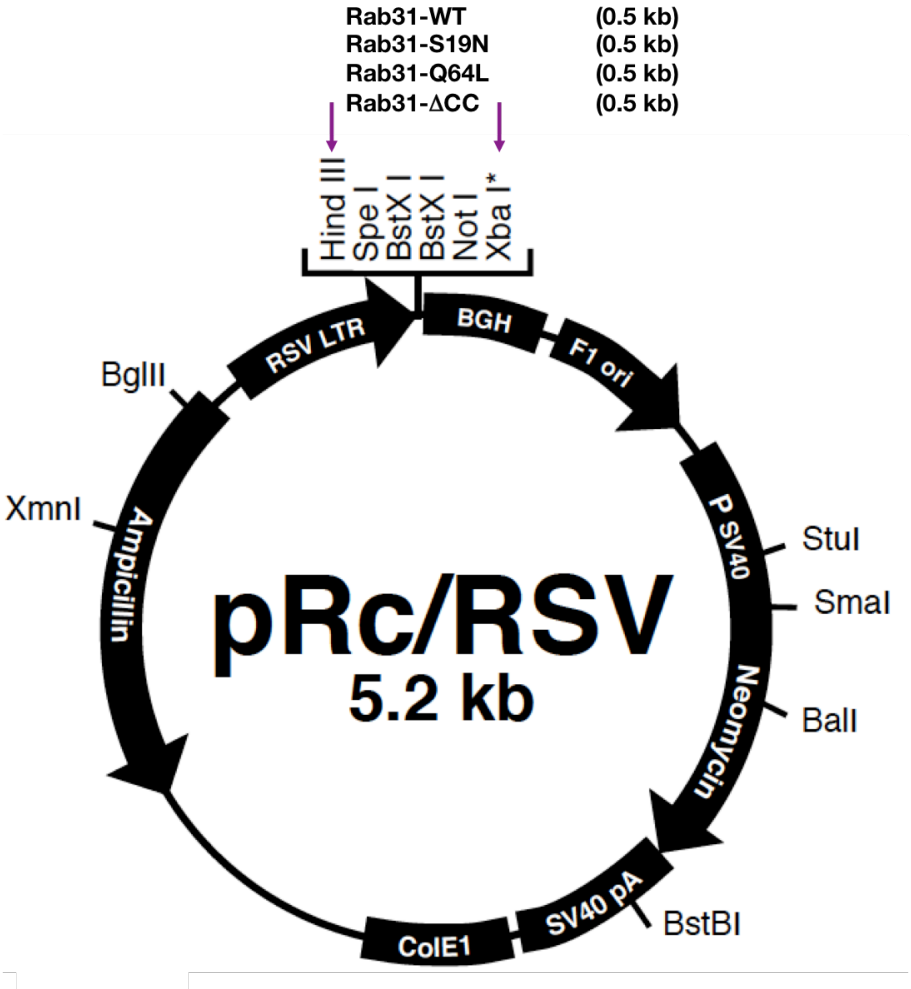

Figure 26 | Map of pRc/RSV vector
The map shows the main features of the pRc/RSV vector: RSV promoter; Polylinker; BGH Poly-A signal; F1 origin; SV40 promoter and origin of replication; Neomycin resistance gene; SV40 Poly-A signal; ColE1 origin; Ampicillin resistance gene; pUC backbone. For cloning of the Rab31 inserts (0.5 kb) into this vector the restriction sites *Hin*d III and *Xba* I were used (chapter 5.1.4). Picture modified from pRc/RSV vector map www.lifetechnologies.com.

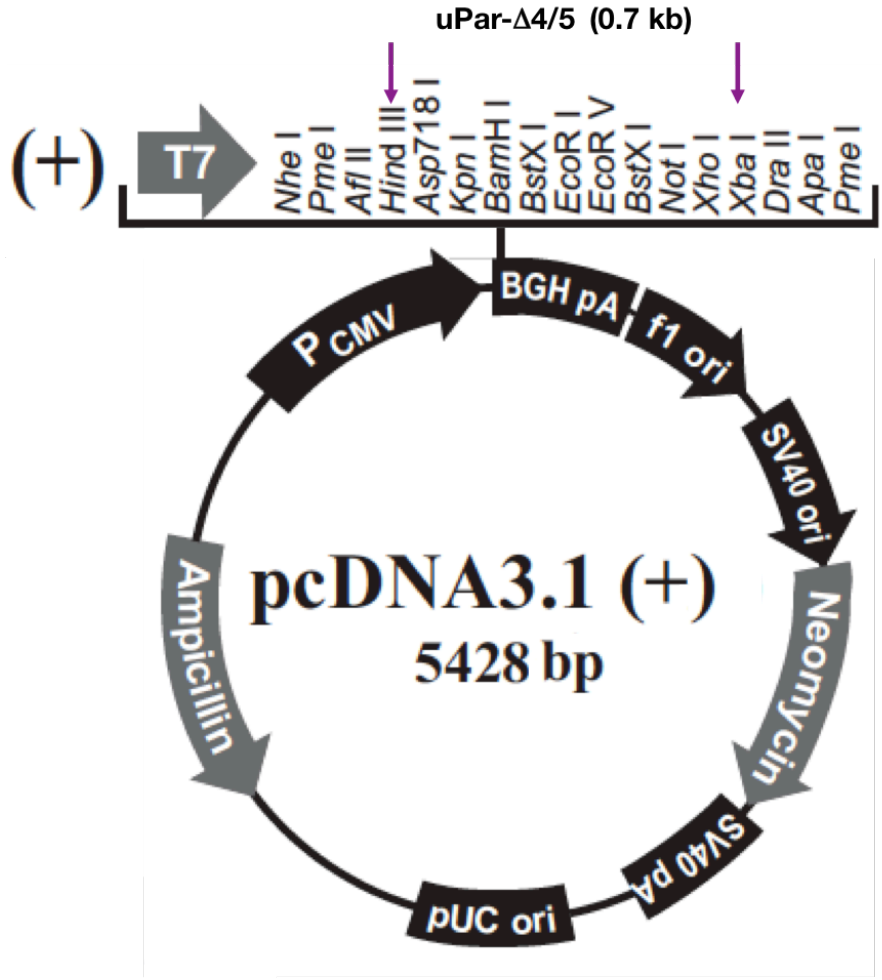

Figure 17 | Map of pcDNA3.1 Hygro(+) vector
The map shows the main features of the pcDNA3.1(+) vector: CMV promoter; T7 promoter/priming site; multiple cloning site; pcDNA3.1/BGH reverse priming site; BGH polyadenylation sequence; F1 origin; SV40 early promoter and origin; Neomycin resistance gene (ORF); SV40 early polyadenylation signal; Ampicillin resistance gene. For cloning of the uPAR-Δ4/5 insert (739 bp) into this vector the *Hin*d III and *Xba* I restriction sites were used (chapter 5.1.4). Picture modified from the pcDNA3.1 Hygro(+) vector map www.lifetechnologies.com

5.2.5 - TRANSIENT TRANSFECTION OF MDA-MB-231 CELLS WITH RAB31-SIRNA

RNA interference (RNAi) is a highly conserved process of posttranscriptional gene silencing, triggered by short, double stranded (ds) RNA molecules (Sharp and Zamore 2000), which are taken up by the RNA-induced silencing complex (RISC). The double stranded siRNA is bound to argonaute 2 (Ago2), the most important part of RISC-complex, and unwound. Subsequently, the passenger strand dissociates and the antisense siRNA guides RISC to the complementary site in the target mRNA. By this, the endonucleolytic activity of Ago2 is activated and Ago2 cleaves the targeted mRNA. The RISC-complex with the siRNA-template is recycled which leads to further cleavage of target mRNA, resulting in the reduction (knock down) of mRNA levels of the gene of interest (Dominska and Dykxhoorn 2010). In the present work, two principal approaches

have been employed to use the RNAi machinery for the knock-down of Rab31 mRNA levels: (i) for transient knock down experiments, treatment with synthetic siRNA nucleotides was applied, (ii) for a more lasting reduction of Rab31 mRNA levels, expression of short-hairpin (sh) RNAs that are processed within the cell into active siRNAs was generated (Figure 28 and 29).

In the liposome-based transient transfection, small double-stranded siRNA is introduced into the cytoplasm of the cells. The knock-down is achieved by silencing genes through mRNA degradation (Figure 28). Different siRNAs targeting Rab31 (Qiagen) were tested for their knock-down capabilities in MDA-MB-231 cells.

On the day of transfection, $2x10^6$ cells were seeded in a 10 cm cell culture dish with 10 ml complete medium and incubated for two hours. The four different siRNAs against Rab31-siRNA #3-#6 FlexiTube GeneSolutions GS113031; Qiagen) were diluted to a final concentration of 6 nM in 2 ml of DMEM without serum. Next, 36 µl of HiPerFect Transfection Reagent (Qiagen) was added to the diluted siRNA. The samples were incubated for 10 min at RT to allow the formation of transfection complexes. The complexes were added onto the cells and incubated for 3 h, followed by supplementing 10 ml of culture medium. The cells were grown for two days. Then in one half of the cells the knock-down was analyzed by Western blotting and qPCR experiments. Three and four days after transfection one half of the cells were analyzed in terms of knock-down efficiency.

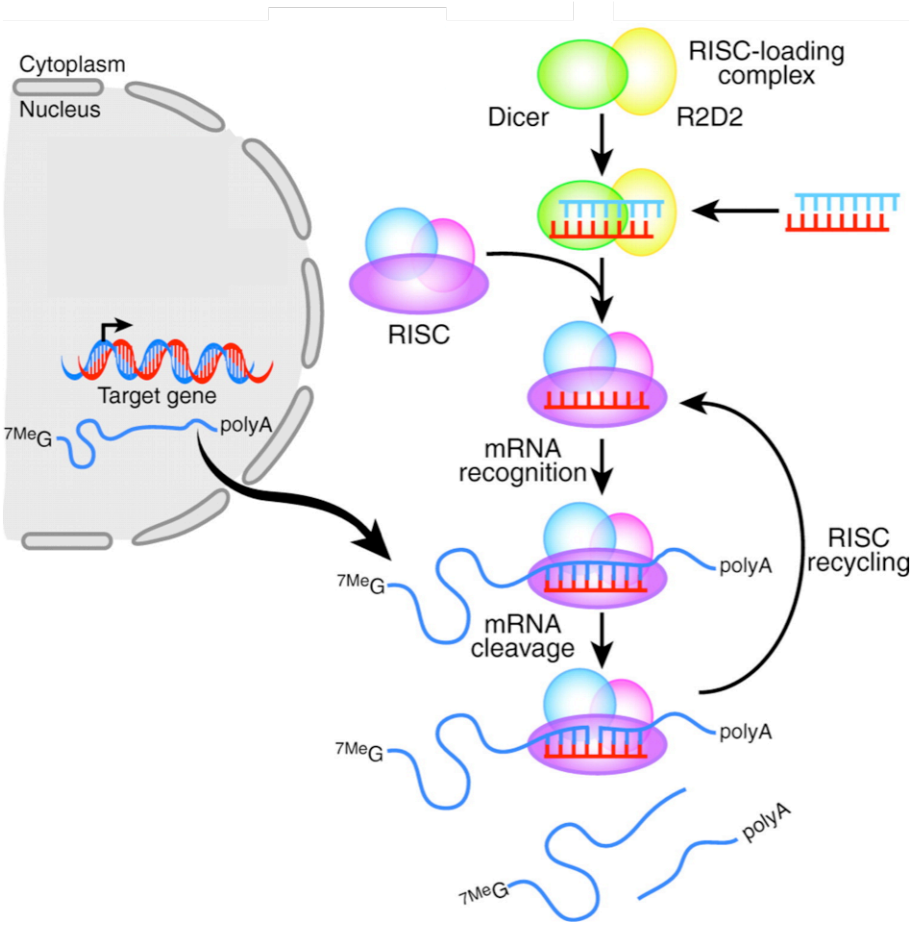

Figure 28 | Schematic representation of the mode of action form short interfering RNA (siRNA)
siRNAs contain a characteristic 19 nucleotide duplexed region with 2-3′ overhangs and 5′-terminal phosphate groups. The siRNAs are taken up by the RNA-induced silencing complex (RISC). The siRNA binds to the Ago2 protein, the central component of RISC. Following unwinding the antisense siRNA guides RISC to the complementary site in the target mRNA. Ago2 then cuts the target mRNA and the siRNA-loaded RISC is recycled for several rounds of mRNA cleavage. Picture modified form Dominska and Dykxhoorn (2010)

5.2.6 - Stable Rab31 knock-down in MDA-MB-231 cells by short hairpin RNA interference

For a stable knock-down of protein expression a short hairpin DNA sequence is integrated into the genome of the cells. Transcription of this sequence results in a short hairpin RNA which degrades the target mRNA (Figure 29).

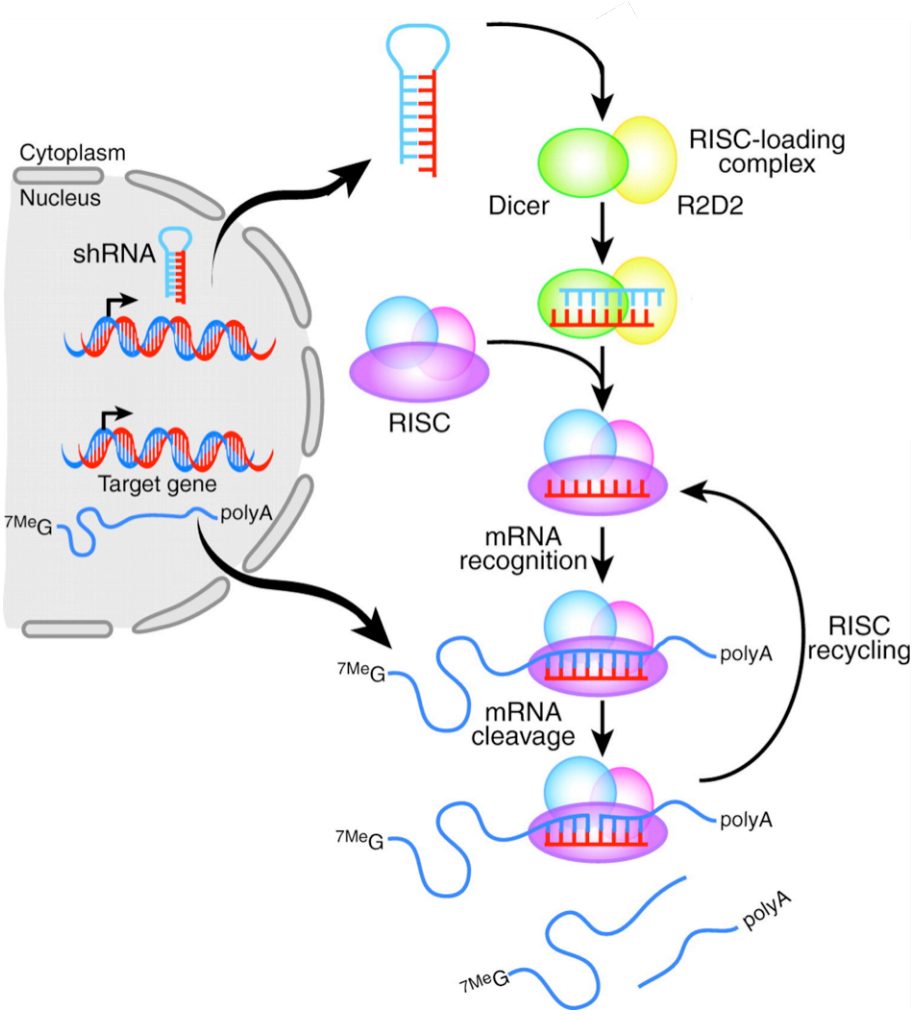

Figure 29 | Schematic representation of the mode of action from short hairpin RNA interference (shRNAi)
Stable knock-down of gene expression can be facilitated with shRNAs expressed from DNA-based vectors. Dicer and the dsRNA-binding protein R2D2 process shRNAs into siRNAs in the cytoplasm. These siRNAs containing the characteristic 19 nucleotide duplexed region with 2-3′ overhangs and 5′-terminal phosphate groups. The siRNAs are taken up by the RNA-induced silencing complex (RISC). The siRNAs are taken up by the RNA-induced silencing complex (RISC). The siRNA binds to the Ago2 protein, the central component of RISC. Following unwinding the antisense sequence siRNA guides RISC to the complementary site in the target mRNA. Ago2 finally cuts the target mRNA. The siRNA-loaded RISC is recycled for several rounds of mRNA cleavage. Picture modified form Dominska and Dykxhoorn (2010)

5.2.6.1 - Generation of Rab31 shRNAi packaging cells for retrovirus production

AmphoPack-293 (Clonetech) is a human embryonic kidney (HEK 293) derived cell line. This cell line is designed for rapid production of high-titer replication-incompetent retroviruses for transient or stable transfections. The AmphoPack-293 cell line was developed using bleomycin and puromycin resistance genes to stably introduce the viral gag, pol and env genes, respectively. Therefore, stable cell lines can be developed

using neomycin and hygromycin for selection. Viruses produced by AmphoPack-293 cells can infect a broad range of mammalian cells.

The cells were grown in DMEM with 10% FCS. Prior to electroporation $3x10^6$ cells / ml were diluted in DMEM and 800 µl were transferred into a 4 mm cuvette (BioRad) with 20 µg pSIREN-RetroQ plasmid (Rab31 shRNA #3, #5 and SCR) (chapter 5.1.4). After 10 min of incubation on ice the cells were pulsed [245V / 960µF / 50Ω] using the Gene Pulser Xcell Total System (BioRad). After electroporation the cells were incubated for 10 min on ice, and then seeded into a flask (75 cm^2) with 20 ml complete medium and 1 µl DNase I (301 U/µl). The electroporated cells were cultivated for three days and after that puromycin (2.5 mg/ml) was added for 24 h. This ensures the selection for transfected cells. At this stage aliquots of transfected cells were frozen for further use (chapter 5.2.3). The retroviral vector was stably inserted into the genome of AmphoPack-293 cells producing viral proteins. These proteins are packed in viral particles that bud off from the cells. After two days the supernatant with the virus particles was stored at -80°C until usage for infection of the target cells (Figure 30).

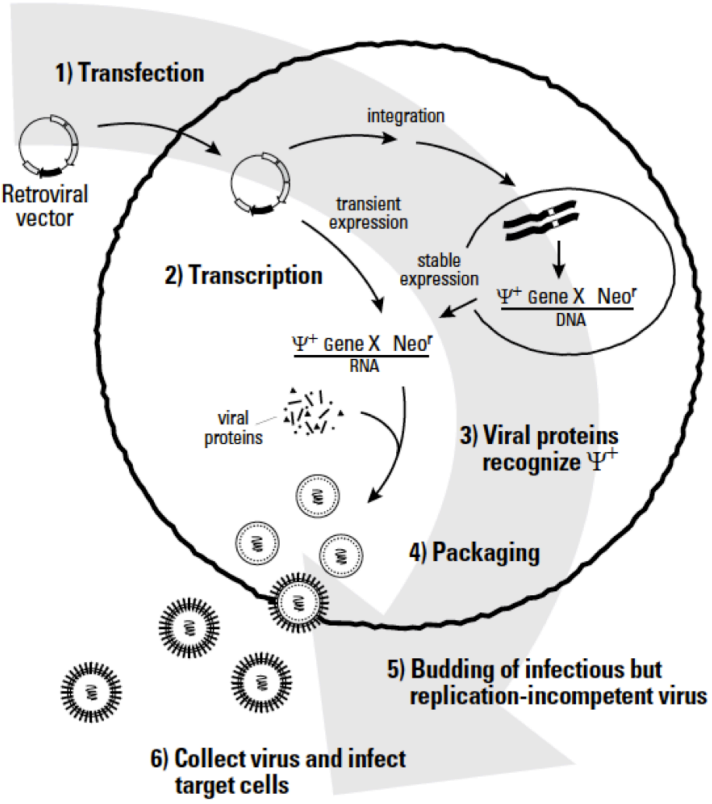

Figure 30 | Virus production in packaging cell lines
1) Transfection of the retroviral pSIREN-RetroQ vector. **2)** The vector is integrated into the genome and transcribed. **3)** Viral proteins recognize the packaging signal Ψ^+. **4)** Viral proteins are packed into new virus particles. **5)** The virions budding from the cells are infectious but replication incompetent. **6)** The supernatant containing the virus particles is collected and can infect target cells. Picture taken from RNAi-Ready pSIREN-RetroQ vector information www.clontech.com

5.2.6.2 - Virus infection of MDA-MB-231 cells

$3x10^5$ MDA-MB-231 cells were seeded per well of a 6-well plate for the infection on the next day. Per well 1 ml of complete medium with 8 µg/ml polybrene and 1 ml of thawed retrovirus supernatant was added. The samples were incubated at 37°C for 48 h. Polybrene is a cationic polymer used to increase the efficiency of infection of cells with a retrovirus in cell culture. It acts by neutralizing the charge repulsion between virions and sialic acid on the cell surface. After infection, 2.5 mg/ml puromycin in 4 ml complete medium was added for selection of the MDA-MB-231 cells that had stably integrated the viral DNA into the genome. The knock-down of Rab31 was tested by qPCR. In case the knock-down turned out to be less efficient subcloning of MDA-MB-231 cells could help to identify cell clones with efficient down-regulation (chapter 5.2.7).

5.2.7 - SUBCLONING OF CELL LINES *VIA* SINGLE SELECTION OF CELLS

Single cell clones were generated by limited dilution to find clones with high efficient knock-down or overexpression of the gene of interest. $1x10^3$ cells were seeded in 10 cm cell culture petri dishes. Colonies that developed from single cell clones were transferred onto 96-well plates for further growth. The expression of uPAR-Δ4/5 or Rab31 was detected thereafter by immunocytochemistry and Western blot analysis. Two rounds of subcloning were performed to secure cell lines with a homogeneous expression of the gene of interest.

5.2.8 - DETECTION OF MYCOPLASMA CONTAMINATION IN CULTURED CELLS

Mycoplasma contamination of cultured cells was regularly checked using mycoplasma specific PCR (3´ primer: 5´-GCG GTG TGT ACA AGA CCC GA- 3´; 5´ primer: 5´-CGC CTG AGT AGT ACG TTC GC- 3´). For this purpose, the cells were detached and the cellular DNA was extracted using the DNA High Pure PCR Template Preparation Kit (Roche Diagnostics) according to the manufacturer's instructions. Mycoplasma PCR was carried out using the following master mix **a)** and according to the following PCR program **b)**.

a)

10x PCR reaction buffer	2.5 µl
dNTPs (2.5 mM each)	2.5 µl
Primer 5´ (20 pM)	0.5 µl
Primer 3´ (20 pM)	0.5 µl
Taq Polymerase (5 U/µl)	0.2 µl
H_2O	17.8 µl
	24.0 µl
Extracted DNA	1.0 µl

b)	Step 1:	5 min	at	94°C
	Step 2:	30 sec	at	94°C
	Step 3:	1 min	at	60°C
	Step 4:	30 sec	at	72°C
	Step 5:	go to step 2		30x
	Step 6:	5 min	at	72°C

The PCR products were analyzed by agarose electrophoresis (1%) with ethidium bromide (0.25 µg/ml). The amplified mycoplasma-DNA PCR product was detected at 500 bp.

5.2.9 -TREATMENT OF MYCOPLASMA INFECTIONS

Myco-3 (AppliChem) is based on the Ciprofloxacin antibiotic, which is a member of the fluoroquinolone group. Many mycoplasma species have been found to be sensitive to Myco-3, including *A. laidlawii*, *M. orale*, *M. hyorhinis*, *M. fermentans* and *M. arginini*. These species generally are involved in mycoplasma contamination in cell culture. Myco-3 was added to the complete medium (1 µg/ml) and the efficacy of Myco-3 treatment was assayed 14 days later by Mycoplasma PCR (chapter 5.2.8).

5.2.10 - 3D CELL CULTURE

QGel (QGel) consists of a synthetic polyethylene glycol (PEG) based hydrogel functionalized with peptides to allow for cell adhesion and to control the degradation properties of the gel. This synthetic matrix mimics key features of the natural extracellular environment of cells *in vivo*. Thus, the artificial matrix provides a microenvironment for cell culture *in vitro* for long-term 3D cell culture experiments.

To reconstitute the gel, 400 µl of the gel-buffer A (provided) was pipetted to one vial of gel-powder and vortexed for 10 sec. $1x10^5$ cells were added to the reconstituted gel in 100 µl phenol red free complete medium and vortexed for 10 sec. Approximately 5 min after the gel is completely polymerized, therefore all subsequent steps have to be carried out quickly. 30 µl droplets of the gel suspension were pipetted on a Sigmacote (Sigma Aldrich) (Ehrbar et al., 2007) coated glass slide with two 3 mm high spacers on the side. The droplets were covered with a second glass slide and fixed with two clamps. For polymerization the gels were transferred in the incubator (37°C) for 45 min. Subsequently PBS was applied between the slides to moisten the gel disks. After removal of the clamps the gels were lifted and transferred in 48-well plates with complete medium using a spatula (Figure 31). The gels were incubated at 37°C for 4 h and then the medium was changed. The medium was changed every three days. In case some cells left the gel and seeded at the bottom of the well plate forming a monolayer the gel discs were transferred to a new well with fresh medium.

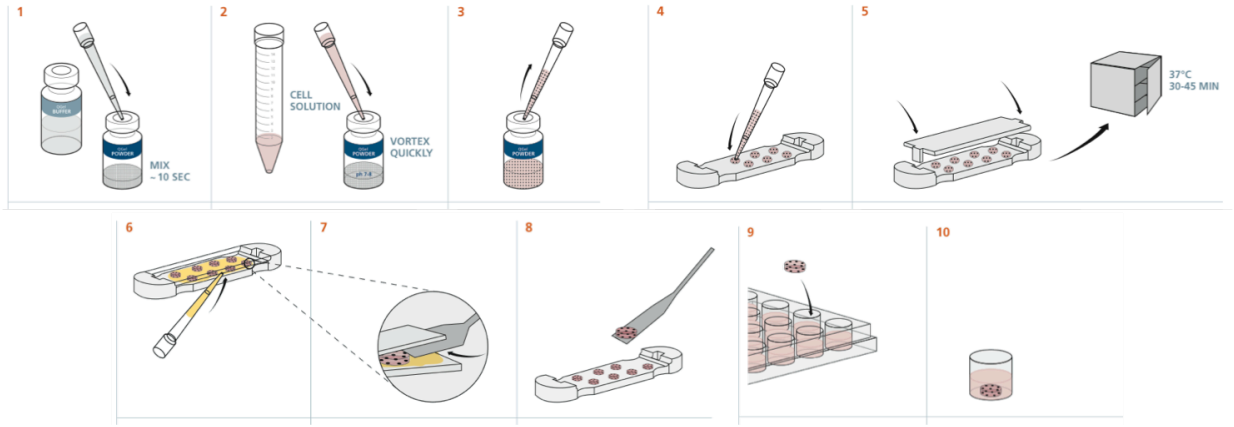

Figure 31 | Schematic representation of how to cast gels QGels
1: Resuspension of the QGel matrix powder with buffer. **2:** addition of the cell suspension. **3:** mixing of the matrix/cell solution. **4:** pipetting the QGel on the caster/glass slide. **5:** closing the caster/glass slides and incubating the cells. **6:** addition of PBS and carefully open the caster. **7:** usage a spatula to avoid that the gel discs stick to the caster. **8:** picking up of the QGels with a spatula. **9:** culturing of the QGel disks in 24-well plates. **10:** long-term culture. Picture modified from QGel user manual www.qgelbio

5.3 - Cellular assays

5.3.1 - Preparation of cellular assays *in vitro*

The cells for all cellular assays were seeded 48 or 72 h prior to the experiment to approximately 70% confluency onto 6-well culture plates.

5.3.2 - Counting Proliferation assay

Transfected MDA-MB-231 ($2x10^4$) and CAMA-1 ($3x10^4$) cells were seeded in triplicates on 24-well plates. Cells were detached in 200 µl, 300 µl, 400 µl and 500 µl of PBS; 0.1% EDTA (1 h at 37°C) after 24 h, 48 h, 72 h and 96 h respectively. To the cell suspension 50 µl trypan blue solution was added and the cell number per well was determined in duplicates using a Neubauer chamber. The cell number of each cell line was set to 100% after 24 h. Proliferation was illustrated as percentage of increase in cell number relative to the 24 h value.

5.3.3 - Proliferation measurement with alamarBlue

The active compound of alamarBlue, resazurin (Life Technologies), is nontoxic, cell permeable and blue, which is basically nonfluorescent. In the cells, resazurin is reduced

to resorufin, which is red fluorescencet (Figure 32). Viable cells continuously reduce resazurin to resorufin, thus allowing quantification of living cells (www.lifetechnologies.com).

Figure 32 | Reduction of resazurin to resorufin as an indicator for cell viability
Resazurin (left), a non-fluorescent indicator dye, is reduced to red–fluorescent resorufin (right) *via* metabolically active cells. The amount of fluorescent resorufin produced is directly proportional to the number of living cells. Picture form alamarBlue product page at www.lifetechnologies.com

Cells were detached and resuspended in DMEM with 10% FCS without phenol red. After counting the cells in a Neubauer chamber, $3x10^3$ cells in 100 µl were seeded eightfold into a black 96 well plate with clear bottom. Every 24 h 0; 2,000; 3,000; 4,000; 6,000; 8,000; 12,000 and 16,000 cells in DMEM with 10% FCS without phenol red were seeded in triplicate for reference. After letting the cells settle down for 4 h at 37°C, 10 µl of alamarBlue was added and incubated for 2 h. The plates were measured with an excitation wavelength of 590 nm and an emission of 530-560 nm (Wallac 3 photometer; PerkinElmer). The cell number in each well was calculated using the reference cells. The cell number of each cell line after 24 h was set to 100%. Proliferation was illustrated as percentage of increase in cell number relative to the 24 h value.

5.3.4 - Proliferation measurement with CyQUANT

CyQUANT measurement is based on the use of the green fluorescent CyQUANT dye, which exhibits strong fluorescence enhancement when bound to cellular nucleic acids. The assay has a linear detection range extending from 50 or fewer to at least 50,000 cells (Figure 33).

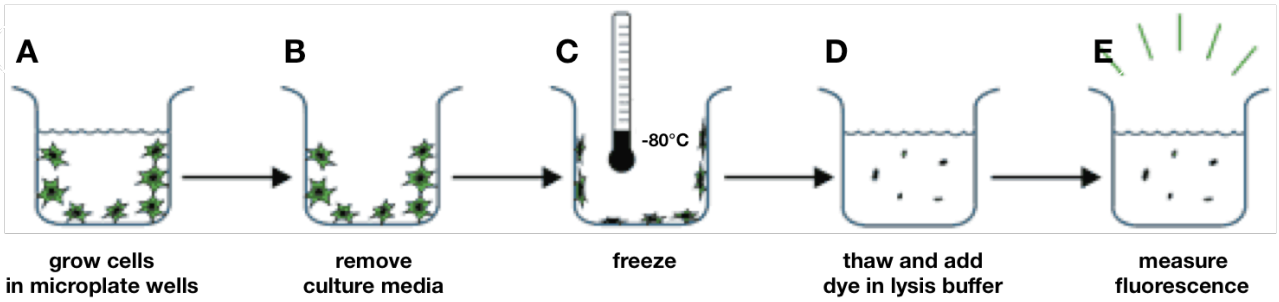

Figure 33 | CyQUANT assay principle
A) Growing of cells in 96-well plates. **B)** Removal of the medium by blotting it against paper towels. **C)** Freezing cells at -80°C. **D)** Thawing of cells at RT and addition of lysis buffer and dye. **E)** Measurement of fluorescence at 520 nm. The DNA amount is proportional to the cell number. Picture modified form CyQUANT manual www.lifetechnologies.com

5.3.4.1 - Measurement of cells in 96-well plates

The plates with the cells that had undergone the alamarBlue assay were blotted onto paper towels to completely remove the medium from the wells. The cells were then frozen at -80°C for at least one day. The freezing step is important for efficient cell lysis. The plates were thawed at RT, the cell standard series (0; 2,000; 3,000; 4,000; 6,000; 8,000; 12,000; 16,000 cells) and the λ-DNA standard series (0; 10; 25; 40; 50; 125; 250; 500 ng/ml) were prepared in 100 µl lysis buffer (provided in the kit) and pipetted in a 96-well plate. 100 µl of 2x CyQUANT dye solution were added to each well and incubated for 2-5 min at RT protected from light. All plates were measured at an excitation wavelength of 485 nm and an emission wavelength of 520 nm. The results were calibrated to the results of λ-DNA standard series (ng) and to the cell numbers of the cell standard series.

5.3.4.2 - Measurement of cells in 3D-QGels

The QGels that had undergone the alamarBlue assay were incubated for 1 h on a shaker in PBS to remove the alamarBlue reagent. The gel discs were then frozen at -80°C in for at least one day. The QGels were then thawed at RT and digested for 1 h in 100 µl RNase A solution (1.35 U/ml in lysis buffer; provided with the kit) at RT. The digested samples were pipetted into a 96-well plate. A λ-DNA standard series (0; 1; 2.5; 10; 25; 50; 100; 200 ng/ml) was prepared in 100 µl RNase A solution (1.35 U/ml in lysis buffer) and pipetted in a 96-well plate. 100 µl of 2x CyQUANT dye solution were added to each well and incubated for 2-5 min at RT protected from light. The plates were measured with an excitation wavelength of 485 nm and an emission wavelength of 520 nm. The results were calibrated to the results of the λ-DNA standard series (ng).

5.3.5 - PROLIFERATION MEASUREMENT BY MEASURING THE CELLULAR IMPEDANCE

Cell proliferation was registered in real-time with a bioelectric xCELLigence device (Roche/ACEA Biosciences) monitoring impedance over gold micro-electrodes at the bottom of electrical-plates (Roche/ACEA Biosciences). $2.5x10^4$ CAMA-1 or $2.0x10^4$ MDA-MB-231 cells were seeded in wells of E-plates in 200 µl complete medium and the cellular impedance was measured periodically.

5.3.6 - ADHESION ASSAYS

To determine cellular adhesion of the transfected cells towards extracellular matrix (ECM) proteins, 100 µl of the matrix proteins were pipetted into 96-well plates and incubated as shown in Table 1.

Table 1 | Incubation of ECM proteins in 96-well plates

ECM protein	Concentration (µg/ml)	Incubation, Temperature
Vitronectin	2	1 h, RT
Fibronectin	5	1 h, RT
Collagen type I	5	3 h, 37°C
Collagen type IV	5	3 h, 37°C
Laminin	5	3 h, 37°C

After incubation, each well was washed once with 100 µl PBS and blocked with 200 µl of 2% (w/v) BSA / PBS for one hour at RT. The coated plates can be stored for one week at 4°C after washing with PBS. Cells were detached, resuspended in adhesion medium [0.5% BSA in DMEM; 20 mM HEPES] and counted. Triplicates of 100 µl cell suspension (MDA-MB-231: $2x10^4$, CAMA-1: $3x10^4$) were added to the coated plates. A standard series in duplicate of 0; 782; 1,563; 3,125; 5,250; 12,500; 25,000 and 50,000 cells in 50 µl PBS was pipetted to the 96-well plate. After letting the cells adhere for 2 h at 37 °C, medium containing non-adherent cells was aspirated. Plates were washed gently twice with 100 µl PBS. Wells containing the reference cells (standard series) remained unwashed. For cell number determination of the adherent cells, 50 µl PBS and 50 µl hexosaminidase substrate [100 mM sodium citrate buffer pH 5; 0.5% Triton-X 100; 10 mM p-Nitrophenyl-N-acetyl-b-D-glucosamidide] were applied to each well. 50 µl hexosaminidase substrate without PBS was added to the reference cells. Viable cells will continuously produce a colored product thereby allowing a quantitative measurement of cells present. After incubation for 90 min at 37°C, the reaction was stopped by addition of 100 µl stop solution [2 M NaOH; 0.5 M EDTA]. Optical density was recorded at 405 nm (SLT Spectra ELISA Reader). The cell number in each well was

calculated using the results of the reference cells. Adherent cell number of vector control cells on each coating was set to 100%.

5.3.7 - Invasion assay

Studies on the invasive capacity of transfected MDA-MB-231 Rab31 mutant cells were performed using the 24-well Costar Transwell chamber system. For this, 24 well transwell plates were coated with the artificial basement membrane Matrigel. The Matrigel used in this assay was extracted from the Engelbreth-Holm-Swarm (EHS) mouse sarcoma. The basement membrane of this tumor mainly consists of laminin, collagen type IV, heparan sulfate, proteoglycans and entactin (according to the product description of BD). Membrane filters with a pore size of 8 µm and a diameter of 6.5 mm were coated with 30 µg growth factor reduced Matrigel (BD) diluted in 100 µl invasion medium [DMEM; 0,1% (w/v) BSA]. The coated transwells were incubated for 3 h at 37°C and dried overnight under the laminar flow. Prior to the experiment, inserts were reconstituted with 200 µl invasion medium for 2 h at 37°C. The bottom chamber was filled with 600 µl of complete medium. The chemoattractant was contained in the FCS of the medium. $4x10^4$ cells were suspended in 200 µl serum-free invasion medium and seeded into the top chamber (Figure 34). The inserts were placed into the 24-well, avoiding bubbles. After 24 h incubation at 37°C, cells and Matrigel at the top of the inserts were removed using a Q-Tip. Cells that had migrated to the bottom of the insert were fixed and stained using the Hemacolor staining kit (Merck). Purple cells on the dried membrane were photographed and quantified. Cell number of invaded vector control cells was set to 100%.

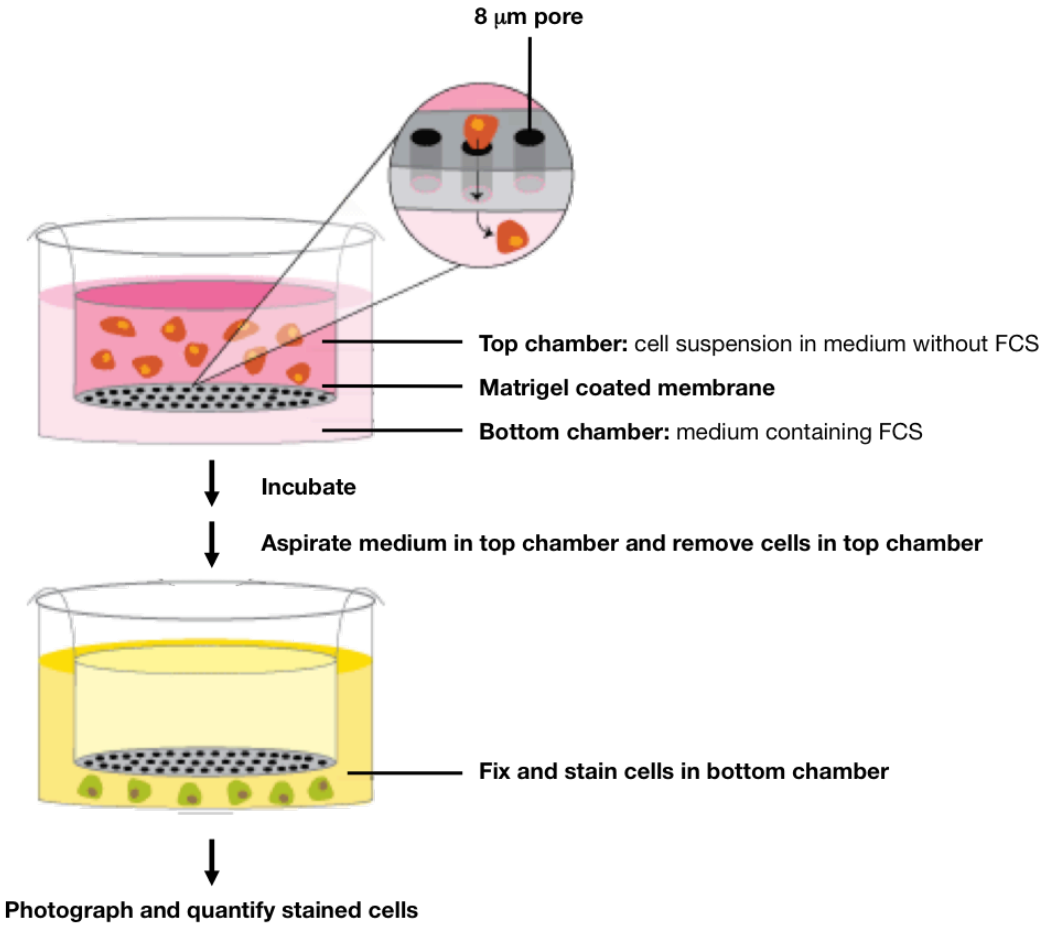

Figure 34 | Principle of invasion assays
Cells are seeded on top of a Matrigel coated membrane in the top chamber. During the 24h incubation cells can, attracted by FCS, migrate trough the 8 mm pores onto the other side of the membrane. There they will be fixed, stained, photographed and counted. The cell number of invaded vector control cells is set to 100%. Picture modified from http://www.rndsystems.com/product_detail_objectname_cell_invasion_assays.aspx

5.3.8 - TGF-β ACTIVITY ASSAY

MFB-F11 cells are embryonic fibroblasts derived from TGF-β-deficient mice, which were stably transfected with an expression plasmid encoding for the secreted alkaline phosphatase (SEAP) under the control of a Smad2-responsive promoter (Tesseur et al. 2006).

$2x10^4$ MFB-F11 cells per well were seeded in a 96-well plate and grown for 24 h. After washing with PBS, cells were serum-starved for 2 h in FCS-free DMEM. The 1:16 concentrated supernatant (chapter 5.7.2) of MDA-MB-231 and CAMA-1 cells, or 1:16 concentrated fresh culture medium (negative control), were either left untreated, or were heated for 10 min at 80°C to activate TGF-β. The resulting media was then added to MFB-F11 cells in two volumes FCS-free DMEM and incubated for 20 h. Cell supernatants were collected and SEAP was measured using a chemiluminescence detection kit (Great EscAPe SEAP; Clontech). Briefly, media were centrifuged for 15 min

at 11,000 g to pellet any floating cell, before 20 µl of medium were transferred in an opaque white 96-well plate, added with 75 µl of dilution buffer, and heated for 20 min at 65°C. After cooling, 100 µl of SEAP substrate solution were added and incubation was carried on for 30 min at RT in the dark. Chemiluminescence was finally measured using the Glomax luminometer (Promega).

5.4 - Flow cytometry

5.4.1 - Annexin V staining

In the early stage of apoptosis, changes occur in the cell membrane. Phosphatidyl serine (PS) located at the cytoplasmic side of the cell membrane is translocated to the cell surface (Figures 35 and 36). PS translocation in apoptotic cells is analyzed by Annexin-V-Fluorescein and propidium iodide (PI) staining followed by fluorescence-activated cell sorting (FACS). Dead cells that have died by apoptosis or necrosis long before staining are Annexin-V-Fluorescein negative and PI positive. Late apoptotic and necrotic cells stain Annexin-V-Fluorescein and PI positive. Early apoptotic cells have a characteristic Annexin-V-Fluorescein positive but a PI negative staining. Viable cells stain negative for both compounds.

Cells were detached and washed with PBS. $1x10^6$ cells were resuspended in 100 µl Hepes buffer [10 mM HEPES/NaOH; 140 mM NaCl; 5 mM $CaCl_2$; pH 7.4] 4 µl of the ready to use Annexin-V-Fluorescein solution (Roche) was added and incubated for 10 min at RT. The samples were washed once with PBS and resuspended in 100 µl Hepes buffer with PI (4 µg/ml). Stained cells were analyzed with a flow cytometer (FACS Calibur; BD Biosciences).

Tumor necrosis factor-related apoptosis-inducing ligand (TRAIL) is a synthetic peptide derived from the amino acids residues 95 – 281 of human TRAIL. TRAIL is a cytokine that binds to receptors and induces apoptosis. Killer TRAIL (Enzo) was used to induce apoptosis in CAMA-1 and MDA-MB-231 cells. The cells were cultivated with 40 ng/ml of Killer TRAIL for 24 h.

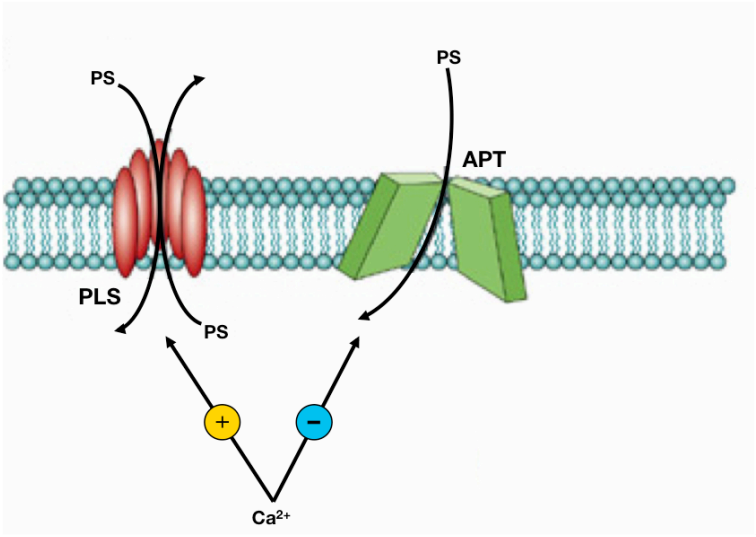

Figure 35 | Mechanism of phosphatidyl serine (PS) regulation during apoptosis
PS distribution between the two leaflets of the plasma membrane is altered at the onset of apoptosis. Phospholipid scramblase (PLS) is Ca^{2+} dependent, and is activated during apoptosis. In contrast aminophospholipid translocase (APT) is inhibited by Ca^{2+}. Picture modified from Orrenius et al. (2003)

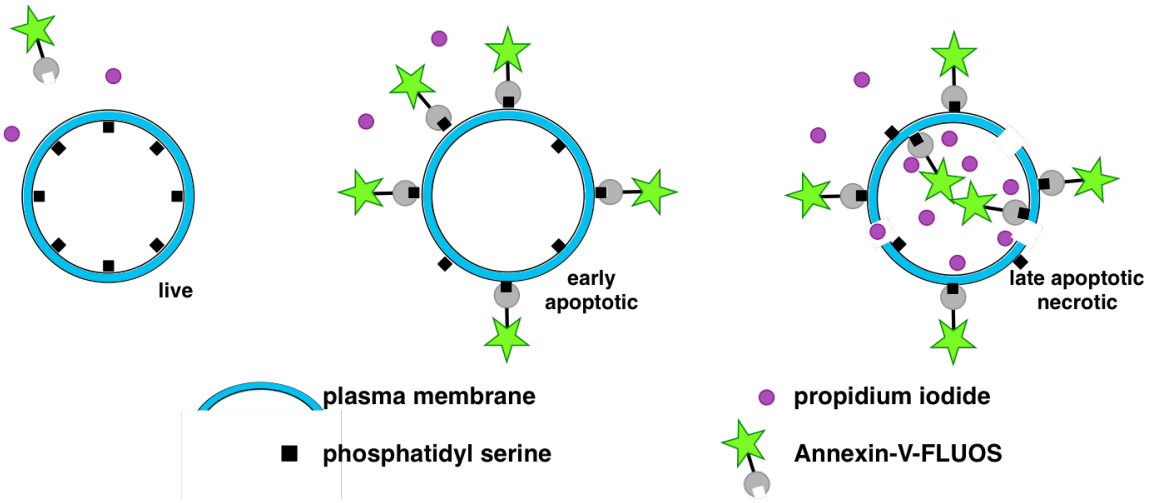

Figure 36 | Annexin-V staining of apoptotic cells
A well-established feature of apoptosis is the externalization of phosphatidyl serine (PS) from the inner leaflet of the plasma membrane to the outer membrane. Because annexin-V specifically binds PS a fluorescent-labeled annexin-V enables the flow cytometric detection of externalized PS. When used in conjunction with the live/dead cell discriminator PI indicating membrane integrity, early apoptotic cells (annexin-V positive only) can be distinguished from late apoptotic/necrotic cells (annexin-V and PI positive). Picture from http://www.lifesci.dundee.ac.uk/services/flow_cytometry/ca/cell-death

5.4.2 – Determination of the percentage of cells in S-phase

This method involves dissolving the cell membrane lipids with a nonionic detergent as well as the digestion of the cytoskeleton and nuclear proteins with trypsin and digestion of the cellular RNA with RNase. For stabilization of the nuclear chromatin spermine is used. The isolated nuclei bind stoichiometrically to Propidium iodide (PI), which are then counted on a flow cytometer. The CycleTEST PLUS DNA Reagent Kit (BD) was used throughout. The cells were detached and washed twice with buffer solution provided with the kit. The cell pellet was resuspended in 1 ml buffer solution and mixed by pipetting. To freeze the cells rapidly a mixture of dry ice and 99% ethanol was used. The cells were stored at -80°C until further use. After thawing the cell suspension was centrifuged at 400 g for 5 min at RT and the supernatant was decanted. 250 µl of solution A (trypsin buffer) was added to each sample, mixed by tapping the tube and incubated for 10 min at RT. To inhibit the trypsin 200 µl solution B (containing RNase) were added and mixed. This mixture was incubated for 10 min at RT. The staining was done by adding 4°C cold solution C (PI staining solution). After mixing the samples were incubated for 10 min on ice in the dark. The analysis was done with a flow cytometer (FACS Calibur; BD Biosciences).

5.5 - Immunocytochemistry

5.5.1 - Immunocytochemistry staining of cells on chamberslides

8-well micro chamber-slides were coated with fibronectin (5 µg/ml) for 1 h at RT. $2x10^4$ cells were seeded per well and cultured for 24 h. Cells were fixed in 4% (w/v) paraformaldehyde [PFA in PBS; pH 7.4] for 15 min and washed once with PBS. For permeabilization, cells were incubated for 5 min in 0.025% (w/v) saponin in PBS. Blocking was achieved with 2% (w/v) BSA in PBS for 30 min. The primary antibodies directed against uPAR (IIIF10) (mouse monoclonal IgG; 0.5 mg/ml; 1:100; Luther et al., 2003) and Rab31 (C15) (rabbit polyclonal IgG; 100 µg/ml; 1:100; Santa Cruz) respectively, were added to the cells for 1.5 h followed by the secondary Alexa-488-conjugated antibody (goat/rabbit polyclonal IgG; 2 mg/ml; 1:1000; Life Technologies) for 45 min in the dark. All steps were done at RT. Slides were mounted with PBS and the fluorescence intensity was determined with a confocal laser-scanning microscope (CLSM) (Zeiss Axio Observer Z1). In order to convert fluorescence staining intensity into colors, the look-up table “glowOv/Un LUT” provided with the CLSM scanning software (ZEN 2011; black edition version 7.0). Negative control staining was done with the secondary Alexa-488-conjugated IgG only.

5.6 - Western blot analysis

5.6.1 - Cell lysis for SDS-PAGE

For preparation of whole cell lysates, cells were detached using PBS/EDTA and washed with PBS. The cell pellet was lysed in 50 to 100 µl of lysis buffer [TBS; 1% (v/v) Triton-X-100; Complete proteases inhibitor cocktail tablet with EDTA (Roche) for 50 ml lysis buffer]. After incubation for 1 h on ice, lysates were centrifuged at 2000 g and the supernatant containing soluble proteins was used for further experiments or frozen at -20°C. The cell debris pellet was discarded. The total protein content was determined using the BCA Protein Assay Kit according to the manufacturer's instructions (Thermo Scientific).

5.6.2 - Western blot analysis (semidry and wet blot)

Reducing sample buffer [1 mM Tris; pH 6.8; 7.5% (w/v) glycerin; 2.6% (v/v) 2-mercaptoethanol; 3% SDS (w/v)] was mixed with 20 µg total protein of each sample and boiled for 10 min at 95°C. Proteins were separated on 12% acrylamide (Rotiphorese 40; CarlRoth) SDS-PAGE (Bio Rad) for 2 h at 125 V. For transfer onto a polyvinylidene difluoride (PVDF) membrane (Immobilon; Millipore) either a semidry or a wet blotting device (Bio Rad) was used.

For semidry blotting different anode buffers [20% (v/v) ethanol; 50 mM boric acid; pH 8.8] and cathode buffers [5% (v/v) ethanol; 50 mM boric acid; pH 8.8] were used. The blotting was performed at 75 mA for 2 h at RT. Wet blotting was done with a glycine buffer [20% (v/v) ethanol; 25 mM Tris; 192 mM glycine] at 350 mA for 1.5 h on ice.

After blotting the PVDF membrane was washed once in TBST [TBS; 1% (v/v) Tween-20]. Membranes were blocked for 1 h at RT in blocking solution [TBST; 5% (w/v) milk powder]. After washing with TBST the primary antibody was applied after dilution in blocking solution overnight at 4°C or for 1 h at RT. The horseradish peroxidase-conjugated secondary antibody was diluted 1:10,000 (1 mg/ml) in TBST with 1% (w/v) milk powder and applied for 1 h at RT followed by three washes with TBST. Proteins were visualized using ECL chemiluminescent 3,3',5,5'-tetramethylbenzidine (TMB; Bio Rad) according to the manufacturer's recommendations. In order to normalize differences in protein loading and blotting efficiency, membranes were subsequently stripped [0.2 M NaOH], blocked for 30 min with 5% (w/v) milk powder in TBST and re-probed with monoclonal antibody directed against the endogenous control glyceraldehyde 3-phosphate dehydrogenase (GAPDH; monoclonal IgG; 1 mg/ml; 1:10,000; Millipore).

5.7 - ELISA

The enzyme-linked immunosorbent assay (ELISA) is a laboratory technique that uses antibodies for quantification of substrates. Here we used a so-called sandwich ELISA as described below (Figure 37).

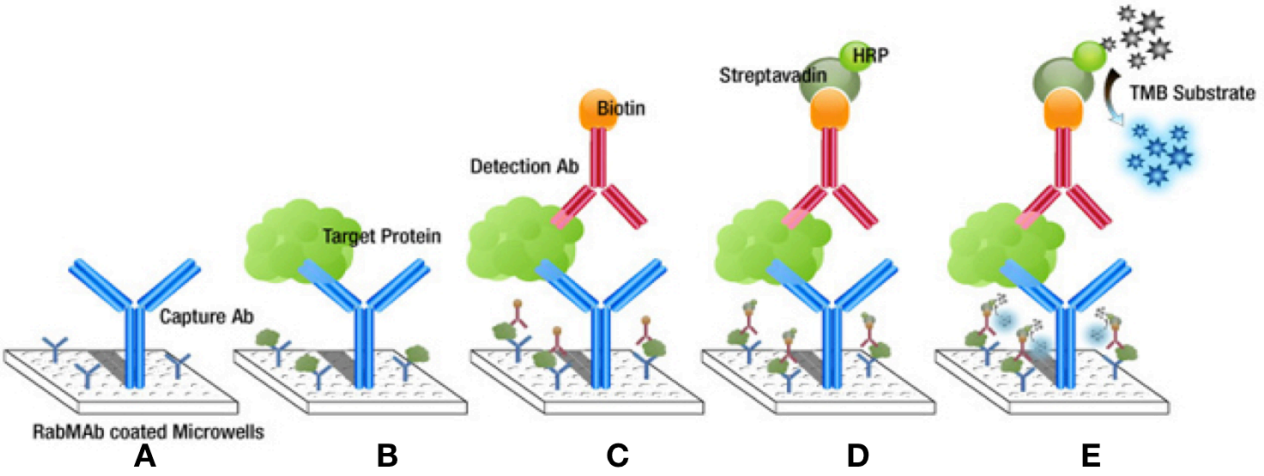

Figure 37 | Schematic representation of the sandwich ELISA assay
A) A 96-well plate is coated with the capture antibody (anti Rab31 or anti TGF-β1). **B)** After washing and blocking, the samples are applied and the protein of interest binds to the capture antibody. **C)** The detection antibody coupled with biotin binds to its substrate. **D)** Streptavidin coupled with horseradish peroxidase is applied. **E)** Addition of 3,3',5,5'-tetramethylbenzidine (peroxidase substrate), the amount of target protein is determined *via* a colorimetric reaction. Picture from http://www.epitomics.com/products/products/c-Jun-antibody-6115-1.html.

5.7.1 - RAB31 ELISA

For detection of Rab31 protein in cell lysates, a newly developed sandwich ELISA was used. The monoclonal anti-Rab31 capture antibody (M01, Novus; 0.5 mg/ml) was diluted 1:2500 in coating buffer [15 mM Na_2CO_3; 33 mM $NaHCO_3$; pH 9.6]. 96-well microplates (NUNC, Denmark) were coated with 100 µl per well of the diluted capture antibody overnight at 4°C. The next day the unbound antibody was aspirated, and plates were washed three times with washing buffer [PBS; 0.05% Tween-20; pH 7.4]. To minimize nonspecific binding, wells were then blocked by adding 200 µl of blocking buffer [PBS; 2% FCS] each and plates were incubated for 30 min at 37°C. Two-fold serial dilutions of a Rab31-His stock solution (25 µg/ml) diluted in sample buffer [TBS; 1% BSA] served as Rab31 standard (0.15; 0.31; 0.62; 1.25; 2.5; 5.0; 10 ng/ml). Plates were incubated with 100 µl of standards or samples, diluted in sample buffer, for 90 min at 37°C. Following three aspiration/wash steps, 100 µl of detection antibody (polyclonal rabbit anti-Rab31, animal 4, IgG-purified) diluted 1:200 in blocking buffer were added to each well and incubated for 90 min at 37 °C. After washing plates three times, 100 µl of peroxidase-labeled goat anti-rabbit IgG antibody (Novus; 0.5 mg/ml) diluted 1:1000 in blocking buffer was added to each well, and plates were incubated for

60 min at 37°C. Following incubation, the aspiration/wash step was repeated three times. A total of 100 µl of 3,3',5,5'-tetramethylbenzidine (TMB; Thermo Scientific), a soluble colorimetric substrate for horseradish peroxidase, was added to each well, and plates were incubated for 20 min at room temperature in the dark. The optical density was measured at 450 nm using a multichannel microplate reader (SLT Spectra). Absorbance values were converted into ng/ml of Rab31 by reference to the standard curve. Finally, Rab31 values were expressed as ng Rab31 per mg of total protein content of cell lysates determined by using the BCA protein assay kit, Sigma).

5.7.2 - TGF-β1 ELISA

TGF-β1 concentration in cell lysates and cell culture supernatants was determined using a specially designed sandwich ELISA (R&D Systems). To activate latent TGF-β1 to the immunoreactive form, an acidification step was necessary. For this an acidification solution [1 M HCl; 1.2 M NaOH; 0.5 M HEPES] and neutralization solution [1.2 M NaOH; 0.5 M HEPES] were prepared. A test activation to exactly define the acid/base volumes for the desired pH-values was performed. To 1 ml complete medium 20 µl of acidification solution were added and mixed. After incubation for 10 min at RT the pH was approximately 2. To neutralize the acidified sample 20 µl of neutralization solution was added and mixed. The pH now was between 7.2 and 7.6. The capture antibody (anti-TGF-β1; 360 µg/ml) was diluted 1:180 in PBS. A 96-well microplate was coated with 100 µl per well of the diluted capture antibody. The plate was sealed and incubated overnight at RT. Each well was washed with wash buffer [PBS; 0.05% Tween20; pH 7.2-7.4] three times. The complete removal of buffer at each step was essential for good performance. The plate was blocked by adding 300 µl of blocking buffer [PBS; 5% Tween20; pH 7.2-7.4] to each well followed by incubation at RT for a minimum of 1 h. The aspiration/wash steps were repeated. All samples were diluted in reagent diluent [PBS; 1.4% BSA (w/v); 0.05% Tween20; pH 7.2-7.4; 0.2 nm filtered] resulting in identical protein concentrations. For preparation of a standard series TGF-β1 was diluted in 100 µl to 0, 31.3, 62.5, 125, 200, 250, 500 and 1000 pg/ml in reagent diluent. The plates were sealed with an adhesive strip and incubated 2 h at RT. The aspiration/wash step was repeated. 100 µl of the detection antibody (54 µg/ml) per well were added after dilution (1:180) in reagent diluent. The plates were covered and incubate 2 h at RT. The aspiration/wash step was repeated. 100 µl of the working dilution (1:200) of Streptavidin-HRP were added to each well and incubated in the dark for 20 min at RT. The aspiration/wash step was repeated. 100 µl of substrate solution [1:1 mixture of Color Reagent A (H_2O_2) and Color Reagent B (Tetramethylbenzidine)] were added to each well and incubated for 20 min at RT in the dark. Subsequently 50 µl of stop solution [2 M H_2SO_4] were added to each well. The optical density of each well was immediately measured at 450 nm, using a microplate reader (SLT Spectra).

The cell culture supernatant for use in TGF-β ELISA was concentrated 16-fold in a spin column (10,000 MW cut off, Vivaspin 6; Sartorius Stedim) at 4°C with 4,500 g.

5.8 - qPCR

5.8.1 - Isolation of RNA

The RNA of MDA-MB-231 and CAMA-1 breast cancer cells was isolated using the RNeasy Mini kit (Qiagen) in combination with the QIAcube (Qiagen) fully automated spin column system. Total RNA was isolated after guanidine-isothiocyanate lysis of cells; ethanol was added to the lysate to provide ideal binding conditions for the silica-membrane purification with a minimum co-purification of DNA. The RNA binds to the column, and all contaminants were efficiently washed away. An on-column DNase (Qiagen) treatment was performed done for every sample. The applied protocol was for animal tissues and cells with an on column DNase digest. All st4eps were conducted according to the manufacturer´s manual. The Nanodrop ND1000 (Peqlab) was used to assess the concentration and purity of the isolated RNA.

5.8.2 - Reverse transcription for qPCR

Reverse transcription of the isolated RNA was conducted using the cloned AMV first-strand cDNA Synthesis Kit (Invitrogen). The cDNA synthesis was performed using total RNA with random hexamers as primers as follows:

Isolated RNA	1.0 µg
Random hexamer primers (50 ng/µl)	1.0 µl
H_2O	x µl
	10.0 µl

Isolated RNA, template and primers were incubated at 65°C for 5 min to remove secondary structures that might impede full-length cDNA synthesis.

For the reverse transcription the following master mix was added to the isolated RNA/primer mixture:

DTT (0.1 M)	1.0 µl
dNTPs (10 mM)	2.0 µl
RNase inhibitor (40 U/µl)	1.0 µl
AMV-rev transcriptase (15 U/µl)	1.0 µl
H_2O	1.0 µl
Buffer (5x)*	4.0 µl
	10.0 µl per well

* [250 mM Tris acetate; pH 8.4; 375 mM potassium acetate; 40 mM magnesium acetate; 20 µg/mL BSA]

The PCR reaction was assembled on ice and the PCR amplification program was started immediately according to this program:

Step 1:	10 min	at	25°C
Step 2:	45 min	at	60°C
Step 3:	5 min	at	85°C

The generated cDNA was diluted 1:5 with H_2O to a concentration of 10 ng/µl and stored at -20°C until use.

5.8.3 - qPCR WITH LINEAR FLUORESCENT PROBES

Linear probes are the most widely used detection chemistry for qPCR applications. In addition to the PCR primers, this chemistry includes a third oligonucleotide in the reaction. A fluorescent reporter dye, *e.g.* FAM, is attached to the 5´-end of the probe. Fluorescence of FAM is quenched by a quencher at the 3´-end of the probe. As long as the reporter dye and the quencher are in close proximity, no fluorescence is detected at the reporter emission wavelength. TaqMan (Life Technologies) probes use the phenomenon called FRET (Fluorescence Resonance Energy Transfer) as the quenching mechanism. The probe is designed to anneal to one strand of the target sequence just slightly downstream of one primer. As the polymerase extends that primer it will degrade the probe with its exonuclease activity. The degradation of the probe releases the reporter dye from the quencher. Now the flourophor emits fluorescence after excitation with an external light source. The quantity of emitted light is proportional to the increase of the generated DNA (Figure 38).

5.8.3.1 - qPCR using Life Technologies primers

The Brilliant III QPCR Master Mix with low ROX (a fluorescein derivate) (Agilent Technologies) in combination with another fluorescein derivate (FAM) labeled probes and primers (Life Technologies) and the Stratagene Mx3005P qPCR System (Agilent Technologies) were used for qPCR quantification of huRAB31, huTGFB1 and huHPRT1. The concentration of cDNA per qPCR run was 30 ng. The different expression levels were normalized to huHPRT1 as a housekeeping gene. For comparison of different expression levels at different time points a calibrator was used. Non-template control (NTC) qPCR, with H_2O instead of cDNA, was used as a negative control. The human RAB31, TGFB1, HPRT1 qPCR master mix was composed as follows:

2x Brilliant II qPCR master mix	10.0 µl
Probe and primer mix (20x)	1.0 µl
H_2O	6.0 µl
	17.0 µl
cDNA (10 ng/µl)	3.0 µl

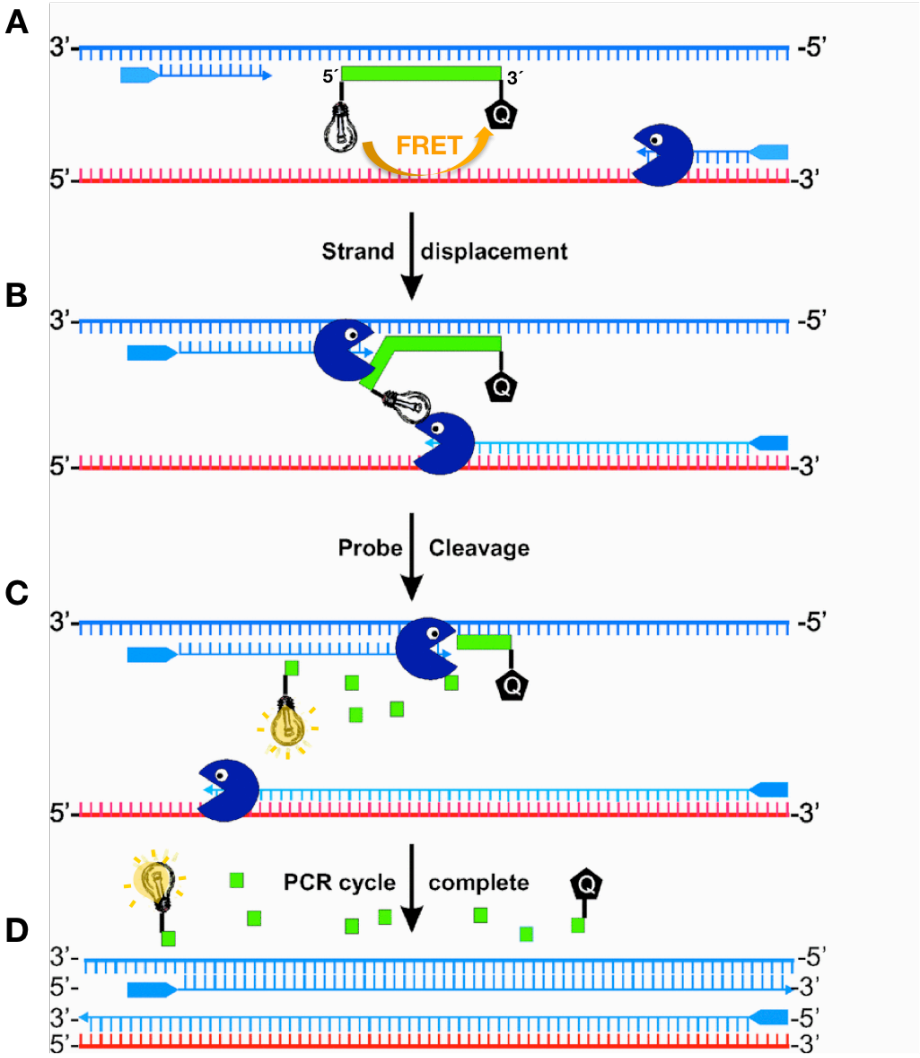

Figure 38 | Schematic representation of qPCR with linear fluorescent probes
A) The probe is designed to anneal to one strand of the target sequence just slightly downstream of one primer. **B)** As the polymerase extends the primer degrades the probe with its 5´-3´exonuclease activity. **C)** The degradation of the probe releases the reporter dye from the quencher. **D)** The fluorescence proportional to the amount of cDNA can be detected. Picture modified from http://www.clinsciusa.org/cs/109/0365/cs1090365f03.htm?resolution=HIGH.

All reactions were performed in triplicates. The samples were pipetted in 96 well plates, sealed with an optical strip and centrifuged for 1 min at low speed to remove air bubbles. According to the recommendation of the manufacturer the following qPCR program was used:

Step 1:	2 min	at	50°C
Step 2:	10 sec	at	95°C
Step 3:	15 sec	at	95°C
Step 4:	1 min	at	60°C
Step 5:	go to step 3		40x

5.8.3.2 - qPCR using the Roche Universal ProbeLibray

To analyze the expression levels of different genes the Universal ProbeLibrary (Roche) was used. The qPCR master mix was composed as follows:

Primer forward (100 µM)	0.25 µl
Primer reverse (100 µM)	0.25 µl
Universal ProbeLibrary probe (10 µM)	0.25 µl
Fast Start TaqMan Probe Master Mix (2x)	12.5 µl
H_2O	1.75 µl
	15.0 µl
cDNA (0,5 ng/µl)	10.0 µl

Normalization of the result was done using 18S RNA expression. The 18S qPCR master mix was composed as follows:

Primers S18 (100 µM)	1.25 µl
Universal ProbeLibrary probe (10 µM)	0.25 µl
Fast Start TaqMan Probe Master Mix (2x)	12.5 µl
H_2O	1.0 µl
	15.0 µl
cDNA (0.1 ng/µl)	10.0 µl

All reactions were performed in triplicates. The samples were pipetted in 96 well plates, sealed with an optical strip and centrifuged for 1 min at low speed to remove air bubbles. The samples were measured in an ABI PRISM 7900HT RealTime-PCR System (Applied Biosystems) with the following program:

Step 1:	2 min	at	50°C
Step 2:	10 min	at	95°C
Step 3:	10 sec	at	95°C
Step 4:	1 min	at	60°C
Step 5:	go to step 3		40x

5.8.4 - SABiosciences array qPCR

The SABiosciences arrays are designed to analyze a panel of genes related to a disease or a biological pathway. The plates contain primers for 84 pathway- or disease-focused genes and five housekeeping genes. In addition, one well contains a genomic DNA control, three wells contain reverse-transcription controls, and three wells contain positive PCR controls. The RT² First Strand Kit provides the first strand cDNA synthesis, one genomic DNA elimination step and a built-in external RNA control. This kit is designed and optimized for real-time PCR-based gene expression analysis with SABiosciences RT² Profiler PCR Arrays. Random hexamer primers were used for the reverse transcription. A built-in external RNA control helps monitor reverse transcription efficiency and test for enzyme inhibitors contaminating RNA samples when used together with RT² Profiler PCR Array. The RNA that was used for the reverse transcription was generated with the RNeasy Mini Kit (Qiagen) (chapter 5.8.1).

5.8.4.1 - Human EMT RT² Profiler PCR Array

The Human Epithelial to Mesenchymal Transition (EMT) RT² Profiler PCR Array (Qiagen) analyses the expression of 84 key genes. The array measures expression changes of EMT key genes (cell surface receptors, extracellular matrix proteins, and cytoskeletal components) or their regulators which control cell development, differentiation, growth, proliferation, transduction and transcription (Qiagen product site).

The procedure begins with the conversion of experimental RNA samples into first-strand cDNA using the First Strand Kit (Qiagen) as described above. Next, the cDNA was mixed with an appropriate SYBR Green master mix. This mixture was pipetted into the wells of the RT² Profiler PCR Array. PCR was performed and finally relative expression is determined using data from the real-time cycler and the ΔΔCt method (Figure 39). For the Human Epithelial to Mesenchymal Transition (EMT) RT² Profiler PCR Array a concentration of 3.0 µg RNA (MDA-MB-231 and CAMA-1) was used in each experiment. The manufacturers recommended protocols were strictly followed. For normalization of the results the five housekeeping genes were used.

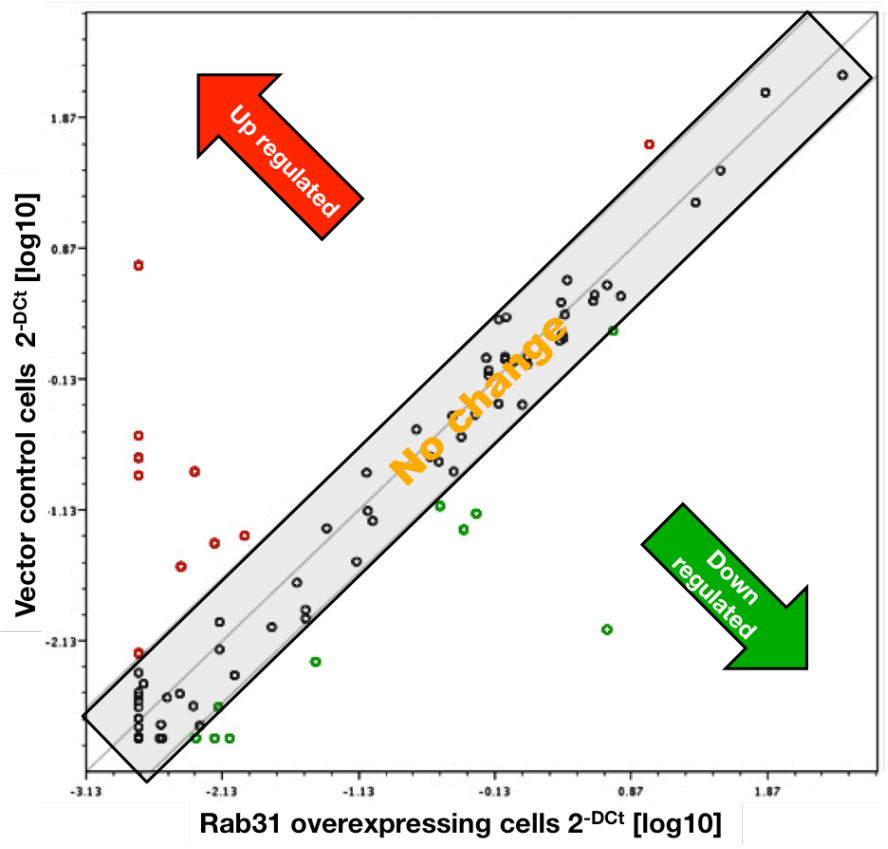

Figure 39 | Scatter blot presentation of the results of RT² Profiler PCR Array analysis
The relative mean expression levels for each gene are plotted against each other, dots in red represent candidate genes potentially up-regulated in Rab31-overexpressing cells, while green dots represent genes potentially down-regulated, each by at least two-fold. Black dots display relative expression changes lying between two-fold up- or down-regulation, the corresponding genes are considered as non-regulated.

5.8.4.2 - Human TGF-β RT² Profiler PCR Array

The Human TGF-β Signaling Target RT² Profiler PCR Array (Qiagen) profiles the expression of 84 key genes involved in TGF-β signal transduction. This array includes TGF-β signaling transcription factors and highly relevant target genes (Qiagen product site).

The procedure was carried out as described for the EMT RT^2 Profiler Array except for usage of 1.5 µg of RNA (MDA-MB-231 and CAMA-1) per array (chapter 5.8.4.1).

5.9 - STATISTICS

Data was analyzed for statistical significance using the Mann-Whitney Utest supported by the software StatView. Differences with a p-value ≤0.05 were denoted as statistically significant (*). P-values ≤0.01 and ≤0.001 were marked (**) and (***), respectively.

6 - RESULTS

6.1 - GENERATION OF BREAST CANCER CELLS CO-OVEREXPRESSING RAB31 AND uPAR-Δ4/5

The urokinase receptor splice variant uPAR-Δ4/5 has been demonstrated to be an independent, so-called pure prognostic factor in breast cancer (Kotzsch et al. 2008). Patients with high uPAR-Δ4/5 levels in tumor tissues have a shorter overall and metastasis free survival. Further studies focusing on the tumor biological role of uPAR-Δ4/5 (Luther et al. 2003; Sato et al. 2010) showed that while uPAR-Δ4/5-overexpression does not enhance proliferation in breast cancer cells, it reduces cell adhesion towards different ECM proteins such as vitronectin, collagen type I and IV, and fibronectin. Additionally, uPAR-Δ4/5-overexpression was found to significantly decrease the invasive capacity of breast cancer cells *in vitro* and to impair metastatic dissemination and growth *in vivo* (Grismayer et al. 2012a).

Similarly, patients with high Rab31 levels have a shorter overall and metastasis-free survival (Kotzsch et al. 2008). Furthermore, the effects of Rab31-overexpression were investigated in different breast cancer cell lines *in vitro* and *in vivo*. Rab31 was found to increase cell proliferation and to decrease the ability to adhere to ECM proteins in a dose-dependent manner. Additionally, in *in vitro* invasion studies, Rab31-overexpressing cells display a significantly decreased invasive capacity through Matrigel. In a xenograft mouse model, a significantly impaired metastatic dissemination of Rab31-overexpressing MDA-MB-231 breast cancer cells to the lung was observed (Grismayer et al. 2012b).

In breast cancer, expression of Rab31 is moderately correlated with uPAR-Δ4/5 (r_s=0.514). Furthermore, both factors independently contribute to patients' prognosis (Kotzsch et al. 2008). Therefore, it seems more likely that Rab31 mRNA may be differentially expressed in tumors with high *versus* low aggressiveness, independent of uPAR-Δ4/5.

To test, whether simultaneous overexpression of both Rab31 and uPAR-Δ4/5 leads to additive or even synergistic effects on proliferation and adhesion batch-transfected breast cancer cell line co-overexpressing both factors was generated.

6.1.1 - STABLE TRANSFECTION OF BREAST CANCER CELLS

To generate Rab31 and uPAR-Δ4/5 co-overexpressing cells, two different expression vectors were introduced into one cell line, either by transfecting an expression vector in an already existing stably transfected cell line or by transfecting two different expression vectors into the parental cell line (Figure 40).

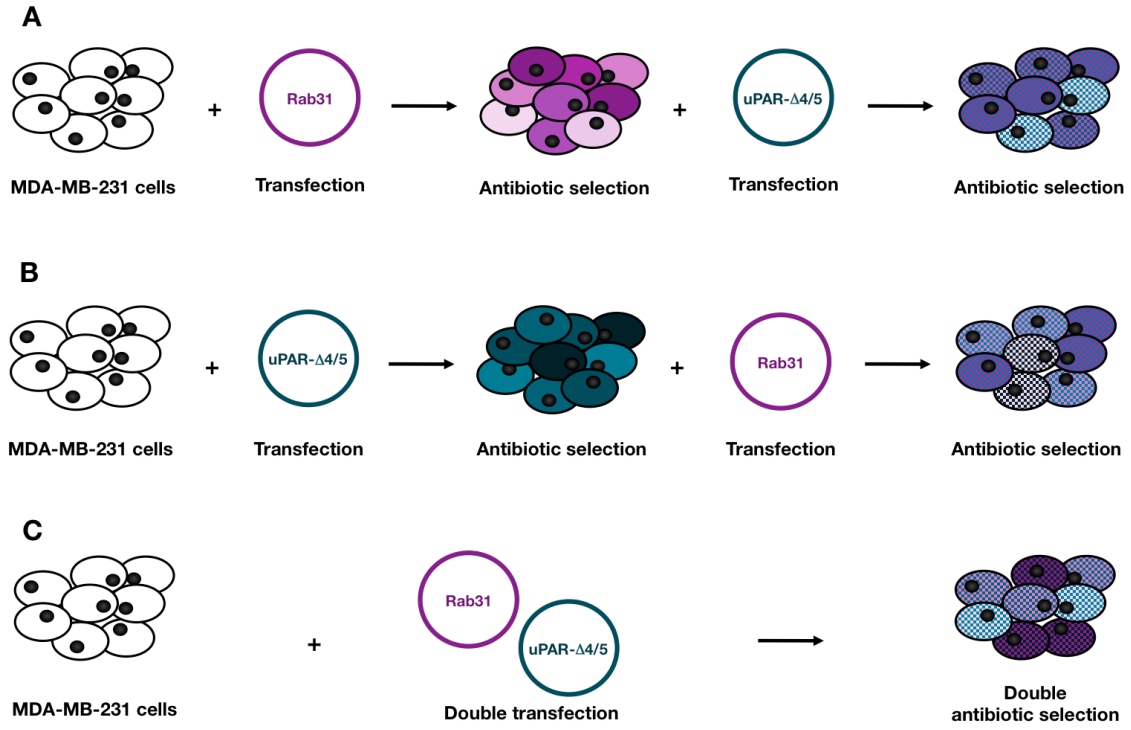

Figure 40 | Three different strategies for generation of MDA-MB-231 cells overexpressing uPAR-Δ4/5 and Rab31
A: MDA-MB-231 cells are first transfected with pRc-RSV-Rab31 vector followed by a geneticin antibiotic selection. After confirmation of Rab31-overexpression, *via* Western blot analysis, a second transfection with pcDNA3.1Hygro$^+$-uPAR-Δ4/5 vector is performed (antibiotic selection with hygromycin).
B: MDA-MB-231 cells are first transfected with pRc-RSV-uPAR-Δ4/5 vector followed by a geneticin antibiotic selection. After confirmation of uPAR-Δ4/5-overexpression, *via* Western blot analysis, a second transfection with pcDNA3.1Hygro$^+$-Rab31 vector is performed (antibiotic selection with hygromycin).
C: MDA-MB-231 cells are co-transfected with both plasmids and antibiotic selection with both antibiotics is performed in parallel.

A pcDNA3.1Hygro$^+$-based uPAR-Δ4/5 expression plasmid was introduced into Rab31-overexpressing MDA-MB-231 cells (based on an incorporated pRc-RSV-Rab31 expression vector) (Grismayer et al. 2012a; Grismayer et al. 2012b) (Figure 40 A). As expected, the resulting cells were resistant against both antibiotics used to select for the incorporation of the vectors. uPAR-Δ4/5 expression was profoundly up-regulated in these cells (as tested by Western blot analysis, data not shown). Strikingly, however, a strong concomitant reduction of the Rab31 expression was observed. The transfection

was repeated several times, but yielded always the same result (data not shown). Similarly, using uPAR-Δ4/5-overexpressing cells for transfection of a pcDNA3.1Hygro^{+}-based Rab31 expression vector (Figure 40 B) resulted in a weak Rab31 expression (data not shown). The only strategy, which gave rise to MDA-MB-231 cells overexpressing both Rab31 and uPAR-Δ4/5, was to transfect both plasmids simultaneously (Figure 40 C).

6.1.2 Characterization of the overexpression of Rab31 and uPAR-Δ4/5 overexpression in MDA-MB-231 cells

The Western blots of the co-transfected MDA-MB-231 batch culture showed that transfection and subsequent overexpression of Rab31 and uPAR-Δ4/5 were successful. As shown in Figure 41, MDA-MB-231 vector control cells display low intrinsic levels of Rab31 und uPAR (left panel). uPAR is highly and heterogenously glycosylated, which results in a broad band in Western blot analysis. Cells transfected with a pRc-RSV-based uPAR-Δ4/5 expression vector result in a strong Western blot band of uPAR-reactive protein (Figure 41; middle left panel). Similarly, the blot of cells transfected with a pRc-RSV-based expression Rab31-vector demonstrate a strong signal of Rab31 (Figure 41; middle right panel). Upon co-transfection of both uPAR-Δ4/5 and Rab31 expression plasmids a simultaneous overexpression of uPAR-Δ4/5 and Rab31 is observed (Figure 41; right panel).

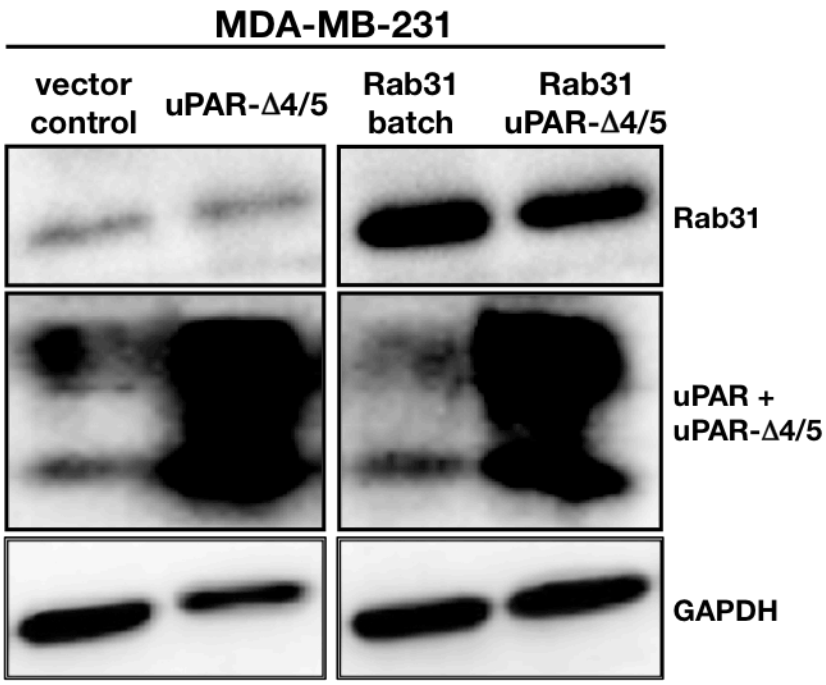

Figure 41 | Western blot analysis of MDA-MB-231 cells stably transfected with Rab31 and/or uPAR-Δ4/5 expression vectors
The vector control cells displays low intrinsic Rab31 and uPAR levels (left panel). A substantial overexpression of uPAR-Δ4/5 (or Rab31 (batch)) is observed in cells stably transfected with the uPAR-Δ4/5 (or Rab31) expression vector (middle left panel for uPAR-Δ4/5; middle right panel for Rab31). The double overexpressing cells (referred as DOC) display significantly up-regulated protein levels for both Rab31 and uPAR-Δ4/5 (right panel). Detection of GAPDH expression served as loading control.

The uPAR-Δ4/5 and Rab31 protein levels were also visualized and quantified *via* confocal laser scanning microscopy after immunocytochemistry (ICC) staining.

The stably transfected MDA-MB-231 cells were grown on glass coverslips; after 24 h the cells were fixed and stained (Figure 42). For ICC staining, the polyclonal rabbit antibody C-15 (Santa Cruz Biotechnology) directed against Rab31 was used, because none of the in house-generated Rab31 antibodies, which were used for Western blot analyses, was found suitable for ICC (data not shown). The primary anti-Rab31 antibody was subsequently visualized using a secondary Alexa488-conjugated goat anti-rabbit-IgG (Invitrogen). To stain uPAR-Δ4/5, the monoclonal antibody IIIF10 (Luther et al. 2003), directed against domain I of uPAR was used. The primary anti-uPAR antibody was visualized with the help of a secondary Alexa488 conjugated goat anti-mouse-IgG (Invitrogen).

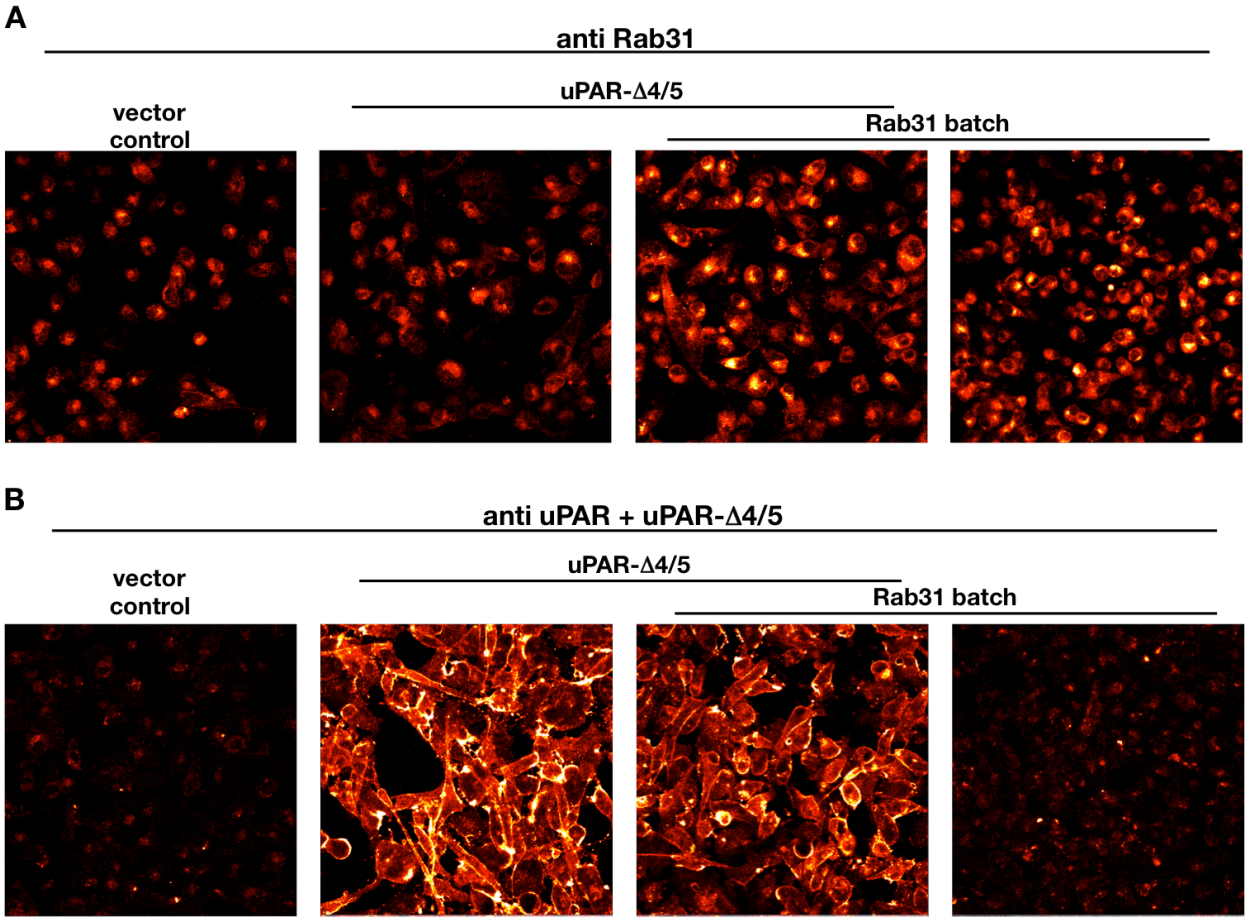

Figure 42 | Immunocytochemistry of MDA-MB-231 cells, stably transfected with Rab31 and/or uPAR-Δ4/5 expression vectors
A: Rab31 staining. Vector control and uPAR-Δ4/5-overexpressing cells display low Rab31 levels (as visualized by the dark red pseudo color). In the double overexpressing cells (DOC), Rab31 expression is high and comparable to cells transfected with a Rab31 expression vector only (orange / yellow pseudo color).
B: uPAR staining. A weak uPAR staining is observed in the vector control and in the Rab31-overexpressing cells. The cells transfected with an uPAR-Δ4/5 expression vector only and the DOC both show a strong and comparable uPAR-Δ4/5 staining. The staining intensity is given by a red to white representation (red: low-expression; white: high-expression). Magnification: 20x.

6.1.3 - Proliferation of MDA-MB-231 cells overexpressing Rab31 and uPAR-Δ4/5

From previous studies (Grismayer et al. 2012a) it is known that Rab31-overexpressing MDA-MB-231 cells proliferate faster than vector control cells, whereas overexpression of uPAR-Δ4/5 does not change their proliferative phenotype. To study the impact of simultaneous overexpression of both factors in MDA-MB-231 DOC cells, proliferation assays were performed (Figure 43). For this, cells were plated in triplicates and manually counted every 24 h for four days.

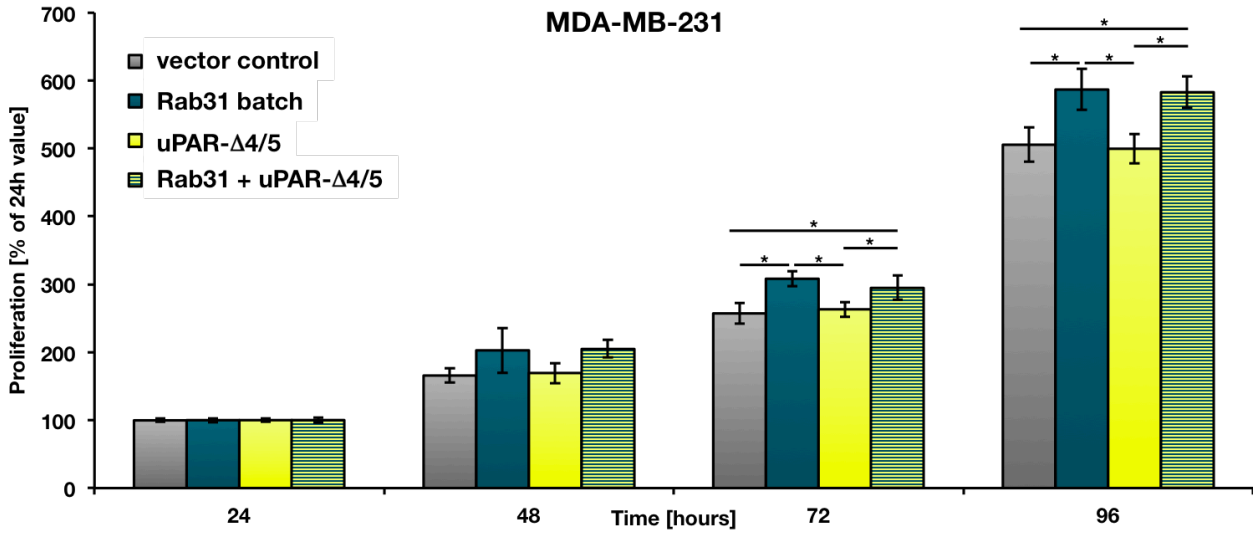

Figure 43 | Proliferation of MDA-MB-231 cells overexpressing Rab31 and/or uPAR-Δ4/5
Rab31-overexpressing and DOC cells proliferated significantly faster than the vector control or uPAR-Δ4/5-overexpressing cells. Cell numbers were normalized against the 24 h value. The graph shows the mean value of three independent experiments preformed in triplicates each. Statistically significant differences ($p<0.05$) are indicated by an asterisk.

Rab31-overexpressing cells displayed a faster proliferation rate than the vector control and the uPAR-Δ4/5-overexpressing cells, respectively. Furthermore, the vector control and uPAR-Δ4/5 cells did not differ in their proliferative behavior. Cells overexpressing both factors proliferated at the same rate as the Rab31-overexpressing cells, both growing significantly faster than vector control or uPAR-Δ4/5-overexpressing cells.

6.1.4 - Adhesive characteristics of MDA-MB-231 cells overexpressing Rab31 and uPAR-Δ4/5

A previous study showed that Rab31 as well as uPAR-Δ4/5-overexpressing breast cancer cells adhere less effectively to ECM proteins than vector control cells (Grismayer et al. 2012a). The question arose whether there is an additive or synergistic effect on the adherence to ECM proteins when both factors are overexpressed. 96 well plates were coated with different ECM proteins, cells were seeded, incubated, and finally, after washing hexosaminidase substrate was added. The chromogenic change was measured and the relative adhesion of the cell lines was normalized to the adhesion of vector control cells on each coating (Figure 44).

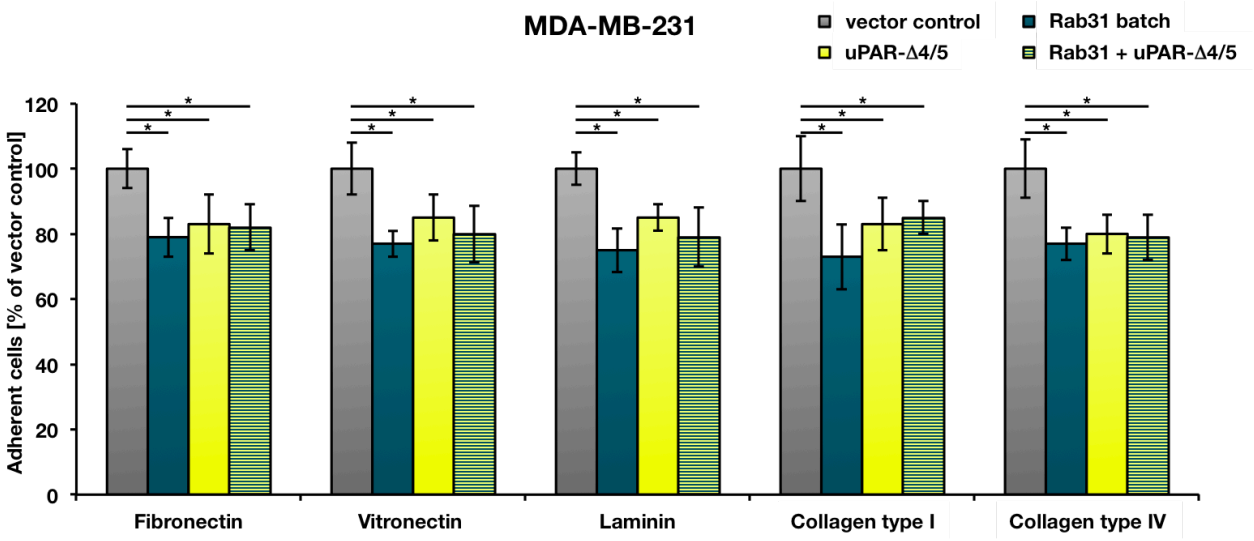

Figure 44 | Adhesion of MDA-MB-231 cells overexpressing Rab31 and/or uPAR-Δ4/5 to ECM proteins

Adhesion of Rab31- uPAR-Δ4/5- and DOC cells was significantly reduced compared to the vector control cells. At least three independent experiments were performed in triplicates each. The results are given in percent relative to the cell number of adherent vector control cells. Statistically significant differences ($p < 0.05$) are indicated by an asterisk.

In fact, in all cell lines overexpressing at least one of both factors (Rab31- uPAR-Δ4/5- or DOC cells) the adherence to different ECM proteins was significantly reduced compared to the vector control cells. However, there was no indication for an additive or synergistic effect on cell adhesion in Rab31/uPAR-Δ4/5 co-overexpressing cells (Figure 44).

6.2 - Knock-down of Rab31 mRNA levels in MDA-MB-231 cells

To further analyze the function of Rab31, we decided to knock-down Rab31 in MDA-MB-231 cells. Since CAMA-1 cells do not express Rab31 no knock-down experiments could be preformed in these cells.

6.2.1 - Transient transfection of siRNAs in MDA-MB-231 cells

Four different Rab31 siRNAs (flexi tube system; Qiagen) were used in transient knock-down (KD) experiments to select the two most efficient siRNAs for further stable knock-down experiments. After liposome-based transfection, the reduction of Rab31 expression on both protein and mRNA level was monitored over 72 h. As a control, scrambled siRNA (SCR) (Qiagen) was used.

6.2.1.1 - Rab31 real-time qPCR analysis in the transient KD MDA-MB-231 cells

Upon transient transfection with four siRNAs and the SCR control, mRNA levels of Rab31 were determined in the MDA-MB 231 cells. Real-time qPCR for Rab31 and HPRT1 as housekeeping gene for normalization was preformed (Figure 45).

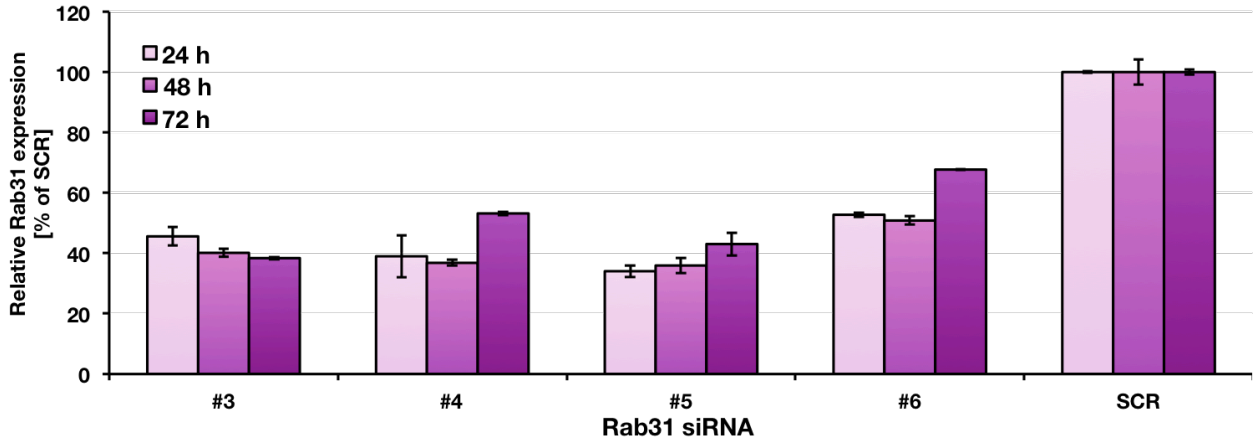

Figure 45 | Down-regulation of Rab31 mRNA levels upon transient transfection of siRNAs into MDA-MB-231 cells
The time points monitored were 24, 48 and 72 h after transfection. Rab31 mRNA reduction in percent is blotted against the SCR control. Three experiments were performed in triplicates each. All data are normalized to HPRT1.

Here, siRNAs #3 and #5 showed the strongest effects (reduction of mRNA levels up to 60%) on Rab31 expression.

6.2.1.2 - Rab31 Western blot analysis

In Western blot analyses, the strongest reduction of Rab31 protein levels was seen with siRNA #3, #5 and #6 after 48 h. Low Rab31 levels were observed up to 72 h (Figure 46).

Based on the results of both mRNA and protein expression, the sequences corresponding to the siRNAs #3 and #5 were selected for the generation of shRNAi expression vectors

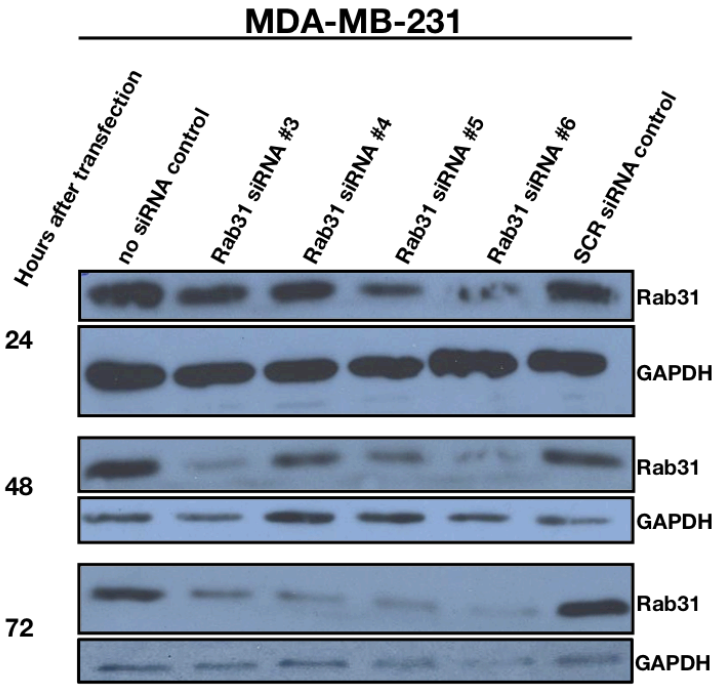

Figure 46 | Western blot analysis of Rab31 protein levels upon transient transfection of siRNAs into MDA-MB-231 cells
The time points monitored were 24, 48 and 72 h after transfection. The non-template control NTC and scrambled siRNA control (SCR) show no Rab31 reduction over time. The most distinct knock-down of Rab31 protein levels are seen after 72 hours. GAPDH served as a loading control.

6.2.2 - Expression of two different shRNAs directed to Rab31 mRNA in MDA-MB-231 cells

For the stable knock-down of Rab31 in MDA-MB-231 cells, the RNAi-Ready pSIREN-RetroQ vector (Clonetech) was used. The two different shRNA-expressing knock-down constructs were designed using the sequence of the siRNA #3 and #5 plus an additional *Sal* I restriction site (Figure 47) to be able to pre-select for insertion of the synthetic short DNA molecules into the vector by restriction analysis.

Figure 47 | Rab31-shRNAi sequences for cloning into the pSIREN-RetroQ vector
The sequence was designed with a *Sal* I restriction site (blue) after the terminator sequence (red). The highlighted sequences in grey (compatible to *Bam* HI and *Eco* RI-restricted DNA, respectively) are for cloning of the oligonucleotides into the pSIREN-RetroQ vector. The hairpin loop is marked in green in between of the two different target sense and anti-sense sequences (#3; #5).

The two shRNAi DNA constructs were synthesized (Metabion) and cloned into the pSIREN-RetroQ vector (restriction sites: *Bam* HI; *Eco* RI). Successful insertion of the short double-stranded DNA leads to a novel *Sal* I restriction site. The plasmids displaying a 1413 bp fragment corresponded to candidate clones harboring an shRNAi construct (Figure 48). Subsequently, the correct sequence of candidate clones encoding pSIREN-RetroQ-shRNA was verified by DNA sequencing (Metabion).

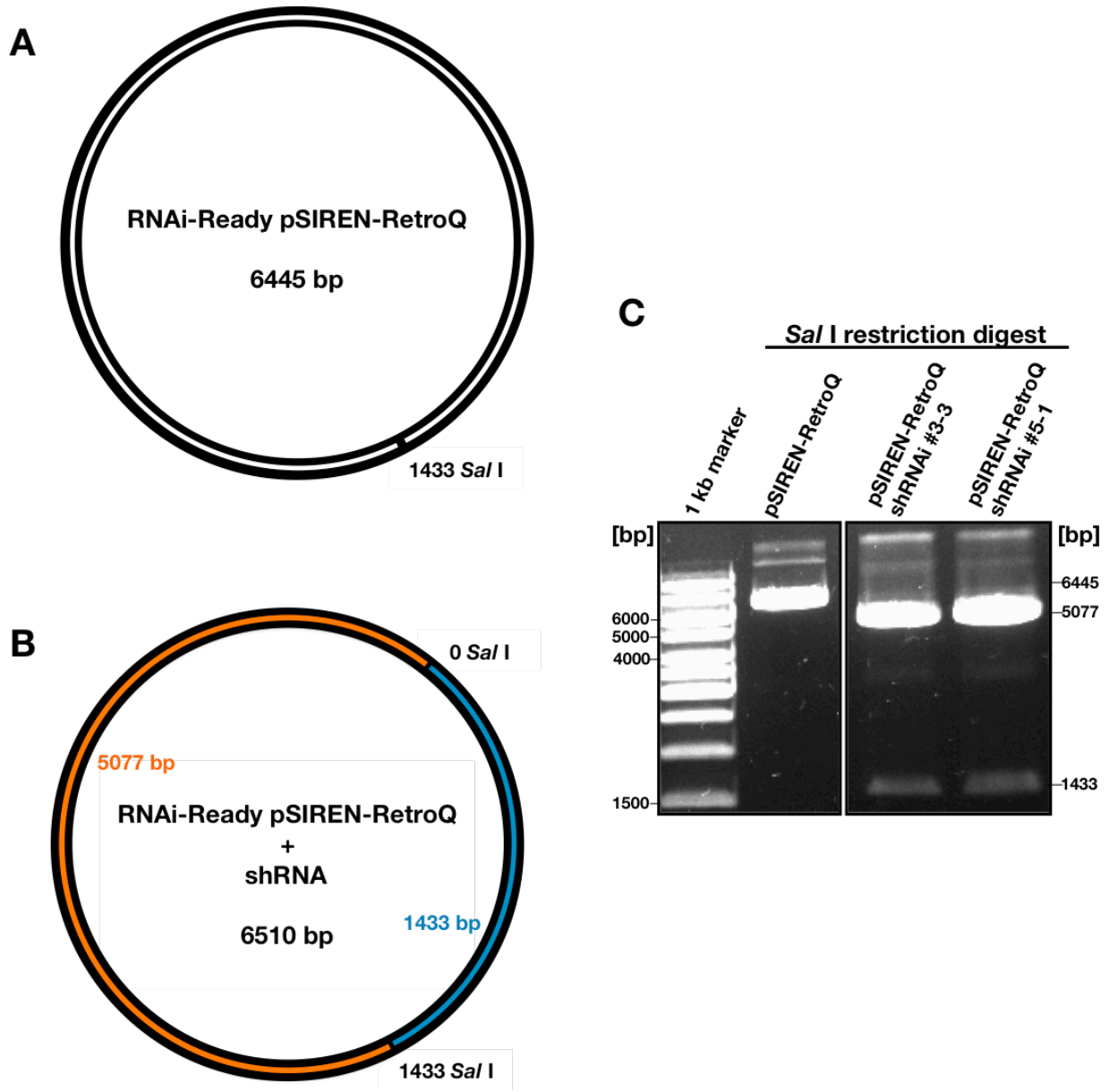

Figure 48 | *Sal*I restriction digest of pSIREN with and without shRNAi insert
A: Restriction map of pSIREN-RetroQ
B: Restriction map of pSIREN-RetroQ-shRNAi (#3 or #5)
C: pSIREN-RetroQ and pSIREN-RetroQ-shRNA digested with *Sal* I and separated on a 1% agarose gel. Whereas pSIREN-RetroQ is linearized only, pSIREN-RetroQ-shRNA displays two fragments (5077 and 1433 bp).

The human embryonic kidney (HEK 293)-derived cell line AmphoPack-293 (Clonetech) was electroporated with the Rab31 shRNAi (#3, #5 and SCR) vector. After stable integration of the vector into the genome of packaging cell line, the virus is produced and infectious virus particles bud into the supernatant. This supernatant is subsequently used to infect MDA-MB-231 cells.

6.2.3 - Analysis of MDA-MB-231 cells expressing Rab31-shRNAi

6.2.3.1 - Rab31 real-time qPCR analysis

To validate a potential down-regulation of RAB31 gene expression in response to expression of Rab31-shRNAi in MDA-MB-231 cells, Rab31 (and HPRT1) mRNA levels were quantified by qPCR (TaqMan gene expression assays; Life Technologies) in these cells (Figure 49). The housekeeping gene HPRT1 was used as reference to normalize the results.

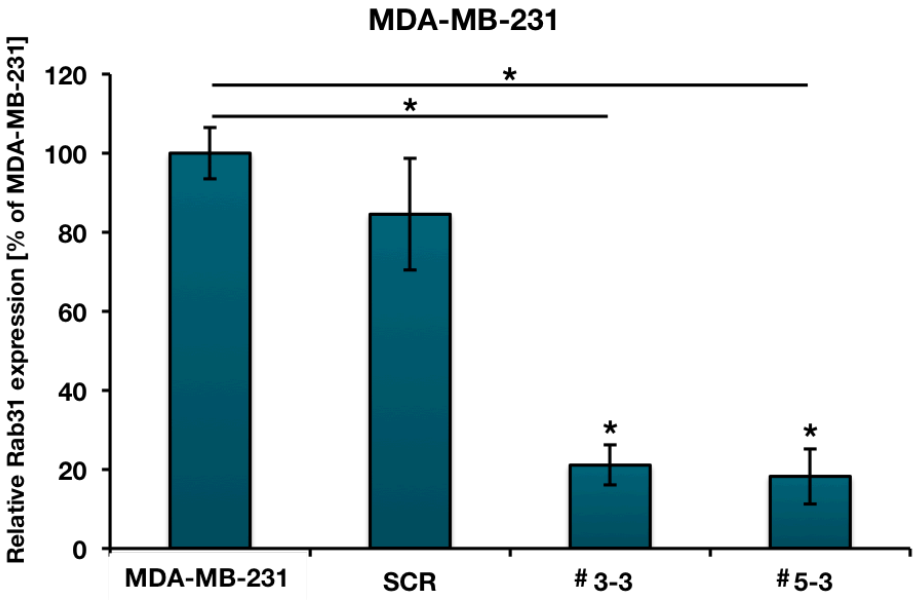

Figure 49 | Rab31 mRNA expression levels upon stable transfection of shRNAi-Rab31 vectors into MDA-MB-231 cells
Real-time qPCR analysis confirms a significant lower Rab31 mRNA expression in the stably transfected pSIREN-RetroQ-Rab31-shRNAi cells (#3-3; #5-3) as compared to parental MDA-MB-231 or stably transfected pSIREN-RetroQ-SCR cells. All samples were normalized to the HPRT1 expression level. At least three experiments were performed in triplicates each. Statistically significant differences ($p<0.05$) are indicated by an asterisk.

Stably transfected MDA-MB-231 cells expressing the scrambled control shRNAi (SCR) displayed similar Rab31 mRNA levels as the parental MDA-MB-231 cells, the cells expressing the selected Rab31-shRNAi (#3, #5) revealed a Rab31 mRNA knock-down of approximately 80%.

6.3.2.2 - Rab31 Western blot analysis

As shown in Figure 50, the Rab31 protein levels were considerably lower in both of the stably transfected MDA-MB-231 cells expressing the different shRNAi molecules (#3-3; #5-3) than in the cells expressing the scramble control shRNAi construct. Furthermore,

it can be seen that the Rab31 levels were similar in the clones expressing either one of the two different shRNAi constructs (#3 *versus* #5).

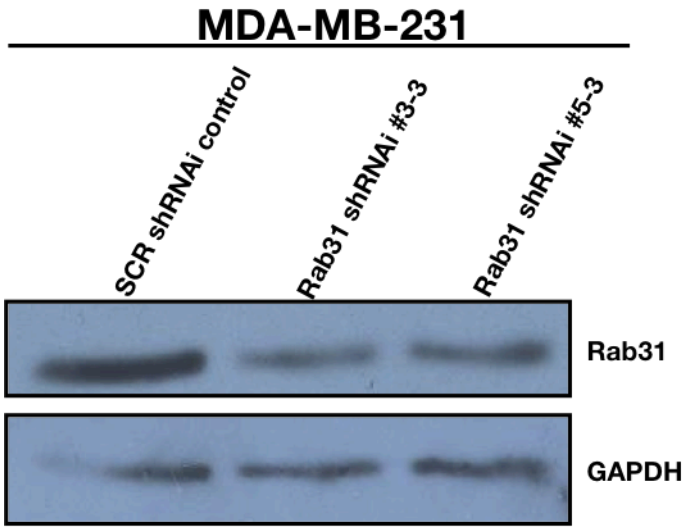

Figure 50 | Rab31 protein expression levels upon stable transfection of shRNAi-Rab31 vectors into MDA-MB-231 cells
Protein levels were determined by Western blot analysis. The knock-down of Rab31 protein expression is equally strong in both shRNAi-expressing cells. The cells expressing the scrambled control shRNAi show higher Rab31 protein levels. GAPDH served as a loading control.

6.2.4 - Proliferative characteristics of MDA-MB-231 cells with reduced Rab31 mRNA levels

Rab31-overexpressing MDA-MB-231 cells proliferate significantly faster than vector control cells displaying a rather low, basal Rab31 expression (Grismayer et al. 2012b and this work). To study the impact of reduced levels of Rab31, we now compared the growth behavior of stably transfected MDA-MB-231 cells expressing the scrambled shRNAi control with those expressing the shRNAi-Rab31 constructs (#3-3; #5-3) using an impedance-based proliferation method (Xcelligence) (Figure 51).

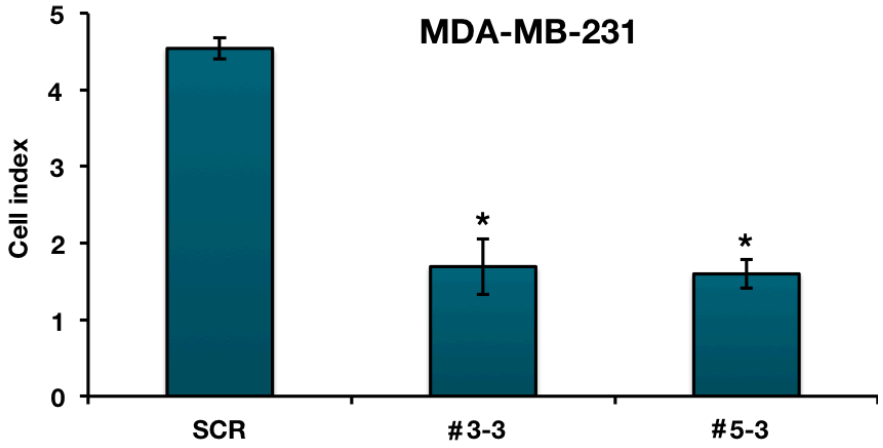

Figure 51 | Proliferation of MDA-MB-231 cells with reduced Rab31 levels compared to SCR control cells
For the measurement of the proliferation rates, the Xcelligence system was used and the impedance-based detection of viable adherent cells (cell index) recorded after 60 h. Each data point is the mean value of three independent experiments. Statistically significant differences ($p<0.05$) are indicated by an asterisk.

The cell index (which is a measure of the proliferation rate) of the Rab31 knock-down cells (#3-3; #5-3) is significantly lower when compared to the scrambled control cell line. Thus, these results indicate that Rab31, depending on its expression level, strongly affects the proliferation rate of the MDA-MB-231 breast cancer cells.

6.3 - Rab31 mutants

6.3.1 - Design of Rab31 mutants affecting the GTP/GDP cycle or membrane association

To analyze whether the function of Rab31 as membrane-bound GTPase is necessary for the observed effects of Rab31 overexpression on cell proliferation and adhesion, we aimed at generating Rab31-mutants resulting in a constitutively active form, an inactive form or a mutant unable to insert into the membrane of the Golgi apparatus (Figure 52).

The following three highly conserved regions were targeted in Rab31 by *in vitro* mutagenesis.

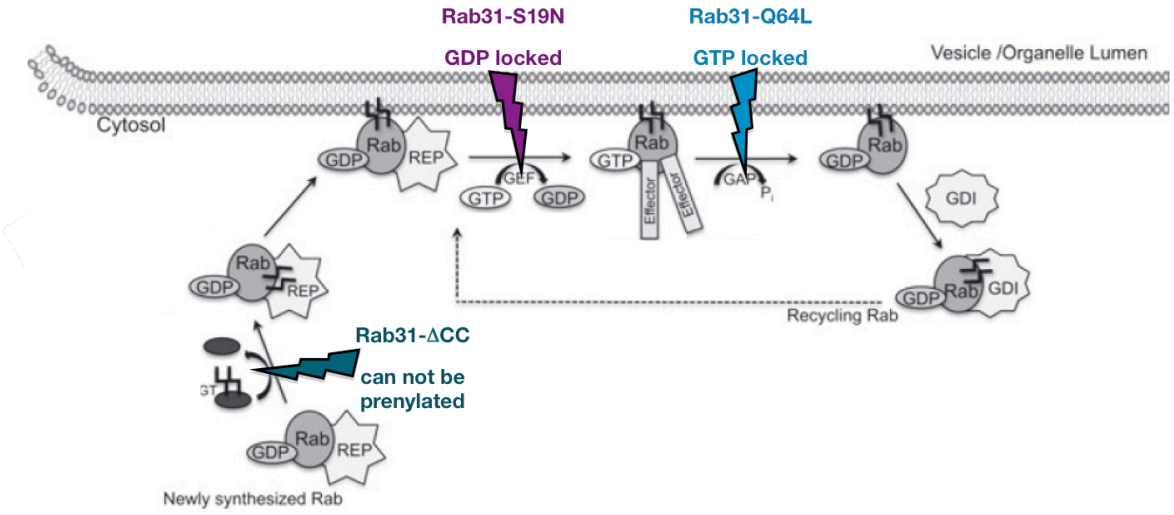

Figure 52 | The Rab31 mutants and their proposed properties within the Rab cycle
Newly synthesized Rab31 forms a complex with the Rab escort protein (REP) in an inactive, GDP-bound state. The geranylgeranyl transferase (GGT) modifies Rab31 with two geranylgeranyl lipid moieties, enabling association of Rab31 with the membrane of the Golgi apparatus. At the membrane, the guanine exchange factor (GEF) activates Rab by exchanging GDP with GTP. In this state, Rab interacts with different proteins and, by this, modulates intracellular vesicle transport. When GTP is hydrolyzed by the GTP activating protein (GAP), Rab31 becomes inactive and can be recycled through the cytosol by the GDP dissociation inhibitor (GDI) (Agola et al. 2011).

6.3.1.1 - GDP/GTP binding site: Rab31-Q64L (Figure 53)

As a GTPase, Rab31 harbors a highly conserved binding site for GDP/GTP. Within this conserved region glutamine 64 by leucine was exchanged by *in vitro* mutagenesis. The Q64L mutation blocks hydrolysis of GTP, therefore, Rab31-Q64L becomes constitutively active (Mesa et al. 2001).

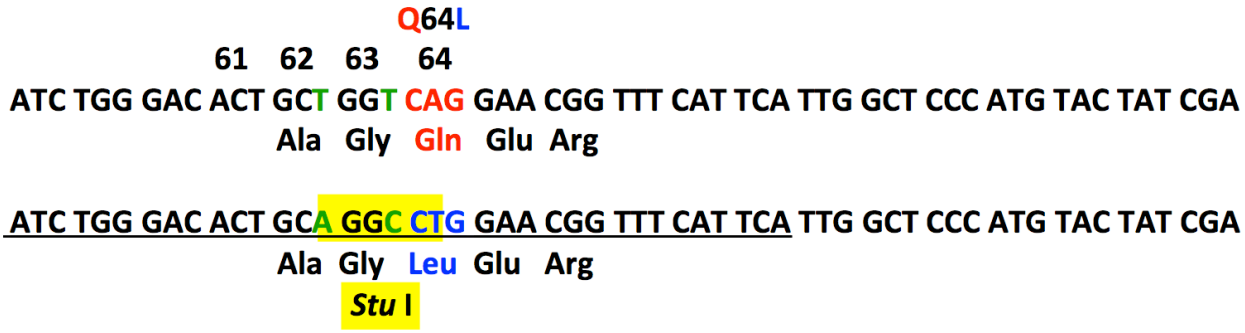

Figure 53 | Design of the Rab-Q64L mutant
The upper sequence shows part of the Rab31 cDNA with codon numbers, its nucleotide sequence and the corresponding amino acids. The lower sequence depicts the newly generated Rab31-Q64L mutation. Furthermore, a restriction site (*Stu* I) was generated (highlighted in yellow). The amino acid sequence was mutated at codon number 64 from a glutamine to a leucine (red and blue). The nucleotides depicted in green were changed to generate the new *Stu* I restriction site without altering the amino acid sequence. The underlined part indicates the primer used in the PCR reaction.

In case of pRc-RSV-Rab31-Q64L, a successful mutation also leads to a novel *Stu* I restriction site in the vicinity of the targeted codon 64. Following *in vitro* mutagenesis, the prepared plasmid DNA of several clones was cleaved with *Stu* I. The Rab31-WT plasmid was linearized whereas the pRcRSV-Rab31-Q64L digest results in two fragments (4173 and 1551 bp) (Figure 54). Subsequently, the correct sequence of candidate clones encoding Rab31-Q64L was verified by DNA sequencing (Metabion) of the complete coding sequence.

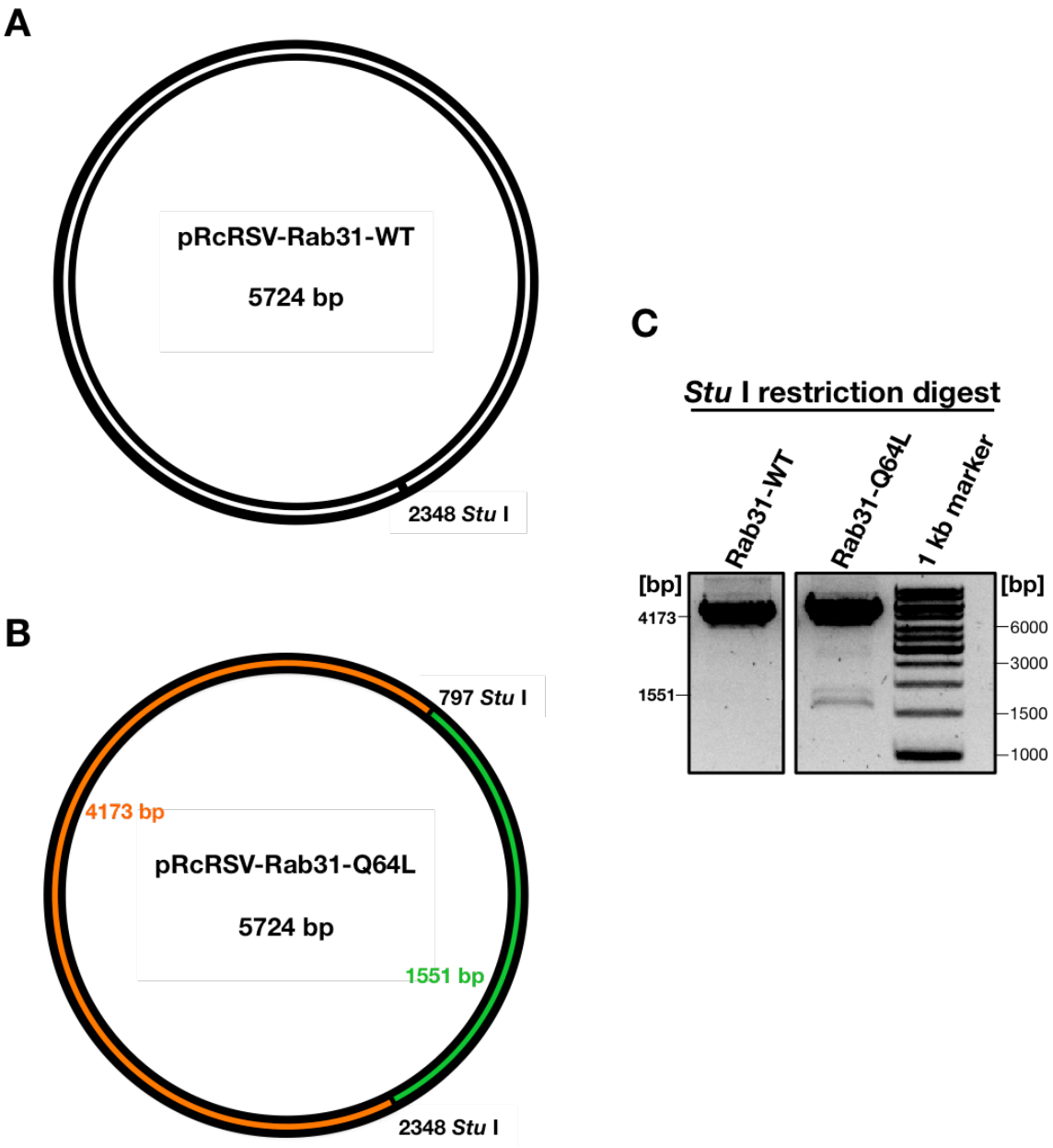

Figure 54 | Restriction digest of pRc-Rab31-WT and -Rab31-Q64L with *Stu* I
A: Restriction map of pRcRSV-Rab31-WT
B: Restriction map of pRcRSV-Rab31-Q64L
C: pRc-Rab31-WT and -Rab31-Q64L digested with *Stu* I and separated on a 1% agarose gel. Whereas pRcRSV-Rab31-WT is linearized, pRcRSV-Rab31-Q64L displays two fragments (4173 and 1551 bp).

6.3.1.2 - Inhibitory-type mutant: Rab31-S19N (Figure 55)

The amino acid serine 19 is highly conserved not only within the Rab family but also the Rho family of small GTPases. The exchange of Ser19 to asparagine has been shown to result in an inactive mutant, still binding to its interaction partners and, thus displaying dominant inhibitory effects, not only in Rab11A and Rab22B.

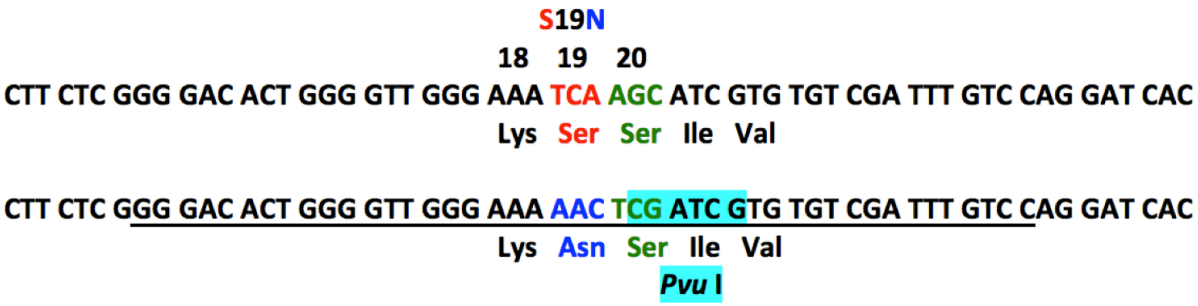

Figure 55 | Design of the Rab31-S19N mutant
The upper sequence shows part of the Rab31 cDNA with codon numbers, its nucleotide sequence and the corresponding amino acids. The lower sequence depicts the newly generated Rab31-S19N mutation. Furthermore, a restriction site (*Pvu* I) was generated (highlighted in light blue). The amino acid sequence was exchanged at codon number 19 from a serine to an asparagine (red and blue). The green depicted nucleotides were changed to generate a novel *Pvu* I restriction site without changing the amino acid sequence. The underlined part indicates the primer used in the PCR reaction.

In case of pRc-RSV-Rab31-S19N, a successful mutation also leads to a novel *Pvu* I restriction site in the vicinity of the targeted codon 19. Following *in vitro* mutagenesis, the prepared plasmid DNA of several clones was cleaved with *Pvu* I. The plasmids displaying a 213 bp fragment corresponded to candidate clones harboring the S19N mutation (Figure 56). Subsequently, the correct sequence of candidate clones encoding Rab31-S19N was verified by DNA sequencing (Metabion) of the complete coding sequence.

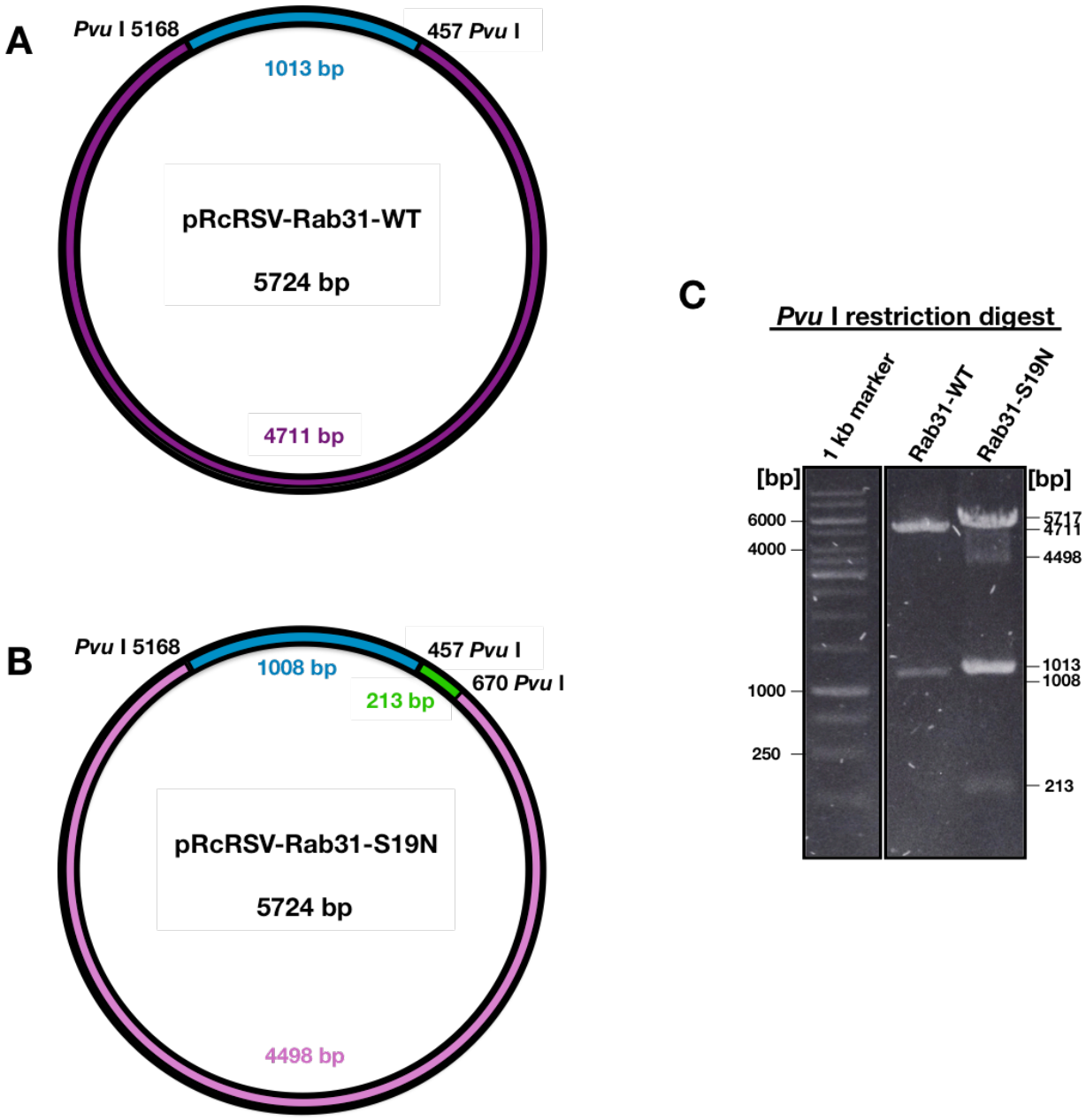

Figure 56 | Restriction digest of pRcRSV-Rab31-WT and -Rab31-S19N with *Pvu* I
A: Restriction map of pRcRSV-Rab31-WT
B: Restriction map of pRcRSV-Rab31-S19N
C: pRcRSV-Rab31-WT and -Rab31-S19N digested with *Pvu* I was separated on a 1% agarose gel. The restriction digest of pRc-RSV-Rab31-WT results in two fragments (4711 and 1013 bp). pRcRSV-Rab31-S19N displays three fragments (4498, 1008 and 213 bp).

6.3.1.3 - C-terminal prenylation site: Rab31-ΔCC (Figure 57)

Rab proteins are intrinsically cytosolic proteins, but only function when bound to membranes. For this, most Rab proteins, including Rab31, are posttranslationally modified with two geranylgeranyl lipid moieties that facilitate their link with membranes (Kauppi et al. 2001). To exclude membrane insertion of Rab31, an expression plasmid lacking the two terminal cysteines was generated. By this, its distribution in the cell is

altered, instead of being bound to the membrane Rab31-ΔCC, it is now located in the cytoplasm. This disruption of the C-terminal prenylation site should not change the properties of this Rab31 variant with respect to GDP/GTP binding and its GTPase activity. Still, its active function should be drastically decreased by not being attached to the membrane.

Figure 53 | Design of the Rab31-ΔCC mutant
The upper nucleotide sequence shows the 3' part of the Rab31 cDNA and the corresponding amino acid sequence. By *in vitro* mutagenesis, the *Xba* I restriction site of the vector (green) was deleted as well as four codon triplets. The lower sequence depicts the mutated Rab31-ΔCC construct with the newly generated stop codon (blue). The underlined part indicates the primer used in the PCR reaction.

In order to select for candidate clones encoding the Rab31-ΔCC mutant, restriction analysis was performed to analyze for the presence (Rab31-WT template) or absence of the *Xba* I restriction site, which is eliminated by the *in vitro* mutagenesis step.

A restriction digest of pRcRSV-Rab31-WT with *Pvu* I and *Xba* I results in three different fragments (3972, 1013 and 739 bp), whereas the pRcRSV-Rab31-ΔCC digest results in only two fragments (4697 and 1310 bp) (Figure 58). After restriction analysis of several clones, the correct sequence of candidate clones encoding Rab31-ΔCC was verified by DNA sequencing (Metabion) of the complete coding sequence.

6.3.2 - Generation of stably transfected breast cancer cells overexpressing Rab31-mutants

Both breast cancer cell lines MDA-MB-231 and CAMA-1 were stably transfected with the eukaryotic expression plasmid pRcRSV harboring the cDNA of wild-type Rab31 (Rab31-WT) or different Rab31-mutants (Rab31-S19N, Rab31-Q64L and Rab31-ΔCC). Transfection of the empty vector pRcRSV served as a control.

The aim was to select stably transfected cells with comparable and high Rab31-S19N, Rab31-Q64L, Rab31-ΔCC and the Rab31-WT levels, respectively. For both cell lines and all constructs, three independent transfections were performed using a liposome-

based transfection method followed by a selection of stably transfected cell clones with the aminoglycoside antibiotic G418.

Untransfected, parental MDA-MB-231 cells have a low intrinsic Rab31 protein expression, whereas CAMA-1 cells do not express Rab31 at all (Grismayer et al. 2012b). The expression levels were determined by Western blot and ICC analysis.

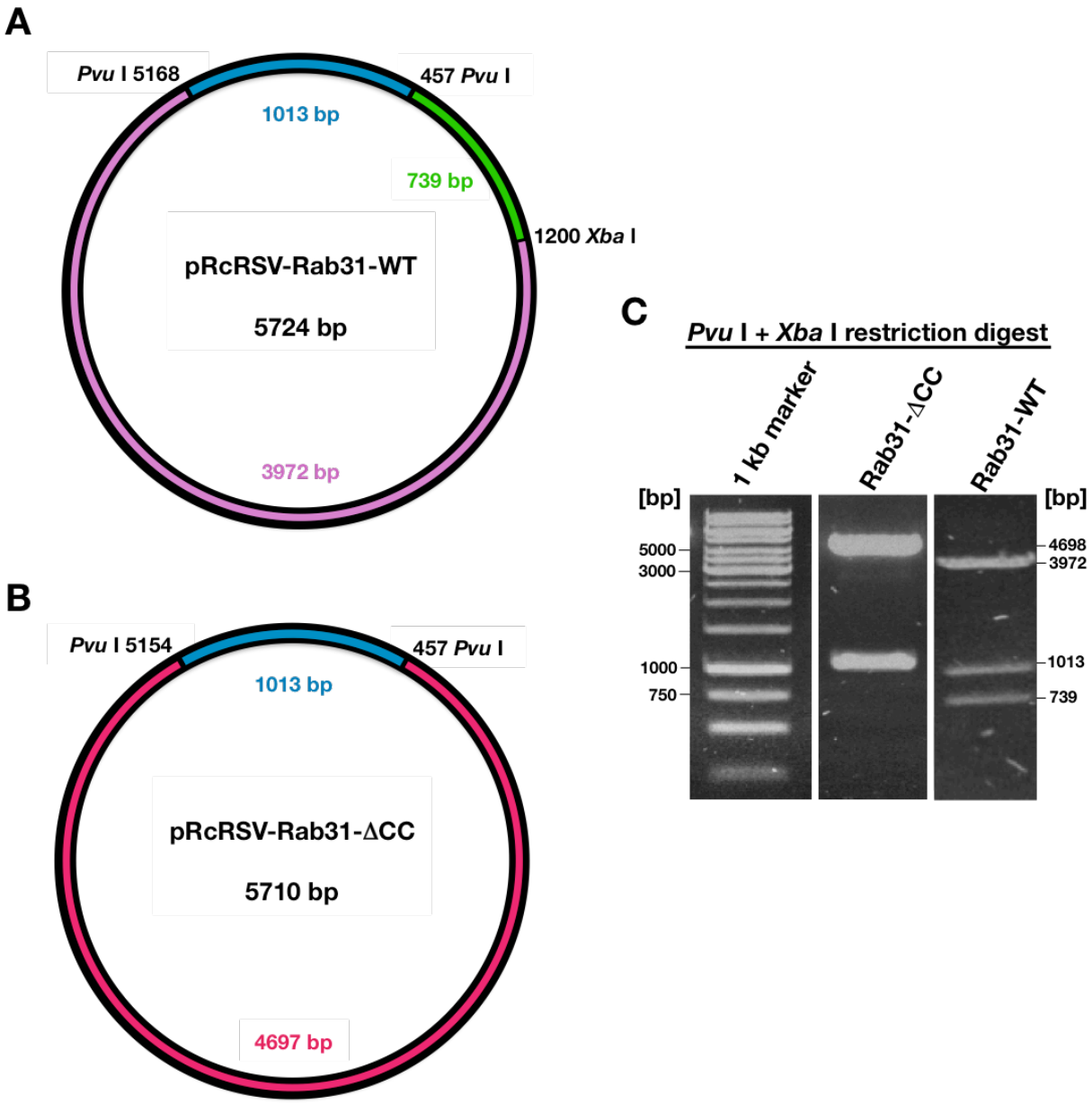

Figure 58 | Restriction digest of pRcRSV-Rab31-WT and -Rab31-ΔCC with *Pvu* I and *Xba* I
A: Restriction map of pRcRSV-Rab31-WT
B: Restriction map of pRcRSV-Rab31-ΔCC
C: pRcRSV-Rab31-WT and -Rab31-ΔCC digested with *Pvu* I and *Xba* I were separated on a 1% agarose gel. The restriction digest of pRc-RSV-Rab31-WT results in three fragments (3972, 1013 and 739 bp). Rab31-ΔCC displays two fragments (4697 and 1013 bp).

In the case of Rab31-S19N, despite the resistance of the cells to G418 selection, no increased Rab31-antigen expression was detectable, neither in MDA-MB-231 nor in CAMA-1 cells (data not shown). This may indicate that there is a selection against Rab31-S19N in the breast cancer cells, possibly due to dominant-negative effects. Therefore, we decided to continue with the analysis of overexpression of the two Rab31-mutants, Rab31-ΔCC and Rab31-Q64L, only.

The MDA-MB-231 Western blots showed that transfection of the plasmids and subsequent overexpression of Rab31-Rab31-WT, Rab31-Q64L and Rab31-ΔCC was successful. As shown in Figure 59, the protein levels of Rab31/Rab31-mutants expression were considerably higher than the intrinsic, basal expression seen in the vector-transfected cells. Furthermore, it can be seen that the Rab31/Rab31-mutant levels were expressed at similarly high levels upon stable transfection.

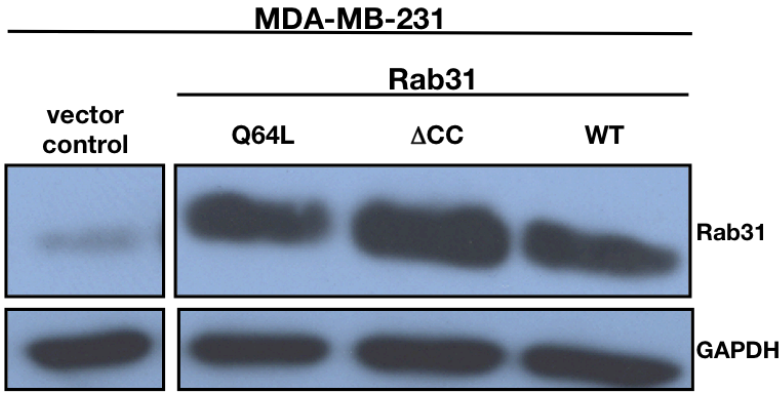

Figure 59 | Western blot analysis of stably transfected MDA-MB-231 cells with expression plasmids encoding Rab31-WT/-mutants
The vector control shows low intrinsic Rab31 expression. Overexpression of the two Rab31-mutants (Q64L and ΔCC) and Rab31-WT was accomplished at high and comparable levels. GAPDH served as loading control.

Rab31 expression levels were also visualized and quantified immunocytochemically in MDA-MB-241 cells. For this, the monoclonal antibody C-15 directed to Rab31 (Santa Cruz Biotechnology) was used for ICC staining.

As expected, endogenous expression of Rab31 in MDA-MB-231 vector control cells was rather low. Whereas the cells overexpressing the two mutant forms of Rab31 displayed homogeneous expression levels in all cells, expression of Rab31-WT was more variably distributed among the cell population (Figure 60).

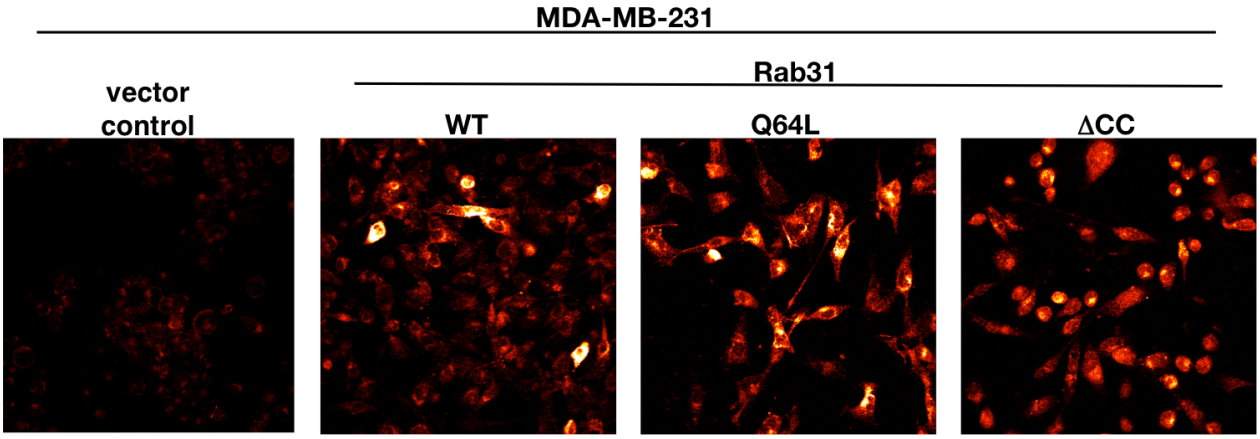

Figure 60 | ICC of MDA-MB-231 cells overexpressing Rab31 mutants
The vector control shows low intrinsic Rab31 expression. Overexpression is seen for the two Rab31-mutants and Rab31 wild-type cells. Red: low-expression, white: high-expression. Magnification: 20x.

In contrast to the MDA-MB-231 cells, batch-transfected CAMA-1 cells did not show comparable (and high) expression levels of Rab31-WT and mutants thereof (data not shown). Therefore, the stably transfected CAMA-1 cells were subcloned, individual subclones analyzed and subclones selected, which displayed similarly high expression levels. Figure 61 depicts the results of a Western blot analysis demonstrating that the Rab31 antigen expression levels of the selected Rab31-Q64L, Rab31-ΔCC and Rab31-WT clones were high and comparable to each other.

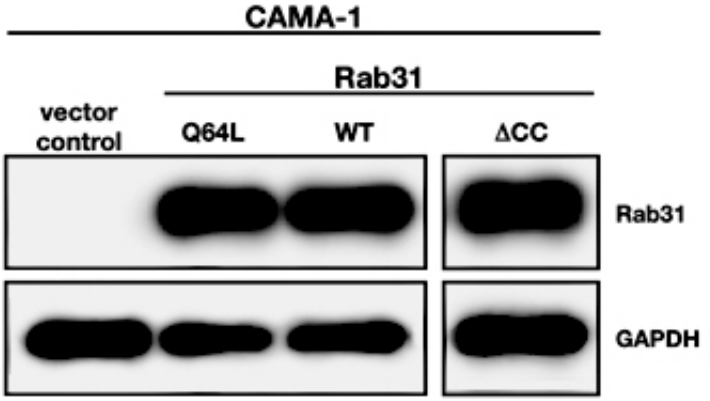

Figure 61 | Western blot analysis of stably transfected CAMA-1 cells with expression vectors encoding Rab31-WT/-mutants
In CAMA-1 cells, the vector control cells show no intrinsic Rab31 expression. Overexpression of the two different Rab31-mutants (Q64L and ΔCC) and Rab31-WT was accomplished at high and comparable levels. GAPDH served as loading control.

In ICC analyses, all three isolated cell clones (overexpressing either Rab31-WT, Rab31-Q64L, or Rab31-ΔCC) are characterized by a homogeneous Rab31 antigen expression throughout all cells. The vector control cells are Rab31-negative (Figure 62).

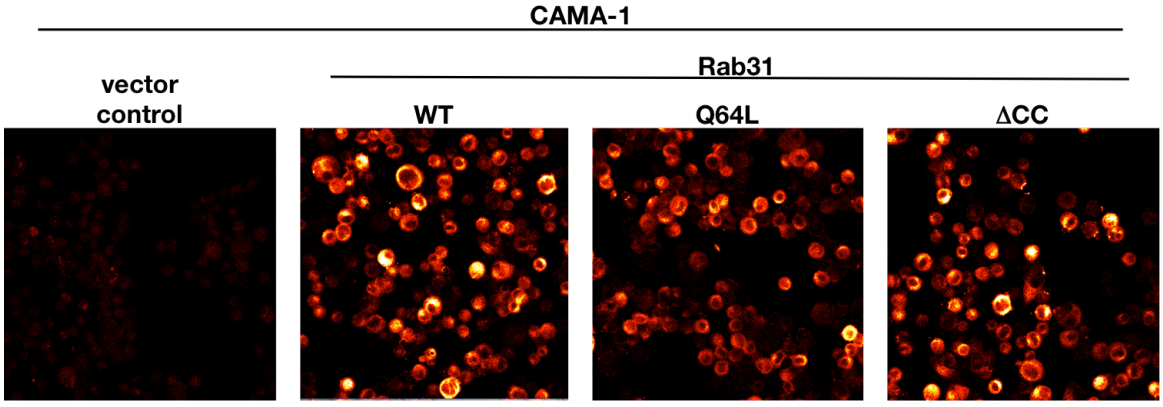

Figure 62 | ICC of CAMA-1 cells overexpressing Rab31-WT/-mutants
The vector control is negative for Rab31 expression. In contrast, distinct overexpression is seen for the two Rab31-mutants and Rab31-WT cells. Red: low-expression, white: high-expression. Magnification: 20x.

6.3.3 - Proliferative characteristics of breast cancer cells overexpressing Rab31-WT/-mutants

From previous studies (Grismayer et al. 2012b), it was known that Rab31-overexpressing MDA-MB-231 and CAMA-1 cells proliferate significantly faster than vector control cells. To study the impact of the two Rab31 mutations on cell growth of MDA-MB-231 cells, we compared the growth behavior of Rab31-Q64L and Rab31-ΔCC overexpressing cells with that of Rab31-WT or vector control cells (Figure 63).

MDA-MB-231 cells overexpressing the constitutively active Rab31-Q64L mutant grew as fast as the Rab31-WT-overexpressing cells. Rab31-WT and Rab31-Q64L cells grew significantly faster than the vector control cells and also the Rab31-ΔCC cells. When comparing the growth rates of vector control *versus* Rab31-ΔCC-overexpressing cells, there was no difference detectable within the margin of error.

Similar proliferation experiments were preformed with CAMA-1 cells overexpressing Rab31-WT, -ΔCC and -Q64L as well as the corresponding vector control cells. The results of the CAMA-1 proliferation assays matched the results of the MDA-MB-231 assays (Figure 64).

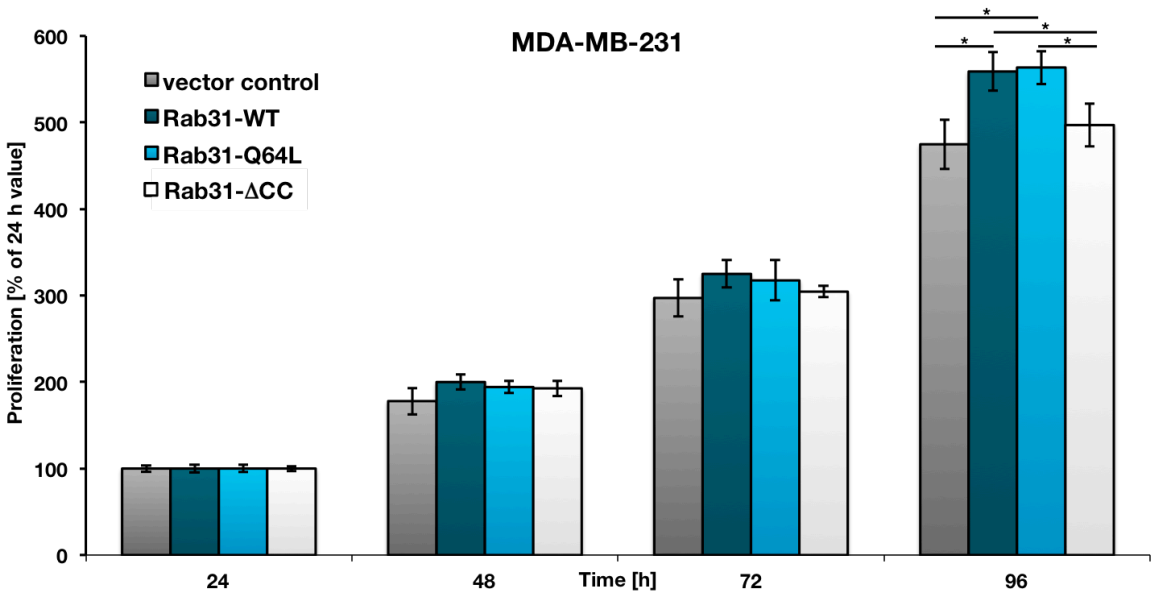

Figure 63 | Growth rates of MDA-MB-231 cells overexpressing Rab31/Rab31-mutants
MDA-MB-231 cells overexpressing the constitutively active mutant Rab31-Q64L proliferate as fast as the Rab31-WT-overexpressing cells. Cells overexpressing the mutant Rab31-ΔCC, which due to the lack of its prenylation site is unable to bind to membranes, proliferate significantly slower than the Rab31-WT and Rab31-Q64L overexpressing cells. The proliferation rate of Rab31-ΔCC and vector control cells is comparable, so is the proliferation rate of Rab31-WT and Rab31-Q64L. Cell numbers are normalized against the 24 h value. The graph shows the mean value of three independent experiments preformed in triplicates each. Statistically significant differences ($p<0.05$) are indicated by an asterisk.

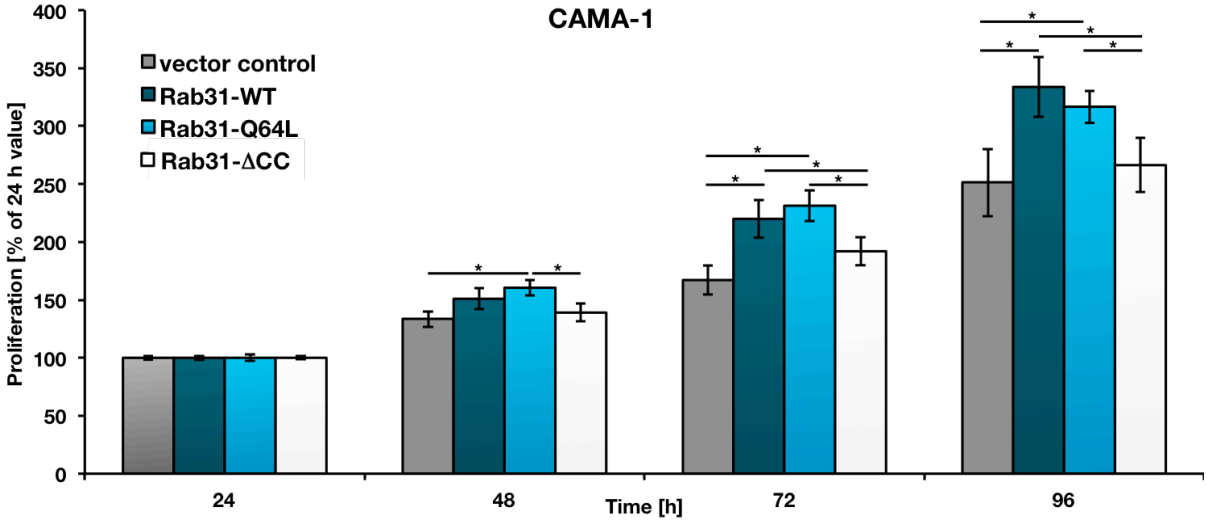

Figure 64 | Growth rates of CAMA-1 cells overexpressing Rab31-WT/-mutants
CAMA-1 cells overexpressing the constitutively active mutant Rab31-Q64L proliferate as fast as the Rab31-WT-overexpressing cells. Cells overexpressing the mutant Rab31-ΔCC, which due to the lack of its prenylation site is unable to bind to membranes, proliferate significantly slower than the Rab31-WT and Rab31-Q64L overexpressing cells. The proliferation rate of Rab31-ΔCC and vector control cells is comparable, so is the proliferation rate of Rab31-WT and Rab31-Q64L. Cell numbers are normalized against the 24 h value. The graph shows the mean value of three independent experiments preformed in triplicates each. Statistically significant differences ($p < 0.05$) are indicated by an asterisk.

Taken together, in both MDA-MB-231 and CAMA-1 cell lines, the cells overexpressing Rab31-WT and Rab31-Q64L proliferate similar and significantly faster than the vector control and Rab31-ΔCC cell lines. The growth rates of Rab31-ΔCC showed no difference compared to vector control cells.

In addition to the above-described manual cell counting assay, the growth rates of the Rab31/Rab31-mutant overexpressing and vector control cells were analyzed by a cell viability assay (AlamarBlue Assay, Life Technologies) and the CyQUANT proliferation assay (Life Technologies). In both cases, similar results were observed (data not shown).

6.3.4 - Adhesive properties of breast cancer cells overexpressing Rab31-WT/-mutants

Previously, we have shown (Grismayer et al. 2012b) that Rab31-overexpressing breast cancer cells adhere less efficiently to ECM proteins than vector control cells. Now, adhesion experiments were additionally performed with the Rab31-mutants. The cells were plated on 96-well plates, which were coated with different extracellular matrix proteins. After incubation and washing, a colorimetric reaction was used to analyze the number of cells adhering to the ECM proteins.

MDA-MB-231 cells overexpressing the constitutively active Rab31-Q64L mutant showed the same reduced adhesive phenotype as the Rab31-WT-overexpressing cells when compared to vector control cells. There was no measurable significant difference in the adhesive capacity between Rab31-ΔCC-overexpressing and vector control cells (Figure 65).

The results obtained with CAMA-1 cells matched those obtained with MDA-MB-231 cells (Figure 66). Firstly, a significant reduction of adhesion to various ECM proteins was observed for Rab31-Q64L compared to the vector control cells. Secondly, there was no difference in the adhesive properties between Rab31-ΔCC and vector control cells. Thirdly, the diminishment of adhesion of Rab31-Q64L and Rab31-WT cells compared to vector control (and Rab31-ΔCC) cells was similar.

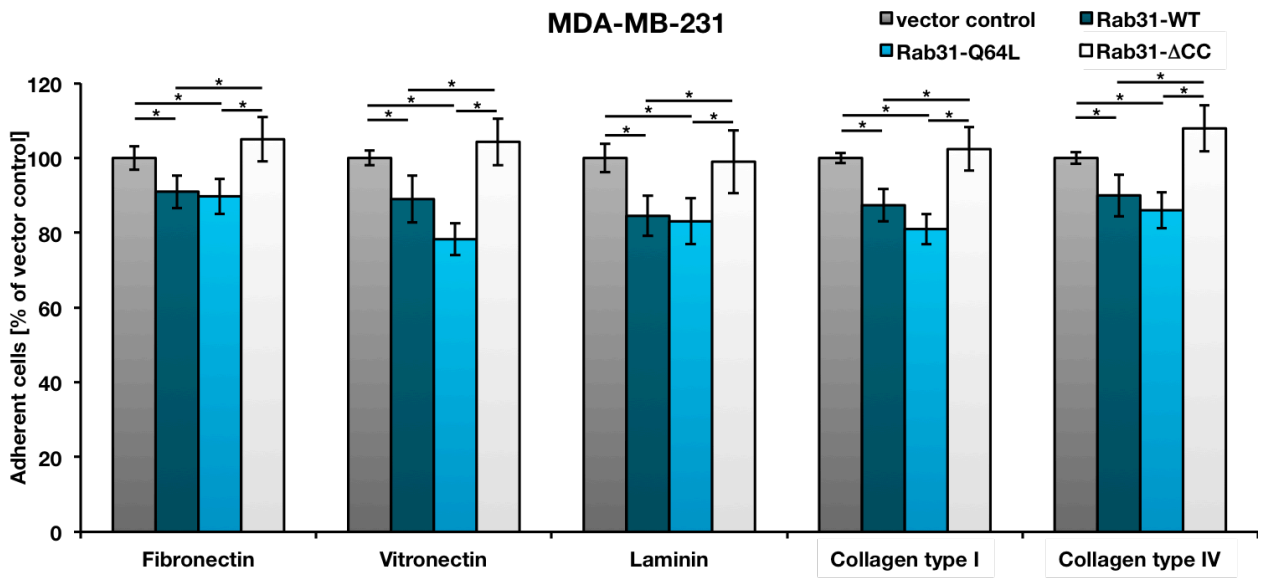

Figure 65 | Adhesion of MDA-MB-231 cells overexpressing Rab31-WT/-mutants to various ECM proteins

Cells overexpressing the constitutively active Rab31-Q64L mutant show a similar reduction of adhesion to the different ECM proteins as the Rab31-WT cells when compared to vector control cells. There is no statistically significant difference in the adhesive capacity between Rab31-ΔCC and vector control cells. At least four independent experiments were performed in triplicates each. The results are given in % relative to the cell number of adherent vector-transfected control cells. Statistically significant differences ($p<0.05$) are indicated by an asterisk.

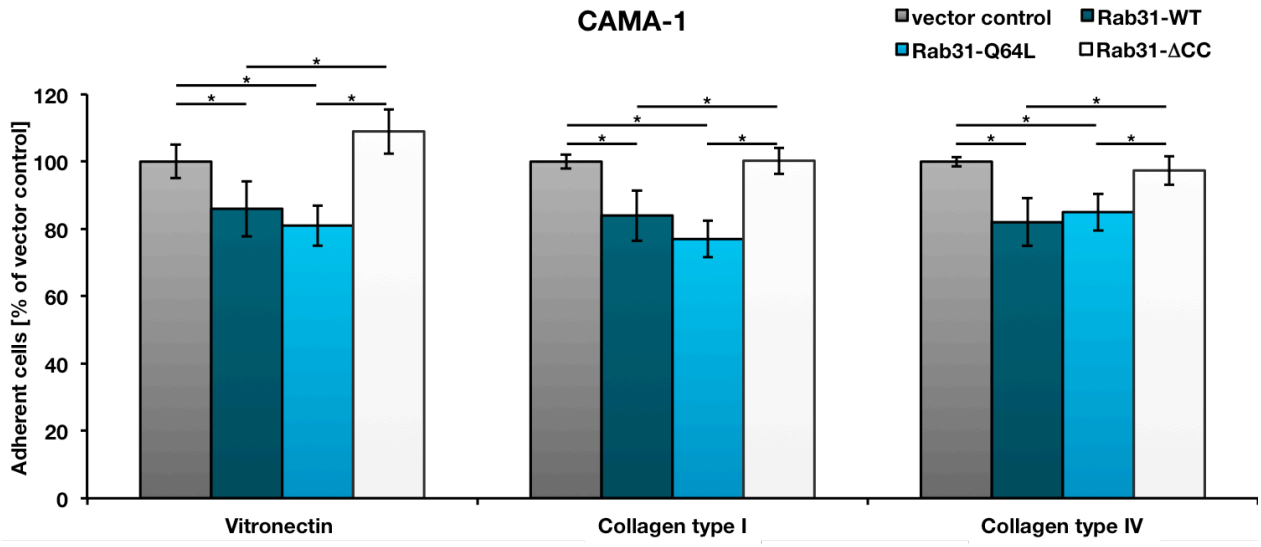

Figure 66 | Adhesion of CAMA-1 cells overexpressing Rab31-WT/-mutants to various ECM proteins

Cells overexpressing the constitutively active Rab31-Q64L mutant show a similar reduction of adhesion to the different ECM proteins as the Rab31-WT cells when compared to vector control cells. There is no difference in the adhesive capacity between Rab31-ΔCC and vector control cells. At least four independent experiments were performed in triplicates each. The results are given in % relative to the cell number of adherent vector-transfected control cells. Statistically significant differences ($p<0.05$) are indicated by an asterisk.

6.3.5 - Invasive capacity of breast cancer cells overexpressing Rab31-WT/-mutants

To explore how the overexpression of Rab31/Rab31-mutant protein impacts the invasive behavior of MDA-MB-231 cells Matrigel transwell assays were preformed. Since CAMA-1 is a non-invasive cell line, no invasion assays could be performed with these cells.

Transwell plates were coated with an artificial extracellular matrix (Matrigel; growth factor reduced; Becton Dickinson). The cells were seeded into the upper part of the chamber in serum-free medium. The lower part of the chamber was filled with medium containing 10 % (v/v) FCS as a chemo-attractant. The plates were incubated for 24 h, allowing the cells to degrade the ECM and migrate through the pores of the transwell to the lower side of the insert. The non-invaded cells in the upper chamber were removed and the cells attached under the filter were fixed, stained and counted. The number of invaded Rab31/Rab31-mutant cells was normalized against the number of invaded vector control cells (Figure 67).

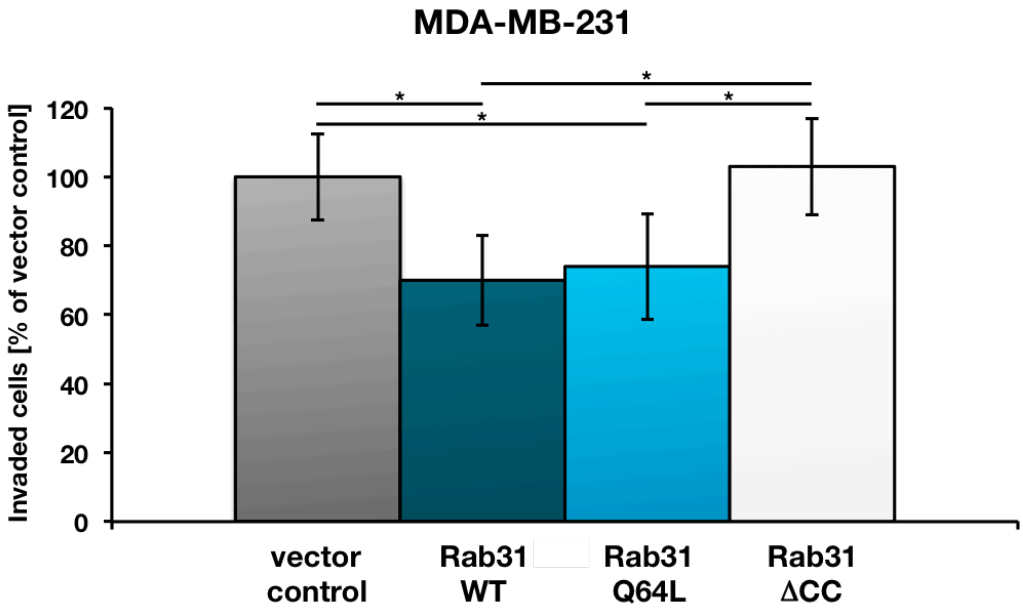

Figure 67 | Invasion of MDA-MB-231 cells overexpressing Rab31-WT/-mutants through Matrigel
Cells overexpressing the constitutively active Rab31-Q64L mutant show a similar reduction of invasive capabilities as the Rab31-WT cells when compared to vector control cells. There is no difference in the invasiveness between Rab31-ΔCC and vector control cells. Three independent experiments were performed in triplicates each. The results are given in % relative to the cell number of invaded vector-transfected control cells. Statistically significant differences ($p<0.05$) are indicated by an asterisk.

In conclusion, the phenotype of Rab31-ΔCC-overexpressing cells concerning proliferation, adhesion, and invasion is similar to that of vector control cells, whereas Rab31-Q64L-overexpressing cells are very similar to Rab31-WT-overexpressing cells. This shows, on one hand, that Rab31 overexpression only displays effects on these cell biological characteristics, if Rab31 can physically interact with membranes. On the other hand, cells overexpressing constitutively active Rab31 behave like cells overexpressing wild-type Rab31.

6.4 - Molecular effects of Rab31 overexpression

Rab31 overexpression affects several tumor biological processes (for analysis of the effects seen in batch-transfected MDA-MB-231 cells see Figure 41, 42 and 43). Thus, the question arises whether Rab31 overexpression levels lead to differential expression of other genes. As demonstrated by our group (Grismayer et al. 2012b), Rab31-mediated effects on cell biological processes are modulated in a concentration-dependent manner. To analyze the strongest possible difference between Rab31 overexpressing versus Rab31-deficient vector control cells, a subclone of the previously characterized batch-transfected cell line MDA-MB-231 that displayed a very high Rab31 expression was used for the following molecular analyses. Prior to gene expression analysis, the clone, Rab31 1-13-10 was thoroughly compared to the vector control cells and characterized in more detail using various cell biological assays.

6.4.1 - Breast cancer cells overexpressing Rab31

6.4.1.1 - Rab31 Western blot analysis

To confirm Rab31 overexpression, we used Western blot analysis of whole cell lysates of the MDA-MB-231 Rab31-overexpressing clone (Rab31 1-13-10), displaying a very high expression versus vector control cells (Figure 68).

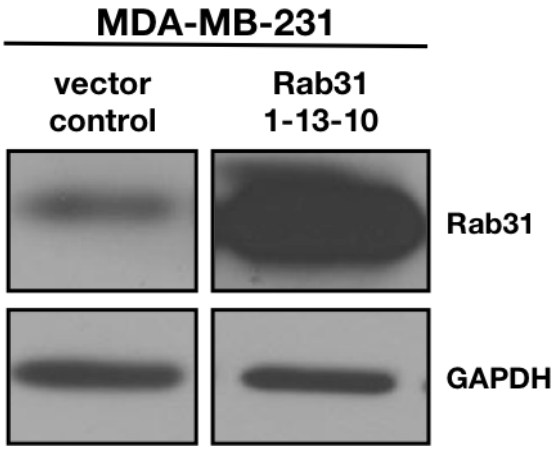

Figure 68 | Western blot analysis of stably transfected MDA-MB-231 cells clones
Western blot analysis indicates a basal Rab31 expression level in vector control cells and significant higher Rab31 levels in cells transfected with pRcRSV-Rab31. Rab31 was visualized with rabbit anti-Rab31 antibodies. GAPDH expression served as loading control.

The data from the Western blot shows that MDA-MB-231 vector control cells display a moderate intrinsic Rab31 expression level, whereas in pRc-RSV-Rab31-transfected cells a distinct increase of Rab31 is observed.

In contrast to MDA-MB-231 cells, CAMA-1 cells display no endogenous Rab31 expression. Upon stable transfection with pRcRSV-Rab31 a strong expression of Rab31 is observed. The Western blot analysis was performed as mentioned above (Figure 69).

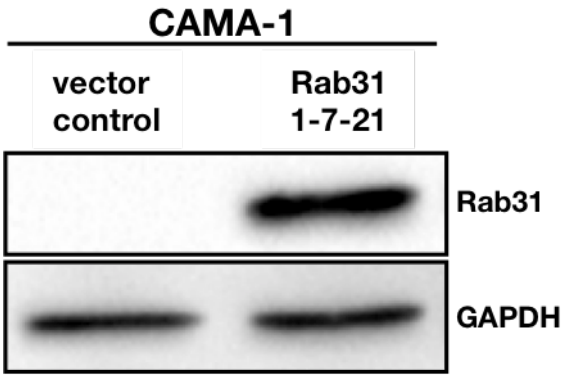

Figure 69 | Western blot analysis of stably transfected CAMA-1 cells with Rab31
The vector control cells are Rab31-deficient. Overexpression of Rab31 (wild-type) was accomplished at a high level. GAPDH expression served as loading control.

6.4.1.2 - Rab31 ELISA analysis

Using a newly developed sensitive ELISA for quantitation of Rab31 (M. Kotzsch, T. Kirchner, S. Schäfer, T. Luther, unpublished), an about 5-fold increase of Rab31 was observed in MDA–MB-231 cells (2.48 ng/mg total protein) as compared to vector control cells (0.37 ng/mg total protein) (Figure 70 A). CAMA-1 vector control cells were negative for Rab31, whereas in CAMA-1 Rab31-overexpressing cells significant amounts of Rab31 antigen was detected (4.08 ng/mg total protein) (Figure 70 B), whereas vector control cells were negative. In a study by Bao et al. (2002) the physiological Rab31 content in platelets was estimated to be approximately 5.0 ng/mg total protein. Thus, the Rab31 levels in Rab31-overexpressing cells seem to be within the physiological range.

6.4.1.3 - Immunocytochemical analysis of Rab31

Protein expression analysis by immunocytochemistry (ICC) confirms overexpression of Rab31 in MDA-MB-231 and CAMA-1, respectively. Moreover, the expression levels in the batch-transfected cells are found to be relatively homogenous (Figure 71).

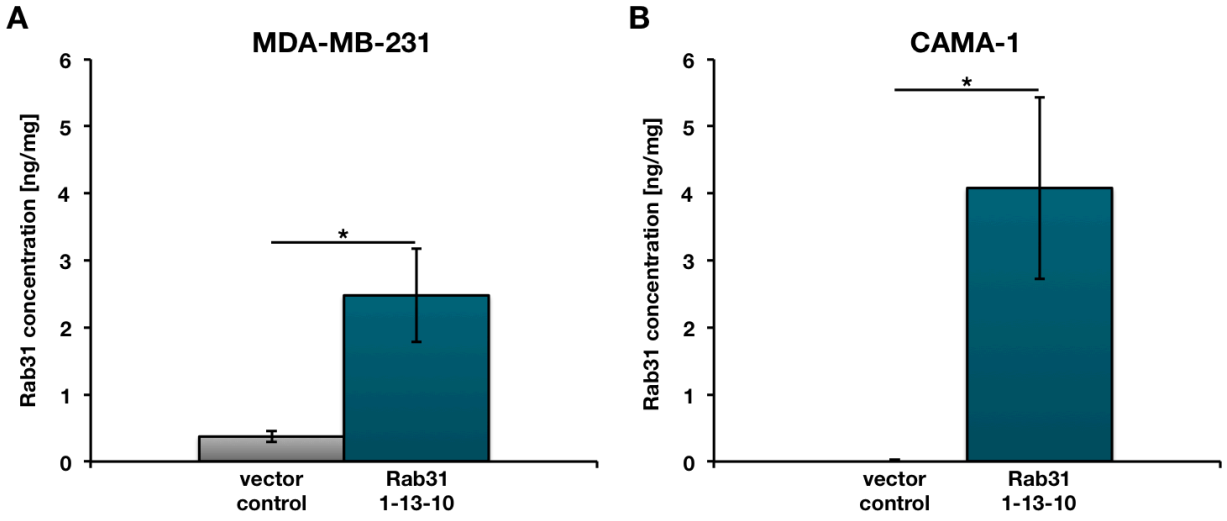

Figure 70 | Rab31 antigen levels in cell culture lysates from Rab31-overexpressing cells, determined by ELISA
A: Rab31 ELISA confirms a significantly higher Rab31 protein expression in MDA-MB-231 cells stably transfected with pRcRSV-Rab31 as compared to the respective vector control.
B: Rab31 ELISA confirms a significantly higher Rab31 protein expression in CAMA-1 cells stably transfected with pRcRSV-Rab31 as compared to the respective vector control.
At least three experiments were performed in triplicates each. Statistically significant differences ($p<0.05$) are indicated by an asterisk.

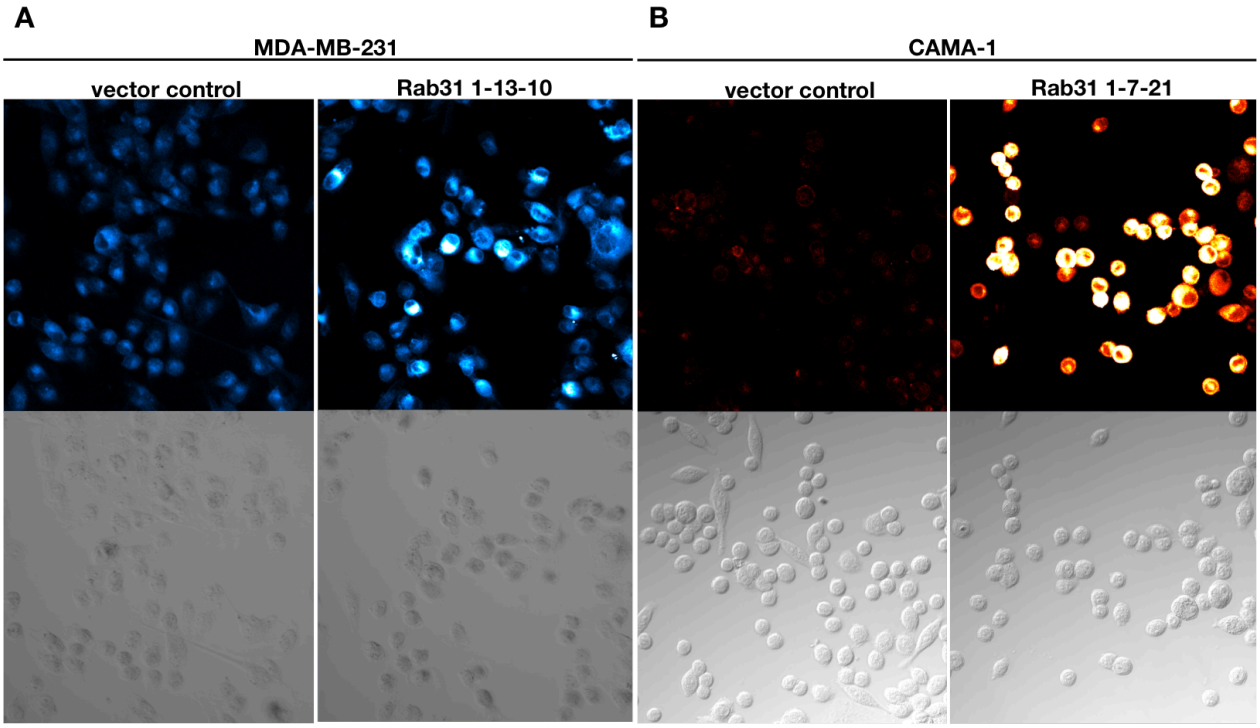

Figure 71 | ICC analysis of CAMA-1 and MDA-MB-231 vector control and Rab31-overexpressing cells
A: MDA-MB-231 cells: the vector control cells display low intrinsic Rab31 expression. Stable transfection with the Rab31 expression plasmid results in high Rab31 protein levels (blue: low expression; white: high expression).
B: CAMA-1 cells: vector control cells are negative for Rab31. Upon stable transfection with the Rab31 expression plasmid, these cells show high levels of protein. (red: low expression; white: high expression). The lower panels show transmission images of the cells. Magnification: 20x

6.4.2 - Proliferative properties of Rab31-overexpressing cells

6.4.2.1 - Conventional 2D cell culture in cell culture dishes

The impact of Rab31 overexpression on MDA-MB-231 and CAMA-1 cell proliferation was analyzed using manual counting in a Neubauer chamber and trypan blue exclusion. The cells were counted every 24 h for 4 days (Figure 72).

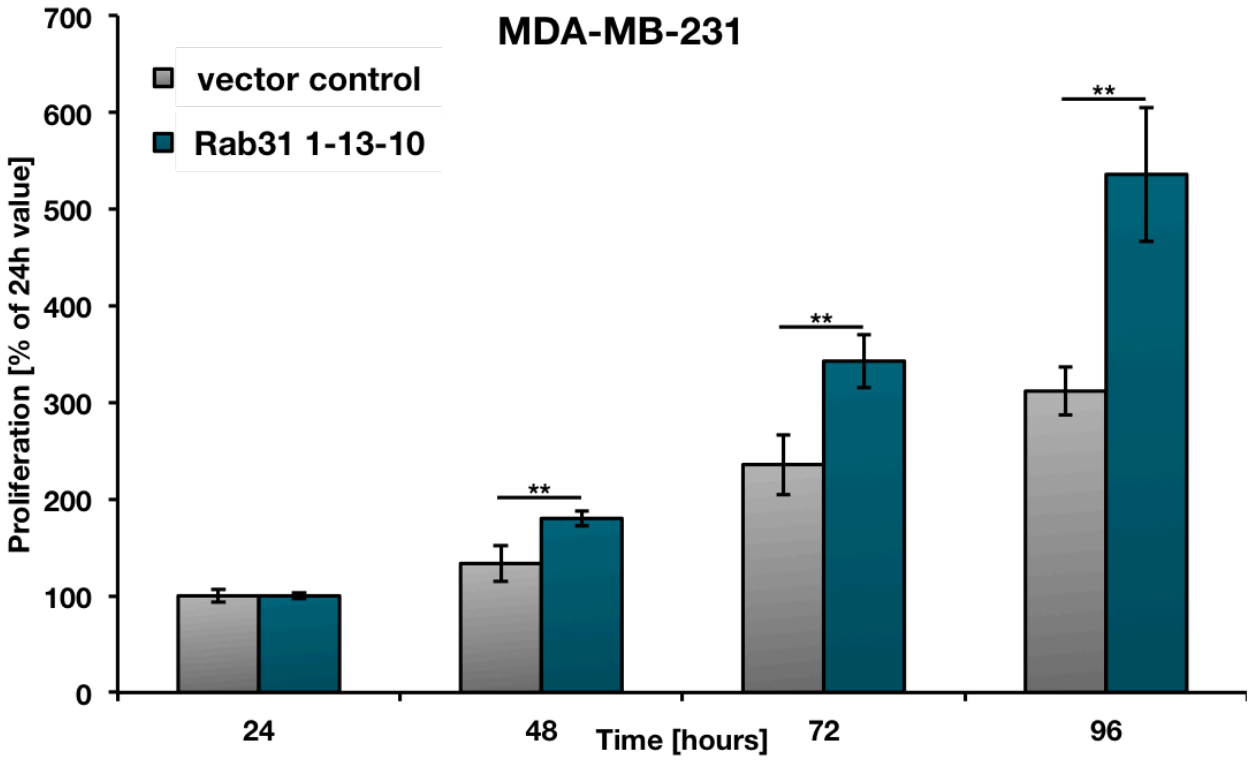

Figure 72 | Proliferation of MDA-MB-231 cells overexpressing Rab31 compared to vector control cells
The cell number at 24 h was set to 100 %. Each data point is the mean value of three independent experiments. Statistically significant differences ($p<0.01$) are indicated by two asterisks.

The MDA-MB-231 Rab31 clone chosen for this experiment has a very high overexpression, which may explain the significantly faster proliferation than the vector control cells under the same culture conditions. The proliferation is known to be dependent on the Rab31 concentration. The stronger effect is shown here by the high overexpessing clone (Figure 72) compared to the batch transfection in Figure 43.

Similarly, proliferation experiments were performed with the CAMA-1 Rab31-overexpressing *versus* vector control cells (Figure 73).

Rab31-overexpressing CAMA-1 cells also showed a significantly accelerated growth rate when compared to vector control cells. As for MDA-MB-231 cells, significant differences in cell number were observed after 48 h and longer time points. These findings suggest that Rab31-overexpressing cells proliferate faster than vector control cells.

In order to exclude another explanation for the observed differences in the growth rates, namely a higher cell death rate in the control cell population, we analyzed the

cells using a FACS-based apoptosis assay. For this, we employed fluorescently labeled annexin (Annexin-V-FLUOS), propidium iodide (PI) staining and FACS analysis to quantify living, apoptotic and dead cells (Figure 74). In the early stage of apoptosis, a translocation of phosphatidylserine (PS) from the inner part of the plasma membrane to the outer layer occurs. Phosphatidylserine can thus be detected *via* Annexin-V-FLUOS staining and indicates early (Annexin-V-FLUOS $^{+}$/PI^{-}) or late apoptotic cells (Annexin-V-FLUOS $^{+}$/PI^{+}). Dead cells with a damaged plasma membrane are characterized by PI staining (Annexin-V-FLUOS $^{-}$/PI^{+}).

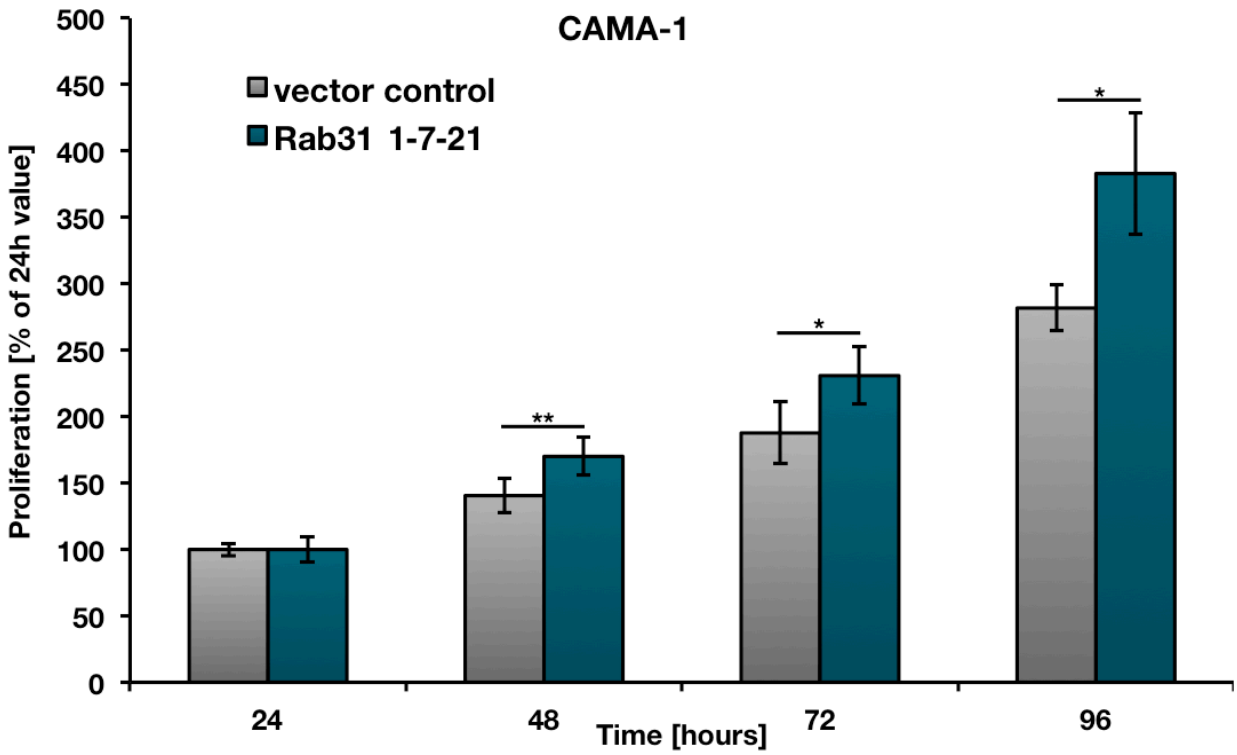

Figure 73 | Proliferation of CAMA-1 cells overexpressing Rab31 compared to vector control cells
The cell number at 24 h was set to 100 %. Each data point is the mean value of three independent experiments. Statistically significant differences are indicated by asterisks (one asterisk: $p<0.05$; two asterisks: $p<0.01$)

Figure 74 shows the results of two independent FACS experiments. Early apoptotic cells display a characteristic Annexin-V-FLUOS-positive, PI-negative staining (pink: lower right quadrant). In both experiments, there was no obvious difference in the amount of apoptotic cells between Rab31-overexpressing and vector control cells. Corresponding experiments with CAMA-1 cells gave similar results (data not shown).

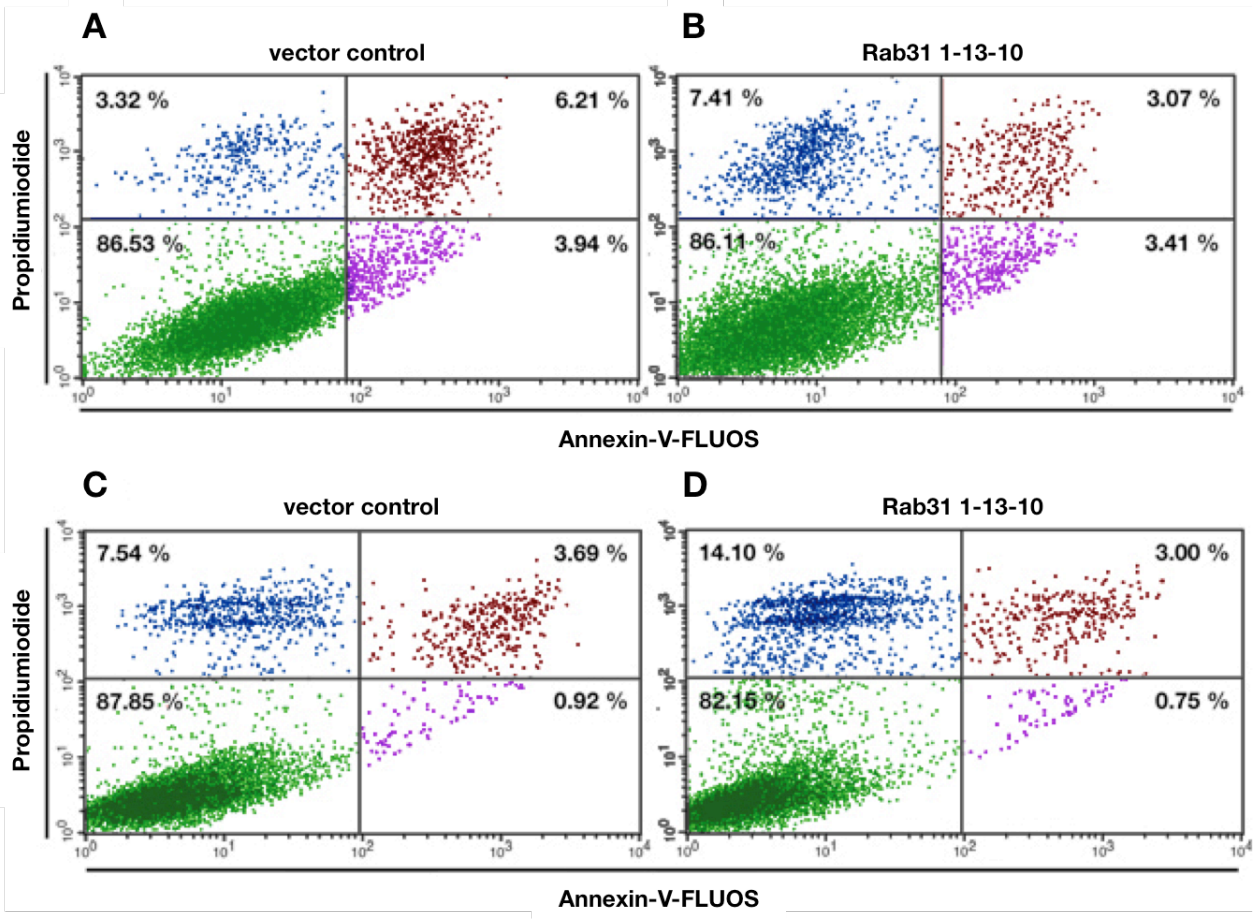

Figure 74 | FACS analysis of MDA-MB-231 cells overexpressing Rab31
Annexin-V-FLUOS and PI staining of cells after 48 h of cultivation (experiment 1: A + B; experiment 2: C + D). **A, C:** MDA-MB-231 vector control cells. **B, D:** MDA-MB-231 Rab31-overexpressing cells. Non-apoptotic cells: Annexin-V-FLUOS $^{-}$/PI^{-} (green); early apoptotic cells: Annexin-V-FLUOS $^{+}$/PI^{-} (pink); late apoptotic and necrotic cells: Annexin-V-FLUOS^{+}/PI^{+} (red); Dead cells: Annexin-V-FLUOS^{-}/PI^{+} (blue).

As a positive control, a synthetic peptide derived from human TRAIL was used, which induces apoptosis by binding to TNF receptors. MDA-MB-231 cells were incubated for 24 h with 40 ng/ml TRAIL followed by Annexin-V staining and FACS analysis (Figure 75).

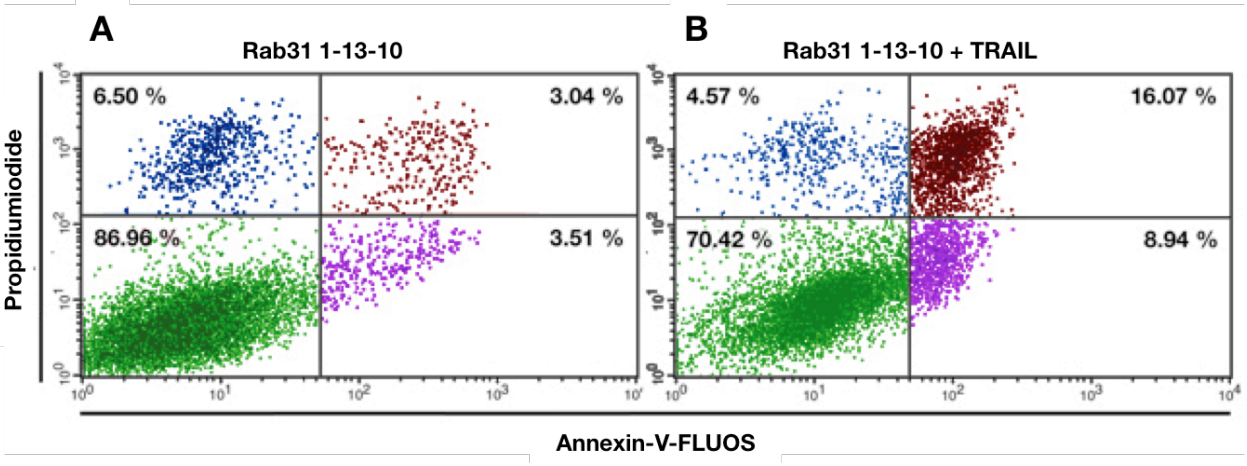

Figure 75 | FACS analysis of MDA-MB-231 cells overexpressing Rab31 with and without treatment with TRAIL
A: Annexin-V-FLUOS and PI staining of MDA-MB-231 Rab31-overexpressing cells after 24 h of cultivation.
B: Annexin-V-FLUOS and PI staining Rab31-overexpressing MDA-MB-231 cells 24 h cultivation with 40 ng/ml TRAIL.
Non-apoptotic cells: Annexin-V-FLUOS$^-$/PI$^-$ (green); early apoptotic cells: Annexin-V-FLUOS$^+$/PI$^-$ (pink); late apoptotic and necrotic cells: Annexin-V-FLUOS$^+$/PI$^+$ (red); Dead cells: Annexin-V-FLUOS$^-$/PI$^+$ (blue).

Incubation of Rab31-overexpressing MDA-MB-231 cells with the TRAIL peptide leads to a strong increase of the number of early as well as late apoptotic cells (Figure 75). Corresponding experiments with CAMA-1 cells gave similar results (data not shown).

To further analyze the accelerated proliferation of Rab31-overexpressing MDA-MB-231 cells, S-phase analyses were performed. The cellular DNA content determined by FACS analyses using PI staining corresponds to different phases of cell division. Compared to the G0/1 phase, the DNA amount steadily increases during the S-phase and leads to a DNA duplication before cell division (mitosis) occurs after the G2-phase.

Figure 76 shows the results of two independent FACS experiments: cells were cultivated for 48 h in the presence of FCS and under starving conditions (*i.e.* without FCS), respectively, prior to S-phase analysis. In both types of experiments, there was an obvious up-regulation in the number/percentage of S-phase cells in Rab31-overexpressing MDA-MB-231 cells compared to vector control cells (22% vs. 14%, and 32% vs. 26% respectively).

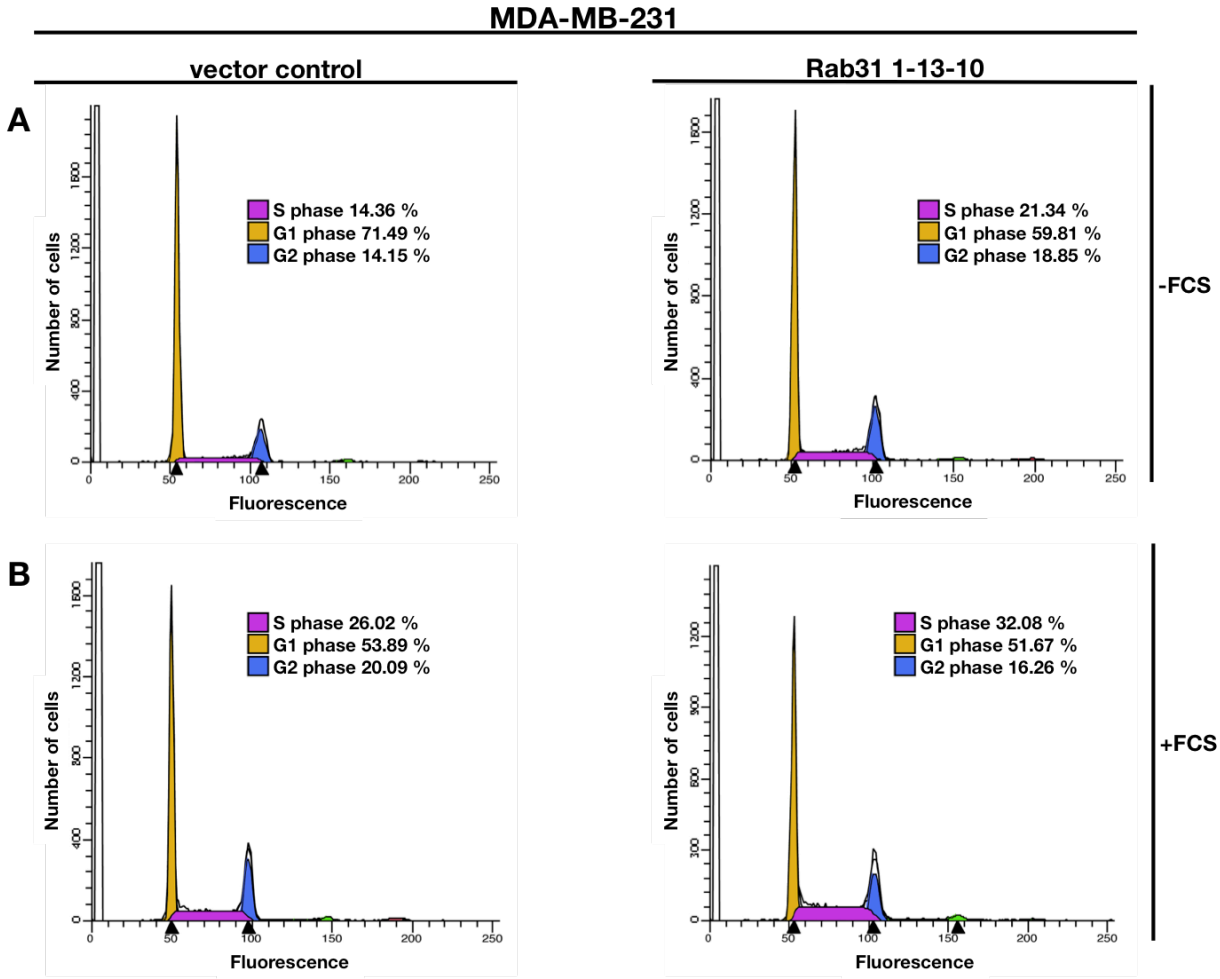

Figure 76 | S-phase analysis of MDA-MB-231 cells overexpressing Rab31 compared to vector control cells.
A: DNA histograms of MDA-MB-231 Rab31-overexpressing and vector control cells after 48 h of cultivation without FCS.
B: DNA histograms of MDA-MB-231 Rab31-overexpressing and vector control cells after 48 h of cultivation with FCS.
G0/1-phase: non-proliferating cells (orange); S-phase: actively proliferating cells (pink); G2/M-phase: dividing cells (blue)

Taken together, the experiments suggest that Rab31 overexpression increased the proliferative activity of MDA-MB-231 cells. Corresponding experiments with CAMA-1 cells give similar results (data not shown).

6.4.2.2 - Assessment of spheroid growth in 3D cell culture

Recently, a bioengineered three-dimensional (3D) culture model was developed based on a polyethylene glycol-based bio-gel (Loessner et al. 2010; Loessner et al. 2012). 3D cell culture models may resemble the natural environment of body-cells more than 2D cell culture and may thus allow better analysis of the role of tumor-associated factors in malignant progression.

We tested whether MDA-MB-231 and CAMA-1 cell lines, respectively, are able to form spheroids. Unfortunately, neither parental MDA-MB-231 cells, nor the vector control cells, nor the Rab31-overexpressing cells were able to form spheroids in the cell culture model (Figure 77). MDA-MB-231 cells are unable to form multicellular aggregates also in other spheroid platforms (B. Mayer, Spherotec GmbH, personal communication).

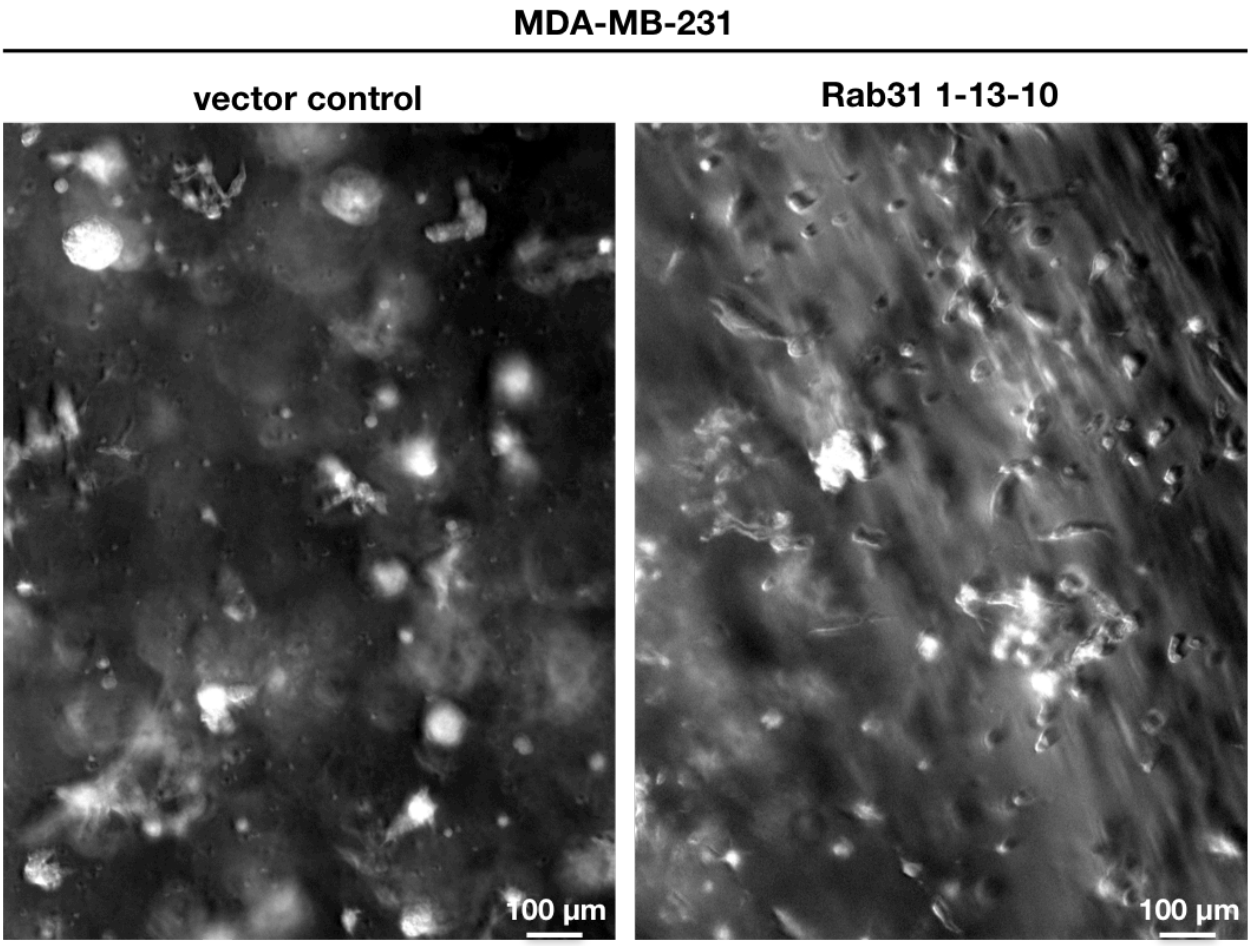

Figure 77 | MDA-MB-231 cells grown for 14 days in QGel
1 x 10^5 cells were seeded into QGel and grown for two weeks. MDA-MB-231 cells were not able to form spheroids.

In contrast, spheroids derived from single cells, were formed by parental (not shown), vector control and Rab31-overexpressing CAMA-1 cells (Figure 78).

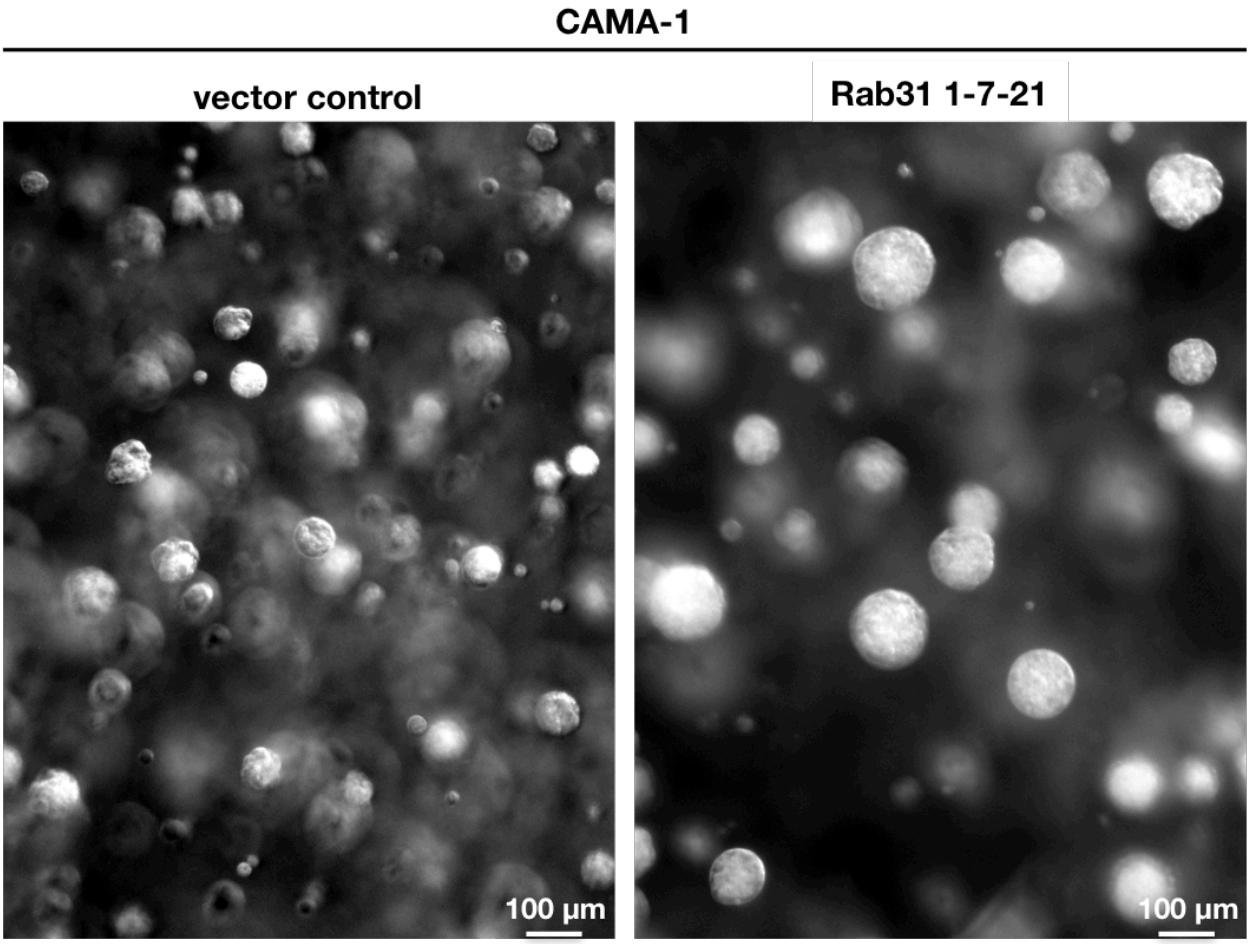

Figure 78 | CAMA-1 cells grown for 14 days in QGel
1 x 10^5 cells were seeded into QGel and grown for two weeks. Both, CAMA-1 vector control and Rab31-overexpressing cells were able to form spheroids. Rab31-overexpressing cells form much larger spheroids indicating a distinctly increased growth rate when compared to vector control cells.

Visual inspection of the size/volume of the formed spheroids strongly indicates a higher growth rate of Rab31-overexpressing compared to vector control cells. Furthermore, measuring the relative cell numbers by AlamarBlue (Figure 79 A) as well as CyQuant-based assays (Figure 79 B) confirmed these findings.

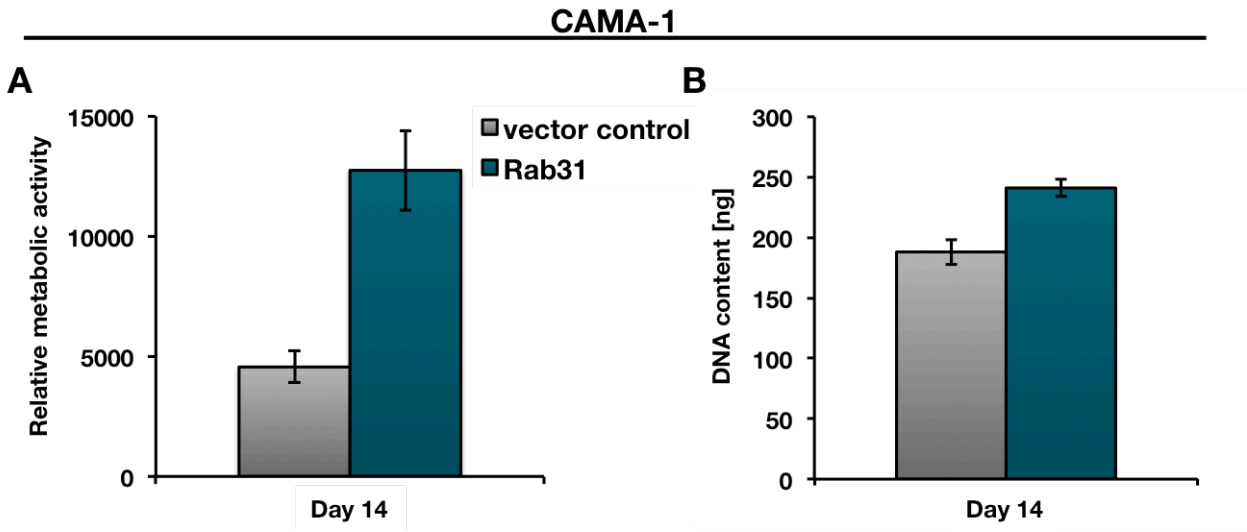

Figure 79 | Proliferation analysis of CAMA-1 Rab31-overexpressing and vector control cells in 3D

A: Viable cells continuously convert the non-fluorescent substrate AlamarBlue into a fluorescent product, thereby allowing a quantitative measurement of cell numbers. Since the same cell number was plated out, Rab31-overexpressing cells display a faster growth rate as compared to vector control cells after 14 days.

B: In the CyQuant assay, the content of DNA is measured by a non-fluorescent substrate, which upon intercalation into genomic DNA exhibits a strong fluorescence. The CyQuant proliferation assay of CAMA-1 cells in 3D QGel culture shows a higher DNA content in Rab31-overexpressing as compared to vector control cells after 14 days, indicating a faster growth rate of Rab31-overexpressing cells.

These results are in line with our observations made in 2D cell culture concerning a distinctly increased growth rate of Rab31-overexpressing *versus* vector control cells.

6.4.3 - Identification of differentially expressed candidate genes in Rab31-overexpressing *versus* control cells by mRNA analysis (SAB EMT array)

All of our data so far suggest that Rab31, depending on its expression level, acts as a switch from an invasive to a proliferative phenotype in breast cancer cells as indicated by an increased cell proliferation, reduced adhesion and invasion *in vitro*, and a reduced capacity to form lung metastases *in vivo* (this work and Grismayer et al. 2012b) Thus, it is tempting to speculate that Rab31 overexpression affects the expression of other genes involved in these processes when compared to Rab31 low expressing cells.

The aim of further work, therefore, was to search for differential expression of tumor-associated genes in Rab31-overexpressing *versus* Rab31-deficient (CAMA-1) or Rab31 low-expressing (MDA-MB-231) vector control cells. We decided to use low-density PCR microarrays and selected the Human EMT RT² Profiler PCR Array (SAB

Biosciences) for the first analyses. This array profiles expression of 84 key genes that have been reported to be involved in the so-called epithelial to mesenchymal transition (EMT) or its reciprocal process mesenchymal to epithelial transition (MET).

EMT/MET play key roles in tumor metastasis. The important steps during EMT are that the epithelial cells lose polarity as well as tight junctions, and degrade basal membrane to become migratory mesenchymal cells. Therefore, the used microarray analyzes gene expression of several tumor-associated genes, which are involved in proliferation, cell adhesion, migration, motility and also in cell signaling.

RNA was isolated from the various cell lines, reverse transcribed and the mRNA expression levels of the various genes evaluated by quantitative PCR using the low-density microarray. Figure 80 depicts the pair-wise comparison of the expression levels of Rab31-overexpressing *versus* vector control cells. A dot (black) lying on the middle diagonal indicates no change of mRNA levels in both types of cells. The outer lines indicate the border for two-fold higher or lower levels in Rab31-overexpressing compared to vector control cells. Thus, those genes that displayed at least two-fold higher (lower) mRNA levels in Rab31-overexpressing cells are indicated by red (green) dots.

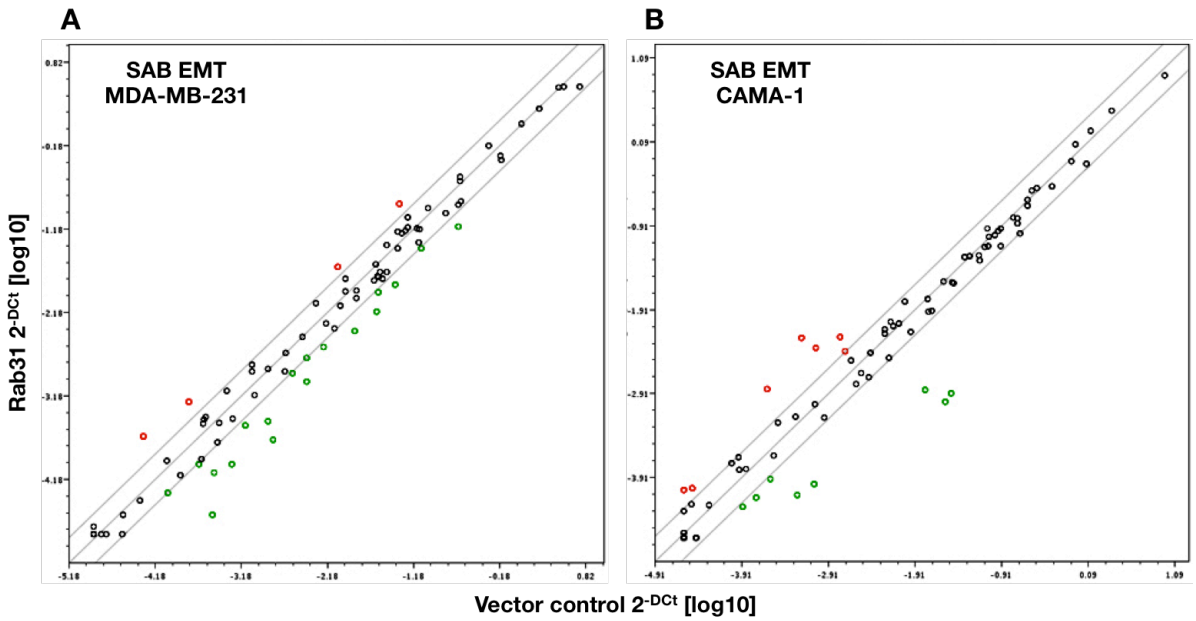

Figure 80 | Low-density qPCR microarrays reveal candidate genes being up- or down-regulated in Rab31-overexpressing *versus* vector control cells
Total mRNA from vector control and Rab31-overexpressing cells was analyzed (A: MDA-MB-231 cells; B: CAMA-1 cells). The relative mean expression levels for each gene in the two samples are plotted against each other, dots in red represent candidate genes potentially up-regulated in Rab31-overexpressing cells, while green dots represent genes potentially down-regulated, each by at least two-fold. Black dots display relative expression changes lying between two-fold up- or down-regulation, the corresponding genes are considered as non-regulated.

Each array allows the measurement of mRNA levels only for one cDNA in a single measurement. Thus, there is a relatively high risk for false-positive or -negative results due to the experimental setting. Therefore, in total, for every cell line two arrays were performed and, thus, each cell line was examined twice with independently generated biological replicates. The average of five housekeeping genes was used to normalize the array. Figure 81, 82, 83 and 84 show the mean values of candidate genes (given as x-fold regulation) of these two measurements. We focused on those genes, which displayed an at least two-fold mean value indicating higher up- or down-regulation.

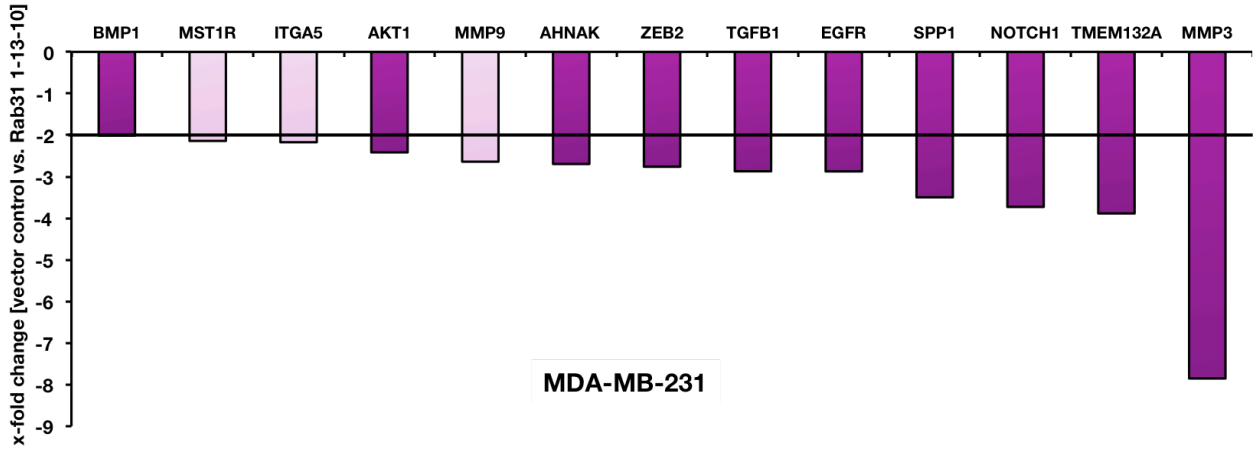

Figure 81 | Down-regulation of candidate genes in MDA-MB-231 Rab31-overexpressing cells compared to the vector control
The mRNA of the depicted genes is at least 2-fold down-regulated in Rab31-overexpressing compared to vector control cells (mean value of two experiments). The purple color indicates that in both experiments a ≥2-fold down-regulation was observed. In the case of the light pink bars only one experiment displayed a ≥2-fold down-regulation, but the mean value was ≥2-fold as well.

Out of 84 analyzed genes, 13 showed ≥2-fold lower mRNA levels in the MDA-MB-231 overexpressing Rab31 compared to the vector control cells (Figure 81).

In contrast, up-regulation of mRNA levels upon Rab31-overexpression was observed in three cases only (mean value of two experiments: ≥2-fold). Furthermore, in two of these three cases, only one of the two experiments revealed an increase of ≥2-fold, whereas in the second experiment only a tendency of up-regulation was observed (Figure 82).

The above-described experiments were subsequently performed with CAMA-1-derived cells as well. On the one hand, seven of 84 genes were found to be potentially down-regulated in Rab31-overexpressing *versus* vector control cells (Figure 83).

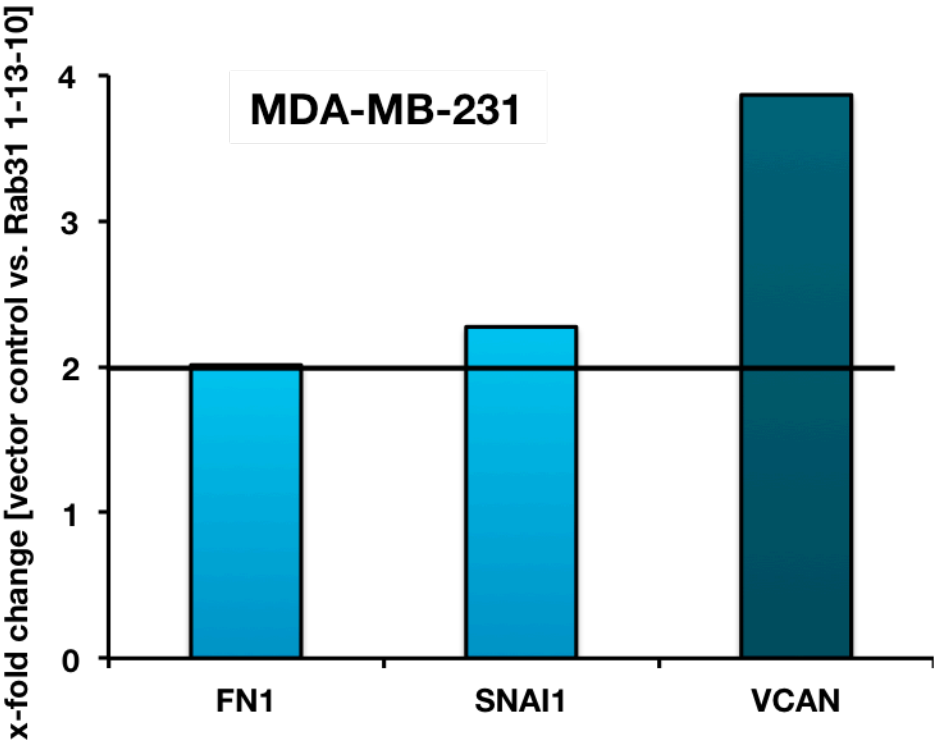

Figure 82 | Up-regulation of candidate genes in MDA-MB-231 Rab31-overexpressing compared to vector control cells

The mRNA of the depicted genes is at least 2-fold up-regulated in Rab31-overexpressing compared to vector control cells (mean value of two experiments). The petrol color indicates that in both experiments a ≥2-fold down-regulation was observed. In the case of the light blue bars only one experiment displayed a ≥2-fold down-regulation, but the mean value was ≥2-fold as well.

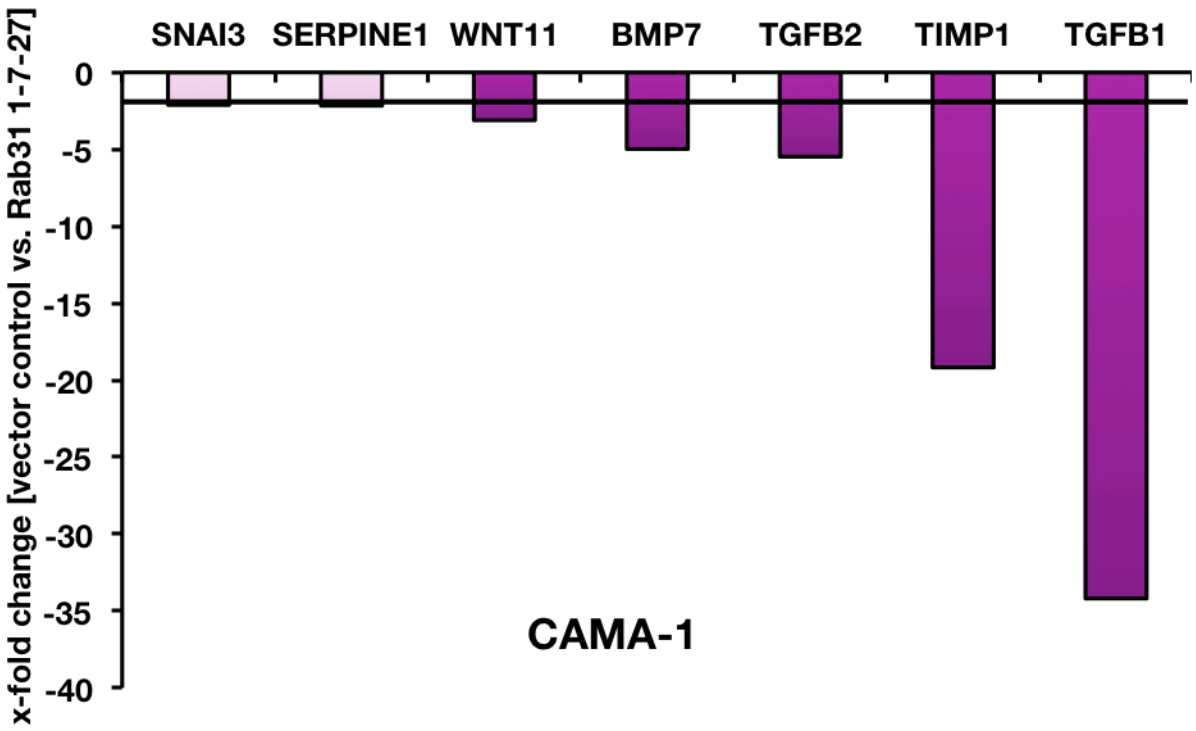

Figure 83 | Down-regulation of candidate genes in CAMA-1 Rab31-overexpressing cells compared to the vector control
The mRNA of the depicted genes is at least 2-fold down-regulated in Rab31-overexpressing compared to vector control cells (mean value of two experiments). The purple color indicates that in both experiments a ≥2-fold down-regulation was observed. In case of the light pink bars only one experiment displayed a ≥2-fold down-regulation, but the mean value was ≥2-fold as well.

On the other hand, six genes were found to be distinctly up-regulated in Rab31-overexpressing *versus* vector control cells (mean value of two experiments: ≥2-fold). Four of the six candidate genes displayed ≥2-fold higher mRNA levels in Rab31-overexpressing cells in both independently performed experiments (Figure 84).

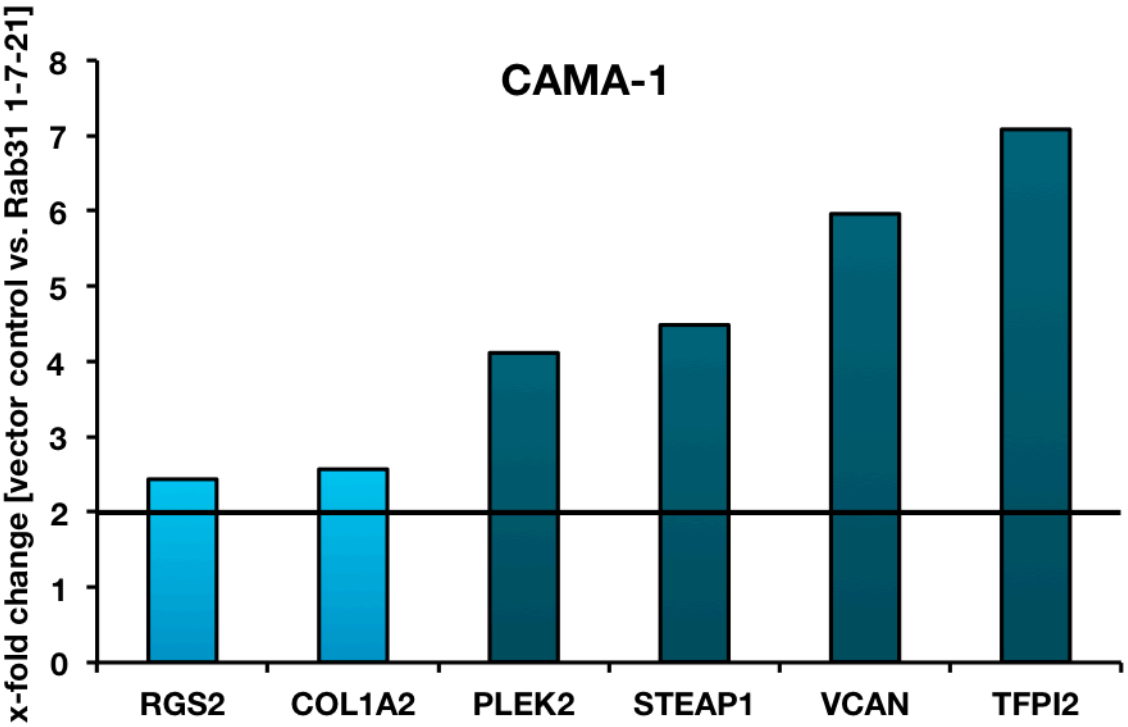

Figure 84 | Up-regulation of candidate genes in CAMA-1 Rab31-overexpressing cells compared to the vector control
The mRNA of the depicted genes is at least 2-fold up-regulated in Rab31-overexpressing compared to vector control cells (mean value of two experiments). The petrol color indicates that in both experiments a ≥2-fold down-regulation was observed. In the case of the light blue bars only one experiment displayed a ≥2-fold down-regulation, but the mean value was ≥2-fold as well.

When we compared the differentially regulated candidate genes from the MDA-MB-231 and CAMA-1 cells, respectively, a single gene, VCAN, encoding for the extracellular matrix proteoglycan versican, was found to be potentially up-regulated in both cell lines upon overexpression of Rab31. Another gene, TGFB1 encoding TGF-β1, was identified to be potentially down-regulated in both cell lines (Figure 85).

Of all candidate genes, the potentially up-regulated gene VCAN and the down-regulated gene TGFB1 also displayed a highly differential expression pattern in Rab31-overexpressing *versus* vector control cells. In the two biologically independent experiments of MDA-MB-321 cells VCAN was approximately 3-fold up-regulated in Rab31-overexpressing cells (Figure 86 A). For Rab31-overexpressing CAMA-1 cells, similar results were obtained. Here, VCAN was found to be 3- to 8-fold up-regulated in Rab31-overexpressing cells (Figure 86 B).

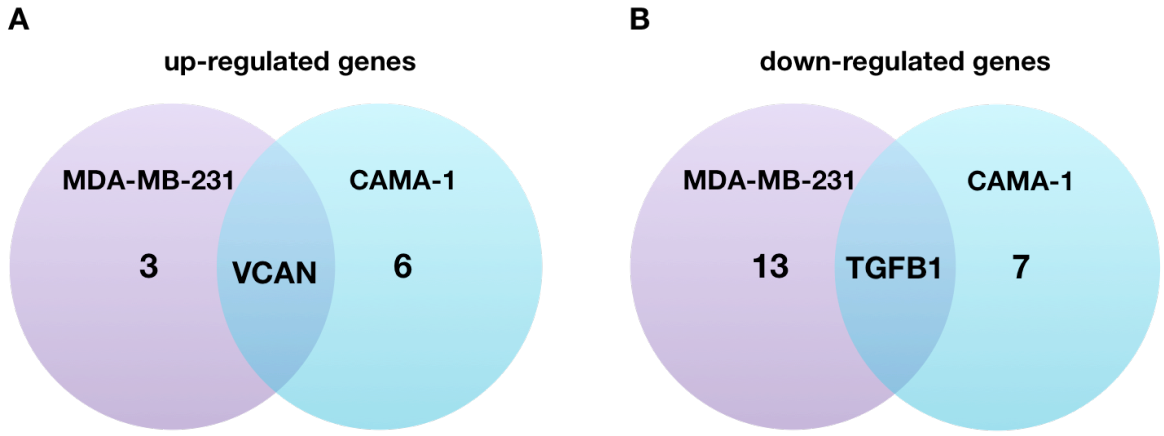

Figure 85 | Venn diagrams of commonly regulated genes between MDA-MB-231 and CAMA-1 cells in the SAB EMT array
In each circle, the cell line and the number of up-regulated genes **(A)** and down-regulated genes **(B)** are depicted. In the intersecting part, the genes that are up- or down-regulated more than 2-fold in both cell lines are given.

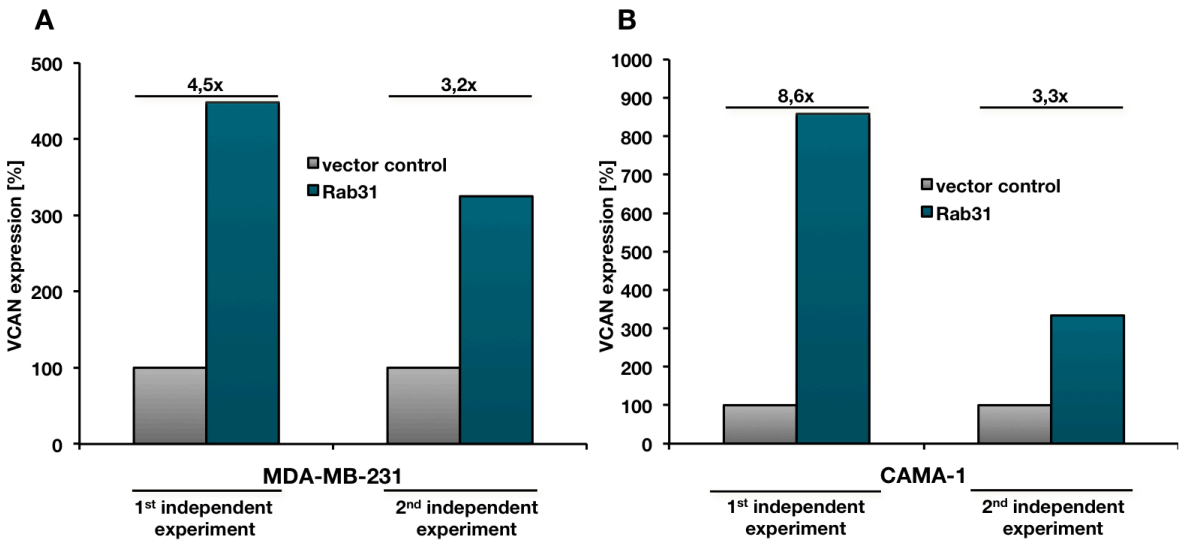

Figure 86 | Versican mRNA expression levels of vector control *versus* Rab31-overexpressing breast cancer cells
A: MDA-MB-231 cells **B:** CAMA-1 cells. Two biologically independent PCR microarray experiments (SAB EMT array) show significant up-regulation of VCAN in Rab31-overexpressing compared to vector control cells.

The data obtained for TGFB1 in the four PCR microarray experiments are depicted in Figure 87. In the two independent experiments using mRNA isolated from MDA-MB-321 cells TGF-β1 mRNA expression was approximately 3-fold down-regulated in Rab31-overexpressing compared to vector control cells (Figure 87 A). For CAMA-1 cells, the differences in the regulation level were even more pronounced. Here, Rab31-overexpressing cells showed approximately 30-fold down-regulated TGF-β1 mRNA levels compared to the vector control cells (Figure 87 B).

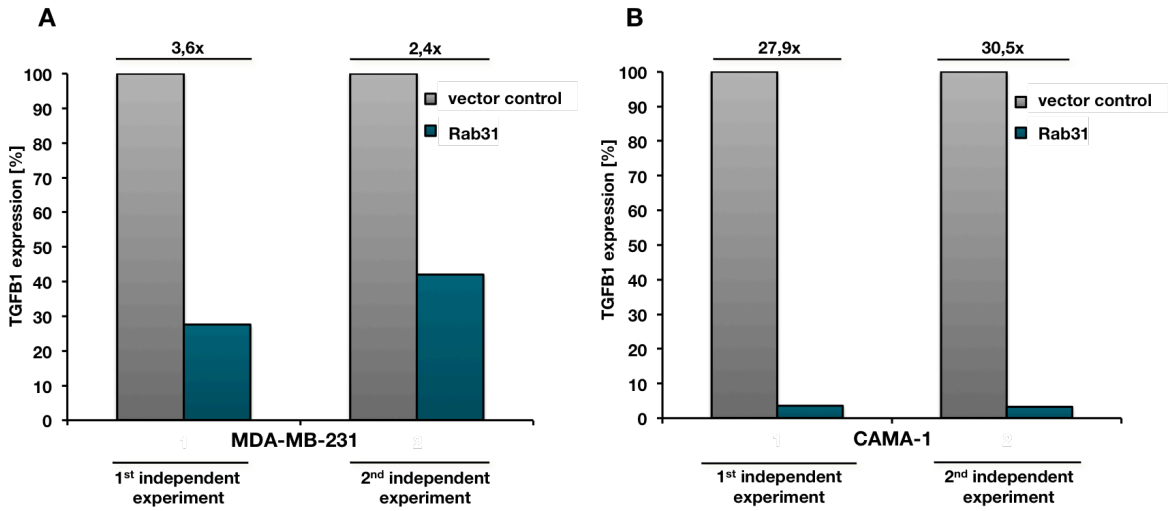

Figure 87 | TGF-β1 mRNA expression levels of vector control *versus* Rab31
A: MDA-MB-231 cells **B:** CAMA-1 cells. Two independent experiments of the SAB EMT array showed that TGFB1 was significantly down-regulated in the Rab31-overexpressing cells compared to the vector control cells.

6.4.4 - Validation of differential VCAN expression in Rab31-overexpressing *versus* vector control breast cancer cells

To validate the potential up-regulation of VCAN gene expression in response to Rab31-overexpression in MDA-MB-231 and CAMA-1 cells, the versican (and Rab31) mRNA levels were quantified using an independent qPCR assay (TaqMan gene expression assay; Life Technologies). Importantly, the VCAN fluorescent probe and primers used in the validation experiments have different sequences than those used in the SAB assay and, thus, these assays can be considered as independent. The housekeeping gene HPRT1 (encoding hypoxanthin-phosphoribosyl-transferase 1) was used as reference to normalize the results.

As expected, overexpression of Rab31 was verified on the mRNA level in both cell lines stably transfected with the Rab31 expression plasmid (Figure 88 A and 88 B, left panel). Although in both cell lines an overall, about 2-fold, up-regulation of VCAN gene expression was seen in response to increased Rab31 expression, the observed differences in the versican mRNA levels between Rab31-overexpressing *versus* vector control cells were not significant. This may, at least in part, be due to the rather high variability of the values obtained in the PCR analyses which points to the need for the development of an improved qPCR assay in further studies.

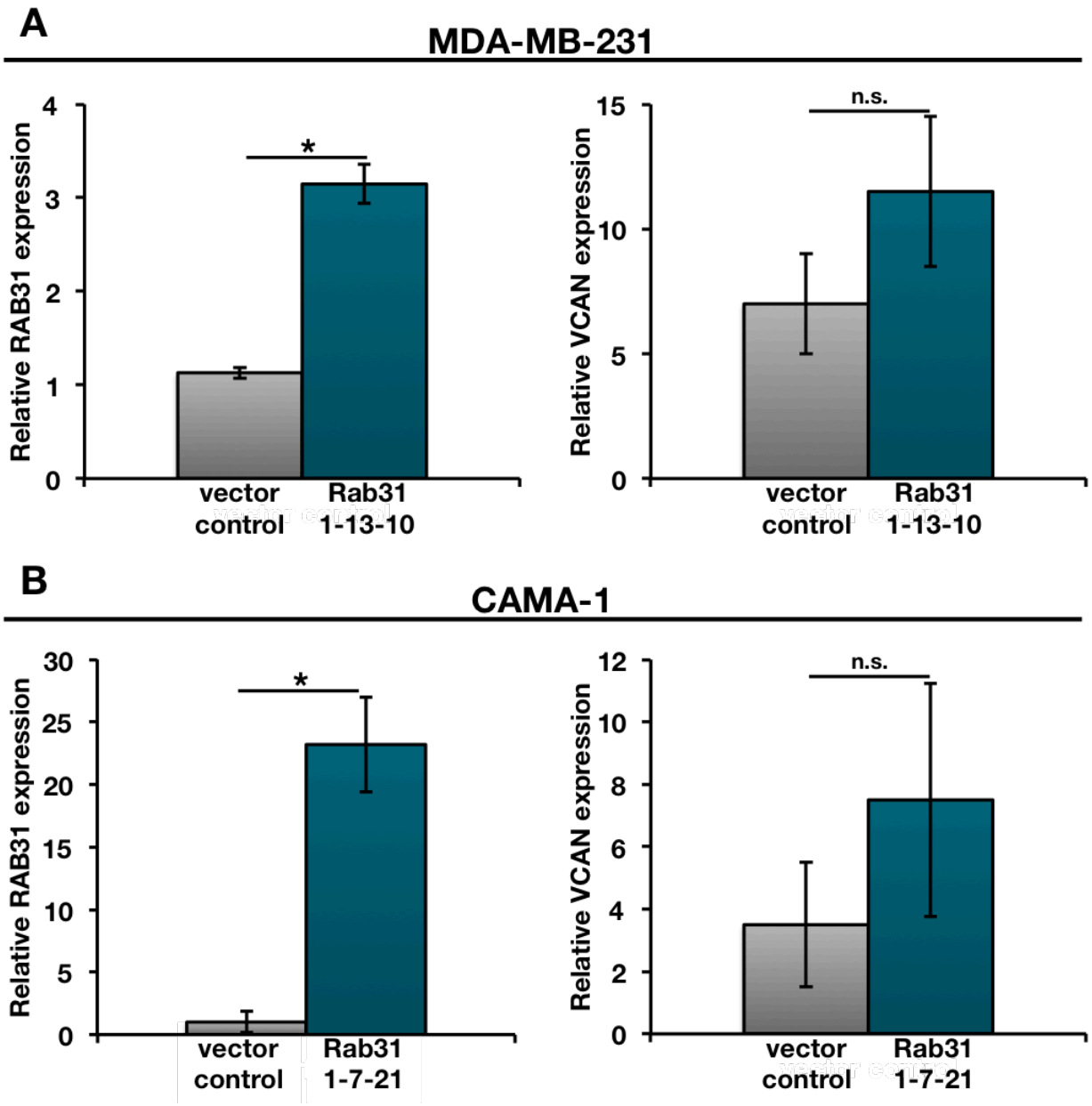

Figure 88 | Versican mRNA levels in MDA-MB-231 and CAMA-1 cells

A: Rab31 qPCR confirms a significant higher Rab31 mRNA expression in MDA-MB-231 cells stably transfected with pRcRSV-Rab31 as compared to the respective vector control (left panel). Versican mRNA expression, although increased, is not significantly up-regulated upon Rab31 overexpression (right panel).

B: Rab31 mRNA expression in CAMA-1 Rab31-overexpressing *versus* vector control cells (left panel). Versican mRNA expression, although increased, is not significantly up-regulated upon Rab31 overexpression (right panel).

All samples were normalized to the HPRT1 mRNA expression level. At least three experiments were performed in triplicates each. Statistically significant differences ($p<0.05$) are indicated by an asterisk.

6.4.5 - VALIDATION OF DIFFERENTIAL TGF-β1 MRNA EXPRESSION IN RAB31-OVEREXPRESSING *VERSUS* VECTOR CONTROL BREAST CANCER CELLS

To validate a potential down-regulation of TGFB1 gene expression in response to Rab31 overexpression in MDA-MB-231 and CAMA-1 cells, the TGF-β1 (and Rab31) mRNA levels were quantified in these cells using an independent qPCR assay (TaqMan gene expression assay; Life Technologies). As in case of the VCAN gene expression analysis, the TGFB1 primers and the probe used in the validation experiments have a different sequence than those used in the SAB assay and, thus, the assays are independent. Again, the housekeeping gene HPRT1 was used as reference to normalize the results.

Although in MDA-MB-231 cells, a trend for the down-regulation of TGFB1 gene expression was seen in response to increased Rab31 expression, the observed differences in the TGF-β1 mRNA levels between Rab31-overexpressing *versus* vector control cells were not significant (Figure 89).

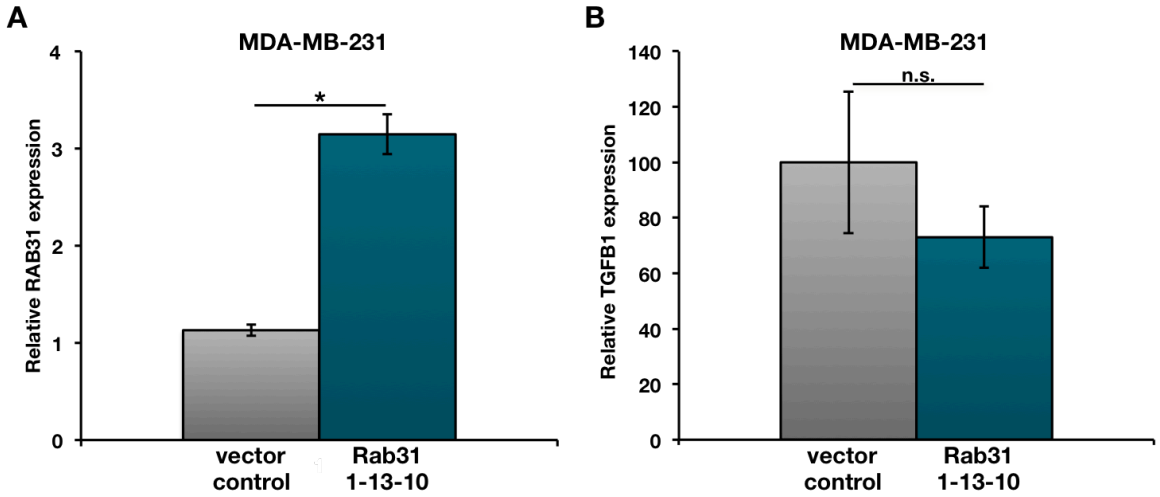

Figure 89 | TGF-β1 mRNA down-regulation in MDA-MB-231 cells with Rab31-overexpressing cells *versus* vector control cells
A: Rab31 qPCR confirms a significant higher Rab31 mRNA expression in MDA-MB-231 cells stably transfected with pRcRSV-Rab31 as compared to the respective vector control.
B: TGF-β1 mRNA expression, although decreased, is not significantly down-regulated upon Rab31-overexpression.
All samples were normalized to HPRT1 expression level. At least three experiments were performed in triplicates each. All data are normalized to HPRT1 mRNA levels. Statistically significant differences ($p<0.05$) are indicated by an asterisk.

However, when the cells were grown for 72 h under starving conditions (*i.e.* in FCS-free medium) or in a synthetic XerumFree (XF) medium (TNC BIO) (data not shown), the differences in TGB-β1 mRNA levels between Rab31-overexpressing and vector control cells were more pronounced and significantly different (Figure 90).

In CAMA-1 cells a strong down-regulation of TGFB1 gene expression was seen already in FCS-containing medium in response to increased Rab31 expression. Here, the

observed differences in the TGF-β1 mRNA levels between Rab31-overexpressing *versus* vector control cells were highly significant (Figure 91).

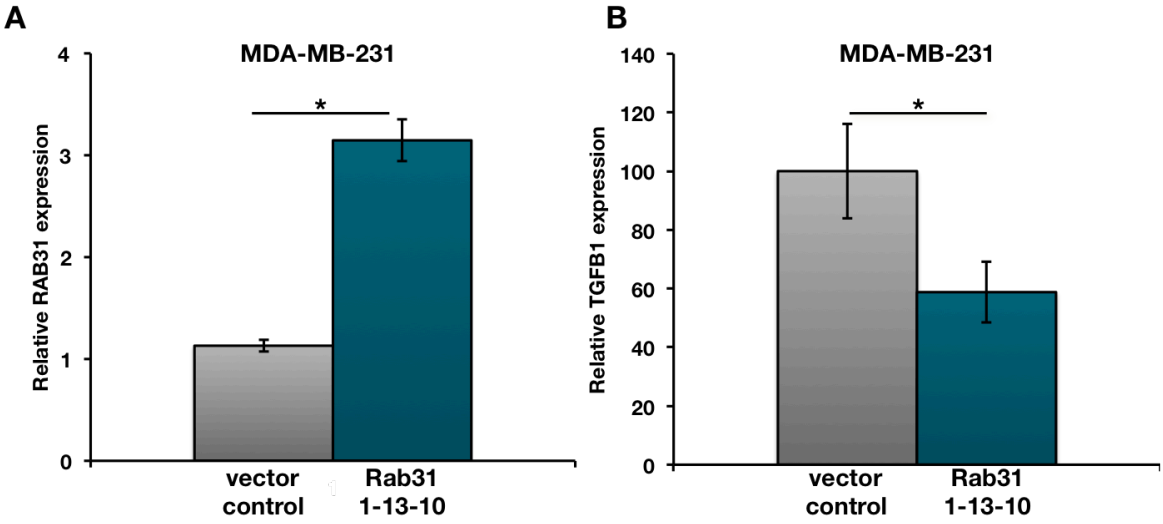

Figure 90 | Rab31 and TGF-β1 mRNA expression levels in MDA-MB-231 cells, grown in FCS-free medium for 72 h

A: Relative Rab31 expression levels in MDA-MB-231 cells. Overexpression of Rab31 in comparison to vector control cells could be verified.

B: Relative TGF-β1 expression levels in MDA-MB-231 cells. The TGF-β1 reduction upon Rab31-overexpression could be verified on mRNA level in FCS-deprived cells.

All samples were normalized to the HPRT1 mRNA expression level. Three experiments were performed each in triplicates. Statistically significant differences ($p<0.05$) are indicated by an asterisk.

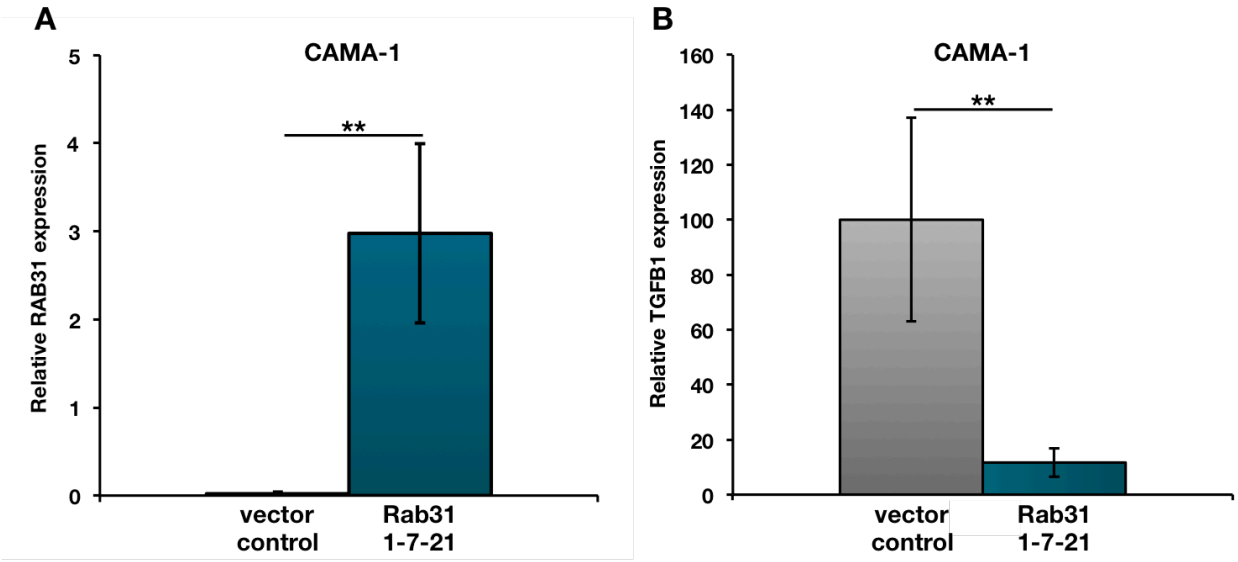

Figure 91 | TGF-β1 mRNA down-regulation in CAMA-1 Rab31-overexpressing cells *versus* vector control cells

A: Rab31 qPCR confirms a significant higher Rab31 mRNA expression in CAMA-1 cells stably transfected with pRcRSV-Rab31 as compared to the respective vector control.

B: TGF-β1 mRNA expression is significantly down-regulated upon Rab31-overexpression.

All samples were normalized to the HPRT1 mRNA expression level. At least three experiments were performed in triplicates each. All data are normalized to HPRT1 mRNA levels. Statistically significant differences ($p<0.05$) are indicated by an asterisk.

Similar results were obtained, when the cells were grown for 72 h under starving (FCS-free) conditions (Figure 92), or in the synthetic medium (data not shown).

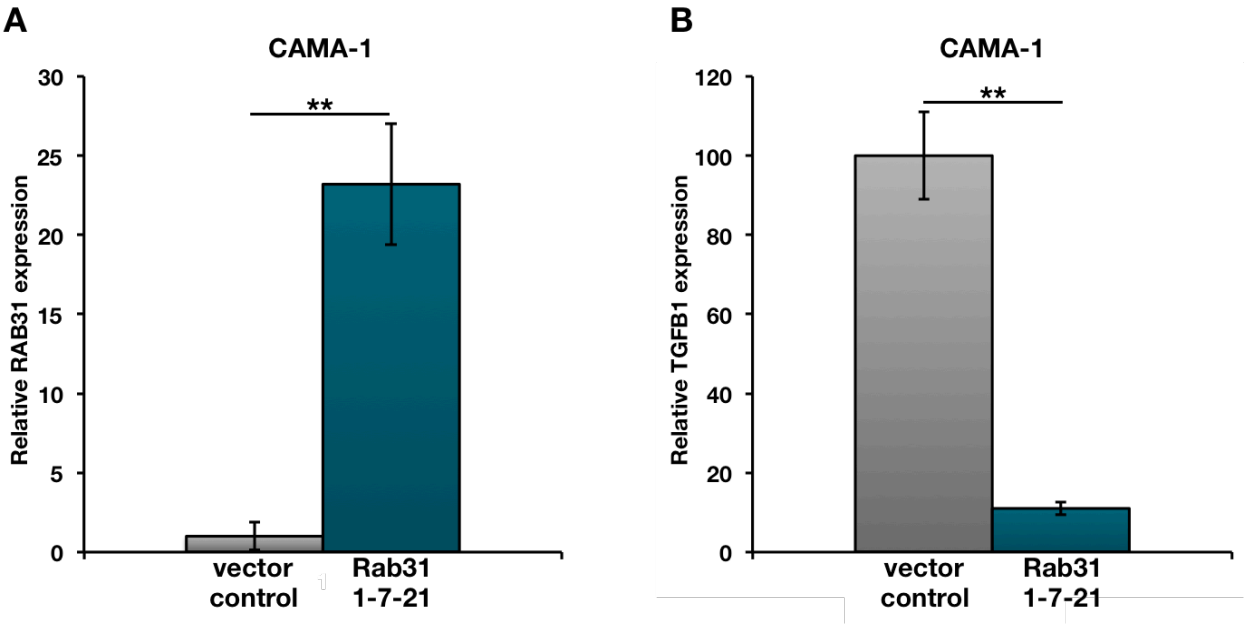

Figure 92 | Rab31 and TGF-β1 mRNA expression levels in CAMA-1 cells, grown in FCS-free medium for 72 h

A: Rab31 qPCR confirms a significant higher Rab31 mRNA expression in CAMA-1 cells stably transfected with pRcRSV-Rab31 as compared to the respective vector control.

B: Relative TGF-β1 expression levels in CAMA-1 cells. When Rab31 was overexpressed the TGF-β1 mRNA expression levels were down-regulated. The TGF-β1 mRNA expression is normalized to the vector control TGF-β1 nRNA expression level.

All samples were normalized to the HPRT1 mRNA expression level. Three experiments were performed each in triplicates. Statistically significant differences ($p<0.05$) are indicated by an asterisk.

All in all, the observed differences in the TGF-β1 mRNA levels between Rab31-overexpressing *versus* vector control cells were considerably higher in CAMA-1 cells than in the MDA-MB-231 cells (Figure 92 B).

6.4.6 - Validation of differential TGF-β1 expression in Rab31 low *versus* high expressing cells on the protein level

6.4.6.1 - TGF-β1 ELISA analysis

To further confirm regulation of TGF-β1 down-regulation by Rab31 overexpression, antigen levels of TGF-β1 were assessed using an ELISA-based approach.

The translated pre-pro-TGF-β-protein consists of the pre-region (signal peptide), the pro-region, which corresponds to the so-called latent associated protein (LAP) part and the actual mature TGF-β peptide. After translation two TGF-β-peptides form a

covalently linked homodimer (Figure 96). This TGF-β dimer is noncovalently associated with two covalently linked LAPs. To activate latent TGF-β1 to the immunoreactive form, an acidification (to pH 2.0) followed by neutralization (to pH 7.4) was necessary.

As TGF-β1 is a secreted protein, its concentration can be measured in cell culture supernatants. Normally, the cells were cultivated in 10 % (v/v) FCS-containing medium. However, we observed that high concentrations of FCS interfered with the ELISA measurements (data not shown). To avoid interference with proteins contained in standard cell culture medium, cells were therefore either cultivated for 48 and 72 hours under starvation conditions (*i.e.* without FCS) or in a synthetic medium. Prior to the ELISA measurements, the supernatant was concentrated (1:16) and the TGF-β1 levels normalized to the total protein content of the cell supernatants. The results demonstrate a considerable reduction TGF-β1 secretion in both MDA-MB-231 and CAMA-1 Rab31-overexpressing cells, respectively, which is more pronounced in CAMA-1 cells (Figure 93). Furthermore, this effect is seen under both cell culture conditions (compare Figure 93, A/B *versus* C/D). Spontaneously active TGF-β is only expressed at very low levels and was not detected in distinct amounts by ELISA.

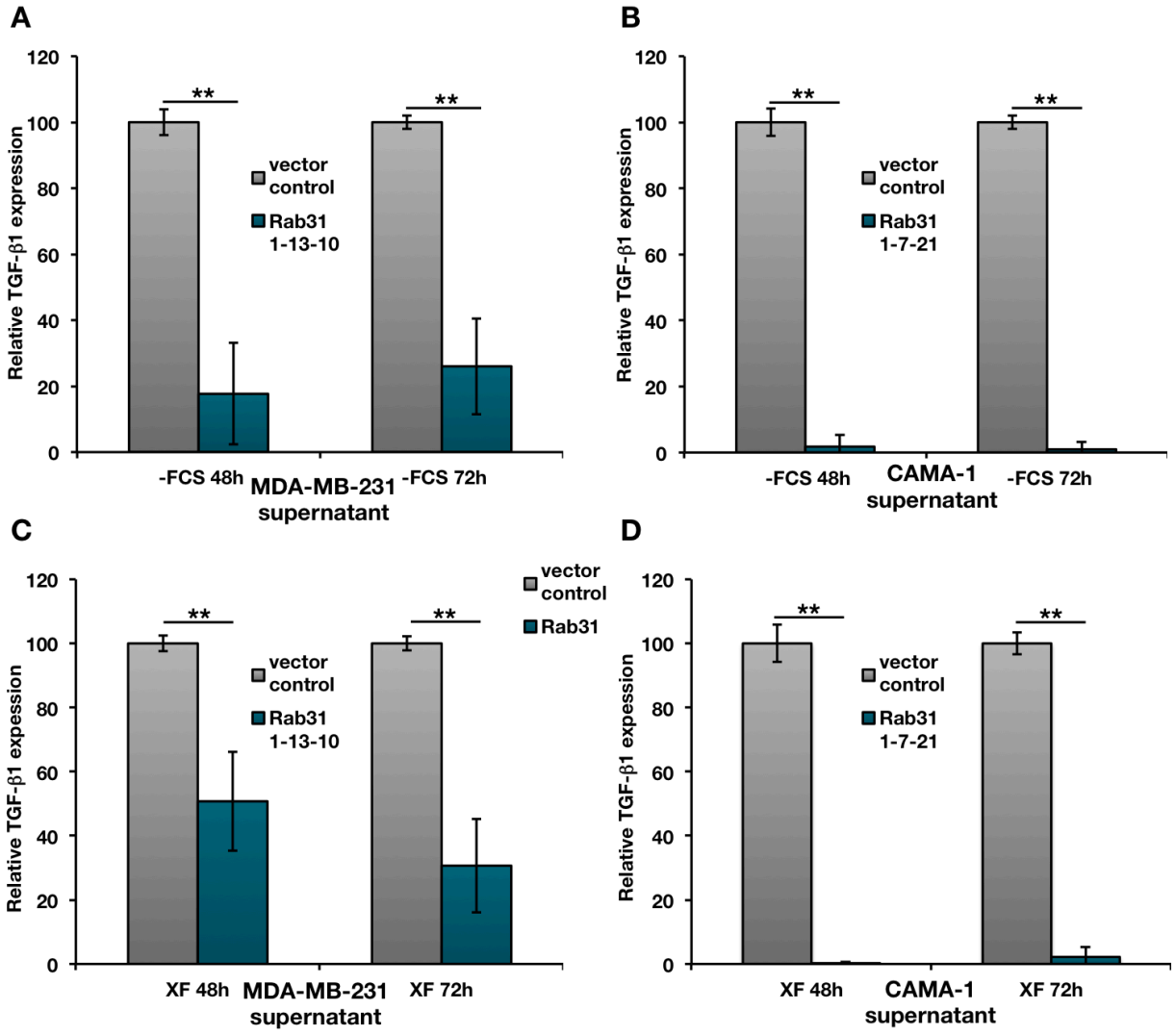

Figure 93 | Relative TGF-β1 protein expression levels in cell culture supernatants from Rab31 low *versus* high expressing cells, determined by ELISA
Cells were grown for 48 or 72 h in FCS-free (**A + B**) or in synthetic XerumFree (**C + D**) medium. Supernatants from Rab31-overexpressing cells contain significantly lower TGF-β1 antigen levels as compared to vector control cells. Three experiments were performed in triplicates each. Statistically significant differences ($p<0.05$) are indicated by an asterisk and ($p<0.01$) are indicated by two asterisks.

In an additional approach, TGF-β1 intracellular antigen levels were also determined in whole cell lysates (Figure 94). These analyses confirmed the results obtained with the cell culture supernatants and the mRNA analysis and showed that TGF-β1 expression is reduced on both protein and mRNA level upon high Rab31 expression in breast cancer cells.

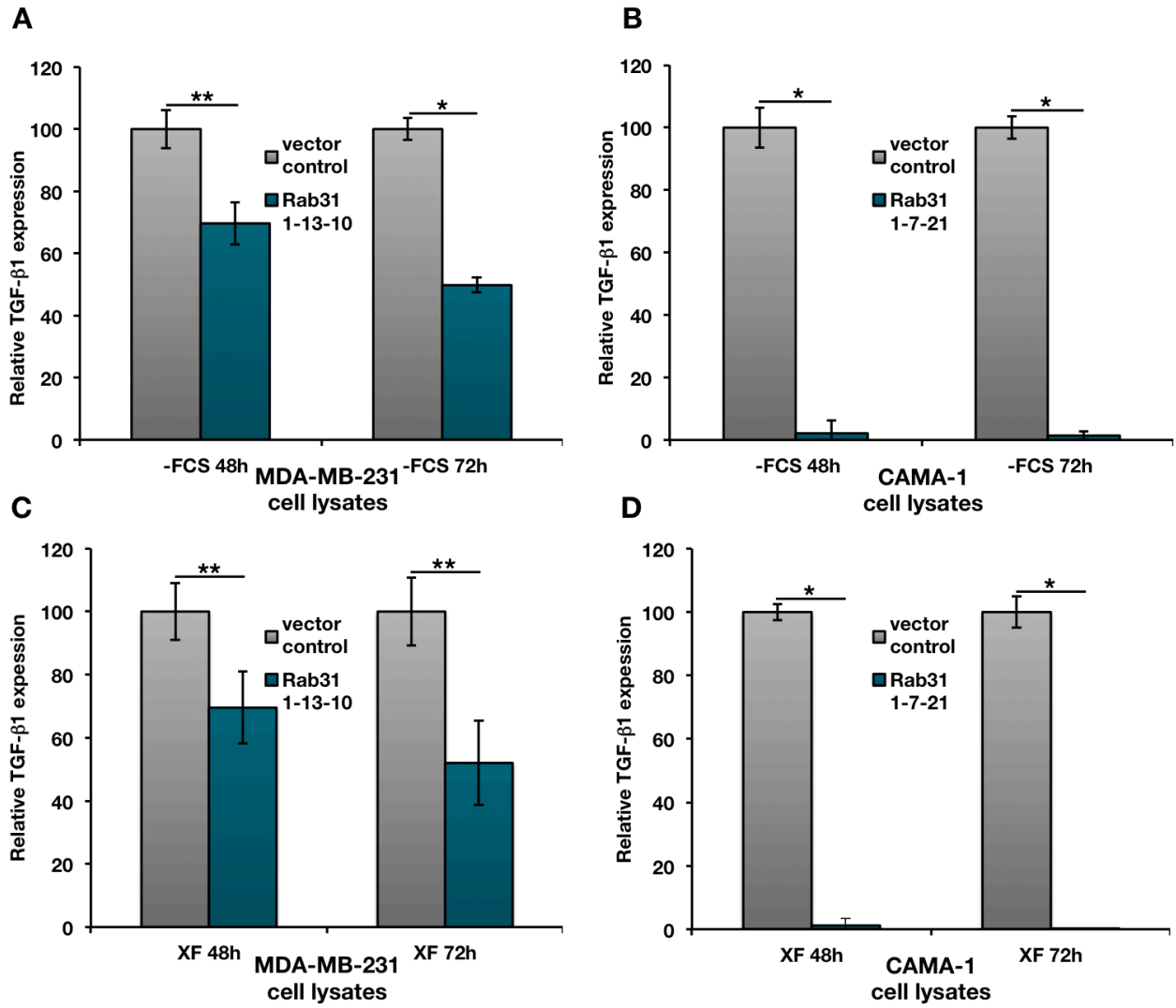

Figure 94 | Relative TGF-β1 antigen levels in whole cell lysates from Rab31 low *versus* high expressing cells, determined by ELISA

Cells were grown for 48 or 72 h in FCS-free (**A + B**), or in XerumFree (**C + D**) medium. Cell lysates from Rab31-overexpressing cells contain significantly reduced TGF-β1 protein levels as compared to vector control cells. The difference in reduction is significant in both cell types but more pronounced in the non-Rab31-expressing CAMA-1 cells. Three experiments were performed in triplicates each. Statistically significant differences ($p<0.05$) are indicated by an asterisk and ($p<0.01$) are indicated by two asterisks.

Since starving cells could change their protein expression patterns, we also analyzed TGF-β1 production in whole cell lysates from cells grown in the presence of 10% FCS in a control experiment using MDA-MB-231 cells. The cells were thoroughly washed before lysis to ensure that none of the ELISA-interfering components of FCS were present (Figure 95).

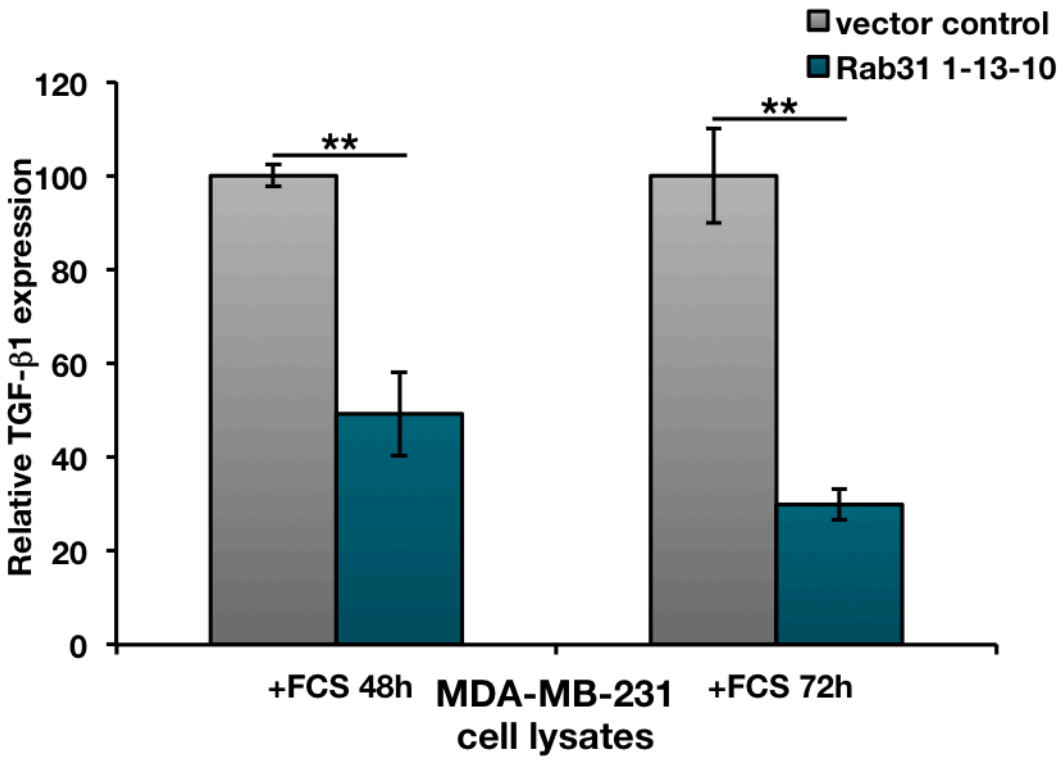

Figure 95 | Relative TGF-β1 antigen levels in whole cell lysates of Rab31 low *versus* high expressing cells, cultivated in FCS-containing medium, determined by ELISA
Cells were grown for 48 or 72 h in medium containing 10 % (v/v) FCS. Cell lysates from Rab31-overexpressing cells contained significantly reduced TGF-β1 protein levels than the vector control cells. Three experiments were performed in triplicates each. Statistically significant differences ($p<0.01$) are indicated by two asterisks.

The results revealed that MDA-MB-231 cells grown in FCS-containing medium matched the results from the FCS-free or XF medium analyses: Rab31 overexpression led to a distinct reduction of TGF-β1 on protein level.

6.4.6.2 - Western Blot

As mentioned above TGF-β is expressed as pre-pro-TGF-β. It consists of the pre-region (signal peptide), the pro-region that corresponds to the latent associated protein (LAP) part and the actual mature TGF-β peptide (Figure 96). After translation two TGF-β-peptides form a covalent bound homodimer. This very stable, active 24 kDa TGF-β dimer is non-covalently associated by two covalently joined pro-regions (LAP), together this is called the small latent complex (SLC). The large latent complex (LLC) is formed when a SLC and a latent TGF-β binding protein (LTBP) bind each other covalently. LAP contains the signal peptide for secretion into the extracellular space, which means both SLC, and LLC are secreted. LLC is important for quick activation and stabilization of the latent TGF-β in the ECM. The ECM acts as a reservoir from which TGF-β can be

recruited without the need for new synthesis (Figure 96). Active TGF-β can be released by proteolytic cleavage (MMP9, MMP2, plasmin), interactions with integrin and even pH changes in the microenvironment (Wakefield and Roberts 2002; Buck and Knabbe 2006).

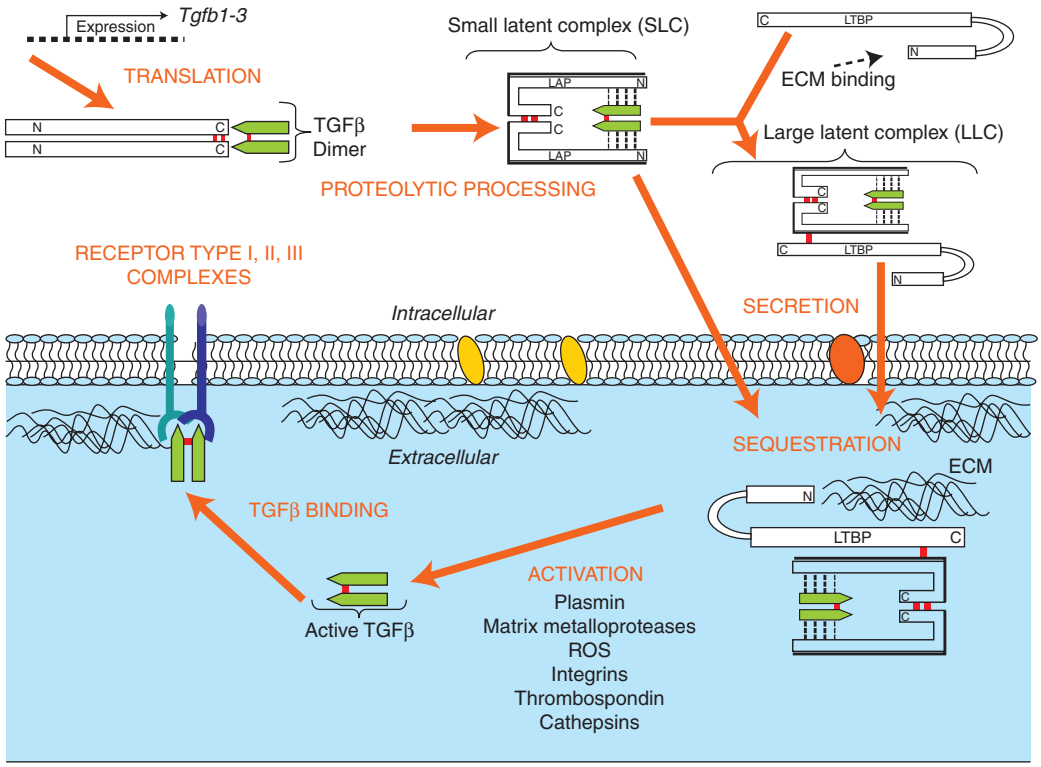

Figure 96 | TGF-β production and regulation
The small latent complex is a homodimer of the pre-pro peptide of TGF-β, designated as latency associated protein, that is non-covalently bound to TGF-β homodimer. When SLC binds covalently to LTBP it is called the large latent complex. LAP contains the signal sequence to be secreted into the extracellular space, which blocks the latent complex until activation. Activation occurs by various mechanisms, resulting in the release of TGF-β for binding to its receptors (type I, II, and III) that then signaling is initiated (Buck and Knabbe 2006).

As free mature TGF-β1 only occurs at a very low level and is rather difficult to detect on Western Blot, we decided to assess pro-TGF-β1 and LAP levels as a measure of TGF-β1 expression (Figure 97).

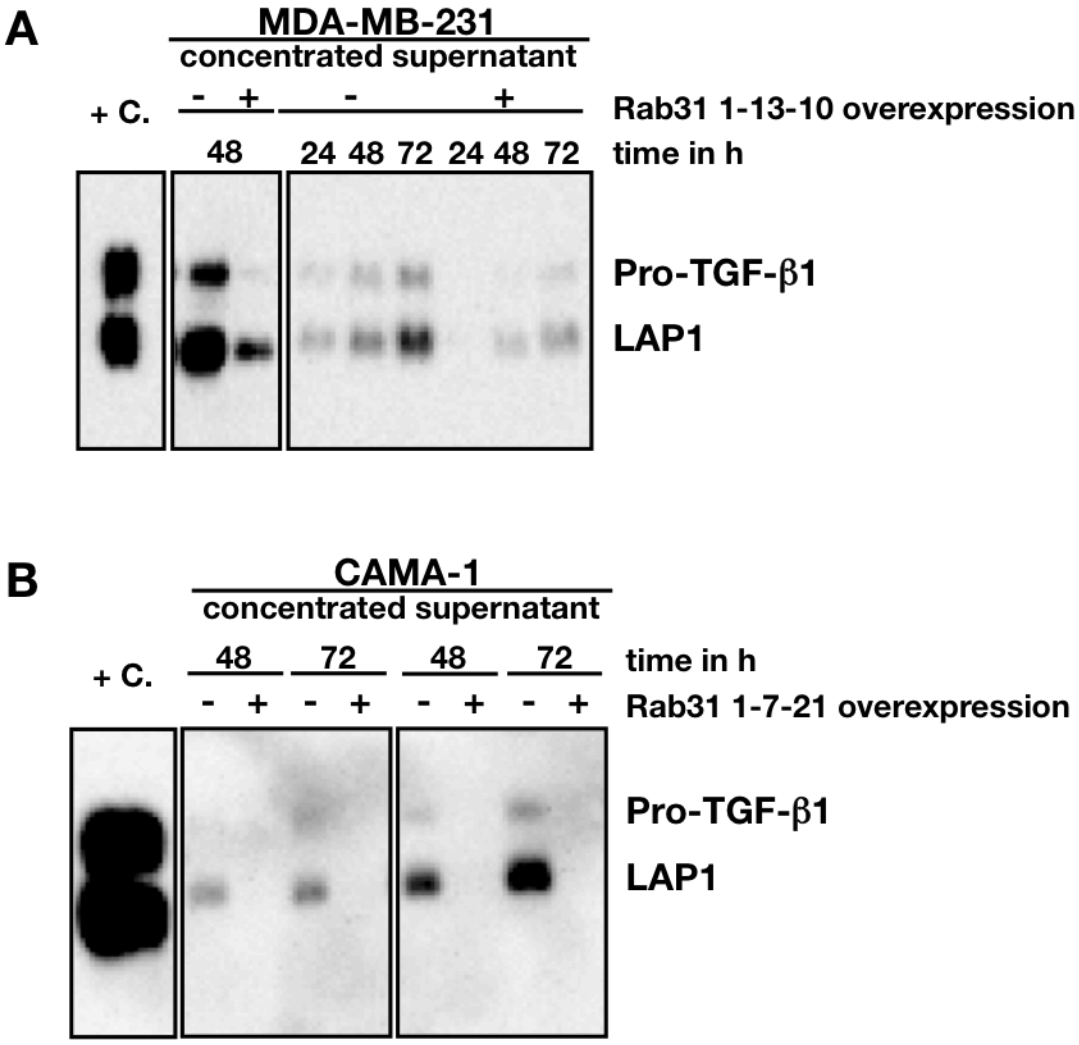

Figure 97 | Western blot analysis of TGF-β1 in cell culture supernatants of Rab31 low *versus* high expressing cells

A: Pro-TGF-β1 and LAP1 protein levels were decreased upon Rab31 overexpression. Concentrated cell culture supernatants of MDA-MB-231 cells are shown at different time points after FCS deprivation.

B: In cell culture supernatants of CAMA-1 cells, both pro-TGF-β1 and LAP1 are present in higher amounts in vector control cells as compared to Rab31-overexpressing cells.

In all analyzed samples, the protein content of corresponding Rab31-overexpressing and vector control pairs were adjusted to the same concentration before loading onto the gel.

6.4.7 - Validation of differential TGF-β activity levels in Rab31-overexpressing *versus* vector control cells

Next, we investigated whether, in addition to mRNA and protein expression, TGF-β activity was also reduced upon Rab31 overexpression using a remarkably sensitive TGF-β bioassay, that allows detection of TGF-β levels as low as 1 pg/ml *versus*

31.2 pg/ml for the ELISA approach (Tesseur et al. 2006). Concentrated supernatants (1:16) from CAMA-1 Rab31-overexpressing and vector control cells were added to murine TGFB1$^{-/-}$ fibroblasts, transfected with a TGF-β reporter plasmid (pSBE-SEAP). The reporter plasmid consists of TGF-β-responsive Smad-binding elements coupled to a secreted alkaline phosphatase. The amount of this enzyme is then determined by a chemiluminescent reaction, which is an indirect measure of active TGF-β1. TGF-β-containing cell culture supernatants were analyzed on one hand without heating to determine the levels of active TGF-β and on the other one after heating to release all of the extracellular TGF-β1 from the latent pool (Figure 98).

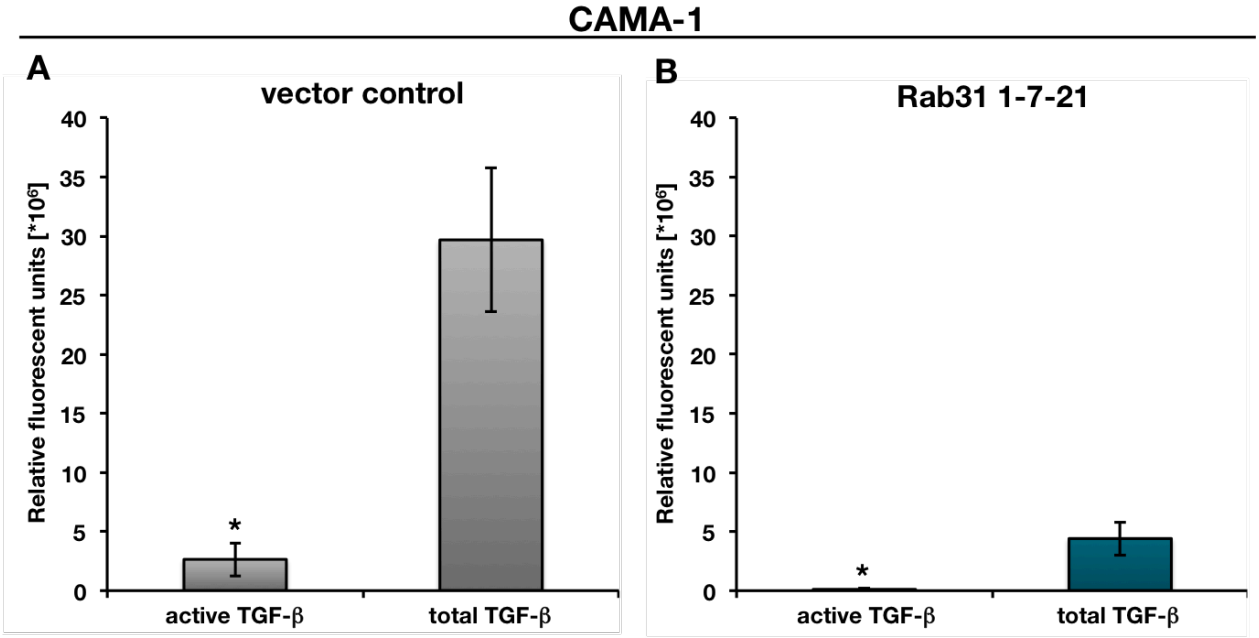

Figure 98 | TGF-ß1 activity assays of concentrated cell culture supernatants from CAMA-1 Rab31-overexpressing and vector control cells
Relative TGF-ß activities in supernatants of vector control **(A)** and Rab31-overexpressing **(B)** cells. Active TGF-β values were measured without prior heat treatment of the cell culture supernatants. The total TGF-β values were measured after acidification.

This experiment illustrates that most of the TGF-β in the supernatant is in its latent state (ratio between total/active TGF-β1 in vector control cells: 11:1; Rab31-overexpressing cells: 39:1). The ratio between active TGF-β1 between CAMA-1 vector control and Rab31-overexpressing cells was 1:24 that of total TGF-ß1 1:7. This may indicate that the vector control CAMA-1 cells not only produce significantly higher amounts of total TGF-β than the Rab31-overexpressing cells, but also release of active TGF-β from its latent form is more efficient.

6.4.8 - Identification of further differentially expressed candidate genes using another mRNA array (SAB TGF-β array)

In the experiments described above, a correlation between TGF-β1 expression and Rab31 levels was demonstrated. To further illuminate this down-regulation of TGF-β1 another low-density microarray was selected (Human TGF-β1/BMP RT² Profiler PCR Array; SAB Biosciences) and used for mRNA profiling studies of CAMA-1 vector control *versus* Rab31-overexpressing cells. This array profiles the expression of 84 key genes that have been reported to be involved in TGF-β signaling like members of the TGFβ superfamily, cytokines, their receptors SMAD family members as well as SMAD target genes. Also TGF-β-related genes like adhesion molecules, extracellular molecules and transcription factors are represented on the array.

RNA was isolated from CAMA-1 cells, reverse transcribed and the mRNA expression levels of the various genes evaluated by quantitative PCR using the low-density microarrays. Figure 99 depicts the pair-wise comparison of the expression levels of Rab31-overexpressing *versus* vector control cells. Those genes that displayed at least two-fold higher (lower) mRNA levels in Rab31-overexpressing cells are indicated by red (green) dots.

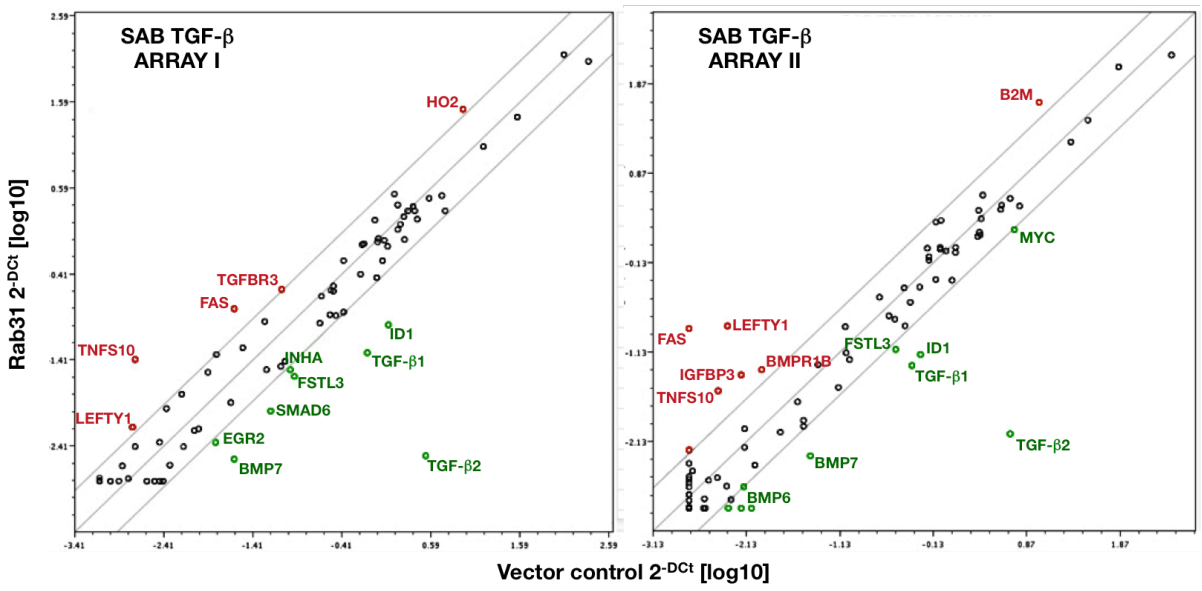

Figure 99 | Low-density qPCR microarrays reveal candidate genes being up- or down-regulated in Rab31-overexpressing *versus* vector control CAMA-1 cells
Total mRNA from CAMA-1 vector control and Rab31-overexpressing cells was analyzed in technical duplicates. The relative mean expression levels for each gene in the two samples are plotted against each other, dots in red represent candidate genes potentially up-regulated in Rab31-overexpressing cells, while green dots represent genes, potentially down-regulated mRNA, each by at least two-fold. Black dots display relative expression changes between two-fold up- or down-regulation.

In total, two arrays were performed and, thus, CAMA-1 cells were examined twice with independently generated biological replicates. HPRT1 was used to normalize the arrays. Figure 100 shows the mean values of candidate genes (given as x-fold regulation) of these two measurements. We focused on those genes, which displayed an at least two-fold mean value indicating higher up- or down-regulation.

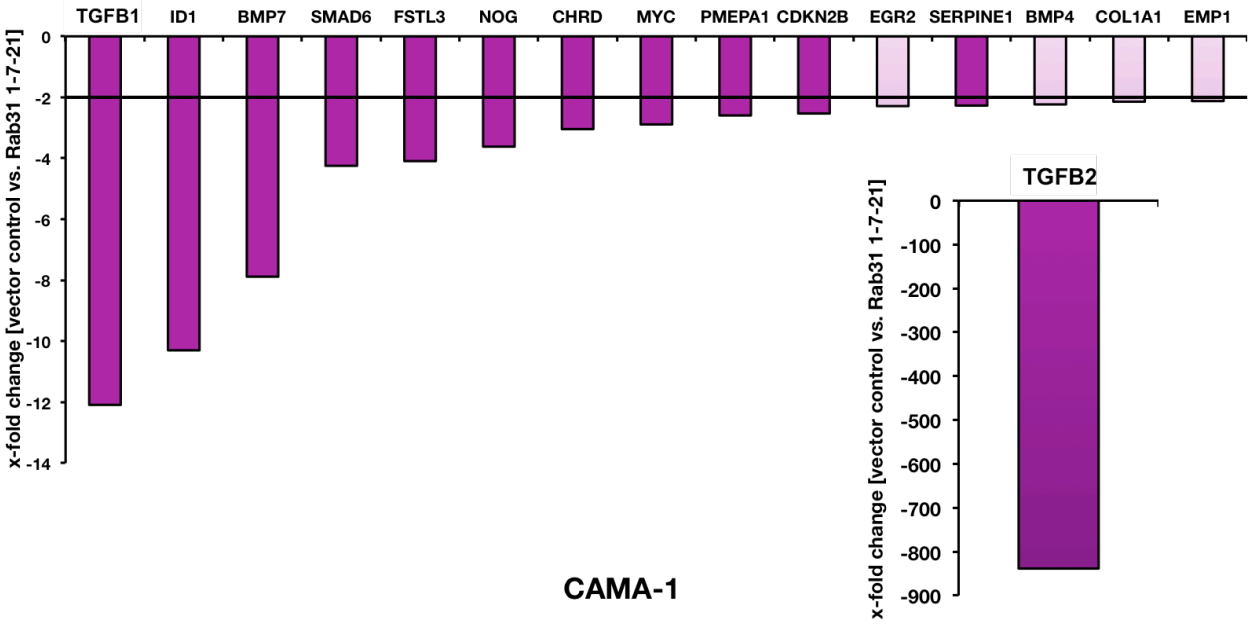

Figure 100 | Down-regulation of candidate genes in CAMA-1 Rab31-overexpressing cells compared to the vector control
The mRNA of the depicted genes is at least 2-fold down-regulated in Rab31-overexpressing compared to vector control cells (mean value of two experiments). The purple color indicates that in both experiments a ≥2-fold down-regulation was observed. In case of the light pink bars only one experiment displayed a ≥2-fold down-regulation, but the mean value was ≥2-fold as well.

In CAMA-1 cells, 16 of 84 mRNAs were significantly reduced and 15 mRNAs were increased upon Rab31 overexpression. The strongest effects concerning down-regulation were found for TGFB2 and TGFB1. Expression of TGFB3 was not affected.

The strongest effects concerning up-regulation were found for LEFTY1 and TNFS10 (Figure 101).

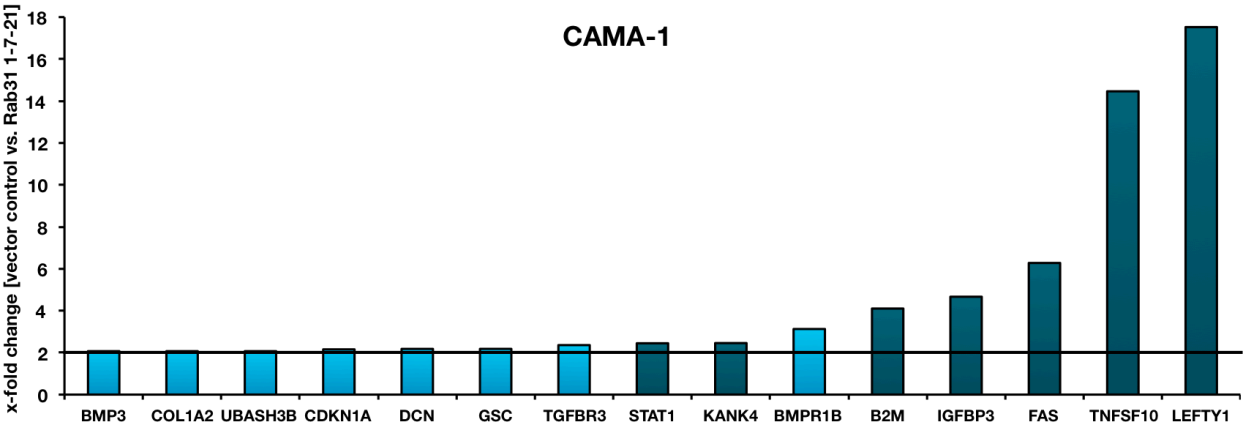

Figure 101 | Up-regulation of candidate genes in CAMA-1 Rab31-overexpressing cells compared to the vector control
The mRNA of the depicted genes is at least 2-fold up-regulated in Rab31-overexpressing compared to vector control cells (mean value of two experiments). The petrol color indicates that in both experiments a ≥2-fold down-regulation was observed. In the case of the light blue bars only one experiment displayed a ≥2-fold down-regulation, but the mean value was ≥2-fold as well.

6.4.9 - Validation of differential mRNA expression of selected candidate genes in Rab31-overexpressing *versus* vector control cells by qPCR

To validate down-regulation of candidate genes in Rab31-overexpressing CAMA-1 cells, we again used qPCR analysis. The following genes were selected: TGFB1, TGFB2, FSTL3, FMP7, SMAD6 and MYC based on the results depicted in Figure 102. In addition, we also analyzed TIMP1 expression, which was found down-regulated in CAMA-1 but not MDA-MB-231 Rab31-overexpessing cells in the initial screen using the Human EMT RT² Profiler PCR Array (SAB Biosciences) (Figure 83).

TaqMan probes and primers for the different genes were used. The primers used in the validation experiments have a different sequence than primers used in the SAB assay to further independently assess mRNA levels. The samples always consisted of a pair of Rab31-overexpressing cells and the vector control cells from the same cell line. The housekeeping gene HPRT1 was used as reference to normalize the results.

All genes with exception of MYC were validated to be differentially regulated in Rab31-overexpressing *versus* vector control cells. In case of MYC even after 40 cycles no PCR product could be detected in both cell lines, and thus has to be considered as a false-positive candidate gene form the microarray analysis.

In a similar manner, we selected four candidate genes indicating a distinct up-regulation in Rab31-overexpressing CAMA-1 cells (Figure 103) B2M, FAS TNFS10 and LEFTY (Figure 103).

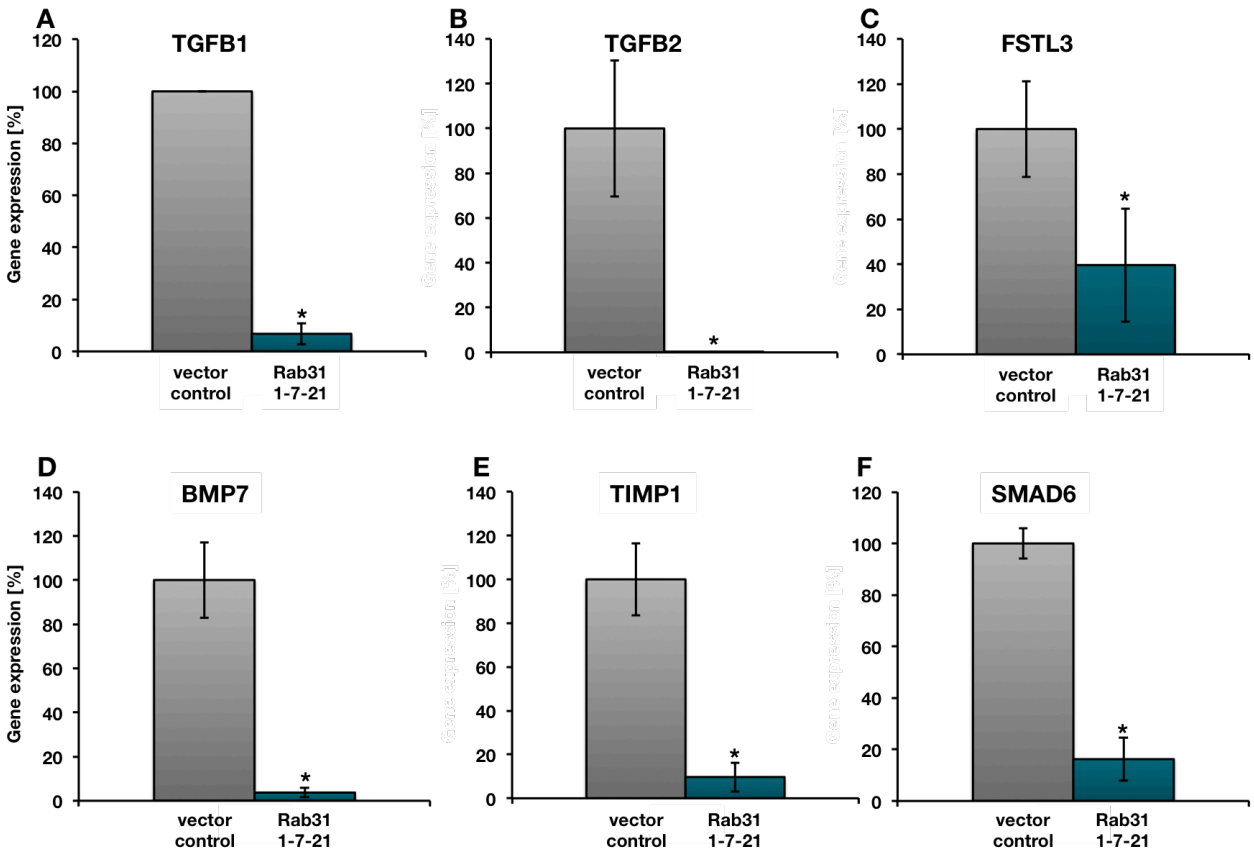

Figure 102 | mRNA analysis of CAMA-1 cells overexpressing Rab31 compared to vector control

The vector control mRNA was set to 100 % and the reduction of mRNA in the Rab31-overexpressing cells was calculated accordingly. All samples were normalized to HPRT1 expression level. Three experiments were performed in triplicates each. Statistically significant differences ($p<0.05$) are indicated by an asterisk. All data is normalized to HPRT1.

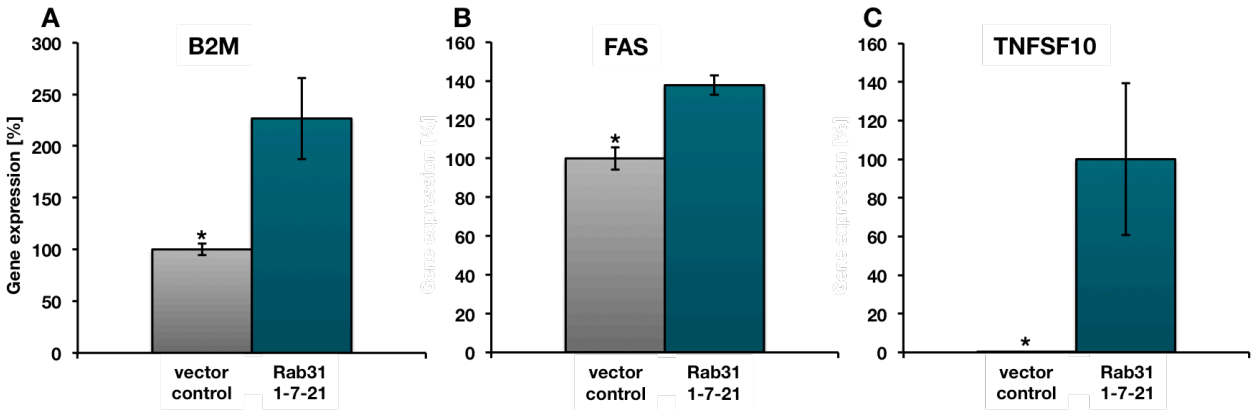

Figure 103 | mRNA analysis of CAMA-1 cells overexpressing Rab31 compared to vector control

A + B: The vector control mRNA was set to 100 %

C: The Rab31 mRNA was set to 100 %

All samples were normalized to HPRT1 expression level. Three experiments were performed in triplicates each. Statistically significant differences ($p<0.05$) are indicated by an asterisk.

Here, all genes with exception of LEFTY, were validated to correspond to be differentially regulated in Rab31-overexpressing *versus* vector control cells. In case of LEFTY, even after 40 cycles no PCR product could be detected in both cell lines.

Table 2 | Differentially regulated genes in Rab31-overexpressing CAMA-1 cells *versus* vector control cells

Symbol	Description	Function	x-fold change [vector control vs. Rab31 1-7-21]
TGFB2	Transforming growth factor, beta 2	proliferation, differentiation, apoptosis **(a)**	-1010.5
BMP7	Bone morphogenetic protein 7	cartilage formation, bone homeogenisis **(b)**	-26.9
TGFB1	Transforming growth factor, beta 1	proliferation, differentiation, apoptosis **(c)**	-14.8
TIMP1	Tissue inhibitor of metalloproteases 1	inhibitor of MMPs, cell signaling **(d)**	-10.3
SMAD6	SMAD family member 6	cell signaling, TGF-β inhibitor **(e)**	-6.2
FSTL3	Follistatin-like 3	cell signaling, TGF-β inhibitor **(f)**	-2.5
TNFSF10	Tumor necrosis factor (ligand) superfamily, member 10	induces apoptosis in tumor cells **(g)**	+16061.5
B2M	Beta-2-microglobulin	activates EMT **(h)**	+2.3
FAS	Fas (TNF receptor superfamily, member 6)	regulator of apoptosis **(i)**	+1.4

a) Sanford et al. 1997; Azhar, 2001; Stauder et al. 2004; Hinshelwood et al. 2007; Buck et al. 2008;
b) Buijs et al. 2007; Alarmo et al. 2009; Rodriguez-Martinez et al. 2011; Naber et al. 2012
c) Sanford et al. 1997; Azhar, 2001; Stauder et al. 2004; Hinshelwood et al. 2007; Buck et al. 2008;
d) Cui et al. 2012; Ries 2013
e) Imamura et al., 1997; Jung et al. 2013
f) Chan et al. 2009; Antsiferova and Werner 2012; Krneta et al. 2012
g) Falschlehner et al. 2007
h) Cooper et al. 1990; Waha et al. 1998; Josson et al. 2011; Nomura et al. 2013
i) Chen et al. 2010

7 - DISCUSSION

uPAR-Δ4/5 AND RAB31 OVEREXPRESSION

Clinical studies in a cohort of nonadjuvantly treated lymph node-negative (LNN) breast cancer patients identified Rab31 as an upregulated factor significantly associated with high expression of uPAR-Δ4/5. Being associated with a significantly shorter distant metastasis-free and overall survival in these patients, both markers, Rab31 and uPAR-Δ4/5 mRNA, were shown to be so-called pure prognostic factors. Furthermore, they display an independent but additive prognostic value (Kotzsch et al. 2008).

uPAR-Δ4/5. In the human uPAR-WT gene, exon 2/3, 4/5 and 6/7 encode the domains D1, D2 and D3, respectively (Figure 9) (Ploug et al. 1991). Luther et al. (2003) described a variant of the wild-type uPAR lacking both exons 4 and 5 (uPAR-Δ4/5), which results in the complete deletion of domain 2. The lack of a complete and independent domain together with the presence of still correctly folded other domains can certainly change the function of the protein. In fact, when uPAR- Δ4/5 was overexpressed in MDA-MB-231 and CAMA-1 cells, the adhesive and invasive properties of these cells were significantly impaired (Table 3), and gene expression of other tumor-associated genes affected (Grismayer et al. 2012a). In an *in vivo* lung colonization model the overexpression of uPAR-Δ4/5 also showed significantly fewer metastases (Sato et al. 2010; Grismayer et al. 2012 a) (Table 3).

Rab31. Small GTPases comprise different families, the largest of which are the Rab proteins. In several studies, it was shown that Rab proteins play an important role in the regulation of transport between organelles, which is supported by the finding that they localize to individual intracellular compartments. Involvement of Rab mutations and the consequences of dysregulation of Rab function in different diseases like neurodegenerative disorders and cancer was established by Agola et al. (2011). Numerous members of the Rab family, *i.e.* Rab5, Rab11, Rab21, Rab25 and Rab27B have been found to be prognostic factors in breast cancer patients (Subramani and Alahari 2010; Yang et al. 2011; Hendrix et al. 2010). Although Rab31 was identified to be associated with poor prognosis of LNN breast cancer (Kotzsch et al. 2008), and Rab31 was found to be overexpressed in ERα-positive breast cancer (Abba et al. 2005), very little is known about its function in cancer. Grismayer et al. (2012 b) showed that overexpression of Rab31 stimulates enhanced proliferation of breast cancer cell lines MDA-MB-231, MDA-MB-435 and CAMA-1. Cell lines lacking endogenous Rab31 expression (MDA-MB-435 and CAMA-1) exhibit a significantly increased proliferation upon expression of moderate levels of recombinant Rab31. MDA-MB-231 cells are characterized by a low endogenous Rab31 expression. Here, enhanced proliferation can only be seen when Rab31 is highly expressed. The invasive capacity and adhesion to ECM proteins in Rab31-overexpressing breast cancer cell lines is reduced. Further data obtained from *in vitro* experiments showed reduced invasiveness in Matrigel

invasion assays. In an *in vivo* mouse model of experimental metastasis, the number of lung metastases was significantly smaller in mice injected with MDA-MB-231 Rab31-overexpressing cells compared to vector control cells (Grismayer et al. 2012 b) (Table 3).

uPAR-Δ4/5 + Rab31. We hypothesized that Rab31 and uPAR-Δ4/5, although possibly *via* different cellular pathways, might work cooperatively to support breast cancer progression. Increased cell proliferation is a pre-requisite for tumor growth while decreased adhesive properties point towards a more anchorage independent survival. Using *in vitro* cell culture experiments, we explored the possibility of an additive effect using MDA-MB-231 cell lines with a dual overexpression of uPAR-Δ4/5 and Rab31. The uPAR-Δ4/5 expression plasmid was introduced into Rab31-overexpressing MDA-MB-231 cells. uPAR-Δ4/5 expression was profoundly up-regulated in these cells Strikingly, however, a strong concomitant reduction of the Rab31 expression was observed, in several independently conducted transfection experiments. Similarly, the usage of uPAR-Δ4/5-overexpressing cells for transfection of a Rab31 expression vector resulted in a weak Rab31 expression. The only strategy, which gave rise to MDA-MB-231 cells overexpressing both Rab31 and uPAR-Δ4/5, was to transfect both plasmids simultaneously. One hypothesis may be that overexpression of either Rab31 or uPAR-Δ4/5 shifts the breast cancer cells into a different physiological state (as reflected by the observed changes on *e.g.* proliferation and/or adhesion), which upon overexpression of the second factor leads to repression of Rab31 expression. When both plasmids are introduced at the same time, the parental physiological state allows - at least initially - simultaneous expression of both factors. Within the time frame of the subsequently performed experiments, Rab31 and uPAR-Δ4/5 expression levels were routinely monitored and found to be stable. Whether Rab31 expression is lost in the double-overexpressing cells after longer time of cultivation in later passages was not analyzed.

By evaluating proliferation and adhesion of the double-overexpressing cells, no additive or synergistic effects were observed. While overexpression of both proteins decreased adhesion to a variety of extracellular matrix proteins, the increased presence of Rab31 and uPAR-Δ4/5 in breast cancer cells had no stronger impact on the adhesive phenotype as the overexpression of one factor alone. With regard to proliferation, Rab31 led to an induction of cell proliferation independent of uPAR-Δ4/5 levels. Therefore, we conclude that at least concerning these two parameters, the increase of uPAR-Δ4/5 expression does not strengthen Rab31 phenotypic changes in breast cancer cells.

MDA-MB-231				
	vector control	uPAR-Δ4/5	Rab31	uPAR-Δ4/5 Rab31
Proliferation	→	→	↑	↑
Adhesion	→	↘	↘	↘
Invasion	→	↘	↘	n. d.
In vivo lung colonization	→	↘	↘	n. d.

Table 3 | Characteristics of MDA-MB-231 cells expressing uPAR-Δ4/5 and/or Rab31
Green arrows, no change as compared to parental cells; vertical pink arrows, increased effect; petrol arrows, decreased effect; n. d., non determined

RAB31 OVEREXPRESSION AND PROLIFERATION

Rab31 overexpression leads to an increased cell growth indicating an induction of proliferation. However, the increased growth could alternatively be due to decreased apoptosis in Rab31-overexpressing cells. Apoptotic assays revealed that the percentage of apoptotic cells in Rab31-overexpressing cells did not differ from the vector control, while the number of cells in S-phase was increased. These data suggest that indeed Rab31 rather induces cell proliferation and may not support cellular survival. Indeed, a pro-proliferative effect of Rab proteins has been described for other protein family members: overexpression of Rab27A increased proliferation of a glioma cell line by increasing the number of cells in S-phase, while suppressing apoptosis (Wu et al. 2013). Furthermore, knock-down of Rab27A displays the complementary effect suggesting a possibly similar role of Rab27A and Rab31. In accordance, a study using ERα-positive human breast cancer cell lines reported that Rab27B strongly increased cell proliferation, again by promotion of G_1 to S phase transition (Hendrix et al. 2010). Additionally, Rab5A overexpression in ovarian cancer increases proliferation, again by support of S-phase transition. Here, its downstream effector APPL1 (adaptor protein containing PH domain, PTB domain, and leucine zipper motif) was identified as a possible secondary transducer protein (Zhao et al. 2010; Yang et al. 2011). Rab25 acts as a regulator of vesicle formation, intracellular trafficking as well as receptor internalization and recycling. Rab25 is upregulated in breast and ovarian cancer tissue and elevated levels of Rab25 in ovarian cancer cells were shown to lead to Akt activation, down-regulation of Bax and Bak, ultimately resulting in increased proliferation and decreased apoptosis (Cheng et al. 2005). Ng et al. (2009) identified EGFR as an interaction partner of Rab31 and showed that Rab31 modulated EGFR

internalization in the epidermoid cancer cell line A431. Rab31 is involved in cellular trafficking, which was demonstrated by Rodriguez-Gabin et al. (2001) showing that Rab31 plays a role in the vesicular transport from TGN to endosomes. The fact that Rab31 and Rab25 share similarities in terms of receptor internalization, cellular localization and the induction of proliferation suggest that signaling pathways regulated by Rab25 might also be affected by Rab31.

The impact of increased Rab31 levels on breast cancer proliferation was further supported using three dimensional (3D) spheroid assays. This 3D system may more closely mimic the nature of the microenvironment than two dimensional (2D) monolayer cultures. Indeed, QGel-based assays revealed a higher cellular DNA content, a higher cellular metabolic activity and cell spheres with an increased diameter, if cells overexpressed Rab31 and, by this, validated the observations obtained with the maybe more artificial 2D cell culture systems. Of note, only CAMA-1 cells were capable of sphere formation, suggesting the need for certain endogenous properties of breast cancer cells to allow initial outgrowth.

RAB31 KNOCK DOWN AND PROLIFERATION

The notion that Rab31 increases proliferation was supported by Rab31 knock down experiments in which Rab31 levels were reduced using siRNA and shRNAi approaches. As the transient transfection of siRNAs reduced Rab31 expression on the protein level only after 48-72 hours, a stable knock down seemed more feasible in order to avoid experimental uncertainties due to the comparable long turnover time of Rab31. Strikingly, reduction of Rab31 mRNA and, in consequence, protein levels reduced cell proliferation rates by 70%.

Increased cell proliferation upon Rab31 overexpression could be discussed as an artifact due to huge amounts of recombinant expressed Rab31 protein in the cell, which may lead to unspecific effects on the cellular machinery. But since the complementary experiment, *i.e.* reduction of Rab31 levels, leads to a decrease of proliferation, it is more likely that Rab31 acts like a molecular switch, *i.e.* it can induce or reduce proliferation depending on its cellular expression level.

RAB31 MUTANTS

Switching between GTP- and GDP-bound states results in two distinct 3D conformations and regulates the biological activity of Rab proteins. Furthermore, Rab proteins shuttle between different locations, cytoplasm and membrane, which also regulates the biological activity of Rabs due to the availability of interaction partners. Rab proteins are associated with transport vesicles while bound to GTP, but are

returned to their inactive state after hydrolysis generates the GDP-bound forms. Different Rab proteins were found to localize in distinct compartments of the endocytotic pathway. Mutants with reduced affinity for GTP (GDP-bound; constitutively inactive mutants) as well as mutants with reduced GTPase activity (GTP-bound; constitutively active mutants) were used to elucidate the biological function of Rab family members (Figure 104). In several Rab family members, the endogenous GTPase activity is inhibited by an exchange of a glutamine (Gln; Q) to leucine (Leu; L) in the GDP/GTP-binding domain, generating constitutively active mutants (Mesa et al. 2001). Overexpression of Rab22A-Q64L, the constitutively active mutant of Rab22A, strongly affects the morphology of endosomes and whereas the wild-type is associated with early and late endosomes only, this mutant also co-localizes with lysosomes. Nevertheless, a serine (Ser; S) to asparagine (Asn; N) or serine to alanine (Ala; A) mutation in GDP/GTP-binding domain leads to a decreased affinity for GTP. Accordingly, Rab22A-S19N was shown to possess reduced affinity for GTP and, consequently, exhibited a cytosolic distribution. (Kauppi et al. 2001; Mesa et al. 2001; Mesa et al. 2005).

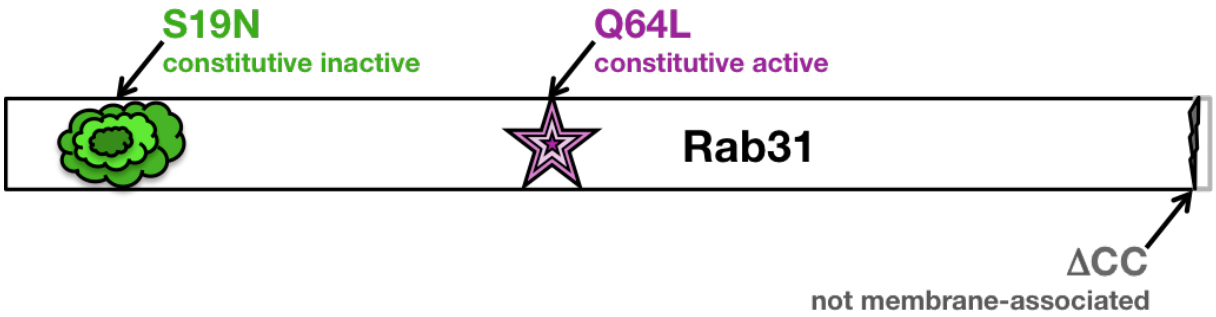

Figure 104 | Schematic representation of Rab31 mutations generated in the present study

Rab31-Q64L. We used point mutations in the GDP/GTP binding site (Q64L) to block GTP hydrolysis, thereby leading to a constitutively active form of Rab31 (Figure 104). The family of Rab GTPases is involved in vesicle trafficking and is regulated by interaction with Rab escort proteins (REPs), guanine exchange factors (GEFs), and GTP activating proteins (GAPs), with the interaction partner depending on Rab GDP/GTP states. Exchange of GTP to GDP and *vice versa* regulates the activation state of Rab proteins and is therefore crucial for proper functioning of Rab31. Interestingly, overexpression of the constitutively GTP-bound Rab31 mutant did not further increase proliferation in comparison to the increase already achieved by overexpression of Rab31-WT. This finding suggests that - at least upon overexpression the GDP/GTP binding status is not the critical effector of Rab31-supported cell proliferation. Furthermore, expression of constitutively active Rab31 does not seem to negatively affect the cell machinery.

Rab31-S19N. We used point mutations in the GTP binding domain (S19N) to block GDP exchange, thereby leading to expression of a constitutively inactive form of Rab31 (Figure 104). A mutation impairing the GTP-binding activity of Rab5 (S34N) and therefore constitutively inactivating the activation of Rab, led to substantial inhibition of endocytosis, when expressed in BHK-21 cells (Li and Liang 1994). A mutant of Rab1, Rab1-S25N, was found to interfere with transport by blocking vesicle formation (Nuoffer and Balch 1994). These experiments point to dominant-negative effects of constitutively inactive Rab-mutants in the cell. Interestingly, generation of cells overexpressing Rab31-S19N was not possible, as transfection with the expression vector in question did not lead to increased Rab31 protein levels in MDA-MB-231 cells. The expression of this potentially dominant-negative mutant also did not give rise to CAMA cells, which do not express at all endogenous levels of wild-type Rab31. Apart from possible technical problems regarding the vector itself, we suggest that expression of this non-functional Rab31 mutant can still interact and thereby scavenge interaction partners, also of other Rab proteins, irrespective of its biological GTPase activity. This mechanism of action might be strongly disadvantageous for breast cancer cells and thereby selective pressure does not allow the stable overexpression of this mutant. Promoter silencing, for example by methylation, would allow the cells to profit from the antibiotic resistance provided by the integration of the vector without the possible side-effects of high levels of Rab31-S19N. It is also possible that regulation took place on the mRNA level, either by an increased degradation or mRNA silencing, for example by an up-regulation of a matching miRNA.

Rab31-ΔCC. Rab proteins are prenylated at their C-terminal region, which is crucial for their binding ability to membranes (and thus their biological activity) and determines their subcellular localization (Figure 104). C-terminal CC or CXC sequences are essential for modification by prenylation. Khosravi-Far et al. (1992) showed that a Rab1B (ΔCC) mutant, lacking both cysteine residues is not a substrate for prenylation (Khosravi-Far et al. 1992). In the case of Rab5 dominant-negative mutants, a secondary mutation (ΔC4), deleting the C-terminal prenylation motif reversed the original dominant-negative effect (Li and Liang 1994). This indicates that interaction of Rab5 with some of its partners is strictly dependent on membrane localization.

Thus, in addition to the analysis of the role of the Rab31 nucleotide binding status, we further assessed the importance of Rab31 localization on cell proliferation. Rab proteins are localized to the membrane by the post-translational modification of two C-terminal cysteines. These cysteines are modified by geranylgeranyl transferases, which add two geranylgeranyl lipid moieties, allowing attachment of Rab proteins to the Golgi membrane. Upon localization in the Golgi membrane, GEF loads Rab31 with GTP, which then enables Rab31 to interact with different binding partners. Following GTP hydrolysis, Rab31 can be recycled. By interaction of GDP dissociation factors (GDI) with its lipid moieties, Rab31, with a GDP in its active center, can again leave the membrane. We constructed a truncated Rab31 mutant, which lacks the C-terminal

cysteines (Rab31-ΔCC), thereby, de-localizing Rab31 from the Golgi membrane without impairing the intrinsic GDP/GTP-binding activity of Rab31. However, due to its altered localization, interaction with other proteins is likely to be strongly impaired. Indeed, the lack of these two cysteines abolished pro-proliferative effects of Rab31 upon overexpression in both CAMA-1 and MDA-MB-231 cells suggesting that membrane localization is dominant over the GTPase function.

Similar to the constitutively inactive Rab31-S19N mutant, in principle the Rab31-ΔCC mutant should be a dominant-negative mutant because it is able to interact and thereby serve as a scavenger for Rab31 interaction partners. Obviously, this is not the case because we were able to overexpress Rab31-ΔCC, which leads to the hypothesis that interaction with important partners of Rab proteins is only possible in a membrane-associated state.

Previous studies utilizing Rab GTPase mutants with altered activity and properties are in accordance with our results. Studies on Rab22A using Q64L mutants also describe a similar phenotype for wild-type and Rab22A-Q64L overexpression. In this study, the authors investigated the impact of Rab22A on EEA1 signaling and endosomal trafficking. Interestingly, the overexpression of Rab22A-WT or the GTP-bound version Rab22A-Q64L interfered with the degradation of EGF, a known pro-proliferative cytokine (Kauppi et al. 2001). Studies on Rab22A using S19A mutants also describe that the S19A variant had no effect on the lysosomal function or the trafficking between endosomes and the Golgi (Mesa et al. 2005). As overexpression of Rab22A-S19A was reported in this study, while we could not express Rab31-S19N, it is tempting to speculate that the interference with cellular pathways by increased amounts of GDP-bound, inactive Rab31 is stronger than that of the Rab22A equivalent. The geranylgeranyl-modification at the C-terminus generally occurs within the Ras superfamily of GTPases. In the case of Rab1A, it was reported that the localization in the Golgi is a pre-requisite for correct function of the Rab protein. In Parkinson's disease Golgi fragmentation is known to be the result of the overabundance of α-synuclein in the nigral dopaminergic neurons. Rab1A overexpression can prevent this Golgi fragmentation, however, this protective feature is lost upon overexpression of Rab1A-ΔCC (Coune et al. 2011).

RAB31 MUTANTS AND ADHESION

As mentioned before, cell adhesion assays using different extracellular proteins, including collagens and fibronectin, revealed a decrease of cell adhesion upon Rab31 overexpression in breast cancer cells. Rab31-Q64L, the mutant constitutively binding GTP behaves similar to the wild-type overexpressing Rab31. In contrast, Rab31-ΔCC, which is not properly localized to the Golgi membrane resembles the vector control and does not show reduced adhesive properties.

Decrease of ECM attachment and the ability of tumor cells to survive without or with fewer contacts to ECM proteins may be a pre-requisite for successful increase of proliferation. Cells displaying a proliferation rate have less contact-surfaces to the ECM and must therefore mostly rely on cell-cell contact to each other. As small GTPases have been thoroughly described to be involved in the regulation of integrins and other cell membrane proteins associated with ECM binding, *e.g.* focal adhesions, the alteration of cellular adhesion upon Rab31 overexpression points towards a change of protein trafficking. Indeed, Rab5 has been shown to regulate stress fiber formation and focal adhesions (Imamura et al. 1998), and Rab21 to influence β1-integrin distribution and trafficking (Pellinen et al. 2006). However, Rab5 and Rab21 increase cell adhesion in PC3 cells upon overexpression. When Rab21 mRNA levels were knocked down, the cell adhesion decreased. The pro-adhesive effects of Rab21 in MDA-MB-231 cells were dependent on its GDP/GTP-exchange (Pellinen et al. 2006). These effects, which at least in part, have opposite effects as described in the present work for Rab31 suggest a different role of Rab31 in cell adhesiveness than Rab21 and Rab5. Indeed, while Rab21 overexpression increased cell migration (Pellinen et al. 2006), that of Rab31 decreased cell invasion. It has been discussed that a switch between a proliferative and an invasive phenotype is a prerequisite for the development of tumor metastases (Gao et al. 2005). The effects of Rab31 overexpression in breast cancer cells indicate that Rab31, dependent on its expression level, may be a candidate protein regulating these tumor biologically relevant processes.

Effects of Rab31 overexpression on gene expression of other tumor-associated genes

The proposed mechanism of Rab31 to act as a molecular switch between a more proliferative *versus* invasive phenotype raised the question whether Rab31 may modulate expression of other tumor-associated genes/proteins involved in these processes. As proliferation, adhesion, motility and invasiveness are strongly associated with a developmental program, the so-called epithelial to mesenchymal transition (EMT), a commercially available EMT low-density qPCR microarray was applied to assess expression of several genes involved in this process. In this screen, we identified and further analyzed two candidate genes, VCAN1 and TGFB1. Whereas VCAN1 encoding for versican, was potentially up-regulated in both MDA-MB-231 and CAMA-1 cells upon Rab31 overexpression, TGFB1, encoding for TGF-β1, was found down-regulated.

VCAN1. Versican is a large extracellular matrix proteoglycan and has been described to play an important role in both malignant transformation and tumor progression (Du et al. 2013). However, in validation experiments, using an independent qPCR assay, the increase of versican was found to be only modest in both cell lines.

TGFB1. In case of TGFB1, the mRNA encoding TGF-β1 was found to be profoundly and significantly down-regulated in Rab31-overexpressing CAMA-1 cells. Also, Rab31-overexpressing MDA-MB-231 cells contained reduced TGF-β1 mRNA levels compared to vector control cells, albeit to a lesser extent. Given the importance of TGF-β1 as signaling molecule, we decided to further analyze TGF-β1 expression also on the protein and activity level.

TGF-β FAMILY

The proteins constituting the TGF-β superfamily share structural homology and contain a variety of subfamilies including Growth Differentiation Factors (GDFs), Bone Morphogenic Proteins (BMPs) and TGF-β proteins (Herpin et al. 2004). Members of this family play significant roles in biological processes like immunoregulation (Li et al. 2006), growth (Gold 1999) and development (Wu and Hill 2009). Homologs of these proteins are found across all species, highlighting their importance (Herpin et al. 2004). The members of the TGF-β subfamily TGF-β1, TGF-β2 and TGF-β3 are functionally closely related and exhibit their biological activity after dimerization and binding to their cognate receptor complex, which is comprised of TGF-β-receptor type I (RI) and TGF-β-receptor type II (RII) subunits (Lin and Moustakas 1994). Ligand binding induces activation of RI through phosphorylation by the RII kinase domain (Massagué and Massagué J 2000; Shi Y and Massagué J 2003; Massagué J 2008) which induces Smad-dependent signaling and leads to altered transcriptional activity of TGF-β responsive genes (Massagué and Massagué J 2000). In contrast, TGF-β-receptor type III (RIII) is not involved in signal transduction, but functions as a co-receptor for TGF-βs (Mythreye and Blobe 2009) and modulates cellular responses (Taylor et al. 2011). Besides the Smad-dependent pathway, several other Smad-independent pathways exist by which TGF-β can regulate gene expression (Figure 105).

RAB31 OVEREXPRESSION AND ITS EFFECTS ON TGF-β1 LEVELS

As TGF-β1 is a secreted protein and Rab31 is involved in protein sorting and trafficking, we analyzed the amount of TGF-β1 in cell culture supernatants and in whole cell lysates by ELISA. In CAMA-1 cells, the reduction of TGF-β1 was very strong in Rab31-overexpressing cells compared to the vector control. The MDA-MB-231 cells displayed a more moderate reduction of TGF-β1, when Rab31 was overexpressed, probably due to the intrinsic Rab31 levels already present in the parental cells. Reduction of TGF-β1 could also be further confirmed by detecting pro-TGF-β1 and LAP1 in both cell lines using Western blot analysis. Most importantly, not only the protein production but also the activity of TGF-β1 was considerably reduced as shown by a highly sensitive cell-

based activity assay. Furthermore, in the cell culture supernatants of Rab31-overexpressing cells, the ratio between total and active TGF-β1 is much higher as in vector control cells. This may indicate that upon Rab31 overexpression not only TGF-β1 production but also the efficiency of active TGF-β1 release from its latent form is considerably reduced.

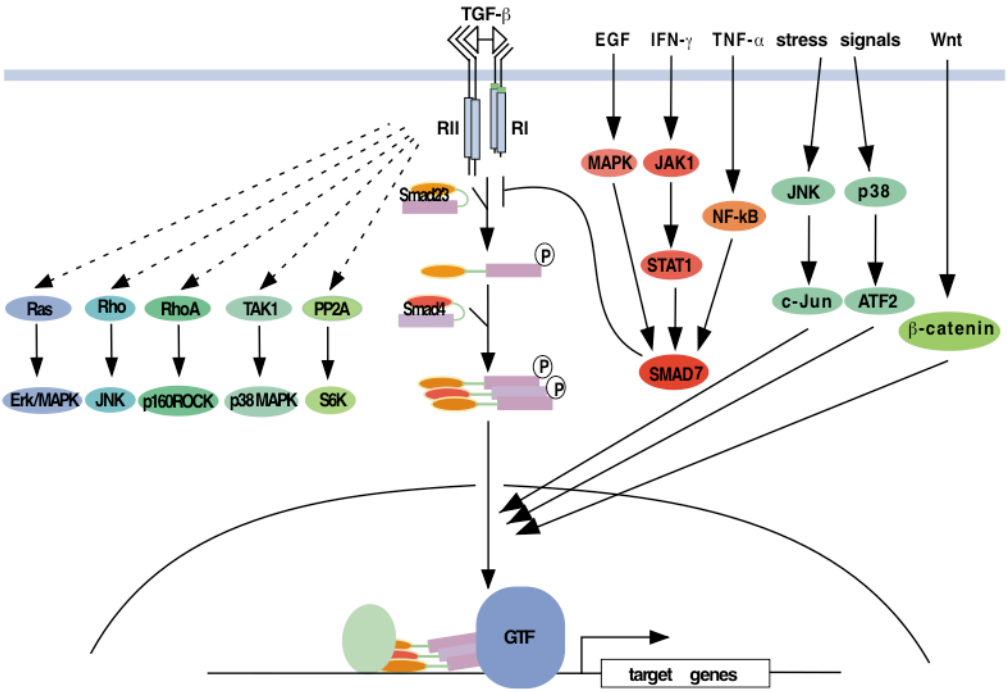

Figure 105 | TGF-β-induced signaling through Smad and non-Smad signaling mechanisms
The receptor is activated when ,Smad2 and/or Smad3 transiently interact with RI. After RI phosphorylates Smad2 and Smad3 at their C-termini a complex, composed of two receptor-activated Smads and Smad4, is formed. After translocation of the Smad-complex into the nucleus, the interaction at promoters with several transcription factors will regulate the expression of different genes. Several other signaling pathways also regulate both signaling by Smads and Smad-mediated gene expression e.g. JNK and p38 MAP kinase as response to stress signals or β-catenin responding to Wnt signaling. In addition TGF-β induces activation of various other signaling pathways (Ras, RhoB, RhoA, TAK1 and PPT2A), These non-Smad signaling events are yet not well understood (Derynck et al. 2001; Ikushima and Miyazono, 2010).

Several other signaling pathways also regulate both signaling by Smads and Smad-mediated gene expression, as exemplified here by the activation of in response to various stress signals, and in response to Wnt proteins.

As an example shown here is the activation of JNK and p38 MAP kinase signaling as response to different signals as well as β-catenin signaling in response to Wnt proteins

TGF-β IN CANCER

The TGF-β pathway is an important pathway in tumor progression, which can have both tumor suppressive and pro-oncogenic effects on tumorigenesis (Figure 106) (Wakefield and Roberts, 2002; Meulmeester and ten Dijke, 2011; Zu et al. 2012). TGF-β is necessary for the maintenance of genomic stability, induction of senescence and suppression of telomerase (Wakefield and Roberts, 2002). It has been shown that TGF-β can induce apoptosis in several normal cell types (Cencetti et al. 2013; Das et al. 2014). Recent studies by Kiyono et al. (2009) demonstrated that TGF-β can induce autophagy and growth inhibition in certain liver and breast cancer cell lines. It has also been shown that TGF-β has a major influence on terminal differentiation of different cell lineages. Furthermore, TGF-β can inhibit cell cycle progression (at the G1-phase) through mobilization of inhibitors and suppression of pro-proliferative factors like c-Myc. In addition to its direct growth-inhibitory effects in cells, TGF-β can also block proliferation by decreasing the production of paracrine factors in stromal and inflammatory cells, thus, acting within the microenvironment (Massagué 2008). In general, TGF-β mainly acts as a tumor suppressor in early stages of cancer development, but later on as a stimulant for invasion and tumor progression. Hence, initially cancer cells must find a way to escape growth inhibition and cell death regulated by the TGF-β pathway. One possible mechanism is the truncation of the pathway with receptor-inactivating mutations and, therefore, silencing of TGF-β signaling altogether. Another mechanism is to selectively amputate the tumor-suppressive arm of the pathway either by mutations within the cascade or by inhibition caused by other altered or mutated pathways (Bierie and Moses 2006; Massagué 2008; Ikushima and Miyazono 2010; Morrison 2013). Repression of TGF-β expression, *e.g.* by Rab31 overexpression, may well be part of the later mechanism to block the tumor-suppressing activities of the TGF-β pathway.

	Tumor suppressor activities	**Pro-oncogenic activities**
tumor cell	Growth Inhibition Apoptosis Negative angiogenic regulator profile Maintenance of genomic stability Induction of replicative senescence Prevention of immortalization Maintenance of tissue architecture	Enhanced epithelial → mesenchymal transition Increased motility Increased invasiveness Increased colonization of bone (PTHrP secretion) Growth stimulation
stromal target	Maintenance of tissue architecture?	Suppression of immune surveillance Increased angiogenesis

Figure 106 | The dual role of TGF-β in tumorigenesis
In context of the tumor microenvironment, both the epithelial target cell and surrounding stromal elements, add to the tumor suppressor and oncogenic actions of TGF-β. In early stages of tumorigenesis TGF-β is thought to be tumor suppressive, whereas in later stages TGF-β may facilitate metastasis formation (Wakefield & Roberts 2002; Bierie and Moses 2006; Ikushima and Miyazono 2010; Morrison 2013).

RAB31 OVEREXPRESSION AND ITS EFFECTS ON TGF-β-ASSOCIATED GENES

To further elucidate the effects of Rab31 overexpression on the TGF-β signaling pathway, the search for differentially regulated genes in Rab31-overexpressing versus vector control cells was extended applying another low-density microarray with a focus on genes of the TGF-β superfamily and related factors. Here, CAMA-1 cells were chosen, since Rab31 overexpression led to a very strong and significant decrease of TGFB1 mRNA with the effect being more pronounced as in MDA-MB-231 cells. In addition to TGFB1, several candidate genes were identified and subsequently validated to be selectively up- or down-regulated upon Rab31 overexpression.

Down-regulated genes

Interestingly, reduction of mRNA levels was not restricted to TGFB1, but significantly lower levels were also found for other family members of the TGF-β superfamily, namely TGFB2, FSTL3, BMP-7, and SMAD6.

TGF-β2. TGFB2 has been ascribed a similar dual role during cancer progression as for TGF-β1. *In vivo* knock out studies as well as *in vitro* experiments, however, suggest further non-redundant roles of the TGF-β isoforms (Sanford et al. 1997; Azhar, 2001; Stauder et al. 2004). In human mammary epithelial cells (HMEC), it was shown that TGF-β2, TGF-βR1, TGF-βR2, and thrombospondin-1 are simultaneously down-regulated during early carcinogenesis by histone modifications (Hinshelwood et al. 2007). Buck et al. (2008) observed that TGF-β2 and TGF-β-RII expression was induced in MCF-7 and T47D breast cancer cells upon treatment with the anti-estrogen tamoxifen, which was paralleled by a significant anti-proliferative activity. Increase of TGF-β2 levels was also observed in tumor tissue of estrogen receptor-positive breast cancer patients after beneficial treatment with the anti-estrogen tamoxifen (Buck et al. 2008). Thus, repression of TGF-β2 expression may exert a pro-proliferative effect on breast cancer cells.

FSTL3. Follistatin-like 3 (FSTL-3) is a glycoprotein, which can act as an inhibitor of a specific part of the TGF-β signaling pathway as it binds and inhibits specific ligands of TGF-b receptors such as the various activin variants. Activins bind and activate type II TGF-b receptors, resulting in recruitment and phosphorylation of type I receptors. Subsequent downstream signaling occurs *via* Smad proteins as well as *via* MAPK pathways. Again, activins were shown to display either pro- or anti-tumorigenic effects (Antsiferova and Werner 2012). In a mammary carcinoma xenograft mouse model, activin-overexpressing human tumor cells were characterized by a faster tumor growth (Krneta et al. 2012). Down-regulation of the activin-antagonist FSTL3 in breast cancer cells may have similar effects. The FSTL family member FSTL-1 was shown to display anti-tumorigenic effects by reversing the effects described in the present work for

Rab31 overexpression: cell cycle progression was reduced upon FSTL-1 overexpression and cell proliferation decreased (Chan et al. 2009).

BMP-7. Bone morphogenic protein 7 (BMP-7) is another member of the TGF-β superfamily, which mRNA expression was decreased upon Rab31 overexpression. BMP-7 expression is known to inhibit cancer progression, as it preserves an epithelial phenotype, similar of TGF-β1, in early cancerogenic stages (Buijs et al. 2007). BMPs are generally described as inhibitors of metastasis. In tumor cells, BMP activity is silenced by the expression of BMP antagonists, such as noggin and gremlin-1 (Rodriguez-Martinez et al. 2011). Miyazaki et al. (2004) showed that BMP-7 inhibits the proliferation of PC-3 and DU-145 prostate cancer cells. Alarmo et al. (2009) have studied the effect of BMP-7 knock down in breast cancer cell lines with high endogenous expression and found elevated proliferation as result of the BMP-7 reduction. When cells with low or no endogenous BMP-7 expression were treated with recombinant BMP-7 in the culture medium, the growth rate was reduced. These results, are in accordance with our study, as Rab31 overexpression reduced BMP-7 mRNA expression accompanied by an increased cell proliferation. In contrast, however, increased BMP-7 expression was found to be associated with early bone metastasis formation by Alarmo et al. (2009) in breast cancer patients. BMP-7 is also described as an inhibitor of invasion by disruption of TGF-β signaling (Naber et al. 2012). Nevertheless, BMP-7 may have an ambivalent and versatile tumor biological role similar to that of other TGF-β family members.

SMAD-6. TGF-β canonical signaling is mediated by a carefully balance of different SMAD-proteins which either act as effectors of TGF-β receptors or as inhibitors by interfering with phosphorylation and subsequent dimerization of effector SMADs. SMAD-6 is described as an inhibitory SMAD protein as it disrupts TGF-β1 signaling transduction and suppresses TGF-β-mediated growth inhibition (Imamura et al., 1997). In contrast to the well-studied canonical TGF-β pathway, not much is known about the non-canonical TGF-β pathways. Recently, SMAD6 was proposed to be a negative regulator of non-canonical TGF-β pathways including the TRAF6-TAK1-p38 MAPK/JNK pathway (Jung et al. 2013).

TIMP-1. Interestingly, TIMP-1, a broad-spectrum inhibitor of metalloproteinases was also found in significantly reduced mRNA levels in CAMA-1 (but not MDA-MB-231) cells overexpressing Rab31. On one hand, one might argue that increase of extracellular proteolytic activity *via* reduction of an inhibitor may lead to a decrease of cell adhesion, which indeed is observed in Rab31-overexpressing cells. On the other hand, however, TIMP-1 gained recognition in recent years as it acts not only as a component of the proteolytic network by tightly regulating MMP activity, but also acts a cytokine (Ries, 2013). Pro-proliferative and anti-apoptotic signaling activated by TIMP-1 involves major signaling pathways, *e.g.*, PI3K/AKT and ERK. A reduction of TIMP-1 by Rab31 overexpression could thus diminish *in vivo* metastasis despite possibly increased MMP

activity. In addition, TIMP-1 is proposed to be a regulator of cell fate decision and might mediate the balance between proliferation and invasion (Cui et al. 2012).

Up-regulated genes

B2M. B2M, encoding β2 microglobulin (β2M), has originally been described as a proper housekeeping gene for normalization of mRNA levels of other genes (Waha et al. 1998). However, β2M mRNA levels increase, *e.g.*, during progression of human breast, prostate, renal, lung and colon cancer (Josson et al. 2011). In Rab31-overexpressing CAMA-1 cells, β2M mRNA levels, as compared to vector control cells, were significantly up-regulated as well. One of its function is the formation of complexes with the heavy chain of major histocompatibility complex class I molecules, which present antigenic peptides to cytotoxic T cells. In addition, β2M has been identified to act as a growth factor and a pleiotropic signaling molecule modulating epithelial-to-mesenchymal transition and supporting growth, survival, and metastasis of cancer cells. Thus, β2M represents a new promising therapeutic target for the treatment of cancer (Josson et al. 2011; Nomura et al. 2013).

FAS/TNFSF10. Moreover, two genes known to encode proteins which are involved in induction of apoptosis, FAS (encoding Fas, a member of the TNF receptor superfamily) and TNFSF10 (encoding TRAIL) were identified as upregulated genes upon Rab31 overexpression in CAMA-1 cells. However, as annexin-V staining did not reveal an altered percentage of apoptotic cells in Rab31-overexpressing *versus* vector control cells, the increase on mRNA level might either not reflect the protein level or the increase of the mRNA/protein level might not suffice to stimulate apoptosis. It should be noted, however, that there is increasing evidence that, *e.g.*, cancer patients frequently have elevated levels of Fas and its ligand Fas-L indicating that Fas could promote tumor growth *via* non-apoptotic activities. In fact, for optimal growth, tumor cells depend on expression of Fas and Fas-L, which signal through a pathway involving JNK and c-jun (Chen et al. 2010). Similarly, TRAIL signaling does not only lead to apoptosis, but it can also induce non-apoptotic pathways *via* activation of NF-κB, Akt or MAPKs which can lead to enhancement of cell proliferation (Falschlehner et al. 2007).

Most of the above discussed genes being either down- or up-regulated in Rab31-overexpressing *versus* control cells have originally been classified to function as oncogene or tumor suppressor gene within a cancer cell. However, it turned out that many of these genes are “chameleons”, which exert opposite effects in different settings, *e.g.* when using different cell lines or tumor samples. This so-called antagonistic duality of cancer genes depends certainly on the genetic context as well as on the environment of the cell, which lead to (in)activation of signaling pathways within a complex network and to the seemingly paradox, opposite responses to the same protein (Stepanenko et al. 2013).

REGULATION OF RAB31 EXPRESSION

Recently, several reports were published shedding some light on the regulation of Rab31 expression in cancer cells.

MUC1-C. The results presented by Jin et al. (2012) point towards an association between Rab31 and mucin 1C (MUC1-C). MUC1-C is linked to anchorage-independent growth and tumorigenicity in breast cancer and provides a possible mechanism on how Rab31 expression is regulated in breast cancer cells. The findings indicate that Rab31 transcription is activated by a complex of ERα and MUC1-C interacting at the estrogen-responsive Rab31 promoter in breast cancer cells. In turn, Rab31 is up-regulated and then MUC1-C levels rise, probably due to Rab31 interfering with MUC1-C degradation. Accordingly, not only is Rab31 expression substantially higher in breast tumors than in healthy tissue, it is also significantly increased in ERα positive tumors to ERα negative ones. Moreover, there was significant co-expression of both Rab31 and MUC1-C in $ER\alpha^+$ breast cancers. MCF-10A cells stably overexpressing Rab31 exhibited increased MUC1-C levels. This was also associated with the ability of the cells to form mammospheres, which is not found in the wild-type cells. This effect was shown to be MUC1-C-dependent and was abolished when overexpressing an inactive Rab31 mutant (Jin et al. 2012). Interestingly, MUC1-C has been associated with increased tamoxifen-resistance. Amongst other effects, MUC1-C counteracts the tamoxifen-induced reduction of ERα occupancy at the Rab31 promoter (Kharbanda et al. 2013).

HuR. In 2011, Rab31 translation was shown to be regulated by the mRNA binding protein HuR (Heinonen et al. 2011). In breast cancer, HuR is abundantly expressed in early stages of the disease and serves as a prognostic marker (Heinonen et al. 2005; Heinonen et al. 2007). HuR binds a broad spectrum of target mRNAs thereby providing enhanced transcript stability and translational regulation (Srikantan et al. 2012). Silencing of HuR expression in 184B5Me epithelial breast cancer cells leads to reduced Rab31 mRNA expression (Heinonen et al. 2011). Induction of HuR overexpression increased cellular proliferation and altered cell cycle kinetics *in vitro*, which is in line with published data for other cancer types (Gubin et al. 2010). Surprisingly, these data do not translate into *in vivo* models. Here, HuR overexpression resulted in decreased tumor growth in comparison with vector control and wild-type MDA-MB-231 cells. This is in line with our former observations, which showed a reduced metastatic potential of MDA-MB-231 cells overexpressing Rab31 in a xenograft mouse model (Grismayer et al. 2012b). Considering the clear association of high levels of both HuR and Rab31 mRNA levels with poor prognosis of breast cancer patients, the results obtained with the xenograft animal models, therefore, may not directly mirror the malignant features of human HuR- and/or Rab31-overexpressing breast cancers, but still demonstrate that expression of both factors are implicated in the modulation of tumor-relevant processes.

CONCLUSION

In breast cancer cells, overexpression of the GTP-binding protein Rab31 (which is involved in intracellular trafficking) leads to a switch from an invasive to a proliferative phenotype as indicated by increased cell proliferation, reduced adhesion and invasion, and a reduced capacity to form lung metastases. In the present work, the tumor biological role of Rab31 was further explored in breast cancer cells:

MDA-MB-231 breast cancer cells, simultaneously overexpressing Rab31 and uPAR-Δ4/5, did not display any additive or synergistic effects of these biomarkers on cell proliferation or adhesion, compared to vector control cells.

Reduction of Rab31 mRNA/protein expression in MDA-MB-231 cells, which endogenously express moderate Rab31 levels, led to significantly lower cell proliferation rates, which matches the effects observed upon Rab31 overexpression.

Breast cancer cells overexpressing a constitutively active Rab31 mutant (Rab31-Q64L) exhibit the same phenotype as Rab31-WT-overexpressing cells concerning proliferation, adhesion and invasion; cells overexpressing a Rab31 mutant unable to insert into the Golgi membrane (Rab31-ΔCC) are characterized by a phenotype comparable to that of vector control cells. Expression of a potentially dominant-negative, constitutively inactive Rab31 variant (Rab31-S19N) could not be achieved, neither in the MDA-MB- 231 nor in the CAMA-1 cells.

Rab31 was found to modulate expression of several tumor biologically relevant genes including TGFB1 (encoding TGF-β1). In both MDA-MB-231 and CAMA-1 cells, not only TGFB1 mRNA was down-regulated upon Rab31-overexpression, but also TGF-β1 protein and activity levels, respectively, were strongly reduced. Repression of TGF-β1 - as well as up-/down-regulation of other factors of the (non-)canonical TGF-β signaling pathways - may elicit the change of the cell biological phenotype (*e.g.* increased proliferation and decreased adhesion) of breast cancer cells upon Rab31 overexpression.

8 - REFERENCES

Abba MC, Hu Y, Sun H, Drake JA, Gaddis S, Baggerly K, Sahin A and Aldaz CM (2005) Gene expression signature of estrogen receptor alpha status in breast cancer. BMC Genomics 6:37

Abdul M and Hoosein N (2000) Changes in beta-2 microglobulin expression in prostate cancer. Urol Oncol 5:168-172

Agola JO, Jim PA, Ward HH, Basuray S and Wandinger-Ness A (2011) Rab GTPases as regulators of endocytosis, targets of disease and therapeutic opportunities. Clin Genet 80:305-18

Alarmo EL, Pärssinen J, Ketolainen JM, Savinainen K, Karhu R and Kallioniemi A (2009) BMP7 influences proliferation, migration, and invasion of breast cancer cells. Cancer Lett 275:35-43

Andreasen PA, Kjoller L, Christensen L and Duffy MJ (1997) The urokinase-type plasminogen activator system in cancer metastasis: a review. Int J Cancer 72:1-22

Antsiferova M and Werner S (2012) The bright and the dark sides of activin in wound healing and cancer. J Cell Sci 125:3929-37

Arias AM (2001) Epithelial mesenchymal interactions in cancer and development. Cell 105:425-31

Azhar M, (2001) Non-redundant tumour supressor functions of transforming growth factor beta in breast cancer. J Biosci 1:9-12

Bao X, Faris AE, Jang EK and Haslam RJ (2002) Molecular cloning, bacterial expression and properties of Rab31 and Rab32. Eur J Biochem 269:259-71

Behrendt N, Ploug M, Patthy L, Houen G, Blasi F and Dano K (1991) The ligandbinding domain of the cell surface receptor for urokinase-type plasminogen activator. J Biol Chem 266:7842-7

Berx G, Raspé E, Christofori G, Thiery JP and Sleeman JP (2007) Pre-EMTing metastasis? Recapitulation of morphogenetic processes in cancer. Clin Exp Metastasis 24:587-97

Bierie B and Moses HL (2006) Tumour microenvironment: TGFbeta: the molecular Jekyll and Hyde of cancer. Nat Rev Cancer 6:506-20

Biermann JC, Holzscheiter L, Kotzsch M, Luther T, Kiechle-Bahat M, Sweep FC, Span PN, Schmitt M and Magdolen V (2008) Quantitative RT-PCR assays for the determination of urokinase-type plasminogen activator and plasminogen activator inhibitor type 1 mRNA in primary tumor tissue of breast cancer patients: comparison to antigen quantification by ELISA. Int J Mol Med 21:251-9

Binder BR and Mihlay J (2008) The plasminogen activator inhibitor „paradox“ in cancer. Immunol Lett 118:116-24

Blasi F, Ciarrocchi A, Luddi A, Strazza M, Riccio M, Santi S, Arcone R, Pietropaolo C, D'Angelo R, Costantino-Ceccarini E und Melli M (2002) Stage-specific gene expression in early differentiating oligodendrocytes. Glia 39:114-23

Blasi F and Carmeliet P (2002) uPAR: a versatile signalling orchestrator. Nat Rev Mol Cell Biol 3:932-43

Blasi F and Sidenius N (2010) The urokinase receptor: focused cell surface proteolysis, cell adhesion and signaling. FEBS Lett 584:1923-30

Buck MB and Knabbe C (2006) TGF-beta signaling in breast cancer. Ann N Y Acad Sci 1089:119-26

Buck MB, Coller JK, Mürdter TE, Eichelbaum M and Knabbe C (2008) TGFbeta2 and TbetaRII are valid molecular biomarkers for the antiproliferative effects of tamoxifen and tamoxifen metabolites in breast cancer cells. Breast Cancer Res Treat 107:15-24.

Buijs JT, Rentsch CA, van der Horst G, van Overveld PG, Wetterwald A, Schwaninger R, Henriquez NV, Ten Dijke P, Borovecki F, Markwalder R, Thalmann GN, Papapoulos SE, Pelger RC, Vukicevic S, Cecchini MG, Löwik CW and van der Pluijm G (2007) BMP7, a putative regulator of epithelial homeostasis in the human prostate, is a potent inhibitor of prostate cancer bone metastasis in vivo. Am J Pathol 171:1047-57

Cailleau R, Young R, Olive M and Reeves WJ, Jr. (1974) Breast tumor cell lines from pleural effusions. J Natl Cancer Inst 53:661-74

Casey JR, Petranka JG, Kottra J, Fleenor DE and Rosse WF (1994) The structure of the urokinase-type plasminogen activator receptor gene. Blood 84:1151-6

Cencetti F, Bernacchioni C, Tonelli F, Roberts E, Donati C and Bruni P (2013) TGFß 1 evokes myoblast apoptotic response via a novel signaling pathway involving S1P4 transactivation upstream of Rho-kinase-2 activation. FASEB J 27:4532-46

Chan QK, Ngan HY, Ip PP, Liu VW, Xue WC and Cheung AN (2009) Tumor suppressor effect of follistatin-like 1 in ovarian and endometrial carcinogenesis: a differential expression and functional analysis. Carcinogenesis 1:114-21

Chen D, Guo J, Miki T, Tachibana M and Gahl WA (1996) Molecular cloning of two novel rab genes from human melanocytes. Gene 174:129-34

Chen L, Park SM, Tumanov AV, Hau A, Sawada K, Feig C, Turnerc JR, Fu YX, Romero I, Lengyel E and Peter ME (2010) CD95/Fas promotes tumour growth. Nature 465: 492–96

Chen Z, Zhang D, Yue F, Zheng M, Kovacevic Z and Richardson DR (2012) The iron chelators Dp44mT and DFO inhibit TGF-β-induced epithelial-mesenchymal transition via up-regulation of N-Myc downstream-regulated gene 1 (NDRG1). J Biol Chem 287:17016-28

Cheng KW, Lahad JP, Gray JW and Mills GB (2005) Emerging role of RAB GTPases in cancer and human disease. Cancer Res 65:2516-9

Chia WJ and Tang BL (2009) Emerging roles for Rab family GTPases in human cancer. Biochim Biophys Acta 1795:110-6

Christofori G and Semb H (1999) The role of the cell-adhesion molecule E-cadherin as a tumour-suppressor gene. Trends Biochem Sci 24:73-6

Cooper MJ, Hutchins GM, Mennie RJ and Israel MA (1990) Beta 2-microglobulin expression in human embryonal neuroblastoma reflects its developmental regulation. Cancer Res 50:3694-700

Corbeel L and Freson K (2008) Rab proteins and Rab-associated proteins: major actors in the mechanism of protein-trafficking disorders. Eur J Pediatr 167:723-9

Cortese K, Sahores M, Madsen CD, Tacchetti C and Blasi F (2008) Clathrin and LRP-1-independent constitutive endocytosis and recycling of uPAR. PLoS One 3:e3730

Coune PG, Bensadoun JC, Aebischer P and Schneider BL (2011) Rab1A over-expression prevents Golgi apparatus fragmentation and partially corrects motor deficits in an alpha-synuclein based rat model of Parkinson's disease. J Parkinsons Dis 1:373-87

Cui H, Grosso S, Schelter F, Mari B and Krüger A (2012) On the pro-metastatic stress response to cancer therapies: evidence for a positive co-operation between TIMP-1, HIF-1α, and miR-210. Front Pharmacol 3:134

Czekay RP, Kuemmel TA, Orlando RA and Farquhar MG (2001) Direct binding of occupied urokinase receptor (uPAR) to LDL receptor-related protein is required for endocytosis of uPAR and regulation of cell surface urokinase activity. Mol Biol Cell 12:1467-79

Das R, Xu S, Quan X, Nguyen TT, Kong ID, Chung CH, Lee EY, Cha SK and Park KS (2014) Upregulation of mitochondrial Nox4 mediates TGF-ß-induced apoptosis in cultured mouse podocytes. Am J Physiol Renal Physiol 306:F155-67

de Bock CE and Wang Y (2004) Clinical significance of urokinase-type plasminogen activator receptor (uPAR) expression in cancer. Med Res Rev 24:13-39

Derynck R, Akhurst RJ and Balmain A (2001) TGF-beta signaling in tumor suppression and cancer progression. Nat Genet 29:117-29

de Visser KE, Eichten A and Coussens LM (2006) Paradoxical roles of the immune system during cancer development. Nat Rev Cancer 6:24-37

Dominska M and Dykxhoorn DM (2010) Breaking down the barriers: siRNA delivery and endosome escape. J Cell Sci 123:1183-9

Du WW, Yang W and Yee AJ (2013) Roles of versican in cancer biology--tumorigenesis, progression and metastasis. Histol Histopathol 6:701-13

Duffy MJ and Duggan C (2004) The urokinase plasminogen activator system: a rich source of tumour markers for the individualised management of patients with cancer. Clin Biochem 37:541-8

Ehrbar M, Rizzi SC, Schoenmakers RG, Miguel BS, Hubbell JA, Weber FE and Lutolf MP (2007) Biomolecular hydrogels formed and degraded via site-specific enzymatic reactions. Biomacromolecules 10:3000-7

Ehrbar M, Rizzi SC, Hlushchuk R, Djonov V, Zisch AH, Hubbell JA, Weber FE and Lutolf MP (2007) Enzymatic formation of modular cell-instructive fibrin analogs for tissue engineering. Biomaterials 26:3856-66

Falschlehner C, Emmerich CH, Gerlach B and Walczak H (2007) TRAIL signalling: decisions between life and death. Int J Biochem Cell Biol 39:1462-75

Gao CF, Xie Q, Su YL, Koeman J, Khoo SK, Gustafson M, Knudsen BS, Hay R, Shinomiya N and Vande Woude GF (2005) Proliferation and invasion: plasticity in tumor cells. Proc Natl Acad Sci U S A 102:10528-33

Gold LI (1999) The role for transforming growth factor-beta (TGF-beta) in human cancer. Crit Rev Oncog 10:303-60

Gotzmann J, Mikula M, Eger A, Schulte-Hermann R, Foisner R, Beug H and Mikulits W (2004) Molecular aspects of epithelial cell plasticity: implications for local tumor invasion and metastasis. Mutat Res 566:9-20

Grismayer B, Sato S, Kopitz C, Ries C, Soelch S, Schmitt M, Baretton G, Krüger A, Luther T, Kotzsch M and Magdolen V (2012 a) Overexpression of the urokinase receptor splice variant uPAR-del4/5 in breast cancer cells affects cell adhesion and invasion in a dose-dependent manner and modulates transcription of tumor-associated genes. Biol Chem 393:1449-55

Grismayer B, Sölch S, Seubert B, Kirchner T, Schäfer S, Baretton G, Schmitt M, Luther T, Krüger A, Kotzsch M and Magdolen V (2012 b) Rab31 expression levels modulate tumor-relevant characteristics of breast cancer cells. Mol Cancer 11:62

Grivennikov SI, Greten F and Karin M (2010). Immunity, inflammation, and cancer. Cell 140:883-99

Gross M, Top I, Laux I, Katz J, Curran J, Tindell C and Agus D (2007) Beta-2-microglobulin is an androgen-regulated secreted protein elevated in serum of patients with advanced prostate cancer. Clin Cancer Res 13:1979-86

Grünert S, Jechlinger M and Beug H (2003) Diverse cellular and molecular mechanisms contribute to epithelial plasticity and metastasis. Nat Rev Mol Cell Biol 4:657-65

Gubin MM, Calaluce R, Davis JW, Magee JD, Strouse CS, Shaw DP, Ma L, Brown A, Hoffman T, Rold TL and Atasoy U (2010) Overexpression of the RNA binding protein HuR impairs tumor growth in triple negative breast cancer associated with deficient angiogenesis. Cell Cycle 9:3337-46

Gupta GP and Massagué J (2006) Cancer metastasis: building a framework. Cell 127:679-95

Hahn WC and Weinberg RA (2002) Modelling the molecular circuitry of cancer. Nat Rev Cancer 2:331-41

Hanahan D and Weinberg RA (2000) The hallmarks of cancer. Cell 100:57-70

Hanahan D and Weinberg RA (2011) Hallmarks of cancer: the next generation. Cell 144: 646-74

Harbeck N, Kates RE, Gauger K, Willems A, Kiechle M, Magdolen V and Schmitt M (2004) Urokinase-type plasminogen activator (uPA) and its inhibitor PAI-I: novel tumor-derived factors with a high prognostic and predictive impact in breast cancer. Thromb Haemost 91:450-6 Review

Heinonen M, Bono P, Narko K, Chang SH, Lundin J, Joensuu H, Furneaux H, Hla T, Haglund C and Ristimaki A (2005) Cytoplasmic HuR expression is a prognostic factor in invasive ductal breast carcinoma. Cancer Res 65:2157-61

Heinonen M, Fagerholm R, Aaltonen K, Kilpivaara O, Aittomaki K, Blomqvist C, Heikkila P, Haglund C, Nevanlinna H and Ristimaki A (2007) Prognostic role of HuR in hereditary breast cancer. Clin Cancer Res 13:6959-63

Heinonen M, Hemmes A, Salmenkivi K, Abdelmohsen K, Vilen ST, Laakso M, Leidenius M, Salo T, Hautaniemi S, Gorospe M, Heikkila P, Haglund C and Ristimaki A (2011) Role of RNA binding protein HuR in ductal carcinoma in situ of the breast. J Pathol 224:529-39

Hendrix A, Braems G, Bracke M, Seabra M, Gahl W, De Wever O and Westbroek W (2010) The secretory small GTPase Rab27B as a marker for breast cancer progression. Oncotarget 1:304-8

Herpin A, Lelong C, Favrel P (2004). Transforming growth factor-beta-related proteins: an ancestral and widespread superfamily of cytokines in metazoans. Dev Comp Immunol 28:461–85

Hinshelwood RA, Huschtscha LI, Melki J, Stirzaker C, Abdipranoto A, Vissel B, Ravasi T, Wells CA, Hume DA, Reddel RR and Clark SJ (2007) Concordant epigenetic silencing of transforming growth factor-beta signaling pathway genes occurs early in breast carcinogenesis. Cancer Res 67:11517-27

Houghton AN and Guevara-Patiño JA (2004) Immune recognition of self in immunity against cancer. J Clin Invest 114:468-71

Huai Q (2008) Crystal structures of two human vitronectin, urokinase and urokinase receptor complexes. Nature Struct Mol Biol 15, 422–423

Huber MA, Beug H and Wirth T (2004) Epithelial-mesenchymal transition: NF-kappaB takes center stage. Cell Cycle 3:1477-80

Hugo H, Ackland ML, Blick T, Lawrence MG, Clements JA, Williams ED and Thompson EW (2007) Epithelial--mesenchymal and mesenchymal--epithelial transitions in carcinoma progression. J Cell Physiol 213:374-83

Hutagalung AH and Novick PJ (2011) Role of Rab GTPases in membrane traffic and cell physiology. Physiol Rev 91:119-49

Ikushima H and Miyazono K (2010) TGFbeta signalling: a complex web in cancer progression. Nat Rev Cancer 10:415-24

Imamura T, Takase M, Nishihara A, Oeda E, Hanai J, Kawabata M and Miyazono K (1997) Smad6 inhibits signalling by the TGF-beta superfamily. Nature 389:622-6

Imamura H, Takaishi K, Nakano K, Kodama A, Oishi H, Shiozaki H, Monden M, Sasaki T and Takai Y (1998) Rho and Rab small G proteins coordinately reorganize stress fibers and focal adhesions in MDCK cells. Mol Biol Cell 9:2561-75

Itzen A and Goody RS (2011) GTPases involved in vesicular trafficking: structures and mechanisms. Semin Cell Dev Biol 22:48-56

Jin C, Rajabi H, Pitroda S, Li A, Kharbanda A, Weichselbaum R and Kufe D (2012) Cooperative interaction between the MUC1-C oncoprotein and the Rab31 GTPase in estrogen receptor-positive breast cancer cells. PLoS One 7:e39432

Jögi A, Rønø B, Lund IK, Nielsen BS, Ploug M, Høyer-Hansen G, Rømer J und Lund LR (2010) Neutralisation of uPA with a monoclonal antibody reduces plasmin formation and delays skin wound healing in tPA-deficient mice. PLoS One 5:e12746

Josson S, Nomura T, Lin JT, Huang WC, Wu D, Zhau HE, Zayzafoon M, Weizmann MN, Gururajan M and Chung LW (2011) Beta2-microglobulin induces epithelial to mesenchymal transition and confers cancer lethality and bone metastasis in human cancer cells. Cancer Res 71:2600-10

Jung SM, Lee JH, Park J, Oh YS, Lee SK, Park JS, Lee YS, Kim JH, Lee JY, Bae YS, Koo SH, Kim SJ and Park SH (2013) Smad6 inhibits non-canonical TGF-β1 signalling by recruiting the deubiquitinase A20 to TRAF6. Nat Commun 4:2562

Kajiho H, Sakurai K, Minoda T, Yoshikawa M, Nakagawa S, Fukushima S, Kontani K and Katada T (2011) Characterization of RIN3 as a guanine nucleotide exchange factor for the Rab5 subfamily GTPase Rab31. J Biol Chem 286:24364-73

Kauppi M, Simonsen A, Bremne B, Vieira A, Callaghan J, Stenmark H and Olkkonen VM (2001) The small GTPase Rab22 interacts with EEA1 and controls endosomal membrane trafficking. J Cell Sci 115, 899-911

Kharbanda A, Rajabi H, Jin C, Raina D and Kufe D (2013) Oncogenic MUC1-C promotes tamoxifen resistance in human breast cancer. Mol Cancer Res 11:714-23

Khosravi-Far R, Clark GJ, Abe K, Cox AD, McLain T, Lutz RJ, Sinensky M and Der CJ (1992) Ras (CXXX) and Rab (CC/CXC) prenylation signal sequences are unique and functionally distinct. J Biol Chem 267:24363-8

Kiyono K, Suzuki HI, Matsuyama H, Morishita Y, Komuro A, Kano MR, Sugimoto K and Miyazono K (2009) Autophagy is activated by TGF-beta and potentiates TGF-beta-mediated growth inhibition in human hepatocellular carcinoma cells. Cancer Res 69:8844-52

Kotzsch M, Sieuwerts AM, Grosser M, Meye A, Fuessel S, Meijer-van Gelder ME, Smid M, Schmitt M, Baretton G, Luther T, Magdolen V and Foekens JA (2008) Urokinase receptor splice variant uPAR-del4/5-associated gene expression in breast cancer: identification of rab31 as an independent prognostic factor. Breast Cancer Res Treat 111:229-40

Kotzsch M, Dorn J, Doetzer K, Schmalfeldt B, Krol J, Baretton G, Kiechle M, Schmitt M and Magdolen V (2011) mRNA expression levels of the biological factors uPAR, uPAR-del4/5 and rab31, displaying prognostic value in breast cancer, are not clinically relevant in advanced ovarian cancer. Biol Chem 392:1047-51

Krneta B, Primozic J, Zhurov A, Richmond S and Ovsenik M (2012) Three-dimensional evaluation of facial morphology in children aged 5-6 years with a Class III malocclusion. Eur J Orthod [Epub ahead of print]

Li G and, Liang Z (2001) Phosphate-binding loop and Rab GTPase function: mutations at Ser29 and Ala30 of Rab5 lead to loss-of-function as well as gain-of-function phenotype. Biochem J 355:681-9

Li MO, Wan YY, Sanjabi S, Robertson AK, Flavell RA (2006). Transforming growth factor-beta regulation of immune responses. Annu Rev Immunol 24:99-146

Llinas P, Le Du MH, Gardsvoll H, Dano K, Ploug M, Gilquin B, Stura EA and Menez A (2005) Crystal structure of the human urokinase plasminogen activator receptor bound to an antagonist peptide. EMBO J 24:1655-63

Lin HY, Moustakas A (1994) TGF-beta receptors: structure and function. Cell Mol Biol 40:337-49

Lodhi IJ, Chiang SH, Chang L, Vollenweider D, Watson RT, Inoue M, Pessin JE and Saltiel AR (2007) Gapex-5, a Rab31 guanine nucleotide exchange factor that regulates Glut4 trafficking in adipocytes. Cell Metab 5:59-72

Loessner D, Stok KS, Lutolf MP, Hutmacher DW, Clements JA and Rizzi SC (2010) Bioengineered 3D platform to explore cell-ECM interactions and drug resistance of epithelial ovarian cancer cells. Biomaterials 31:8494-506

Loessner D, Quent VM, Kraemer J, Weber EC, Hutmacher DW, Magdolen V and Clements JA (2012) Combined expression of KLK4, KLK5, KLK6, and KLK7 by ovarian cancer cells leads to decreased adhesion and paclitaxel-induced chemoresistance. Gynecol Oncol 127:569-78

Look MP, van Putten WLJ, Duffy MJ (2002) Pooled analysis of prognostic impact of uPA and PAI-1 in 8,377 breast cancer patients. J Natl Cancer Inst 94:116-28

Luther T, Kotzsch M, Meye A, Langerholc T, Fussel S, Olbricht N, Albrecht S, Ockert D, Muehlenweg B, Friedrich K, Grosser M, Schmitt M, Baretton G and Magdolen V (2003) Identification of a novel urokinase receptor splice variant and its prognostic relevance in breast cancer. Thromb Haemost 89:705-17

Lutz V, Reuning U, Kruger A, Luther T, von Steinburg SP, Graeff H, Schmitt M, Wilhelm OG and Magdolen V (2001) High level synthesis of recombinant soluble urokinase

receptor (CD87) by ovarian cancer cells reduces intraperitoneal tumor growth and spread in nude mice. Biol Chem 382:789-98

Madsen CD and Sidenius N (2008) The interaction between urokinase receptor and vitronectin in cell adhesion and signalling. Eur J Cell Biol 87:617-29

Mangone FR, Walder F, Maistro S, Pasini FS, Lehn CN, Carvalho MB, Brentani MM, Snitcovsky I and Federico MH (2010) Smad2 and Smad6 as predictors of overall survival in oral squamous cell carcinoma patients. Mol Cancer 9:106

Massagué J (2008) TGFbeta in Cancer. Cell 134:215-30

Massagué and Massagué J (2000) How cells read TGF-beta signals. Nat Rev Mol Cell Biol 1:169-78

Mengele K, Napieralski R, Magdolen V, Reuning U, Gkazepis A, Sweep F, Brunner N, Foekens J, Harbeck N and Schmitt M (2010) Characteristics of the level-of-evidence-1 disease forecast cancer biomarkers uPA and its inhibitor PAI-1. Expert Rev Mol Diagn 10:947-62

Mercatante DR, Sazani P and Kole R (2001) Modification of alternative splicing by antisense oligonucleotides as a potential chemotherapy for cancer and other diseases. Curr Cancer Drug Targets 1:211-30

Mesa R, Salomón C, Roggero M, Stahl PD und Mayorga LS (2001) Rab22a affects the morphology and function of the endocytic pathway. Cell Sci 114:4041-9

Mesa R, Magadán J, Barbieri A, López C, Stahl PD and Mayorga LS (2005) Overexpression of Rab22a hampers the transport between endosomes and the Golgi apparatus. Exp Cell Res 304:339-53

Meulmeester E and Ten Dijke P (2011) The dynamic roles of TGF-β in cancer. J Pathol 223:205-18

Mitra S, Cheng KW, and Mills GB (2011) Rab GTPases implicated in inherited and acquired disorders. Semin Cell Dev Biol 22:57–68

Miyazaki H, Watabe T, Kitamura T and Miyazono K (2004) BMP signals inhibit proliferation and in vivo tumor growth of androgen-insensitive prostate carcinoma cells. Oncogene 23:9326-35

Montuori N, Visconte V, Rossi G and Ragno P (2005) Soluble and cleaved forms of the urokinase-receptor: degradation products or active molecules? Thromb Haemost 93:192-8

Morrison CD, Parvani JG and Schiemann WP (2013) The relevance of the TGFβ paradox to EMT-MET programs. Cancer Lett 341:30-40

Mukherjee A, Sidis Y, Mahan A, Raher MJ, Xia Y, Rosen ED, Bloch KD, Thomas MK and Schneyer AL (2007) FSTL3 deletion reveals roles for TGF-beta family ligands in glucose and fat homeostasis in adults. Proc Natl Acad Sci USA 104:1348-53

Mythreye K and Blobe GC (2009) The type III TGFbeta receptor regulates directional migration: new tricks for an old dog. Cell Cycle 8:3069-70

Naber HP, Wiercinska E, Pardali E, van Laar T, Nirmala E, Sundqvist A, van Dam H, van der Horst G, van der Pluijm G, Heckmann B, Danen EH and Ten Dijke P (2012) BMP-7 inhibits TGF-β-induced invasion of breast cancer cells through inhibition of integrin ß(3) expression. Cell Oncol (Dordr) 35:19-28

Ng EL, Ng JJ, Liang F and Tang BL (2009) Rab22B is expressed in the CNS astroglia lineage and plays a role in epidermal growth factor receptor trafficking in A431 cells. J Cell Physiol 221:716-28

Nomura T, Huang WC, Zhau HE, Josson S, Mimata H and Chung LW (2013) Beta2-Microglobulin-mediated Signaling as a Target for Cancer Therapy. Anticancer Agents Med Chem [Epub ahead of print]

Nuoffer C and Balch WE (1994) GTPases: multifunctional molecular switches regulating vesicular traffic. Annu Rev Biochem 63:949-90

O'Halloran TV, Ahn R, Hankins P, Swindell E and Mazar AP (2013) The many spaces of uPAR: delivery of theranostic agents and nanobins to multiple tumor compartments through a single target. Theranostics 3:496-506

Oldknow KJ, Seebacher J, Goswami T, Villen J, Pitsillides AA, O'Shaughnessy PJ, Gygi SP, Schneyer AL and Mukherjee A (2013) Follistatin-like 3 (FSTL3) mediated silencing of transforming growth factor β (TGFβ) signaling is essential for testicular aging and regulating testis size. Endocrinology 154:1310-20

Orrenius S, Zhivotovsky B and Nicotera P (2003) Regulation of cell death: the calcium-apoptosis link. Nat Rev Mol Cell Biol 4:552-65

Park SH (2005) Fine tuning and cross-talking of TGF-beta signal by inhibitory Smads. J Biochem Mol Biol 38:9-16

Parker AL, Newman C, Briggs S, Seymour L and Sheridan PJ (2003) Nonviral gene delivery: techniques and implications for molecular medicine. Expert Rev Mol Med 5:1-15

Pellinen T, Arjonen A, Vuoriluoto K, Kallio K, Fransen JA and Ivaska J (2006) Small GTPase Rab21 regulates cell adhesion and controls endosomal traffic of beta1-integrins. J Cell Biol 173:767-80

Perik PJ, De Vries EG, Boomsma F, Messerschmidt J, Van Veldhuisen DJ, Sleijfer DT, Gietema JA and Van der Graaf WT (2006) The relation between soluble apoptotic proteins and subclinical cardiotoxicity in adjuvant-treated breast cancer patients. Anticancer Res 26:3803-11

Ploug M, Ronne E, Behrendt N, Jensen AL, Blasi F and Dano K (1991) Cellular receptor for urokinase plasminogen activator. Carboxyl-terminal processing and membrane anchoring by glycosyl-phosphatidylinositol. J Biol Chem 266:1926-33

Ploug M and Ellis V (1994) Structure-function relationships in the receptor for urokinase-type plasminogen activator. Comparison to other members of the Ly-6 family and snake venom alpha-neurotoxins. FEBS Lett 349:163-8

Pyke C, Eriksen J, Solberg H, Nielsen BS, Kristensen P, Lund LR and Dano K (1993) An alternatively spliced variant of mRNA for the human receptor for urokinase plasminogen activator. FEBS Lett 326:69-74

Qian BZ and Pollard JW (2010) Macrophage diversity enhances tumor progression and metastasis. Cell 141:39-51

Ries C (2013) Cytokine functions of TIMP-1. Cell Mol Life Sci [Epub ahead of print]

Ragno P (2006) The urokinase receptor: a ligand or a receptor? Story of a sociable molecule. Cell Mol Life Sci 63:1028-37

Rodriguez-Gabin AG, Cammer M, Almazan G, Charron M and Larocca JN (2001) Role of rRAB22b, an oligodendrocyte protein, in regulation of transport of vesicles from trans Golgi to endocytic compartments. J Neurosci Res 66:1149-60

Rodriguez-Gabin AG, Ortiz E, Demoliner K, Si Q, Almazan G and Larocca JN (2001) Interaction of Rab31 and OCRL-1 in oligodendrocytes: its role in transport of mannose 6-phosphate receptors. J Neurosci Res 88:589–604

Rodriguez-Gabin AG, Yin X, Si Q, and Larocca JN (2009) Transport of mannose-6-phosphate receptors from the trans Golgi network to endosomes requires Rab31.” Exp Cell Res 315:2215–30

Rodriguez-Martinez A, Alarmo EL, Saarinen L, Ketolainen J, Nousiainen K, Hautaniemi S and Kallioniemi A (2011) Analysis of BMP4 and BMP7 signaling in breast cancer cells unveils time-dependent transcription patterns and highlights a common synexpression group of genes. BMC Med Genomics 4:80

Sanford LP, Ormsby I, Gittenberger-de Groot AC, Sariola H, Friedman R, Boivin GP, Cardell EL and Doetschman T (1997) TGFbeta2 knockout mice have multiple developmental defects that are non-overlapping with other TGFbeta knockout phenotypes. Development 124:2659-70

Sato S, Kopitz C, Grismayer B, Beaufort N, Reuning U, Schmitt M, Luther T, Kotzsch M, Krüger A and Magdolen (2010) Overexpression of the urokinase receptor mRNA splice variant uPAR-del4/5 affects tumor-associated processes of breast cancer cells in vitro and in vivo. Breast Cancer Res Treat 127:649-57

Schmitt M, Harbeck N, Thomssen C, Wilhelm O, Magdolen V, Reuning U, Ulm K, Hofler H, Janicke F and Graeff H (1997) Clinical impact of the plasminogen activation system in tumor invasion and metastasis: prognostic relevance and target for therapy. Thromb Haemost 78:285-96

Schmitt M, Mengele K, Napieralski R, Magdolen V, Reuning U, Gkazepis A, Sweep F, Brunner N, Foekens J and Harbeck N (2010) Clinical utility of level-of-evidence-1 disease forecast cancer biomarkers uPA and its inhibitor PAI-1. Expert Rev Mol Diagn 10:1051-67

Sharp PA and Zamore PD (2000) Molecular biology. RNA interference. Science 287:2431-3

Shi Y and Massagué J (2003) Mechanisms of TGF-β Signaling from Cell Membrane to the Nucleus Cell 113: 685–700

Sidenius N and Blasi F (2003) The urokinase plasminogen activator system in cancer: recent advances and implication for prognosis and therapy. Cancer Metastasis Rev 22:205-22

Siegel R, Naishadham D and Jemal A (2012) Cancer statistics, 2012 CA Cancer J Clin 62:10–29

Singan VR, Handzic K and Simpson JC (2012) Quantitative image analysis approaches for probing Rab GTPase localization and function in mammalian cells. Biochem Soc Trans 40:1389-93

Smith HW and Marshall CJ (2010) Regulation of cell signalling by uPAR. Nat Rev Mol Cell Biol 11:23-36

Srikantan S, Tominaga K and Gorospe M (2012) Functional interplay between RNA-binding protein HuR and microRNAs. Curr Protein Pept Sci 13:372-9

Stauder G, Bischof A, Egger T, Hafner M, Herrmuth H, Jachimczak P, Kielmanowicz M, Schlingensiepen R and Schlingensiepen KH (2004) TGF-ß2 suppression by the antisense oligonucleotide AP 12009 as treatment for pancreatic cancer: preclinical efficacy data. J Clin Oncol 22, 14S Suppl:4106

Stenmark H and Olkkonen VM (2001) The Rab GTPase family. Genome Biol 2:3007

Stenmark H (2009) Rab GTPases as coordinators of vesicle traffic. Nat Rev Mol Cell Biol 10:513-25

Stepanenko AA, Vassetzky YS and Kavsan VM (2013) Antagonistic functional duality of cancer genes. Gene 529:199-207

Subramani D and Alahari SK (2010) Integrin-mediated function of Rab GTPases in cancer progression. Mol Cancer 9:312

Tang CH and Wei Y (2008) The urokinase receptor and integrins in cancer progression. Cell Mol Life Sci 65:1916-32

Tatsis G, Tsoukalas G, Boulbasakos G, Platsouka E, Anagnostopoulou M, Pirounaki M, Paniara O, Sioula E, Raptis J and Saroglou G (1998) Efficacy and tolerance of roxithromycin versus clarithromycin in the treatment of lower respiratory tract infections. J Antimicrob Chemother 41, Suppl B:69-73

Tatsis N, Lannigan DA and Macara IG (1998) The function of the p190 Rho GTPase-activating protein is controlled by its N-terminal GTP binding domain. J Biol Chem 273:34631-8

Taylor MA, Lee YH and Schiemann WP (2011) Role of TGF-β and the tumor microenvironment during mammary tumorigenesis. Gene Expr 15:117-32

Tesseur I, Zou K, Berber E, Zhang H and Wyss-Coray T (2006) Highly sensitive and specific bioassay for measuring bioactive TGF-beta. BMC Cell Biol 7:15

Thiery JP (2002) Epithelial-mesenchymal transitions in tumour progression. Nat Rev Cancer 6:442-54

Thiery JP and Sleeman JP (2006) Complex networks orchestrate epithelial-mesenchymal transitions. Nat Rev Mol Cell Biol 7:131-42

Ulisse S, Baldini E, Sorrenti S and D'Armiento M (2009) The urokinase plasminogen activator system: a target for anti-cancer therapy. Curr Cancer Drug Targets 1:32-71

Visse R and Nagase H (2003) Matrix metalloproteinases and tissue inhibitors of metalloproteinases: structure, function, and biochemistry. Circ Res 92:827-39 Review

Waha A, Sturne C, Kessler A, Koch A, Kreyer E, Fimmers R, Wiestler OD, von Deimling A, Krebs D and Schmutzler RK (1998) Expression of the ATM gene is significantly reduced in sporadic breast carcinomas. Int J Cancer 78:306-9

Wakefield LM and Roberts AB (2002) TGF-beta signaling: positive and negative effects on tumorigenesis. Curr Opin Genet Dev 1:22-9

Wu MY, Hill CS (2009) Tgf-beta superfamily signaling in embryonic development and homeostasis. Dev Cell 16:329-43

Wu X, Hu A, Zhang M and Chen Z (2013) Effects of Rab27a on proliferation, invasion, and anti-apoptosis in human glioma cell. Tumour Biol 34:2195-203

Yang PS, Yin PH, Tseng LM, Yang CH, Hsu CY, Lee MY, Horng CF and Chi CW (2011) Rab5A is associated with axillary lymph node metastasis in breast cancer patients. Cancer Sci 102:2172-8

Zang YE, (2009) Non-Smad pathways in TGF-β signaling. Cell Res 1:128-39

Zerial M and McBride H (2001) Rab proteins as membrane organizers. Nat Rev Mol Cell Biol 2:107-17

Zhao Z, Liu XF, Wu HC, Zou SB, Wang JY, Ni PH, Chen XH and Fan QS (2010) Rab5a overexpression promoting ovarian cancer cell proliferation may be associated with APPL1-related epidermal growth factor signaling pathway. Cancer Sci 101:1454-62

Zu X, Zhang Q, Cao R, Liu J, Zhong J, Wen G and Cao D (2012) Transforming growth factor-β signaling in tumor initiation, progression and therapy in breast cancer: an update. Cell Tissue Res 347:73-84

9 - PUBLICATIONS

Grismayer B, Sato S, Kopitz C, Ries C, **Soelch S**, Schmitt M, Baretton G, Krüger A, Luther T, Kotzsch M and Magdolen V (2012a) Overexpression of the urokinase receptor splice variant uPAR-del4/5 in breast cancer cells affects cell adhesion and invasion in a dose-dependent manner and modulates transcription of tumor- associated genes. Biol Chem 393:1449-55

Grismayer B, **Sölch S**, Seubert B, Kirchner T, Schäfer S, Baretton G, Schmitt M, Luther T, Krüger A, Kotzsch M and Magdolen V (2012b) Rab31 expression levels modulate tumor-relevant characteristics of breast cancer cells. Mol Cancer 11:62

Sölch S, Beaufort N, Seubert B, Alterauge D, Luther T, Krüger A, Kotzsch M, Napieralski R, and Magdolen V (2014) Effect of overexpression of the GTPase Rab31 on TGF-β1 expression in breast cancer cells. *In preparation*

Grismayer B, **Sölch S**, Seubert B, Kirchner T, Schäfer S, Schmitt M, Luther L, Krüger K, Kotzsch M, and Magdolen V (2012) Overexpression of the GTP-binding protein Rab31 induces a switch from an invasive to a proliferative phenotype in breast cancer cells. 14th International Biennial Conference on Metastasis Research, Brisbane, Australia, *Oral presentation*

Sölch S, Schmitt M, Kotzsch M, Magdolen V, Grismayer B (2012) Overexpression of the urokinase receptor splice variant uPAR-Δ4/5 or the GTP binding protein Rab31 in breast cancer cells affects tumor biological processes. 29th Winter School on Proteases and Their Inhibitors, Tiers, Italy, *Oral presentation*

10 - ACKNOWLEDGEMENTS

First and foremost, I want to thank **Prof. Dr. Viktor Magdolen** for giving me the opportunity to work on such a challenging project in his great lab. Viktor, you supervised me in an ideal fashion, which letting me work independently, but never alone. I really appreciate all you have done for me. Thank you very much.

A very big thank you goes to **all my colleagues** in the lab. You guys make the place friendly, fun, full of cake and a very good place to work. Furthermore I want to thank **Prof. Dr. Schmitt**, **Dr. Christof Seidl**, **Dr. Rudolf Napieralski**, **Dr. Bettina Grismayer**, **Sabine Creutzburg**, **Anke Benge**, **Marita Zoma**, **Athina Vakrakou**, **Dimitra Mazaraki** amd **Tom Schulze** for helpful discussions and the collaborate work on the Rab31 project. I want to thank all members of the **"underground guerilla army"** it was always a pleasure to see you guys!

The last few months **Kasia Falkowski** and **Dominik Alterauge** joined the Magdolen lab, which showed me that a great working environment is good, but working with friends is something so special. Thank you for making the most stressful time of this thesis also the best! And by the way you guys are now my friends, whether you want to or not, so join the family below!

My thanks also go out to the people, which I have been fortunate to cooperate with, to learn from, to talk to about my project and to meet during this thesis. They all have contributed to this work and I very much appreciate it.

Bastian Seubert, with whom I was able to cooperate on the Rab31 overexpression project. My Ph.D. committee: **Prof. Dr. Achim Krüger** and PD Dr. **Günther Richter** who both allowed me to work in their labs and discussed my projects with me. **Dr. Matthias Kotzsch** who welcomed me in his lab in Dresden and collaborated with us. **Dr. Nathalie Beaufort** shared her knowledge and her lab with me. **Dr. Daniela Lössner** was a great supervisor during my time in Brisbane and a friend. **Prof. Dr. Ute Reuning** always had an open ear and taught me how to use the CLSM. **Wolfgang Skala** the men of all the papers we don't get!

My mom has also always backed me up during my studies and this thesis. Her total (moral) support made it easier to believe that the end to my studies would finally come.

I want to thank **my dad**; he had given me financial support during all my studies but this is by far not the biggest gift he had for me. Just some weeks before his sudden death he gave me his blessing to do whatever (job) makes me happy. I am glad that I can now be a Ph.D., which he placed so much value on and find my way towards a life that fulfills me.

Some say…

Friends are the family you choose and I picked the very best one!

This is why I want to thank **all my friends**, being **my family** scattered around the globe, but still has taken an interest in my wellbeing and my work. They always found time to help me, and very interesting ways to motivate me in the last month while writing up my thesis! A lot of them even read this “master piece”. I hope, I can give back to my family what they have given me so generously and party with them when this is over.

Last, but definitely not least, I want to thank **Olrich -mein Held-**. You are one of the nicest, greatest, kindest, craziest and funnies person on earth and every day you inspire me to be the best possible version of myself. Thank you for every femtosecond of your time and your love.